Fernando Luiz de Campos Carvalho

Estudos de Nova Física em Aceleradores

Guaratinguetá
2014

Fernando Luiz de Campos Carvalho

Estudos de Nova Física em Aceleradores

Texto Sistemático Crítico Apresentado à Faculdade de Engenharia da Universidade Estadual Paulista "Júlio de Mesquita Filho- Câmpus de Guaratinguetá para o Concurso de Livre-Docência.

Guaratinguetá, abril de 2014
2014

Carvalho, Fernando Luiz de Campos

Estudos de Nova Física em Aceleradores

148 páginas

Texto Sistemático Crítico - Faculdade de Engenharia - Campus de Guaratinguetá - Universidade Estadual Paulista "Júlio de Mesquita Filho". Departamento de Física e Química.

I. Universidade Estadual Paulista "Júlio de Mesquita Filho". Faculdade de Engenharia - Campus de Guaratinguetá. Departamento de Física e Química.

Dedicatória

Dedico este trabalho à minha família e às pessoas que participam de minha vida, na busca incessante da felicidade.

Agradecimentos

Gostaria de agradecer aos colaboradores que participaram do desenvolvimento do trabalho de pesquisa ao longo de minha vida acadêmica, nesses dezessete anos de UNESP. Devo primeiro agradecer ao Prof. Dr. José Wagner Furtado Valle, orientador e colaborador desde 1991. Aprendi com ele a importância da dedicação e da seriedade no trabalho acadêmico. O privilégio de ter participado de um período, ainda que curto, da trajetória científica que ele traçou no CSIC-Espanha ajudou a definir muitos dos valores científicos acadêmicos que trago até hoje. Também é de fundamental importância agradecer aos colaboradores Prof. Dr. Oscar José Pinto Éboli, Prof. Dr. Sérgio Ferraz Novaes e ao Prof. Dr. Maurício Bernardino Magro, que me acompanham no trabalho em Física de Partículas Elementares antes mesmo do meu início da vida acadêmica na UNESP. Aos colaboradores A. Belyaev, Diego Restrepo, M. C. Gonzalez-Garcia, Martin Hirsch, Miguel Angel García-Jareño, M. A. Díaz, P. G. Mercadante, Rogério Rosenfeld, S. M. Lietti, S. P. Das, W. Porod . Gostaria de agradecer também aos novos colaboradores, professor Júlio Marny Hoff da Silva e Marco André Ferreira Dias. A consciência de que ainda sou capaz de aprender com profissionais tão dedicados é motivo de grande alegria.

Dentre as pessoas que me acompanham na vida acadêmica, é primordial agradecer aos amigos que apoiam, aconselham e com os quais convivi no Departamento de Física e Química (DFQ) nos últimos quinze anos. Especiais agradecimentos aos professores Maurício Antonio Algatti e Rogério Pinto Mota e demais professores do Grupo de Plasma, aos professores da área de Ensino de Física e aos professores do Grupo de Partículas e Campos, companheiros no Programa de

Pós-Graduação em Física, na FE - Guaratinguetá. Imperdoável seria deixar de citar e prestar meus agradecimentos a duas pessoas importantíssimas na vida acadêmica: Vânia Cristina e Ana Cristina Leme, por seu trabalho na secretaria do DFQ, pelas qualidades profissionais e humanas.

O trabalho de pesquisa na academia não se limitou á área de Física de Part ículas Elementares. A área de Ensino de Física, embora não seja o tema abordado, também é parte de minha trajetória acadêmica e deve ser mencionada. Neste caso, o trabalho foi desenvolvido graças à colaboração e apoio das Profas. Dras. Alice Assis e Valéria Silva Dias, com as quais tive o imenso prazer de trabalhar, e com esta última, dividir sala nos últimos dois anos. A convivência foi um verdadeiro processo de construção, tal qual o conhecimento. Agradeço imensamente a oportunidade da convivência e da aprendizagem. Agradeço também ao Insituto de Ciência e Tecnologia, de São José dos Campos, por sua repecção acolhedora. Espero poder contribuir com tudo o que aprendi ao longo dos anos de UNESP no Campus de Guaratinguetá para o crescimento e fortalecimento da UNESP no Vale do Paraíba.

Por fim, agradeço às pessoas que me apoiaram ao longo dessa jornada, à minha família, sempre generosa, e ao amor, que me faz caminhar mais feliz.

À FAPESP e ao CNPq pelo suporte financeiro.

Fernando Luiz de Campos Carvalho

Texto Sistemático Crítico

Apresentado à Faculdade de engenharia da Universidade Estadual Paulista - Campus de Guaratinguetá para o Concurso de Livre-Docência

Guaratinguetá, abril de 2014

.

Texto Sistemático Sobre Nossas
Contribuições ao "Estudo de
Nova Física em Aceleradores"

Elaborado por

Fernando Luiz de Campos Carvalho

APRESENTAÇÃO

Decidi apresentar uma análise crítica de alguns trabalhos desenvolvidos após a conclusão do pós-doutoramento, no Instituto de Física Teórica - UNESP, em continuidade aos trabalhos desenvolvidos no doutoramento, no Instituto de Física Corpuscular - IFIC/CSIC, na Universidad de Valencia, Espanha, em substituição à tradicional tese de Livre-Docência elaborada por vários pesquisadores. A maioria desses trabalhos foram desenvolvidos na UNESP, em parceria com a USP e a Universidad de Valencia, desde 1997 até o momento.

A opção por esta sistemática, de leitura crítica dos trabalhos desenvolvidos, visa ressaltar a contribuição dos referidos trabalhos para a área bem como as perspectivas de sua continuidade ou extensão.

Sumário

1 Introdução **1**

2 O Modelo Padrão e algumas extensões possíveis **1**

3 Acoplamentos Anômalos **7**

3.1 Acoplamentos Anômalos - $e^+e^- \to W^+W^-\gamma$ 9

3.2 Acoplamentos Anômalos - o bóson de Higgs 19

3.3 Acoplamentos Anômalos - Três jatos 30

4 Modelos Supersimétricos com quebra de paridade R **39**

4.1 Modelo BRPV–mSUGRA 44

4.2 Modelo BRpV-AMSB 45

4.3 Determinação dos parâmetros associados aos modelos 74

4.4 Os modelos BRpV e a Física de Neutrinos 75

4.5 Sinais em aceleradores: o Tevatron, LEP II e o LHC 105

5 Quebra de simetria de Lorentz **141**

6 Considerações Finais **151**

Capítulo 1

Introdução

A tentativa de entender e descrever a Natureza é um desafio que o ser humano se propõe a enfrentar e tem no conhecimento científico o seu maior aliado. A divisão do conhecimento científico nas diferentes áreas se faz necessária à medida que ampliamos e aprofundamos nossa capacidade de descrever os mais diferentes fenômenos da Natureza. Mesmo tendo em vista a busca da unificação do conhecimento produzido para que se atinja o objetivo inicial, e a consequente perda da perspectiva geral, a eficácia da fragmentação se manifesta quando observado o desenvolvimento das diferentes áreas das ciências. Na Física, cujos primórdios se confundem com o desenvolvimento do próprio conhecimento científico, nossa busca por descrever fenômenos físicos e utilizar a matemática como nossa estrutura a partir da qual nos comunicamos, nos levou, ao mesmo tempo, à separação dos estudos em diferentes áreas e à busca de uma forma unificada de entendê-las dentro dessas áreas. No caso da Física das Partículas Elementares essa unificação faz parte do seu desenvolvimento. Assim, as propostas para se descrever as interações fundamentais da natureza convergem para sua expressão mais elaborada no

chamado Modelo Padrão das Interações Fundamentais, que incluem as interações eletrofracas e as interações fortes e, espera-se que em algum momento, a interação gravitacional. Ou seja, a unificação aqui aparece como nossa meta, a partir da qual, se supõe, teremos uma visão geral de todo o conhecimento produzido na área e a partir do qual será possível responder às questões que nos são apresentadas pelos diferentes resultados obtidos em experimentos ou da observação direta da natureza, em fenômenos astrofísicos. É nesse contexto que inciamos nossos trabalhos de pesquisa, e seguimos, tentando entender questões que permanecem à espera de respostas consistentes, sem perder de vista a possibilidade de contato com outros temas de estudo na Física de Partículas Elementares. O foco de nossa atenção está no Modelo Padrão das Interações Eletrofracas. Sempre buscamos uma abordagem fenomenológica, tendo como base de nossos estudos os resultados experimentais publicados pelas diferentes colaborações dos principais laboratórios do mundo. Este tipo de trabalho deve, essencialmente, ser realizado em grupo, visto que diferentes aspectos relacionados à teoria, análise dos resutlados experimentais, geração e uso de códigos computacionais são necessários. Os grupos dos quais participei, contaram sempre com professores da UNESP, do Insituto de Física da USP, da Universidad Católica do Chile, Universidad de Medellín, Colômbia, Fundação Santo André e da Universidad de Valencia, Espanha. Assim, iniciamos nossa apresentação com algumas considerações sobre o Modelo Padrão das Interações Eletrofracas e, a seguir, passamos aos trabalhos desenvolvidos e que queremos apresentar e tecer algumas considerações.

Capítulo 2

O Modelo Padrão e algumas extensões possíveis

O Modelo Padrão (SM) de interações eletrofracas tem sido testado em todos os experimentos de altas energias. Todos os resultados experimentais encontrados até o momento corroboram os resultados teóricos previstos. A geração de massa das partículas elementares sempre foi um dos principais problemas nesse modelo. O Mecanismos de Higgs, baseado na quebra da simetria $SU(3) \otimes U(1)$, tem como consequencia o surgimento do bóson de Higgs, cuja descoberta foi uma das principais empreitadas de grande parte dos físicos experimetais de altas energias, e referencia para propostas de extensões do SM. Além desse aspecto, relacionado à geração de massa das partículas elementares, outros não menos importantes e intrigantes, também servem de guia para os estudos das possíveis extensões do SM. Dentre aqueles que nos servem de referência estão a geração de massa para os neutrinos no SM e a estabilidade da teoria a altas energias.

A recente descoberta do bóson de Higgs, como a último bloco fundamental do

SM, na verificação das partículas previstas nesse Modelo, consolida o SM como a base para a descrição das interações eletrofracas na escala de energia acessível nos aceleradores. Assim, começam a ser respondidas duas das questões fundamentais do SM: qual a origem das massas das partículas e qual a natureza da quebra da simetria eletrofraca. Com o funcionamento do Large Hadron Collider (LHC), temos a possibilidade de estudar ambas questões, a partir da análise dos dados, que começam a ser publicadas. Tais resultados são de fundamental importância no estudo das possíveis extensões do SM. Neste caso o objetivo é estudar a física a energias mais altas que a escala de quebra da simetria eletrofraca. O anúncio da detecção do bóson de Higgs permite que respostas possam surgir dessa análise de dados coletados no período de funcionamento do LHC. Tais resultados certamente serão utilizados para a discussão de outros pontos chaves a serem compreendidos na busca de uma teoria unificada, a partir da qual aspectos associados à astrofísica também possam ser considerados na elaboração dessa teoria. As extensões do Modelo Padrão visam contribuir para esse estudo. Dentre as extensões propostas para o SM, nos dedicamos, ao longo desses anos, principalmente, ao estudo de duas delas. A primeira baseia-se na extensão do SM por meio da introdução de acoplamentos anômalos na Lagrangeana. O aspecto a ser estudado aqui se associa à estabilidade da teoria, ou seja, como a presença de termos que podem interferir na renormalizabilidade da teoria tem efeito nos sinais em experimentos de altas energias, a energias acessíveis nos aceleradores. Desse modo, estudamos os sinais em aceleradores advindos desse tipo extensão, no sentido de estabelecer possíveis limites sobre os acoplamentos associados a esses termos. A segunda, e mais debatida na área de Física de Partículas e Campos, é o Modelo Padrão Supersimétrico Mínimo (MSSM). Nesse modelo, se introduz uma nova simetria, a

Supersimetria, cuja principal característica é a associação entre férmions e bosons, de tal forma que toda partícula do SM tenha um parceiro supersimétrico, ou seja, a cada férmion temos um bóson associado e a cada bóson, um férmion. Como não foi observada até o momento, considera-se que a supersimetria esteja quebrada à escala de energia acessível. Nosso interesse reside no fato de, na construção do referido modelo, serem impostas "a priori"algumas simetrias, dentre elas a simetria associada à conservação de número bariônico e leptônico, expressa na forma de paridade, a chamada paridade R. Estudamos extensões do MSSM, nos quais a paridade R não se conserva (BRpV), e analisamos as conseqüências da quebra dessa simetria em aceleradores. Como consequência da quebra de paridade R, a partícula supersimétrica mais leve pode decair. Estudam-se, principalmente, duas possibilidades de se realizar tal quebra: explícita ou espontânea. No caso da quebra espontânea, temos a geração de um bóson de Goldstone, o majoron, a partícula mais leve, que acarretará no decaimento da partícula supersimétrica mais leve. A quebra explícita também é estudada como um modelo efetivo, comparado ao caso da quebra espontânea. Nas extensões do MSSM onde a partícula supersimétrica mais leve (LSP) pode decair, é possível acomodar a geração massa para os neutrinos, cujos valores são compatíveis com os resultados experimentais conhecidos, e nos quais a massa e os ângulos de misturas dos neutrinos podem ser expressos em termos de parâmetros do modelo.

Nesses modelos, o sinal característico deixado no acelerador pela LSP ao decair pode ser composto de multi-leptons ou multi-jets,a partir de um vértice deslocado. De acordo com os resultados já obtidos a partir de simulações, uma ampla região no espaço de parâmetros dos modelos pode ser testada nos aceleradores em funcionamento. Nosso objetivo é o estudo detalhado das taxas de decaimento

da LSP em modelos com quebra de paridade R nos cenários em que a quebra da supersimetria é mediada por termos de origem gravitacional (mSUGRA), anômala (AMSB) ou via termos de gauge (GMSB)em aceleradores (como foi realizado para o Tevatron, o LEP e mas recentemente para o LHC), assim como os possíveis limites sobre o setor de neutrinos desses modelos, tendo como base os resultados experimentais fornecidos pelas colaborações associadas a esses experimentos. No caso de modelos em física de neutrinos, o que se pretende é utilizar o resultado obtidos nos aceleradores para estudar os possíveis limites sobre acoplamentos e ângulos de mistura para os neutrinos, e contribuir para ampliar nosso conhecimento na área de Física de Neutrinos, que abarca resultados de aceleradores, assim como da Astrofísica.

Além dos estudos abrangendo estes dois aspectos citados, recentemente participamos de estudos de sinais em aceleradores devido ao acoplamento do bóson de Higgs com partículas de espín semi-inteiro e dimensão de massa 1, o chamado Elko - *Eigenspinoren des Ladungskonjugationsoperators*. Sabendo que termos de dimensão superior a 4 devem estar suprimidos por uma escala de massa fundamental e a renormalizabilidade da teoria deve ser mantida, o espinor Elko pode ter auto acoplamento quártico ou se acoplar ao bóson de Higgs, aparecendo como candidato para a matéria escura. Desse modo, pode-se estudar uma possível extensão do Modelo Padrão de forma a incluir os limites associados à Astrofísica para matéria escura no Universo. Inclua-se nas características dos Elko a não localidade, derivada na quebra de simetria de Lorentz associada a este tipo de acoplamento.

Apresentamos a seguir, de forma resumida, algumas características relevantes no caso das extensões consideradas, os resultados obtidos bem como a discussão

das possibilidades e alternativas de estudos possíveis, quando for o caso. Incluimos também os trabalhos produzidos, selecionados por sua importância e que incluem referências sobre o assunto. Desse modo, optamos por indicá-las também como as referências do trabalho que ora se apresenta.

Capítulo 3

Acoplamentos Anômalos

A tentativa de descrever as interações fundamentais da Natureza em alta escala de energia permitiria identificar os efeitos de uma teoria mais ampla, na qual seria possível englobar o Modelo Padrão (SM), e, buscar indicações de uma proposta de modelo unificado no qual seja possível abarcar as interações fundamentais da Natureza. O primeiro passo nesse sentido é estudar possíveis sinais de nova física, por meio da busca de seus efeitos a energias acessíveis atualmente nos aceleradores, com o objetivo de propor possíveis extensões do SM. Uma das formas de se buscar os efeitos dessa nova física em aceleradores é o estudo de extensões realizados por meio da adição de termos na Lagrangeana, com o objetivo de parametrizá-los. Assim, temos uma Lagrangena Efetiva, contendo operadores de dimensão superior a quatro, que incluem os campos presentes na escala de energia acessível, assegurando as simetrias do Modelo Padrão. Este tipo de extensão consiste numa aproximação independente de quais modelos poderão ser propostos, limitada por uma escala de energia, Λ, muito maior que a escala de energia na qual os experimentos se realizam. Desse modo, a Lagrangeana na escala de energia

dos aceleradores, pode conter termos associados aos efeitos das possíveis novas interações a escala de energias mais altas. A forma da Lagrangeana, invariante sob $SU(3)_C \otimes SU(2)_L \otimes U(1)_Y$ é:

$$L = L_{SM} + \sum_{n=1...} \frac{f_{(n+4)}}{\Lambda^n} O_{(n+4)} \tag{3.1}$$

na qual L_{SM} é a Lagrangeana correspondente do Modelo Padrão, Λ é a escala característica da nova física e $O_{(n+4)}$ são os operadores locais de dimensão (n+4). Como diferentes cenários podem gerar o mesmo tipo de operador, indicam-se os diferentes acoplamentos efetivos f_{n+4}. A classificação dos operadores indicados foi realizada e, a partir dela, vários estudos sobre a possíveis implicações fenomenológicas no setor bosôsonico, assim como no setor fermiônico e no setor de gluons. A análise do setor bosônico se faz, considerando-se todos os possíveis termos de dimensão 6 que possam contribuir para os acoplamentos entre os bóson do Modelo Padrão, isto é, γ, W^+, W^-, Z^0 e H, invariantes sob o mesmo grupo de simetria do Modelo Padrão. No caso do setor fermiônico o mesmo tipo de procedimento é adotado, isto é, considera-se todos os termos de dimensão 6 que possam contribuir para a modificação do acoplamentos desses férmions, tendo em vista as possíveis restrições obtidas da análise de dados então conhecidos (LEP I, LEP II, Tevatron). Nossa contribuição nesse aspecto foi o estudo de alguns acoplamentos anômalos, com a finalidade de estabelecer os possíveis limites a partir desses dados.

3.1 Acoplamentos Anômalos - $e^+e^- \to W^+W^-\gamma$

Inicialmente estudamos os limites para os coeficientes dos termos de dimensão 6 da Lagrangena que parametrizam os possíveis efeitos da nova física no processo $e^+e^- \to W^+W^-\gamma$ para energias acessíveis no LEP II e no NLC. Nesse estudo incluimos todas as poíveis interações incluindo bosons vetoriais e o boson de Higgs, levando em conta o estudo do "background"irredutível. A forma da Lagrangeana, invariante sob $SU(3)_C \otimes SU(2)_L \otimes U(1)_Y$ é:

$$L = L_{SM} + \frac{1}{\Lambda^2}(f_{WWW}\,O_{WWW} + f_{WW}\,O_{WW} + f_W\,O_W + f_{BB}\,O_{BB} + f_B\,O_B) \quad (3.2)$$

na qual L_{SM} é a Lagrangeana correspondente do Modelo Padrão, Λ é a escala característica da nova física e $O_{(n+4)}$ são os operadores locais de dimensão (n+4) associados às contribuições efetivas para o sinal estudado. Os operadores mencionados são definidos da seguinte forma:

$$O_{WWW} = Tr[\hat{W}_{\mu\nu}\hat{W}^{\nu\rho}\hat{W}^{\mu}_{\rho}] \quad (3.3)$$

$$O_{WW} = \Phi^{\dagger}\hat{W}_{\mu\nu}\hat{W}^{\mu\nu}\Phi \quad (3.4)$$

$$O_W = (D_\mu\Phi)^{\dagger}\hat{W}^{\mu\nu}(D_\nu\Phi) \quad (3.5)$$

$$O_{BB} = \Phi^{\dagger}\hat{B}_{\mu\nu}\hat{B}^{\mu\nu}\Phi \quad (3.6)$$

$$O_B = (D_\mu\Phi)^{\dagger}\hat{B}^{\mu\nu}(D_\nu\Phi) \quad (3.7)$$

Incluimos nesse estudo os efeitos de polarição dos eletrons incidentes e dos W finais e estudamos a distribuição de energia dos fótons para obtermos os referidos

limites. Nesse caso, o interesse foi estudar o possível efeitos advindos de operadores que não pudessem ser testados em processos de produção de pares de W. Para o caso do bóson de Higgs com massa na faixa 170GeV$<m_H<$300GeV, o espectro de energia do fóton apresenta uma contribuição via acoplamento anômalo do Higgs.

Anomalous couplings in $e^+e^- \to W^+W^-\gamma$ at CERN LEP 2 and NLC

F. de Campos, S. M. Lietti, S. F. Novaes, and R. Rosenfeld
Instituto de Física Teórica, Universidade Estadual Paulista,
Rua Pamplona 145, CEP 01405–900 São Paulo, Brazil
(Received 21 March 1997; revised manuscript received 16 June 1997)

We present sensitivity limits on the coefficients of a dimension-6 effective Lagrangian that parametrizes the possible effects of new physics beyond the standard model. Our results are based on the study of the process $e^+e^- \to W^+W^-\gamma$ at CERN LEP 2 and NLC energies. In our calculations, we include *all* the new anomalous interactions, involving vectors and Higgs bosons, and take into account the standard model irreducible background. We analyze the impact of these new interactions on the total cross section, including the effects of the initial electron and final W polarizations. We then focus on the operators that will not be constrained by the $e^+e^- \to W^+W^-$ process, obtaining limits based on the photon energy distribution. [S0556-2821(97)05019-4]

PACS number(s): 14.80.Cp, 13.10.+q

I. INTRODUCTION

One of the main physics goals of the CERN e^+e^- collider LEP 2 and future e^+e^- colliders is to directly test the gauge nature of couplings among the electroweak gauge bosons. The process with a largest cross section at LEP 2 involving these couplings is the W-pair production $e^+e^- \to W^+W^-$, which is sensitive to the trilinear $WW\gamma$ and WWZ couplings. The measurement of these couplings and the sensitivity to possible deviations from the standard model (SM) predictions have been extensively studied in the recent years [1].

The most general phenomenological parametrization for these couplings [2] can be achieved by means of an effective Lagrangian [3] that involves operators with dimension higher than 4, containing the relevant fields at low energies and respecting the symmetries of the standard model. The effective Lagrangian approach is a model-independent way to describe new physics that can occur at an energy scale Λ much larger than the scale where the experiments are performed.

The effective Lagrangian depends on the particle content at low energies and since the Higgs boson has not yet been found, there are two logical possibilities to describe the new physics effect at low energies. In one of them, the Higgs boson can be light, being present in the higher dimensional operators, in addition to the electroweak gauge bosons, and the SM symmetries are linearly realized [4,5]. Alternatively, the Higgs boson can be very heavy and it must be integrated out at low energies. In this case, the relevant fields at low energies are only electroweak gauge bosons and the SM symmetries are realized nonlinearly [6]. Here we focus on a linearly realized $SU_L(2)\times U_Y(1)$-invariant effective Lagrangian to describe the bosonic sector of the standard model, keeping the fermionic couplings unchanged.

The same effective Lagrangian used to describe anomalous trilinear gauge couplings can, in general, lead to anomalous quartic interaction among gauge bosons and also to anomalous couplings of these particles with the Higgs field. All these interactions should also be investigated at LEP 2 and at the Next Linear Colliders (NLC) in order to search for hints about the nature of the new physics described by these higher dimensional operators.

New quartic gauge boson couplings have been studied before in many different processes at future e^+e^-, $e\gamma$, $\gamma\gamma$, e^-e^-, and pp colliders [7]. However, most of these previous works have focused on the so-called genuinely quartic operators, i.e., operators that give rise only to quartic gauge boson interactions without altering the trilinear couplings [8]. Since these operators do not appear in a dimension-6 linearly realized $SU(2)_L\times U_Y(1)$ invariant effective Lagrangian [9], they will not be considered here. Anomalous Higgs boson couplings have also been studied before in Higgs and Z boson decays [10], in e^+e^- [11,12] and $\gamma\gamma$ colliders [13].

The process with largest cross section in e^+e^- colliders that also involves quartic couplings, and possibly anomalous Higgs couplings, besides the trilinear couplings, is $e^+e^- \to W^+W^-\gamma$. Therefore, it is the most promising channel to look for possible deviations from the standard model predictions. This process has been considered by Bélanger and Boudjema [8] and by Leil and Stirling [14] in the context of genuinely quartic operators, where the Higgs and trilinear couplings were set to the standard model values and 3σ deviations in the total cross section were used to determine the reach of this reaction. Grosse-Knetter and Schildknecht [15] have considered the effect of a *single* higher dimensional operator usually denoted by $\mathcal{O}_W$ (see below) in the above process, taking into account modifications on both trilinear and quartic couplings. However, they assumed that the Higgs boson mass lies above the energy region to be investigated and therefore they disregarded its contribution.

The purpose of this work is to study the sensitivity to these anomalous couplings of the process $e^+e^- \to W^+W^-\gamma$ at LEP 2 and the NLC. We consistently include in our calculations *all* new couplings introduced by the effective Lagrangian that has become widely adopted to describe new physics beyond the standard model. In particular, this process is sensitive to operators related to anomalous Higgs boson couplings that do *not* affect the self-coupling of gauge bosons and hence are not constrained by the LEP 2 measurements of $e^+e^- \to W^+W^-$. Therefore, the process $e^+e^- \to W^+W^-\gamma$ may provide important information about these operators at the NLC.

This paper is organized as follows. In Sec. II, we review

the framework of effective Lagrangians that we use to parametrize anomalous couplings and explain the methodology used to study the $W^+W^-\gamma$ production. In Sec. III, we analyze the sensitivity at LEP 2 based on the total cross section. In Sec. IV, we study the improvements arising from going to NLC energies, the effects of having a polarized electron beam, and the impact of being able to measure the W boson polarization. We then concentrate on the analysis of operators which will not be probed by the $e^+e^-\to W^+W^-$ process, obtaining limits based on the photon energy spectrum. We present our conclusions in Sec. V.

II. EFFECTIVE LAGRANGIAN AND THE PROCESS $e^+e^-\to W^+W^-\gamma$

In order to write down the most general dimension-6 effective Lagrangian containing all SM bosonic fields, i.e., γ, $W^\pm$, Z^0, and H, we adopt the notation of Hagiwara *et al.* [5]. This Lagrangian has eleven independent operators in the linear representation that are locally $SU_L(2)\times U_Y(1)$ invariant, C and P even. We discard the four operators which affect the gauge boson two-point functions at the tree level and therefore are strongly constrained by LEP 1 measurements. We also do not consider the two operators that modify only the Higgs boson self–interactions, since they are not relevant for our calculations. We are then left with five independent operators, and the Lagrangian is written as

$$\mathcal{L}_{\rm eff}=\mathcal{L}_{\rm SM}+\frac{1}{\Lambda^2}(f_{WWW}\mathcal{O}_{WWW}+f_{WW}\mathcal{O}_{WW}+f_{BB}\mathcal{O}_{BB}+f_W\mathcal{O}_W+f_B\mathcal{O}_B), \tag{1}$$

with each operator $\mathcal{O}_i$ defined as

$$\mathcal{O}_{WWW}=\mathrm{Tr}[\hat{W}_{\mu\nu}\hat{W}^{\nu\rho}\hat{W}^{\mu}_{\rho}], \tag{2}$$

$$\mathcal{O}_{WW}=\Phi^\dagger\hat{W}_{\mu\nu}\hat{W}^{\mu\nu}\Phi, \tag{3}$$

$$\mathcal{O}_{BB}=\Phi^\dagger\hat{B}_{\mu\nu}\hat{B}^{\mu\nu}\Phi, \tag{4}$$

$$\mathcal{O}_W=(D_\mu\Phi)^\dagger\hat{W}^{\mu\nu}(D_\nu\Phi), \tag{5}$$

$$\mathcal{O}_B=(D_\mu\Phi)^\dagger\hat{B}^{\mu\nu}(D_\nu\Phi), \tag{6}$$

where Φ is the Higgs field doublet, which in the unitary gauge assumes the form

$$\Phi=\begin{pmatrix}0\\(v+H)/\sqrt{2}\end{pmatrix},$$

and

$$\hat{B}_{\mu\nu}=i\frac{g'}{2}B_{\mu\nu},\quad \hat{W}_{\mu\nu}=i\frac{g}{2}\sigma^a W^a_{\mu\nu}, \tag{7}$$

with $B_{\mu\nu}$ and $W^a_{\mu\nu}$ being the field strength tensors of the U(1) and SU(2) gauge fields, respectively.

The operator $\mathcal{O}_{WWW}$ contributes only to anomalous gauge couplings, $\mathcal{O}_{WW}$ and $\mathcal{O}_{BB}$ contribute only to anomalous Higgs couplings HZZ and $HZ\gamma$, whereas $\mathcal{O}_W$ and $\mathcal{O}_B$ give rise to both types of new couplings. Therefore, the existence of anomalous trilinear gauge couplings could be related to the anomalous quartic gauge couplings and Higgs interaction, which are the subject of our investigation.

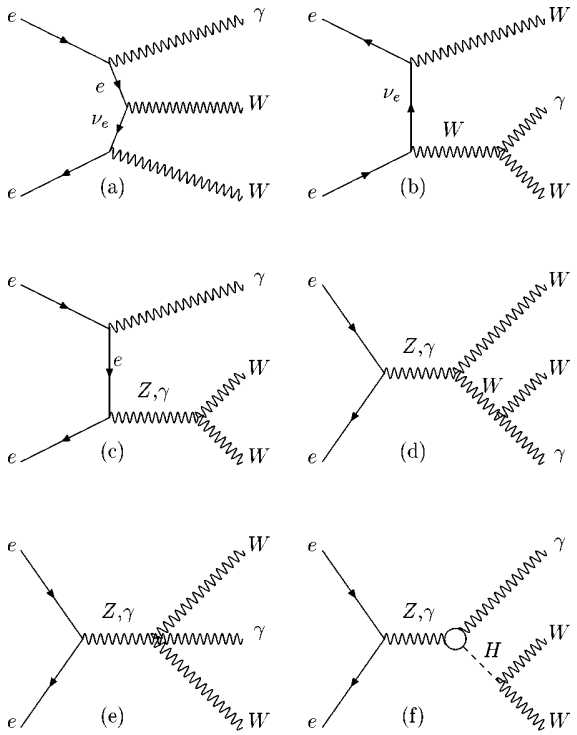

FIG. 1. Feynmam diagrams for the standard model process $e^+e^-\to W^+W^-\gamma$. Crossed diagrams are not shown.

Studies of anomalous trilinear gauge boson couplings from W-pair production will significantly constrain combinations of the parameters f_{WWW}, f_W, and f_B. However they are ''blind'' with respect to f_{WW} and f_{BB}. We chose to study the reaction $e^+e^-\to W^+W^-\gamma$ since it is the process with the largest cross section involving triple, quartic gauge boson couplings and also anomalous Higgs-gauge boson couplings. Therefore, it is also sensitive to f_{WW} and f_{BB}, offering an excellent possibility for a detailed study of these couplings.

The standard model cross section for the process $e^+e^-\to W^+W^-\gamma$ was evaluated in Ref. [16]. When we neglect the electron mass, Higgs contributions for this reaction do not appear at tree level since the couplings $H\gamma\gamma$ and the $HZ\gamma$ are generated only at one loop [17,18]. Taking into account these contributions, there are 16 Feynman diagrams involved in the reaction $e^+e^-\to W^+W^-\gamma$, which are represented in Fig. 1 (the crossed diagrams are not shown) which yields

$$\sigma^{\rm SM}_{WW\gamma}=46(418)\ \text{fb},\quad \text{with } E_\gamma>20(5)\ \text{GeV at } \sqrt{s}=190\ \text{GeV},$$
$$12\ \ \sigma^{\rm SM}_{WW\gamma}=144\ \text{fb},\quad \text{with } E_\gamma>20\ \text{GeV at } \sqrt{s}=500\ \text{eV}, \tag{8}$$

where we have required that the angle between any two particles is larger than 15°. The cross section peaks at roughly $\sqrt{s}=300$ GeV and is typically two orders of magnitude

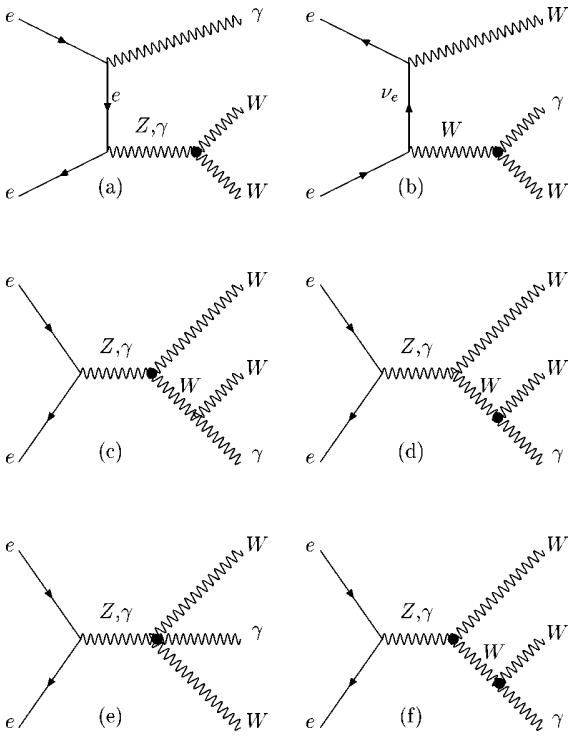

FIG. 2. The vector bosons anomalous contributions to $e^+e^-\to W^+W^-\gamma$. Crossed diagrams are not shown.

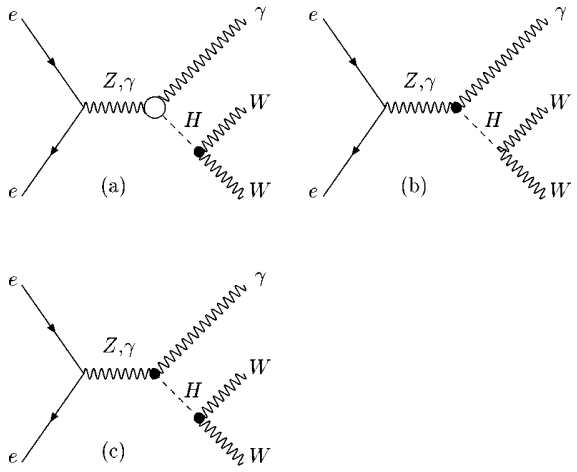

FIG. 3. The Higgs boson anomalous contributions to $e^+e^-\to W^+W^-\gamma$.

smaller than the two-body process $e^+e^-\to W^+W^-$, used to constrain anomalous trilinear couplings.

In order to compute the contribution from all possible anomalous couplings, we have developed a MATHEMATICA code to automatically generate the Feynman rules for the Lagrangian (1) that were then incorporated in HELAS-type [19] subroutines. These new subroutines were used to extend a MADGRAPH [20] generated code to include all the anomalous contributions and to numerically evaluate the helicity amplitudes and the squared matrix element. In our calculations, we have taken into account the standard loop Higgs contributions besides all the relevant anomalous couplings, which give rise to the 42 contributions shown in Figs. 1, 2, and 3. We have checked that our code passed the nontrivial test of electromagnetic gauge invariance. We employed VEGAS [21] to perform the Monte Carlo phase space integration with the appropriate cuts to obtain the differential and total cross sections. Moreover, we have studied the angular variables in order to find optimal cuts to improve the anomalous contribution over the SM signal.

III. $WW\gamma$ PRODUCTION AT LEP 2

We studied the reaction $e^+e^-\to W^+W^-\gamma$ at LEP 2 assuming a center-of-mass energy of $\sqrt{s}=190$ GeV and an integrated luminosity of $\mathcal{L}=0.5$ fb^{-1}. We applied a cut in the photon energy ($E_\gamma>5$ GeV), and we required the angle between any two particles to be larger than $\theta_{ij}>15°$.

Our results for the sensitivity of LEP 2 to the operators appearing in the effective Lagrangian (1), from an analysis of the total cross section, are summarized in Fig. 4 for a fixed value of the Higgs boson mass $M_H=170$ GeV. We plot the contributions of the five different operators separately, assuming that only one operator contributes each time. We also show the result for an extension of the so-called Hagiwara-Ishihara-Szalapski-Zeppenfeld (HISZ) scenario [5], where all the coefficients are considered equal, i.e., $f_{WWW}=f_{WW}=f_{BB}=f_W=f_B=f$, in order to reduce the number of free parameters to only one (f). The standard model cross section and its value with 1, 2, and 3 σ deviations are depicted as horizontal lines.

The most sensitive contribution comes from $\mathcal{O}_{WWW}$, $\mathcal{O}_W$, and $\mathcal{O}_B$. A 1σ deviation in the total cross section would be observed for the following ranges of the coefficients of these operators, for $\Lambda=1$ TeV,

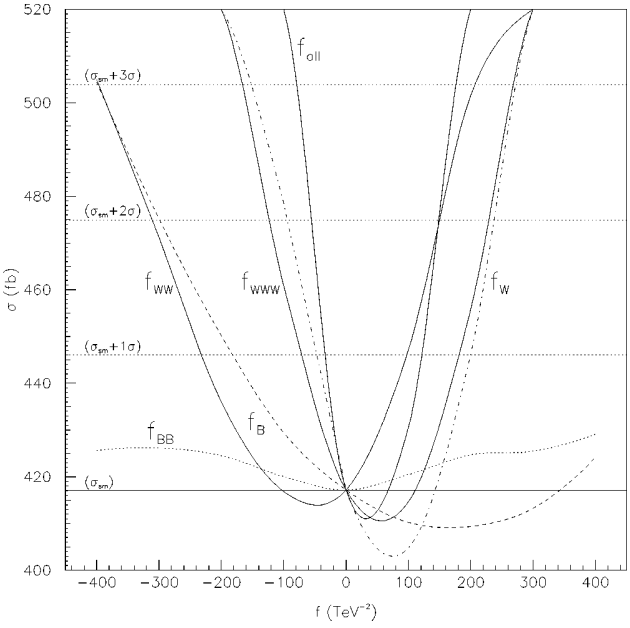

FIG. 4. Total cross section (SM+anomalous) for the process $e^+e^-\to W^+W^-\gamma$, at LEP 2 as a function of different anomalous coefficients and also for the HISZ scenario ($f_{\rm all}$). We assumed $m_H=170$ GeV and $\mathcal{L}=0.5$ fb^{-1}. The results for the SM and for 1, 2, and 3σ deviations are displayed (see text for energy and angular cuts).

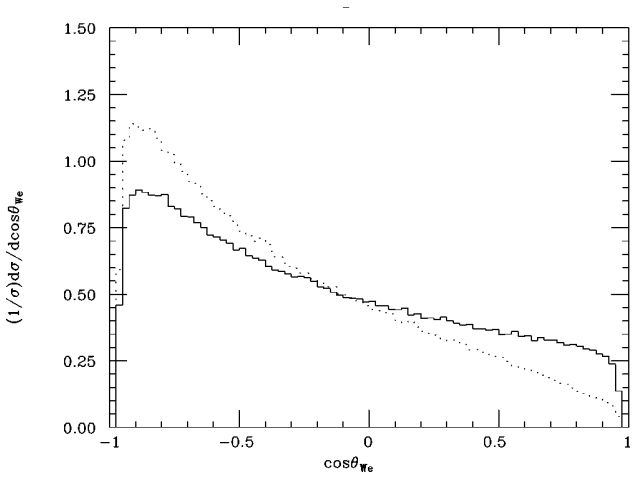

FIG. 5. Normalized W^+-e^+ angular distribution. The solid (dashed) line represents the SM (SM+anomalous) contribution for $f_{\rm all}/\Lambda^2=150$ TeV^{-2} and $m_H=170$ GeV.

$$-75<f_{WWW}<178, \quad -48<f_W<192,$$
$$-188<f_B<550, \quad -253<f_{WW}<110; \tag{9}$$

whereas for the extended HISZ scenario, we have

$$-33<f<119. \tag{10}$$

Of course, the operators that also give rise to changes in the triple vector boson couplings can also be constrained at LEP 2 via the reaction $e^+e^- \to W^+W^-$. A recent analysis of W-boson pair production based on a log-likelihood fit to a fivefold differential cross section obtained the 1σ limits [22], $|f_{WWW}|<10$, $|f_W|<7.1$, and $|f_B|<46$. However, one should keep in mind that this reaction is insensitive to f_{WW} and f_{BB}, and therefore the study of the process $e^+e^- \to W^+W^-\gamma$ can provide further information on these operators, as we show in this paper.

The contribution of the anomalous couplings involving only the Higgs boson, i.e., f_{WW} and f_{BB} (see Fig. 3), is dominated by on-mass-shell Higgs production with the subsequent $H \to W^+W^-$ decay:

$$\sigma(e^+e^- \to W^+W^-\gamma) \propto \sigma(e^+e^- \to H\gamma)\frac{\Gamma(H \to W^+W^-)}{\Gamma(H \to \text{all})}. \tag{11}$$

For large values of the operator coefficients, the total Higgs boson width is dominated by the anomalous decay $H \to \gamma\gamma$ [10], which is also proportional to f_{WW} and f_{BB}. On the other hand, the anomalous width $\Gamma(H \to W^+W^-)$ depends only on f_{WW}. Therefore, the contribution from the anomalous coupling f_{BB} is much less sensitive than the contributions from the other operators since $\sigma(e^+e^- \to W^+W^-\gamma)$ becomes almost independent of this coefficient. Fortunately, this is not the case if one is sensitive to small values of the coefficients, as will occur at the NLC study in the next section.

We have investigated various distributions to try to improve the LEP 2 sensitivity. The most promising distribution is the angular distribution of the W bosons with respect to the beam direction (see Fig. 5). We computed the total cross section with the extra cut $\cos\theta_{W^+e^+}>0$, as suggested by this distribution, and found an increase in sensitivity from 2σ to 2.8σ. However, due to the small deviations in the shape of the kinematical distributions and small statistics, no further improvement seems to be possible.

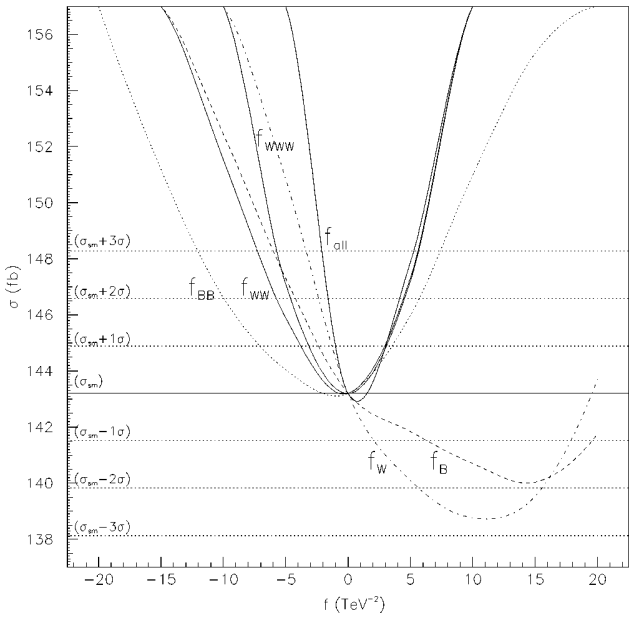

FIG. 6. The same as Fig. 4 for NLC, with $\sqrt{s}=500$ GeV and $\mathcal{L}=50$ fb^{-1}.

IV. $WW\gamma$ PRODUCTION AT NLC

The effect of the anomalous operators becomes more evident with the increase of energy, and we are able to put tighter constraints on the coefficients by studying their contribution to different processes at the Next Linear Collider. We studied the sensitivity of NLC to the process $e^+e^- \to W^+W^-\gamma$ assuming $\sqrt{s}=500$ GeV and an integrated luminosity $\mathcal{L}=50$ fb^{-1}. We adopted a cut in the photon energy of $E_\gamma>20$ GeV and required the angle between any two particles to be larger than 15°. We have analyzed this process for different values of the Higgs boson mass.

In Fig. 6, we show the results for the total cross section, for $M_H=170$ GeV, including the effects of the anomalous operators. The values of the coefficients f's for which a 2σ deviation is obtained are shown in Table I, being typically of

TABLE I. The minimum and maximum values (min,max) of the coefficients f_i/Λ^2 in units of TeV^{-2} for a 2σ deviation of the unpolarized total cross section.

Anomalous couplings	Unpolarized
$f_{\rm all}/\Lambda^2$	$(-2, 5)$
f_B/Λ^2	$(-5, 31)$
f_{BB}/Λ^2	$(-11, 7)$
f_W/Λ^2	$(-3, 23)$
f_{WW}/Λ^2	$(-8, 4)$
f_{WWW}/Λ^2	$(-5, 5)$

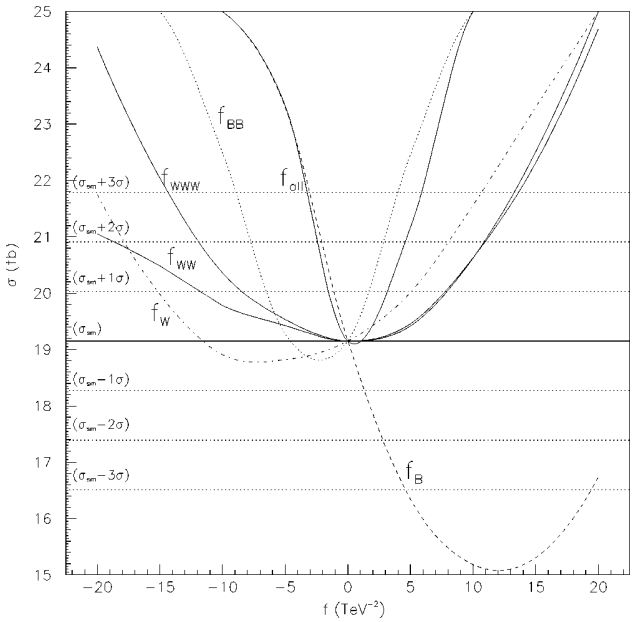

FIG. 7. The same as Fig. 6 for a 90% right-handed polarized electron, with $\sqrt{s}=500$ GeV and $\mathcal{L}=50$ fb^{-1}.

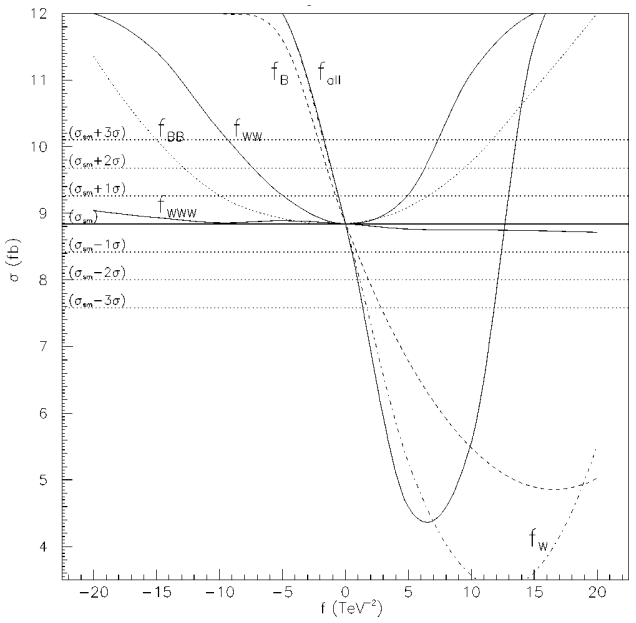

FIG. 8. The same as Fig. 6 for longitudinal W bosons (W_LW_L), with $\sqrt{s}=500$ GeV and $\mathcal{L}=50$ fb^{-1}.

the order of $1-10$ TeV^{-2}. As we could expect, the W pair production at NLC is able to put a limit that is one order of magnitude better for the coefficients $f_{B,W,WWW}$ [22]. However, this latter reaction is *not* able to constrain $f_{BB,WW}$.

In an attempt to increase the sensitivity, we looked at the effects of a 90% polarized electron beam in order to reduce the SM background, mainly the one coming from diagrams of Figs. 1(a) and 1(b) were just left-handed electrons are present. We have considered both left-handed (LH) and right-handed (RH) polarizations, expecting a larger anomalous sensitivity for RH electrons.

In Fig. 7, we show the results for the total cross section, for a 90% right-handed (RH) polarized electron, for $M_H=170$ GeV. Comparing Fig. 6 and Fig. 7, we notice that the effect of the anomalous contributions in the total cross section are larger for the polarized case. However, the small absolute value of the cross section for the polarized case reduces the statistics and leads to no improvement in the established limits, as shown in Table II.

Since we expect the new interactions to involve mainly longitudinally polarized gauge bosons, we studied the sensitivity for different combinations of the polarizations of the W pair. In Fig. 8, we show the analogous of Fig. 6 for the W_LW_L case. Again, the effect of the anomalous contributions to the total cross section is increased, but no further improvements are found due to the small statistics. The results for the bounds on the anomalous coefficients for the W_LW_L, W_TW_T, and $(W_LW_T+W_TW_L)$ cases can be seen in Table III. These bounds were obtained requiring a 2σ effect on the total cross section.

It is important to notice that the kinematical distributions of the longitudinally polarized W's are quite different from the SM results. As we could expect, the new physics effects becomes more evident for longitudinal W's since the decay $H\to W^+W^-$ is dominated by this state of polarization. In Fig. 9, we present the angular distribution of the longitudinal W^+ boson with the initial positron and with the final photon, the energy and the transverse momentum distributions. We can see, for instance, that the W energy distribution is very different from the SM prediction. Its characteristic behavior for $100<E_W<175$ GeV is due to the presence of the Higgs boson, which decays into the W pair giving rise, at the same time, to a monochromatic photon.

We present in Fig. 10 the percent deviation of the SM

TABLE II. The minimum and maximum values (min,max) of the coefficients f_i/Λ^2 in units of TeV^{-2} for a 2σ deviation of the total cross section with 90% polarized LH and RH electrons for a reduced luminosity of $\mathcal{L}=25$ fb^{-1}.

Anomalous couplings	e^-_{LH}	e^-_{RH}
$f_{\rm all}/\Lambda^2$	$(-2, 5)$	$(-3, 5)$
f_B/Λ^2	$(-11, 42)$	$(-2, 26)$
f_{BB}/Λ^2	$(-19, 17)$	$(-8, 3)$
f_W/Λ^2	$(-2, 26)$	$(-17, 9)$
f_{WW}/Λ^2	$(-7, 5)$	$(-15, 11)$
f_{WWW}/Λ^2	$(-5, 5)$	$(-12, 11)$

TABLE III. The minimum and maximum values (min,max) of the coefficients f_i/Λ^2 in units of TeV^{-2} for a 2σ deviation of the total cross section for different combinations of the final state W-pair polarization.

Anomalous Couplings	W_LW_L	W_TW_T	$(W_LW_T+W_TW_L)$
$f_{\rm all}/\Lambda^2$	$(-1, 14)$	$(-5, 3)$	$(-2, 7)$
f_B/Λ^2	$(-2, 35)$	$(-29, 29)$	$(-9, 36)$
f_{BB}/Λ^2	$(-12, 9)$	$(-14, 10)$	$(-13, 8)$
f_W/Λ^2	$(-1, 25)$	$(-36, 22)$	$(-4, 23)$
f_{WW}/Λ^2	$(-8, 6)$	$(-9, 6)$	$(-8, 5)$
f_{WWW}/Λ^2	$(-51, 96)$	$(-6, 4)$	$(-5, 25)$

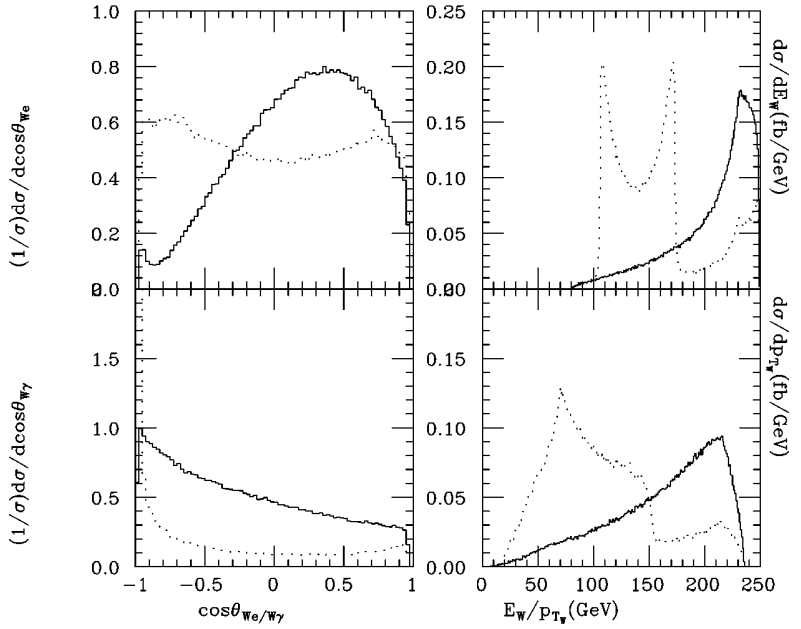

FIG. 9. Kinematical distributions of the longitudinally polarized W^+ vector boson for the SM (solid histogram) and for the anomalous contribution (dotted histogram).

prediction in the photon transverse momentum distribution: i.e.,

$$\Delta = \left(\frac{d\sigma_{\rm ANO}/dp_{T_\gamma}}{d\sigma_{\rm SM}//dp_{T_\gamma}} - 1 \right) \times 100\%,$$

for the different polarization of the W's. Once again the relevance of the $W_L W_L$ case is evident: $\Delta > 100\%$ for $p_{T_\gamma} > 120$ GeV. When a cut of $p_{T_\gamma} > 100$ GeV is implemented, the background is drastically reduced and the ratio of anomalous over SM events per year goes from 576/442 to 424/74, for $f_{\rm all} = 15$ TeV^{-2}.

Using the reaction $e^+e^- \to W^+W^-\gamma$, we are also able to establish bounds on the values of the coefficients f_{WW} and f_{BB}, for which the W-pair process is insensitive, since they only affect the Higgs boson couplings. In Fig. 11, we present the results of a combined sensitivity analysis in the form of a contour plot for the two free parameter, f_{BB} and f_{WW}, for $M_H = 170$ GeV. These are the most relevant coefficients for the anomalous Higgs boson phenomenology and they are not constrained by the W-pair production. We should keep in mind that the $WW\gamma$ production at LEP 2 can put a 1σ bound on f_{WW} (9) while it is not possible to impose a limit on f_{BB} since the cross section is quite insensitive to this coefficient.

If the Higgs boson is found with a mass in the range from 170 to 300 GeV, one would have a large sensitivity for the

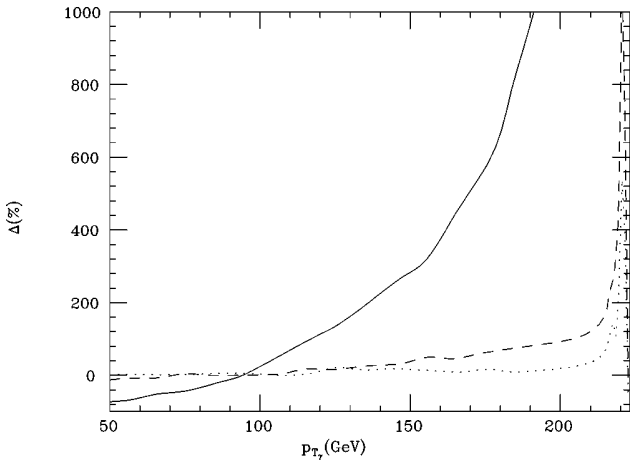

FIG. 10. Plot of deviation (Δ) in the photon P_{T_γ} distribution for the cases of $W_L W_L$ (solid line), $W_L W_T + W_T W_L$ (dashed line), and $W_T W_T$ (dotted line).

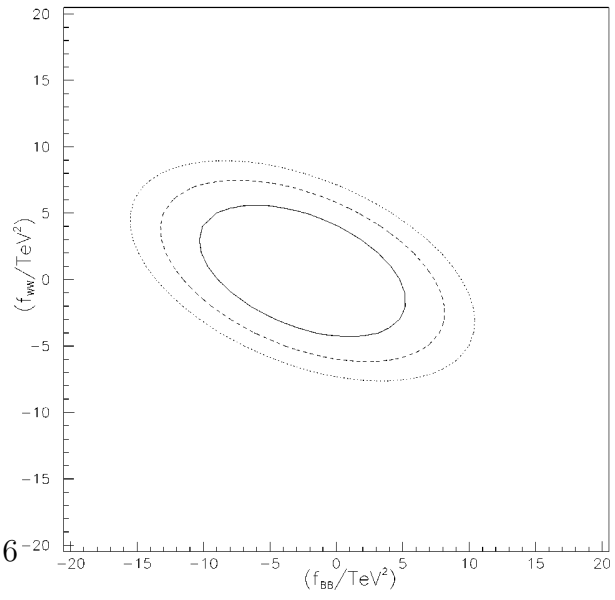

FIG. 11. Contour plot of $f_{BB} \times f_{WW}$, for $M_H = 170$ GeV. The curves show the one, two, and three σ deviations from the standard model value of the total cross section.

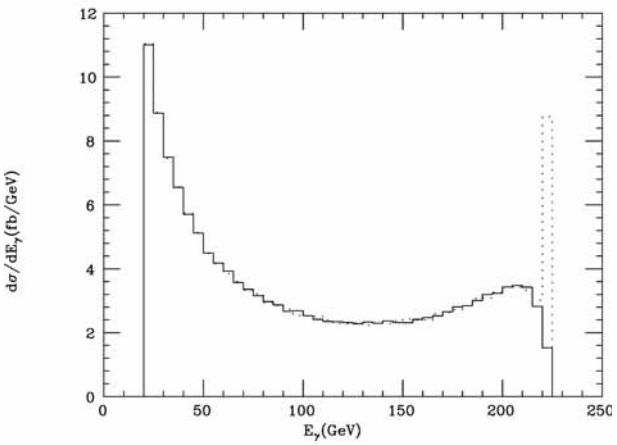

FIG. 12. Photon energy distribution for the SM (solid line) and for the SM+anomalous (dashed line), for $f_{WW}/\Lambda^2 = f_{BB}/\Lambda^2 = 5\text{TeV}^{-2}$, and $M_H = 170$ GeV, with a 5 GeV bin.

anomalous Higgs couplings f_{WW} and f_{BB} in the photon energy distribution of the process $e^+e^- \to W^+W^-\gamma$. This increased sensitivity comes about because the existence of a peak in the photon energy spectrum due to the two-body nature of the dominant contribution, i.e., $e^+e^- \to H\gamma$ followed by the subsequent decay $H \to W^+W^-$ (see Fig. 3). In Fig. 12, we illustrate this effect with a typical photon energy distribution, for $f_{WW}/\Lambda^2 = f_{BB}/\Lambda^2 = 5$ TeV^{-2} and $M_H = 170$ GeV, where the Higgs peak appears very clearly in the photon spectrum of the anomalous contribution.

In order to analyze the significance of the signal based on the photon energy spectrum, we took different energy bins of 1, 3, and 5 GeV. The reason is to roughly mimic the effects of a realistic simulation including the finite energy resolution of the detector and the small spread in the real center-of-mass energy due to initial state radiation. We have not considered the experimental efficiency ϵ_{eff} for W reconstruction. It can be easily incorporated by multiplying the obtained significances by $\sqrt{\epsilon_{\text{eff}}}$. Table IV shows the improvement on the sensitivity compared to the total cross section analysis for the $f_{WW}/\Lambda^2 = f_{BB}/\Lambda^2 = 5$ TeV^{-2} and $M_H = 170$GeV cases.

In Table V, we present our results for the sensitivity on f_{BB}/Λ^2 and f_{WW}/Λ^2, assuming $f_{BB} = f_{WW}$, for the three energy bins above. We obtained a sensitivity of the order of a TeV^{-2} for $M_H = 170$ GeV, decreasing by a factor of roughly four for $M_H = 300$ GeV, which does not depend in a significant way of the bin size. For larger Higgs boson masses, the cross section is reduced due to phase space suppression. For smaller Higgs boson masses, the cross section is reduced since the Higgs boson is off-mass shell, and in this case it would be better to study processes such as $e^+e^- \to b\overline{b}\gamma$ or $e^+e^- \to \gamma\gamma\gamma$ [12].

TABLE IV. Number of standard deviations σ from the standard model from a sensitivity analysis based on the total cross section compared to a sensitivity analysis based on the peak of the photon energy distribution, considering a 1, 3, and 5 GeV bin for different values of the Higgs mass. We fixed $f_{WW}/\Lambda^2 = f_{BB}/\Lambda^2 = 5$ TeV^{-2}.

M_H (GeV)	Total cross section	1 GeV bin	3 GeV bin	5 GeV bin
170	4.2	52.2	43.1	35.8
200	2.8	17.8	20.9	17.8
250	1.8	8.3	10.7	9.9
300	1.0	2.5	3.8	4.3

V. CONCLUSION

The search for the effect of higher dimensional operators that give rise to anomalous bosonic couplings should be pursued in all possible processes since the results may provide important information on physics beyond the standard model. We have studied here the production of a W pair plus a photon in e^+e^- colliders in order to analyze the contributions of anomalous couplings arising from dimension-6 operators of a linearly realized $\text{SU}_L(2) \times \text{U}_Y(1)$ invariant effective Lagrangian. We have included *all* the anomalous trilinear and quartic gauge couplings, as well as the anomalous Higgs couplings with gauge bosons.

We present the limits attainable at LEP 2 and at NLC, including the standard model irreducible background. Polarization of the electron beam and of the W pair are found to be insufficient to improve the limits obtained from the total cross section.

We also focused on the operators $\mathcal{O}_{WW}$ and $\mathcal{O}_{BB}$, which cannot be tested in the W-pair production process. We showed, in particular, that for Higgs boson masses in the range $M_H = 170$–300 GeV, the photon energy spectrum provides a sensitive signature for the anomalous Higgs couplings. Typical sensitivities of a few TeV^{-2} at the NLC are obtained for these coefficients, providing complementary information on different higher dimensional operators.

ACKNOWLEDGMENTS

This work was supported by Conselho Nacional de Desenvolvimento Científico e Tecnológico (CNPq), and by Fundação de Amparo à Pesquisa do Estado de São Paulo (FAPESP).

TABLE V. The minimum and maximum values (min, max) of the coefficients f_i/Λ^2 (for $f_{BB} = f_{WW} = f$) in units of TeV^{-2} that generate a 95% C.L. signal for the total cross section analysis and for the photon energy spectrum analysis with 1, 3, and 5 GeV energy bins for different values of the Higgs mass.

M_H (GeV)	Total cross section	1 GeV bin	3 GeV bin	5 GeV bin
170	(−5.9, 2.8)	(−3.9, 0.3)	(−3.9, 0.4)	(−3.9, 0.5)
200	(−6.4, 3.6)	(−4.4, 0.9)	(−4.1, 0.8)	(−4.2, 0.9)
250	(−7.0, 4.9)	(−4.2, 1.8)	(−3.9, 1.6)	(−4.0, 1.6)
300	(−8.3, 6.9)	(−6.2, 4.3)	(−5.1, 3.2)	(−4.9, 3.0)

[1] H. Aihara *et al.*, in *Electroweak Symmetry Breaking and New Physics at the TeV Scale*, edited by T. Barklow, S. Dawson, H. Haber, and J. Siegrist (World Scientific, Singapore, 1997); Z. Ajaltuoni *et al.*, in *Proceedings of the CERN Workshop on LEPII Physics*, edited by G. Altarelli *et al.* (CERN Report No. 96-01, Geneva, Switzerland, 1996), Vol. 1, p. 525, hep-ph/9601233; T. Barklow *et al.*, in Proceedings of the 1996 DPF/DPB Summer Study on New Directions in High-Energy Physics, 1996, Snowmass, CO (unpublished), hep-ph/9611454.

[2] K. Gaemers and G. Gounaris, Z. Phys. C **1**, 259 (1979); K. Hagiwara, K. Hikasa, R. D. Peccei, and D. Zeppenfeld, Nucl. Phys. **B282**, 253 (1987).

[3] S. Weinberg, Physica A **96**, 327 (1979); see also, H. Georgi, *Weak Interactions and Modern Particle Theory* (Benjamim/Cummings, Menlo Park, CA, 1984); J. F. Donoghue, E. Golowich, and B. R. Holstein, *Dynamics of the Standard Model* (Cambridge University Press, Cambridge, England 1992).

[4] W. Buchmüller and D. Wyler, Nucl. Phys. **B268**, 621 (1986); C. J. C. Burgess and H. J. Schnitzer, *ibid.* **B228**, 454 (1983); C. N. Leung, S. T. Love, and S. Rao, Z. Phys. C **31**, 433 (1986); A. De Rújula, M. B. Gavela, P. Hernández, and E. Massó, Nucl. Phys. **B384**, 3 (1992).

[5] K. Hagiwara, S. Ishihara, R. Szalapski, and D. Zeppenfeld, Phys. Lett. B **283**, 353 (1992); Phys. Rev. D **48**, 2182 (1993).

[6] S. Coleman, J. Wess, and B. Zumino, Phys. Rev. **177**, 2239 (1969); C. Callan, S. Coleman, J. Wess, and B. Zumino, *ibid.* **177**, 2247 (1969); T. Appelquist and C. Bernard, Phys. Rev. D **22**, 200 (1980); A. Longhitano, Nucl. Phys. **B188**, 118 (1981); T. Appelquist and G.-H. Wu, Phys. Rev. D **48**, 3235 (1993).

[7] For a review, see, S. Godfrey, in ''International Symposium on Vector Boson Self-Interactions,'' Los Angeles, CA, 1995, Report No. OCIP/C-95-5, hep-ph/9505252, and references therein.

[8] G. Bélanger and F. Boudjema, Phys. Lett. B **288**, 201 (1992); **288**, 210 (1992); O. J. P. Éboli, M. C. Gonzalez-Garcia, and S. F. Novaes, Nucl. Phys. **B411**, 381 (1994); O. J. P. Éboli, M. B. Magro, P. G. Mercadante, and S. F. Novaes, Phys. Rev. D **52**, 15 (1995).

[9] Genuine quartic operators, without anomalous trilinear couplings, are only possible in the nonlinear realization of the gauge symmetry for $ZZZZ$, $WWZZ$, and $WWWW$ couplings [22].

[10] K. Hagiwara, R. Szalapski, and D. Zeppenfeld, Phys. Lett. B **318**, 155 (1993).

[11] K. Hagiwara and M. L. Strong, Z. Phys. C **62**, 99 (1994); B. Grzadowski and J. Wudka, Phys. Lett. B **364**, 49 (1995); G. J. Gounaris, F. M. Renard, and N. D. Vlachos, Nucl. Phys. **B459**, 51 (1996); W. Killian, M. Krämer, and P. M. Zerwas, Phys. Lett. B **381**, 243 (1996).

[12] S. M. Lietti, S. F. Novaes, and R. Rosenfeld, Phys. Rev. D **54**, 3266 (1996); F. de Campos, S. M. Lietti, S. F. Novaes, and R. Rosenfeld, Phys. Lett. B **389**, 93 (1996).

[13] G. J. Gounaris, J. Layssac, and F. M. Renard, Z. Phys. C **69**, 505 (1996); G. J. Gounaris and F. M. Renard, *ibid.* **69**, 513 (1996).

[14] G. A. Leil and W. J. Stirling, J. Phys. G **21**, 517 (1995).

[15] C. Grosse-Knetter and D. Schildknecht, Phys. Lett. B **302**, 309 (1993).

[16] V. Barger, T. Han, and R. J. N. Phillips, Phys. Rev. D **39**, 146 (1989).

[17] J. Ellis, M. K. Gaillard, and D. V. Nanopoulos, Nucl. Phys. **B106**, 292 (1976); A. I. Vainshtein, M. B. Voloshin, V. I. Zakharov, and M. S. Shifman, Sov. J. Nucl. Phys. **30**, 711 (1979).

[18] L. Bergstrom and G. Hulth, Nucl. Phys. **B259**, 137 (1985); A. Barroso, J. Pulido, and J. C. Romão, *ibid.* **B267**, 509 (1986).

[19] H. Murayama, I. Watanabe, and K. Hagiwara, KEK Report No. 91–11 (unpublished).

[20] T. Stelzer and W. F. Long, Comput. Phys. Commun. **81**, 257 (1994).

[21] G. P. Lepage, J. Comput. Phys. **27**, 192 (1978).

[22] K. Hagiwara, T. Hatsukano, S. Ishihara, and R. Szalapski, Nucl. Phys. **B496**, 66 (1997).

3.2 Acoplamentos Anômalos - o bóson de Higgs

Posteriormente, nosso interesse se voltou para o estudo da produção do boson de Higgs, tendo em vista os acoplamentos anômalos. Estudamos os limites para os coeficientes dos termos de dimensão 6 que poderiam contribuir no processo de produção do Higgs, considerando em nossa análise os dados do Tevatron, que permitiram estabelecer limites restritivos sobre coeficientes dos termos que contribuiriam para os acoplamentos Higgs-boson vetorial no seu processo de produção. No mesmo estudo, trabalhamos no estabelecimento de novos limites nos termos associados aos acoplamentos triplos, em especial, limites sobre o acoplamento anômalo ao vértice $WW\gamma$. Além disso, utilizando os dados do Tevatron, também é possível impor limites sobre os operadores que contribuiriam para novas interações do boson de Higgs, no caso de massa acima da acessível no LEP II. Ainda no escopo do estudo dos termos que poderiam contribuir para desvios no acoplamento do bosos de Higgs, estudamos os possíveis limites nos acoplamentos entre o boson de Higgs e bosons vetorias por meio da produção de três fotons, utilizando dados do CDF. Neste caso, consideramos todas as interações entre o Higgs e os bosons γ e Z^0.

Limits on Anomalous Couplings from Higgs Boson Production at the Fermilab Tevatron Collider

F. de Campos,[1] M. C. Gonzalez-Garcia,[1,2] and S. F. Novaes[1]
[1]*Instituto de Física Teórica, Universidade Estadual Paulista, Rua Pamplona 145, 01405-900, São Paulo, Brazil*
[2]*Instituto de Física Corpuscular-IFIC/CSIC, Departament de Física Teòrica, Universitat de València, 46100 Burjassot, València, Spain*
(Received 18 July 1997)

We estimate the attainable limits on the coefficients of dimension-6 operators from the analysis of Higgs boson phenomenology, in the framework of a $SU_L(2) \times U_Y(1)$ gauge-invariant effective Lagrangian. Our results, based on the data sample already collected by the collaborations at Fermilab Tevatron, show that the coefficients of Higgs-vector boson couplings can be determined with unprecedented accuracy. Assuming that the coefficients of all "blind" operators are of the same magnitude, we are also able to impose more restrictive bounds on the anomalous vector-boson triple couplings than the present limit from double gauge boson production at the Tevatron collider. [S0031-9007(97)04882-5]

PACS numbers: 14.70.Fm, 13.40.Em, 13.85.Qk, 14.80.Cp

Despite the impressive agreement of the standard model (SM) predictions for the fermion-vector boson couplings with the experimental results, the couplings among the gauge bosons are not determined with the same accuracy. The gauge structure of the model completely determines these self-couplings, and any deviation can indicate the existence of new physics.

Effective Lagrangians are useful to describe and explore the consequences of new physics in the bosonic sector of the SM [1–4]. After integrating out the heavy degrees of freedom, anomalous effective operators can represent the residual interactions between the light states. Searches for deviations on the couplings WWV ($V = \gamma, Z$) have been carried out at different colliders and recent results [5] include the ones by CDF [6], and D0 Collaborations [7,8]. Forthcoming perspectives on this search at LEP II CERN Collider [9,10], and at upgraded Fermilab Tevatron Collider [11] were also reported.

In the framework of effective Lagrangians respecting the local $SU_L(2) \times U_Y(1)$ symmetry linearly realized, the modifications of the couplings of the Higgs field (H) to the vector gauge bosons (V) are related to the anomalous triple vector boson vertex [2–4,12]. In this Letter, we show that the analysis of an anomalously coupled Higgs boson production at the Fermilab Tevatron is able to furnish tighter bounds on the coefficients of the effective Lagrangians than the present available limits. We study the associated HV process

$$p\bar{p} \to q\bar{q} \to W/Z(\to f\bar{f}') + H(\to \gamma\gamma)\,, \qquad (1)$$

and the vector boson fusion process

$$p\bar{p} \to q\bar{q}' WW(ZZ) \to j + j + H(\to \gamma\gamma)\,, \qquad (2)$$

taking into account the 100 pb^{-1} of integrated luminosity already collected by the Fermilab Tevatron Collaborations. Recently, the D0 Collaboration has presented their results for the search of high invariant–mass photon pairs in $p\bar{p} \to \gamma\gamma jj$ events [13]. We show, based on their results, that it may be possible to obtain a significant indirect limit on anomalous WWV coupling under the assumption that the coefficients of the "blind" effective operators contributing to the Higgs-vector boson couplings are of the same magnitude. It is also possible to restrict the operators that involve just Higgs boson couplings HVV, and therefore cannot be bounded by the W^+W^- production at LEP II.

Let us start by considering a general set of dimension-6 operators involving gauge bosons and the Higgs field, respecting local $SU_L(2) \times U_Y(1)$ symmetry, and C and P conserving which contains eleven operators [2,3]. Some of these operators either affect only the Higgs self-interactions or contribute to the gauge boson two-point functions at tree level and can be strongly constrained from low energy physics below the present sensitivity of high energy experiments [3,4]. The remaining five blind operators can be written as [2–4]

$$\mathcal{L}_{\text{eff}} = \sum_i \frac{f_i}{\Lambda^2}\mathcal{O}_i = \frac{1}{\Lambda^2}\{f_{WWW}\,\text{Tr}[\hat{W}_{\mu\nu}\hat{W}^{\nu\rho}\hat{W}_{\rho}^{\mu}] + f_W(D_\mu\Phi)^\dagger\hat{W}^{\mu\nu}(D_\nu\Phi) + f_B(D_\mu\Phi)^\dagger\hat{B}^{\mu\nu}(D_\nu\Phi) + f_{WW}\Phi^\dagger\hat{W}_{\mu\nu}\hat{W}^{\mu\nu}\Phi + f_{BB}\Phi^\dagger\hat{B}_{\mu\nu}\hat{B}^{\mu\nu}\Phi\}, \qquad (3)$$

where Φ is the Higgs field doublet, and

$$\hat{B}_{\mu\nu} = i(g'/2)B_{\mu\nu}, \qquad \hat{W}_{\mu\nu} = i(g/2)\sigma^a W^a_{\mu\nu}\,,$$

 0031-9007/97/79(26)/5210(4)$10.00

with $B_{\mu\nu}$ and $W^a_{\mu\nu}$ being the field strength tensors of the U(1) and SU(2) gauge fields, respectively.

In the unitary gauge, the operators $\mathcal{O}_W$ and $\mathcal{O}_B$ give rise to both anomalous Higgs-gauge boson couplings and to new triple and quartic self-couplings among the gauge bosons, while the operator $\mathcal{O}_{WWW}$ solely modifies the gauge boson self-interactions [12].

The operators $\mathcal{O}_{WW}$ and $\mathcal{O}_{BB}$ affect only HVV couplings, like HWW, HZZ, $H\gamma\gamma$, and $HZ\gamma$, since their contribution to the $WW\gamma$ and WWZ tree-point couplings can be completely absorbed in the redefinition of the SM fields and gauge couplings. Therefore, one cannot obtain any constraint on these couplings from the study of anomalous trilinear gauge boson couplings. These anomalous couplings were extensively studied in electron-positron collisions [12,14,15].

We consider in this Letter Higgs production at the Fermilab Tevatron collider with its subsequent decay into two photons [16]. This channel in the SM occurs at the one-loop level and it is quite small, but due to the new interactions (3), it can be enhanced and even become dominant. We focus on the signatures $\ell\nu\gamma\gamma$, ($\ell = e, \mu$), and $jj\gamma\gamma$, coming from the reactions (1) and (2). Our results show that the cross section for the $\ell\ell\gamma\gamma$ final state is too small to give any reasonable constraints.

We have included in our calculations all SM (QCD plus electroweak), and anomalous contributions that lead to these final states. The SM one-loop contributions to the $H\gamma\gamma$ and $HZ\gamma$ vertices were introduced through the use of the effective operators with the corresponding form factors in the coupling [17]. Neither the narrow-width approximation for the Higgs boson contributions, nor the effective W boson approximation were employed. We consistently included the effect of all interferences between the anomalous signature and the SM background. A total of 42 (32) SM (anomalous) Feynman diagrams are involved in the subprocesses of $\ell\nu\gamma\gamma$ [18] for each leptonic flavor, while 1928 (236) participate in $jj\gamma\gamma$ signature [19]. The SM Feynman diagrams were generated by Madgraph [20] in the framework of Helas [21]. The anomalous contributions arising from the Lagrangian (3) were implemented in Fortran routines and were included accordingly. We have used the MRS (G) [22] set of proton structure functions with the scale $Q^2 = \hat{s}$.

The cuts applied on the final state particles are similar to those used by the experimental collaborations [6–8]. In particular, when studying the $\gamma\gamma jj$ final state we have closely followed the results recently presented by the D0 Collaboration [13], i.e., for the photons

$$\begin{gathered} |\eta_{\gamma 1}| < 1.1 \quad \text{or} \quad 1.5 < |\eta_{\gamma 1}| < 2, \\ p_T^{\gamma 1} > 20 \text{ GeV}, \\ |\eta_{\gamma 2}| < 1.1 \quad \text{or} \quad 1.5 < |\eta_{\gamma 2}| < 2.25, \\ p_T^{\gamma 2} > 25 \text{ GeV}, \\ \sum \vec{p}_T^{\,\gamma} > 10 \text{ GeV}. \end{gathered} \tag{21}$$

For the $l\nu\gamma\gamma$ final state

$$|\eta_e| < 1.1 \quad \text{or} \quad 1.5 < |\eta_e| < 2, \qquad |\eta_\mu| < 1,$$
$$p_T^{e,\mu} > 20 \text{ GeV}, \qquad \not{p}_T > 20 \text{ GeV}.$$

For the $jj\gamma\gamma$ final state

$$|\eta_{j1}| < 2, \qquad p_T^{j1} > 20 \text{ GeV},$$
$$|\eta_{j2}| < 2.25, \qquad p_T^{j2} > 15 \text{ GeV},$$
$$\sum \vec{p}_T^{\,j} > 10 \text{ GeV}, \qquad R_{\gamma j} > 0.7,$$
$$40 \le M_{jj} \le 150 \text{ GeV}.$$

We also assumed an invariant-mass resolution for the two photons of $\Delta M_{\gamma\gamma}/M_{\gamma\gamma} = 0.15/\sqrt{M_{\gamma\gamma}} \oplus 0.007$ [16]. Both signal and background were integrated over an invariant-mass bin of $\pm 2\Delta M_{\gamma\gamma}$ centered around M_H.

The signature of the $jj\gamma\gamma$ process receives contributions from both associated production and WW/ZZ fusion. For the sake of illustration, we show in Fig. 1(a) the invariant mass distribution of the two photons for $M_H = 70$ GeV and $f_{BB}/\Lambda^2 = 100$ TeV^{-2}, without any cut on $M_{\gamma\gamma}$ or M_{jj}. We can clearly see from Fig. 1(b) that after imposing the Higgs mass reconstruction, there is a significant excess of events in the region $M_{jj} \sim M_{W,Z}$ corresponding to the process of associate production (1). It is also possible to distinguish the tail corresponding to the Higgs production from WW/ZZ fusion (2), for

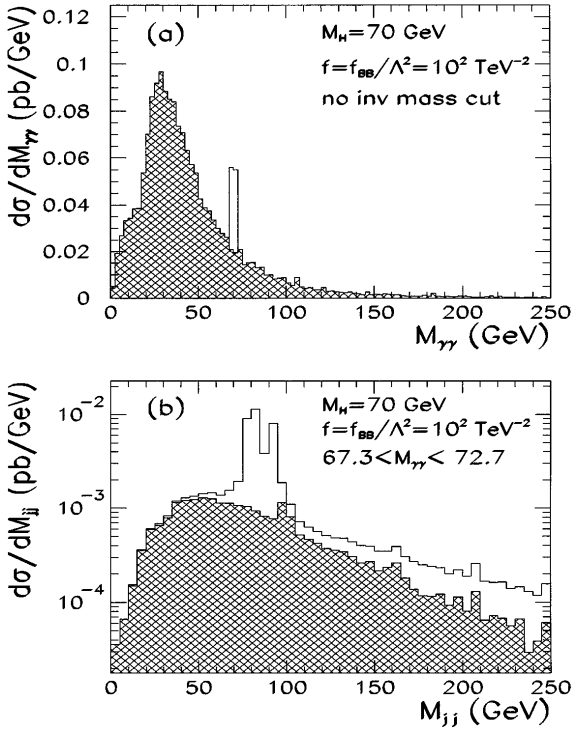

FIG. 1. (a) Two photon invariant mass distribution for the background (shaded histogram) and for the signal (clear histogram) before applying any cut, for $M_H = 70$ GeV and $f_{BB}/\Lambda^2 = 100$ TeV^{-2}. (b) Two jet invariant mass distribution, after the cut on the two photon invariant mass.

$M_{jj} > 100$ GeV. We isolate the majority of events due to associated production, and the corresponding background, by integrating over a bin centered on the W or Z mass, which is equivalent to the invariant mass cut listed above.

After imposing all the cuts, we get a reduction on the signal event rate which depends on the Higgs mass. For the $jj\gamma\gamma$ final state the geometrical acceptance and background rejection cuts account for a reduction factor of 15% for $M_H = 60$ GeV rising to 25% for $M_H = 160$ GeV. We also include in our analysis the particle identification and trigger efficiencies which vary from 40% to 70% per particle lepton or photon [7,8]. For the $jj\gamma\gamma$ ($\ell\nu\gamma\gamma$) final state we estimate the total effect of these efficiencies to be 35% (30%). We therefore obtain an overall efficiency for the $jj\gamma\gamma$ final state of 5.5% to 9% for $M_H = 60$–160 GeV in agreement with the results of Ref. [13].

For the $l\nu\gamma\gamma$ signature, the main physics background comes from $W\gamma\gamma$. After imposing all cuts and efficiencies the background is reduced far below the experimental sensitivity. For the $jj\gamma\gamma$ final state the dominant physics background is a mixed QCD-QED process. Again, when cuts and efficiencies are included, it is reduced to less than 0.2 events for the present luminosity [13].

Dominant backgrounds, however, are due to misidentification when a jet fakes a photon that has been estimated to occur with a probability of a few times 10^{-4} [7]. Although this probability is small, it becomes the main source of background for the $jj\gamma\gamma$ final state because of the very large multijet cross section. In Ref. [13] this background is estimated to lead to 3.5 ± 1.3 events with invariant mass $M_{\gamma\gamma} > 60$ GeV, and it has been consistently included in our derivation of the attainable limits.

In the $l\nu\gamma\gamma$ channel the dominant fake background is the $W\gamma j$ channel, when the jet mimics a photon. We estimated the contribution of this channel to yield $N_{\text{back}} < 0.01$ events [7] at 95% C.L. We have also estimated the various QCD fake backgrounds such as jjj, $jj\gamma$, and $j\gamma\gamma$, with the jet faking a photon and/or electron plus fake missing, which are to be negligible.

The coupling $H\gamma\gamma$ derived from (3) involves f_{WW} and f_{BB} [12]. In consequence, the anomalous signature $f\bar{f}\gamma\gamma$ is possible only when those couplings are not vanishing. The couplings f_B and f_W, on the other hand, affect the production mechanisms for the Higgs boson. In what follows, we present our results for three different scenarios of the anomalous coefficients: (i) Suppressed VVV couplings compared to the $H\gamma\gamma$ vertex: $f_{BB,WW} = f \gg f_{B,W}$ (ii) All coupling with the same magnitude and sign: $f_{BB,WW,B,W} = f$. (iii) All coupling with the same magnitude but different relative sign: $f_{BB,WW} = f = -f_{B,W}$. In order to establish the attainable bounds on the coefficients, we imposed an upper limit on the number of signal events based on Poisson statistics [23]. For the $jj\gamma\gamma$ final state we use the results from Ref. [13], where no event has been reported in the 100 pb^{-1} sample. For the other cases, the limit on the number of signal events was conservatively obtained assuming that the number of observed events coincides with the expected background.

Table I shows the range of f/Λ^2 that can be excluded at 95% C.L. with the present Tevatron luminosity in the scenario (i). We should remind the reader that this scenario will not be restricted by LEP II data on W^+W^- production since there are no trilinear vector boson couplings involved. As seen in the table, the best limits are obtained for the $jj\gamma\gamma$ final state, and they are more restrictive than the ones coming from $e^+e^- \to \gamma\gamma\gamma$ or $b\bar{b}\gamma$ at LEP II [15].

For the scenarios (ii) and (iii), the limits derived from our study lead to constraints on the triple gauge boson coupling parameters. The most general parametrization for the WWV vertex can be found in Ref. [1]. When only the operators (3) are considered, it contains three independent parameters. If it is further assumed that $f_B = f_W$, only two free parameters remain, which are usually chosen as $\Delta\kappa_\gamma$ and λ_γ. This is usually quoted in the literature as the HISZ scenario [4].

Since we are assuming $f_B = f_W$ our results can be compared to the derived limits from triple gauge boson studies in the HISZ scenario. In Fig. 2, we show the region in the $\Delta\kappa_\gamma \times M_H$ that can be excluded through the analysis of the present Tevatron data, accumulated in Run I, with an integrated luminosity of 100 pb^{-1} [13], for scenarios (ii) and (iii).

For the sake of comparison, we also show in Fig. 2 the best available experimental limit on $\Delta\kappa_\gamma$ [5,8] and the expected bounds, from double gauge boson production, from an updated Tevatron Run II, with 1 fb^{-1}, and TeV33 with 10 fb^{-1} [11], and from LEP II operating at 190 GeV with an integrated luminosity of 500 fb^{-1} [10]. In all cases the results were obtained assuming the HISZ scenario. We can see that, for $M_H \lesssim 200[170]$ GeV, the

TABLE I. Allowed range of f/Λ^2 in TeV^{-2} at 95% C.L., assuming the scenario (i) ($f_{BB} = f_{WW} \gg f_B, f_W$) for the different final states, and for different Higgs boson masses for an integrated luminosity of 100 pb^{-1}.

M_H (GeV)		100	150	200	250
$\ell\nu\gamma\gamma$	Run I	(−41−74)	(−83−113)	(<−200−>200)	(<−200−>200)
	Run II	(−13−36)	(−22−46)	(−57−135)	(−195−>200)
	TeV33	(−3.8−8)	(−4.8−20)	(−28−60)	(−45−83)
$jj\gamma\gamma$	Run I	(−20−49)	(−26−64)	(−96−>100)	(<−100−>100)
	Run II	(−8.4−26)	(−11−31)	(−36−81)	(−64−>100)
	TeV33	(−4.2−6.5)	(−4.5−12)	(−19−40)	(−28−51)

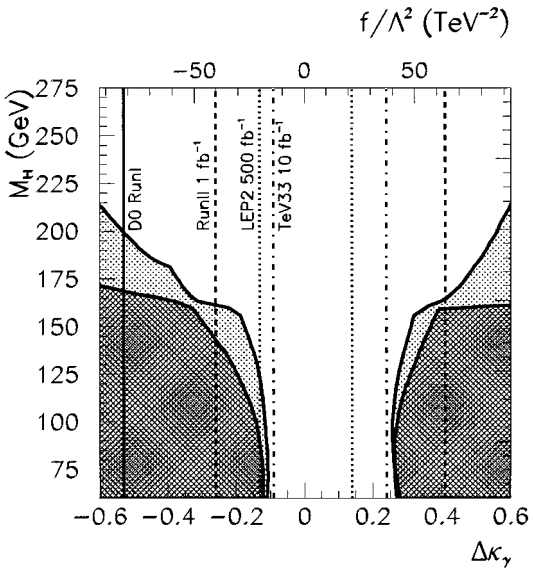

FIG. 2. Excluded region in the $\Delta\kappa_\gamma \times M_H$ plane for an integrated luminosity of 100 pb^{-1}, and for scenarios (ii) (clear shadow) and (iii) (dark shadow). The present and future bounds on $\Delta\kappa_\gamma$ are also shown (see text for details).

limit that can be established at 95% C.L. from the Higgs production analysis for scenario (ii) [(iii)], based on the present Tevatron luminosity is tighter than the present limit coming from gauge boson production.

When the same analysis is performed for the upgraded Tevatron, a more severe restriction on the coefficient of the anomalous operators is obtained. For instance, from $p\bar{p} \to jj\gamma\gamma$, in scenario (ii) we get, for $M_H = 150$ GeV: For RunII with 1 fb^{-1}, $-9 < f < 25$ ($-0.06 < \Delta\kappa_\gamma < 0.16$); for TeV33 with 10 fb^{-1}, $-4 < f < 15$ ($-0.03 < \Delta\kappa_\gamma < 0.1$).

In conclusion, we have shown that the Fermilab Tevatron analysis of an anomalous Higgs boson production may be used to impose strong limits on new effective interactions. Under the assumption that the coefficients of the four "blind" effective operators contributing to Higgs-vector boson couplings are of the same magnitude, the study can give rise to a significant indirect limit on anomalous $WW\gamma$ couplings. Furthermore, the Tevatron is able to set constraints on those operators contributing to new Higgs interactions for Higgs masses far beyond the kinematical reach of LEP II.

We want to thank R. Zukanovich Funchal for useful discussion on the Poisson statistics in the presence of background. M. C. G.-G. is grateful to the Instituto de Física Teórica for its kind hospitality. This work was supported by FAPESP, by DGICYT under Grant No. PB95-1077, by CICYT under Grant No. AEN96-1718, and by CNPq.

23

[1] K. Hagiwara, H. Hikasa, R. D. Peccei, and D. Zeppenfeld, Nucl. Phys. **B282**, 253 (1987).

[2] C. J. C. Burguess and H. J. Schnitzer, Nucl. Phys. **B228**, 464 (1983); C. N. Leung, S. T. Love, and S. Rao, Z. Phys. **31**, 433 (1986); W. Buchmüller and D. Wyler, Nucl. Phys. **B268**, 621 (1986).

[3] A. De Rujula, M. B. Gavela, P. Hernandez, and E. Masso, Nucl. Phys. **B384**, 3 (1992); A. De Rujula, M. B. Gavela, O. Pene, and F. J. Vegas, Nucl. Phys. **B357**, 311 (1991).

[4] K. Hagiwara, S. Ishihara, R. Szalapski, and D. Zeppenfeld, Phys. Lett. B **283**, 353 (1992); Phys. Rev. D **48**, 2182 (1993); K. Hagiwara, T. Hatsukano, S. Ishihara, and R. Szalapski, Nucl. Phys. **B496**, 66 (1997).

[5] For a review, see T. Yasuda, Report No. FERMILAB-Conf-97/206-E; hep-ex/9706015.

[6] F. Abe *et al.*, CDF Collaboration, Phys. Rev. Lett. **74**, 1936 (1995); **74**, 1941 (1995); **75**, 1017 (1995); **78**, 4536 (1997).

[7] S. Abachi *et al.,* D0 Collaboration, Phys. Rev. Lett. **75**, 1023 (1995); **75**, 1028 (1995); **75**, 1034 (1995); **77**, 3303 (1996); **78**, 3634 (1997); **78**, 3640 (1997).

[8] B. Abbott *et al.,* D0 Collaboration, Phys. Rev. Lett. **79**, 1441 (1997).

[9] For a review, see Z. Ajaltuoni *et al.*, in Proceedings of the CERN Workshop on LEPII Physics, edited by G. Altarelli, T. Sjöstrand, and F. Zwirner (CERN 96–01, 1996), Vol. 1, 525.

[10] T. Barklow *et al., in* Proceedings of the 1996 DPF/DPB Summer Study on New Directions in High-Energy Physics, Snowmass, Colorado, 1996 (to be published).

[11] D. Amidei *et al.*, Report No. FERMILAB-PUB-96-082, 1996.

[12] K. Hagiwara, R. Szalapski, and D. Zeppenfeld, Phys. Lett. B **318**, 155 (1993).

[13] D0 Collaboration, B. Abbott *et al.,* in Proceedings of the Lepton-Photon Conference, Hamburg, 1997 (FERMILAB-CONF-97/325-E, 1997).

[14] K. Hagiwara and M. L. Stong, Z. Phys. C **62**, 99 (1994); B. Grzadkowski and J. Wudka, Phys. Lett. B **364**, 49 (1995); G. J. Gounaris, J. Layssac, and F. M. Renard, Z. Phys. C **65**, 245 (1995); G. J. Gounaris, F. M. Renard, and N. D. Vlachos, Nucl. Phys. **B459**, 51 (1996).

[15] S. M. Lietti, S. F. Novaes, and R. Rosenfeld, Phys. Rev. D **54**, 3266 (1996); F. de Campos, S. M. Lietti, S. F. Novaes, and R. Rosenfeld, Phys. Lett. B **389**, 93 (1996).

[16] A. Stange, W. Marciano, and S. Willenbrock, Phys. Rev. D **49**, 1354 (1994); **50**, 4491 (1994).

[17] J. F. Gunion, H. E. Haber, G. Kane, and S. Dawson, *The Higgs Hunter's Guide* (Addison-Wesley, Reading, MA, 1990).

[18] R. Keiss, Z. Kunszt, and W. J. Stirling, Phys. Lett. B **253**, 269 (1991); J. Ohnemus and W. J. Stirling, Phys. Rev. D **47**, 336 (1993); U. Baur, T. Han, N. Kauer, R. Sobey, and D. Zeppenfeld, Phys. Rev. D **56**, 140 (1997).

[19] V. Barger, T. Han, D. Zeppenfeld, and J. Ohnemus, Phys. Rev. D **41**, 2782 (1990).

[20] T. Stelzer and W. F. Long, Comput. Phys. Commun. **81**, 357 (1994).

[21] H. Murayama, I. Watanabe, and K. Hagiwara, KEK Report No. 91-11 (unpublished).

[22] A. D. Martin, W. J. Stirling, and R. G. Roberts, Phys. Lett. B **354**, 155 (1995).

[23] O. Helene, Nucl. Instrum. Methods Phys. Res. **212**, 319 (1983).

ELSEVIER

10 September 1998

PHYSICS LETTERS B

Physics Letters B 435 (1998) 407–412

Testing anomalous Higgs couplings in triple photon production at the Tevatron collider

F. de Campos [a], M.C. Gonzalez–Garcia [b,c], S.M. Lietti [c], S.F. Novaes [c], R. Rosenfeld [c]

[a] *Depto. de Física e Química, Universidade Estadual Paulista, Av. Dr. Ariberto Pereira da Cunha 333, 12500 Guaratinguetá, Brazil*
[b] *Instituto de Física Corpuscular IFIC / CSIC, Departament de Física Teòrica, Universitat de València, 46100 Burjassot, València, Spain*
[c] *Instituto de Física Teórica, Universidade Estadual Paulista, Rua Pamplona 145, 01405–900, São Paulo, Brazil*

Received 2 June 1998
Editor: R. Gatto

Abstract

We derive bounds on Higgs and gauge–boson anomalous interactions using the CDF data for the process $p\bar{p} \to \gamma\gamma\gamma + X$. We use a linearly realized $SU_L(2) \times U_Y(1)$ invariant effective Lagrangian to describe the bosonic sector of the Standard Model, keeping the fermionic couplings unchanged. All dimension–six operators that lead to anomalous Higgs interactions involving γ and Z are considered. We also show the sensitivity that can be achieved for these couplings at Fermilab Tevatron upgrades.

PACS: 14.80.Cp

We certainly expect the Standard Model (SM), despite its astonishing success in describing all the precision high energy experimental data so far [1], to be an incomplete picture of Nature at high energy scales. In particular, the Higgs sector of the model, responsible for the spontaneous electroweak symmetry breaking and for mass generation, is not fully satisfactory since it has to be introduced in an *ad hoc* fashion. Furthermore, this scalar sector has not yet been experimentally verified.

Although we do not know the specific model which will eventually supersede the SM, we can always parametrize its effects at low energies by means of an effective Lagrangian [2] that involves operators with dimension higher than four, containing the relevant fields at low energies and respecting the symmetries of the Standard Model. The effective Lagrangian approach is a model–independent way to describe new physics that can occur at an energy scale Λ much larger than the scale where the experiments are performed.

The effective Lagrangian depends on the particle content at low energies and here we will consider the possibility that the Higgs boson can be light, being present in the higher dimensional operators, in addition to the electroweak gauge bosons. Hence we will use a linearly realized [3,4] $SU_L(2) \times U_Y(1)$ invariant effective Lagrangian to describe the bosonic sector of the Standard Model, keeping the fermionic couplings unchanged. The new interactions can alter considerably the low energy phenomenology. For instance, some operators can give rise to anomalous

0370-2693/98/$ - see front matter
PII: S0370-2693(98)00829-6

$H\gamma\gamma$ and $HZ\gamma$ couplings which may affect the Higgs boson production and decay [5].

It is important to notice that, since the linearly realized effective Lagrangian relates the modifications in the Higgs couplings to the ones in the vector boson vertex [5,3,4], the search for Higgs bosons can be used not only to study its properties, but also to place bounds on the gauge boson self–interactions. This approach is more efficient when the analysis is performed for decays of the Higgs boson that are suppressed in the SM, such as $H \to \gamma\gamma$ that occurs only at the one loop level, and are enhanced by new anomalous interactions.

Events containing two photons plus additional missing energy, photons or charged fermions represent a signature for several models involving physics beyond the SM such as some classes of supersymmetric models [6]. Recently, the CDF collaboration have reported the search for the signature $\gamma\gamma + X$, where $X =$ jets, leptons, gauge bosons (W, Z, γ) or just missing energy in $p\bar{p}$ collisions at $\sqrt{s} = 1.8$ TeV [7]. Their analysis indicates a good agreement with the expectations from the Standard Model (SM). In this way, they were able to set limits on the production cross section $\sigma(p\bar{p} \to \gamma\gamma \not{E}_T + X)$ in particular in the light gravitino scenario.

In this work, we point out that the experimental search for $\gamma\gamma\gamma$ events contained in the CDF analysis can place constraints on new physics in the bosonic sector of the SM. For instance, associated Higgs–γ boson production, with the subsequent decay of the Higgs into two photons can yield this signature. In the SM, the decay width $H \to \gamma\gamma$ is very small since it occurs just at one–loop level [8]. However, the existence of new interactions can enhance this width in a significant way. These anomalous Higgs boson couplings have also been studied before in Higgs and Z boson decays [5], in e^+e^- [9,10], $p\bar{p}$ [11] and $\gamma\gamma$ colliders [12]. Here we shall show how to bound these new couplings by analyzing their effects on the process $p\bar{p} \to \gamma\gamma\gamma + X$ at the Fermilab Tevatron.

In order to write down the most general dimension–6 effective Lagrangian containing all SM bosonic fields, *i.e.* γ, $W^{\pm}$, Z^0, and H, we adopt the notation of Hagiwara et al. [4]. This Lagrangian has eleven independent operators in the linear representation that are locally $SU_L(2) \times U_Y(1)$ invariant, C and P even. We discard the four operators which affect the gauge boson two–point functions at tree–level and therefore are strongly constrained by LEP measurements. We also do not consider the three operators that modify only the Higgs or vector boson self–interactions, since they are not relevant for our calculations. We are then left with four independent operators, and the Lagrangian is written as,

$$\mathscr{L}_{\rm eff} = \mathscr{L}_{\rm SM} + \frac{1}{\Lambda^2}\left(f_{WW}\mathscr{O}_{WW} + f_{BB}\mathscr{O}_{BB} + f_W\mathscr{O}_W + f_B\mathscr{O}_B \right), \tag{1}$$

with the operators $\mathscr{O}_i$ defined as,

$$\mathscr{O}_{WW} = \Phi^\dagger \hat{W}_{\mu\nu}\hat{W}^{\mu\nu}\Phi,$$

$$\mathscr{O}_{BB} = \Phi^\dagger \hat{B}_{\mu\nu}\hat{B}^{\mu\nu}\Phi,$$

$$\mathscr{O}_W = \left(D_\mu\Phi\right)^\dagger \hat{W}^{\mu\nu}\left(D_\nu\Phi\right),$$

$$\mathscr{O}_B = \left(D_\mu\Phi\right)^\dagger \hat{B}^{\mu\nu}\left(D_\nu\Phi\right), \tag{2}$$

where Φ is the Higgs field doublet, $\hat{B}_{\mu\nu} = i(g'/2)B_{\mu\nu}$, and $\hat{W}_{\mu\nu} = i(g/2)\sigma^a W^a_{\mu\nu}$, with $B_{\mu\nu}$ and $W^a_{\mu\nu}$ being the field strength tensors of the $U(1)$ and $SU(2)$ gauge fields respectively.

Anomalous $H\gamma\gamma$, $HZ\gamma$, and HZZ couplings are generated by (1), which, in the unitary gauge, are given by

$$\mathscr{L}^{\rm H}_{\rm eff} = g_{H\gamma\gamma}HA_{\mu\nu}A^{\mu\nu} + g^{(1)}_{HZ\gamma}A_{\mu\nu}Z^\mu\partial^\nu H + g^{(2)}_{HZ\gamma}HA_{\mu\nu}Z^{\mu\nu} + g^{(1)}_{HZZ}Z_{\mu\nu}Z^\mu\partial^\nu H + g^{(2)}_{HZZ}HZ_{\mu\nu}Z^{\mu\nu}, \tag{3}$$

where $A(Z)_{\mu\nu} = \partial_\mu A(Z)_\nu - \partial_\nu A(Z)_\mu$. The effective couplings $g_{H\gamma\gamma}$, $g^{(1,2)}_{HZ\gamma}$, and $g^{(1,2,3)}_{HZZ}$ are related to the coefficients of the operators appearing in (1) through,

$$g_{H\gamma\gamma} = -\left(\frac{gM_W}{\Lambda^2}\right)\frac{s^2(f_{BB}+f_{WW})}{2},$$

$$g^{(1)}_{HZ\gamma} = \left(\frac{gM_W}{\Lambda^2}\right)\frac{s(f_W - f_B)}{2c},$$

$$g^{(2)}_{HZ\gamma} = \left(\frac{gM_W}{\Lambda^2}\right)\frac{s\left[2s^2 f_{BB} - 2c^2 f_{WW}\right]}{2c},$$

$$g^{(1)}_{HZZ} = \left(\frac{gM_W}{\Lambda^2}\right)\frac{c^2 f_W + s^2 f_B}{2c^2},$$

$$g^{(2)}_{HZZ} = -\left(\frac{gM_W}{\Lambda^2}\right)\frac{s^4 f_{BB} + c^4 f_{WW}}{2c^2}, \tag{4}$$

with g being the electroweak coupling constant, and $s(c) \equiv \sin(\cos)\theta_W$.

The calculation of the reaction $p\bar{p} \to \gamma\gamma\gamma$ was performed using the Helas package [13]. We have constructed new subroutines in order to incorporate the anomalous contributions. The irreducible background subprocesses $q\bar{q} \to \gamma\gamma\gamma$ for $q = u, d, s$ were generated by MadGraph [14] and the new contributions were included. In this way, all the anomalous contributions and their respective interference with the SM were evaluated. We convoluted this subprocess cross sections, using a Monte Carlo integration [15], with the corresponding parton distributions using the MRS (G) [16] set of proton structure functions with the scale given by the parton–parton center–of–mass energy.

The CDF Collaboration [7] search for anomalous $\gamma\gamma$ events has included events that have two photons in the central region of the detector ($|\eta| < 1$), with a minimum transverse energy of 12 GeV, plus an additional photon with $E_T > 25$ GeV. The photons were required to be separated by an angle larger the 15°. After applying these cuts, no event was observed, while the expect number from the background is 0.1 ± 0.1 in the 85 pb^{-1} collected. Therefore, at 95 % CL this experimental result implies that the signal should have less than 3 events. The efficiency of identification of an isolated photon is $68 \pm 3\%$, for $E_T > 12$ GeV, and grows to $84 \pm 4\%$, for $E_T > 22$ GeV. We have taken into account these efficiencies in our estimate.

It is important to notice that the dimension-six operators (1) do not induce 4–point anomalous couplings like $ZZ\gamma\gamma$, $Z\gamma\gamma\gamma$, and $\gamma\gamma\gamma\gamma$, being these terms generated only by dimension–eight and higher operators. Since the production and decay of the Higgs boson also involve two dimension–six operators, we should, in principle, include in our calculations dimension–eight operators that contribute to the above processes. Notwithstanding, we can neglect the higher order interactions and bound the dimension–six couplings under the naturalness assumption that no cancelation takes place amongst the dimension–six and –eight contributions that appear at the same order in the expansion.

We start our analysis by examining which are the bounds that can be placed on the anomalous coefficients from the negative search of 3 photon events made by the CDF Collaboration. We start by assuming that the only non–zero coefficients are the ones that generate the anomalous $H\gamma\gamma$, i.e., f_{BB} and f_{WW}. Our results for the 95% CL exclusion region in the plane $f_{BB} \times f_{WW}$, obtained from the CDF data, are presented in Fig. 1. For $f_{BB} = -f_{WW}$ the anomalous contribution to $H\gamma\gamma$ becomes zero, independently of the values of f_W and f_B, and the bounds become very weak in this region.

As mentioned above, the coupling $H\gamma\gamma$ derived in Eq. (4) involves f_{WW} and f_{BB}. In consequence, the anomalous $\gamma\gamma$ signature is only possible when those couplings are non–vanishing. The couplings f_B and f_W, on the other hand, affect the production mechanisms for the Higgs boson. In order to reduce the number of free parameters one can make the assumption that all blind operators affecting the Higgs interactions have a common coupling f, i.e. $f = f_W = f_B = f_{WW} = f_{BB} = f$ [1,4,5]. In this scenario we can relate the Higgs boson anomalous coupling f with the LEP conventional parametrization of the vertex WWV ($V = Z, \gamma$) [17] can be written as,

$$\alpha = \alpha_{B\Phi} = \alpha_{W\Phi} = \frac{M_W^2}{2\Lambda^2} f. \tag{5}$$

Table 1 shows the 95% CL allowed region of the anomalous couplings in the above scenario. As could be expected, these bounds become weaker as the Higgs boson mass increases. We also show the related bounds in $\alpha = \alpha_{B\Phi} = \alpha_{W\Phi}$ in Table 2.

We now extend our analysis to the upgraded Tevatron collider. We first study the possible improvements in the kinematical cuts in order to get better sensitivity to the anomalous coefficients. First of all, we order the three photons according to their transverse energy, *i.e.* $E_{T_1} > E_{T_2} > E_{T_3}$, and we adopt a preliminary cut of $E_{T_i} > 12$ GeV and $|\eta_i| < 1$, for all the three photons. In Fig. 2, we show the transverse energy distribution for the three photons for $\sqrt{s} = 2$ TeV. Comparison is made between the SM background and the new anomalous distribution for $f = 100$ TeV^{-2}, and for a Higgs boson mass of 100 GeV.

These distributions strongly suggest that a cut on the transverse energy of the most energetic photon with a simultaneous cut in transverse energy of the two softest photons can improve the sensitivity. We

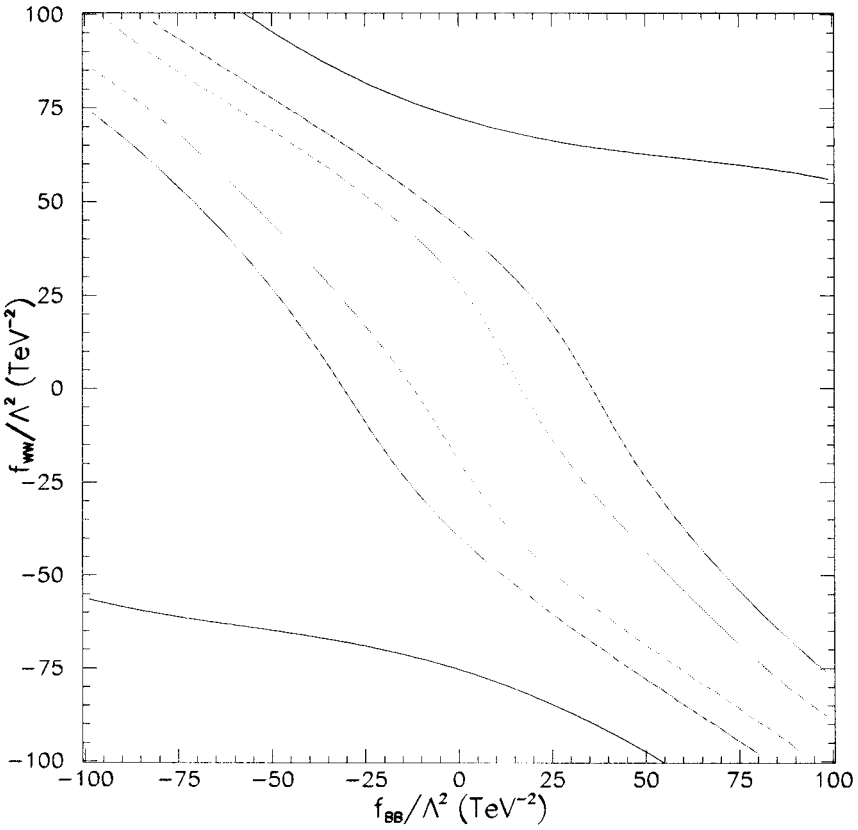

Fig. 1. Exclusion region outside the curves in the $f_{BB} \times f_{WW}$ plane, in TeV^{-2}, based on the CDF analysis [7] and Tevatron upgrades of $\gamma\gamma\gamma$ production, assuming $M_H = 100$ GeV. The curves show the 95% CL deviations from the SM total cross section. The outermost curves are based on the CDF analysis, the intermediate curves on the Tevatron Run II analysis, and the innermost curves are based on the Tevatron TeV33 upgrade.

tried two sets of cuts: (a) $E_{T_1} > 40$ GeV while $E_{T_{2,3}} > 25$ GeV, and (b) $E_{T_1} > 40$ GeV, with $E_{T_{2,3}} > 12$ GeV. Cut (a) leads to a large background reduction of a factor 5.5 but it also reduces the number of signal events by a factor two 2. So the significance of the signal over the background ($S = N_{\text{Signal}}/\sqrt{N_{\text{Background}}}$) is enhanced only by 17%. Cut (b) however leads to a smaller background rejection of a factor of 2 without significantly changing the signal. The significance is now improved by a factor of 41%, so we present our results considering this set of cuts. We always require the photons to be in the central region of the detector ($|\eta_i| < 1$) where there is sensitivity for electromagnetic showering. In our es-

Table 1
The minimum and maximum values (min, max) of f/Λ^2, at 95% CL, from $\gamma\gamma\gamma$ production at CDF and Tevatron upgrades, assuming that all f_i are equal

M_H (GeV)	f/Λ^2(TeV^{-2})		
	CDF	Tevatron Run II	Tevatron TeV33
100	(−61.7 , 64.5)	(−23.2 , 23.3)	(−13.7 , 13.9)
120	(−75.5 , 76.9)	(−25.0 , 25.0)	(−14.4 , 14.5)
140	(−92.0 , 93.2)	(−29.1 , 29.5)	(−15.3 , 15.7)
160	(−113 , 115)	(−34.0 , 35.8)	(−16.1 , 17.8)

Table 2
The minimum and maximum values (min, max) of $\alpha = \alpha_{B\Phi} = \alpha_{W\Phi}$, at 95% CL, from $\gamma\gamma\gamma$ production at CDF and Tevatron upgrades, assuming that all f_i are equal

M_H (GeV)	$\alpha = \alpha_{B\Phi} = \alpha_{W\Phi}$		
	CDF	Tevatron Run II	Tevatron TeV33
100	(−0.197 , 0.206)	(−0.074 , 0.075)	(−0.044 , 0.044)
120	(−0.242 , 0.246)	(−0.080 , 0.080)	(−0.046 , 0.046)
140	(−0.294 , 0.298)	(−0.093 , 0.094)	(−0.049 , 0.050)
160	(−0.362 , 0.368)	(−0.109 , 0.115)	(−0.052 , 0.057)

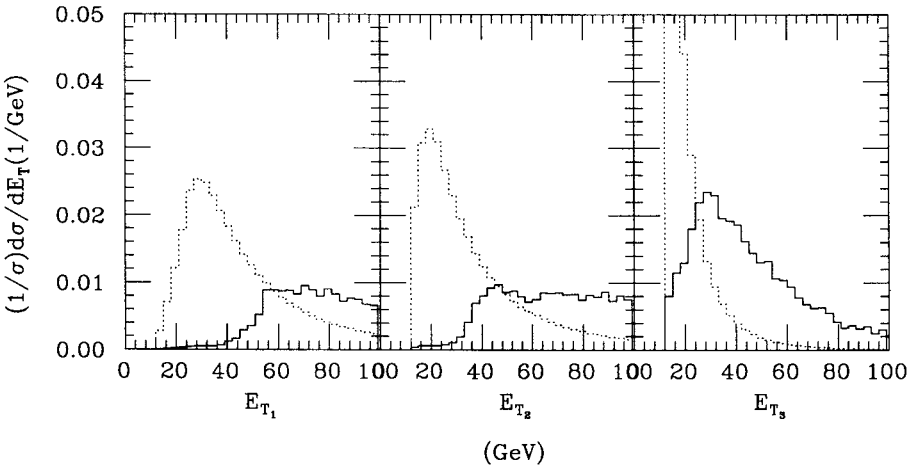

Fig. 2. Transverse momentum distribution of the three photons for $\sqrt{s} = 2$ TeV, for the SM background (dotted line) and for the anomalous contributions (full line). We have taken $M_H = 100$ GeV, and $f_i/\Lambda^2 = 100$ TeV^{-2}.

timates we assume the same detection efficiency for photons as the present CDF efficiencies given above.

After applying the cuts, we obtain the 95% CL exclusion region in the plane $f_{BB} \times f_{WW}$ shown in Fig. 1. We have assumed that the upgraded Tevatron collider will reach a centre–of–mass energy of $\sqrt{s} =$ 2 TeV with an integrated luminosity of 1 fb^{-1}, in the Run II, and of 10 fb^{-1}, in the TeV33 run [18]. Again, the $f_{BB} = -f_{WW}$ line is unbounded since the anomalous contribution to $H\gamma\gamma$ is zero in this case.

In Table 1, we present the 95% CL limit of the anomalous couplings when all couplings are taken to be equal, for different Higgs boson masses. The associated bounds in $\alpha = \alpha_{B\Phi} = \alpha_{W\Phi}$ are also shown in Table 2. These bounds are comparable with the preliminary results of the combinations of measurements from the individual LEP and DØ experiments [19], $\alpha_{B\Phi} = -0.05^{+0.22}_{-0.20}$, and $\alpha_{W\Phi} = -0.03^{+0.06}_{-0.06}$. The comparison is to be taken with a pinch of salt as the LEP–DØ bounds are given for only one coupling different from zero while our bounds hold for $\alpha_{B\Phi} = \alpha_{W\Phi}$

Summarizing, in this work we have estimated the limits on anomalous dimension–six Higgs boson interactions that can be derived from the investigation of three photon events at the Fermilab Tevatron. We have used the present data from the CDF collaboration and we have estimated the attainable sensitivity at the upgraded Tevatron. Under the assumption of equal coefficients for all anomalous Higgs operators, these bounds also lead to limits on triple–gauge–boson couplings.

We would like to thank Alexander Belyaev for very useful discussions. This work was supported by Conselho Nacional de Desenvolvimento Científico e Tecnológico (CNPq), and by Fundação de Amparo à Pesquisa do Estado de São Paulo (FAPESP).

References

[1] See, for instance, G. Altarelli, preprint CERN-TH. 97-278, hep-ph/9710434 and references therein; H. Aihara et al., Summary of the Working Subgroup on Anomalous Gauge Boson Interactions of the DPF Long–Range Planning Study, to appear in Electroweak Symmetry Breaking and Beyond the Standard Model, edited by T. Barklow, S. Dawson, H. Haber, J. Siegrist, hep-ph/9503425; Z. Ajaltuoni et al., Triple Gauge Boson Couplings, in Proceedings of the CERN Workshop on LEPII Physics edited by G. Altarelli et al., CERN 96-01, Vol. 1, p. 525 (1996) hep-ph/9601233; T. Barklow et al., Summary of the Snowmass Subgroup on Anomalous Gauge Boson Couplings, to appear in the Proceedings of the 1996 DPF/DPB Summer Study on New Directions in High-Energy Physics June 25 — July 12 (1996), Snowmass, CO, USA, hep-ph/9611454.

[2] S. Weinberg, Physica 96A (1979) 327; see also H. Georgi, Weak Interactions and Modern Particle Theory (Benjamim/Cummings, Menlo Park, 1984), J.F. Donoghue, E. Golowich, B.R. Holstein, Dynamics of the Standard Model (Cambridge University Press, 1992).

[3] W. Buchmüller, D. Wyler, Nucl. Phys. B 268 (1986) 621; C.J.C. Burgess, H.J. Schnitzer, Nucl. Phys. B 228 (1983)

454; C.N. Leung, S.T. Love, S. Rao, Z. Phys. 31 (1986) 433; A. De Rújula, M.B. Gavela, P. Hernández, E. Massó, Nucl. Phys. B 384 (1992) 3.
[4] K. Hagiwara, S. Ishihara, R. Szalapski, D. Zeppenfeld, Phys. Lett. B 283 (1992) 353; idem Phys. Rev. D 48 (1993) 2182.
[5] K. Hagiwara, R. Szalapski, D. Zeppenfeld, Phys. Lett. B 318 (1993) 155.
[6] For a recent review on the phenomenological aspects of supersymmetry see for instance: X. Tata, in the Proceedings of the IX Jorge André Swieca Summer School: Particles and Fields, São Paulo, Brazil, report UH-511-872-97, and hep-ph/9706307.
[7] F. Abe et al., CDF Collaboration, hep-ex/9801019 (1998).
[8] J. Ellis, M.K. Gaillard, D.V. Nanopoulos, Nucl. Phys. B 106 (1976) 292; M.A. Shifman, A.I. Vainshtein, M.B. Voloshin, V.I. Zakharov, Sov. J. Nucl. Phys. 30 (1979) 711.
[9] K. Hagiwara, M.L. Stong, Z. Phys. 62 (1994) 99; B. Grzadowski, J. Wudka, Phys. Lett. B 364 (1995) 49; G.J. Gounaris, F.M. Renard, N.D. Vlachos, Nucl. Phys. B 459 (1996) 51; W. Killian, M. Krämer, P.M. Zerwas, Phys. Lett. B 381 (1996) 243.
[10] S.M. Lietti, S.F. Novaes, R. Rosenfeld, Phys. Rev. D 54 (1996) 3266; F. de Campos, S.M. Lietti, S.F. Novaes, R. Rosenfeld, Phys. Lett. B 389 (1996) 93.
[11] F. de Campos, M.C. Gonzalez-Garcia, S.F. Novaes, Phys. Rev. Lett. 79 (1997) 5210; M.C. Gonzalez-Garcia, S.M. Lietti, S.F. Novaes, Phys. Rev. D (in press).
[12] G.J. Gounaris, J. Layssac, F.M. Renard, Z. Phys. 69 (1996) 505; G.J. Gounaris, F.M. Renard, Z. Phys. 69 (1996) 513.
[13] H. Murayama, I. Watanabe, K. Hagiwara, KEK report 91-11 (unpublished).
[14] T. Stelzer, W.F. Long, Comput. Phys. Commun. 81 (1994) 357.
[15] G.P. Lepage, J. Comp. Phys. 27 (1978) 192.
[16] A.D. Martin, W.J. Stirling, R.G. Roberts, Phys. Lett. B 354 (1995) 155.
[17] G. Gounaris et al., Triple Gauge Boson Couplings in Proceedings of the CERN Workshop on LEP II Physics ed. G. Altarelli et al., preprint CERN 96-01, Vol. 1, p. 525 (1996)
[18] D. Amidei et al., Future Electroweak Physics at the Fermilab Tevatron: Report of the TeV–2000 Study Group preprint FERMILAB–PUB–96–082 (1996).
[19] See the public LEP TGC web page: http://www.cern.ch/LEPEWWG/tgc/.

3.3 Acoplamentos Anômalos - Três jatos

Finalmente, estudamos as contribuições desses operadores de dimensão 6 na produção de jatos, especificamente eventos de três jatos, para o LEP e para o NLC. Em nosso estudo, indicamos como o estudo da produção de tres jatos em aceleradores do tipo e^+e^- poderiam ser utilizados para o estudo do acoplamento qqg. Neste caso, consideramos os operadores cujas contribuições envolvem quarks, bosons vetoriais e o bóson de Higgs:

A forma da Lagrangeana é:

$$L = L_{SM} + \frac{1}{\Lambda^2}\sum_i A_i O_i \tag{3.8}$$

na qual L_{SM} é a Lagrangeana correspondente do Modelo Padrão e os operadores locais de dimensão (n+4) associados às contribuições efetivas para o sinal estudado são definidos da seguinte forma:

$$O_{Qg} = i(\bar{Q}\lambda^a\gamma^\mu D^\nu Q)G^a_{\mu\nu} + h.c. \tag{3.9}$$

$$O_{Ug} = i(\bar{U}\lambda^a\gamma^\mu D^\nu U)G^a_{\mu\nu} + h.c. \tag{3.10}$$

$$O_{Dg} = i(\bar{D}\lambda^a\gamma^\mu D^\nu D)G^a_{\mu\nu} + h.c. \tag{3.11}$$

$$O_{Ug\phi} = (\bar{Q}\sigma^{\mu\nu}\lambda^a U)\tilde{\phi}G^a_{\mu\nu} + h.c. \tag{3.12}$$

$$O_{Dg\phi} = (\bar{Q}\sigma^{\mu\nu}\lambda^a D)\phi G^a_{\mu\nu} + h.c. \tag{3.13}$$

Estimamos os possíveis limites a partir dos resultados experimentais do LEP II e do NLC. Considerando a taxa de produção total, bem como algumas variáveis

cinemáticas, como "thrust (T)", "spherocity (S)"e "C-variable".

ELSEVIER

11 February 1999

PHYSICS LETTERS B

Physics Letters B 447 (1999) 331–335

Three jet events and new strong couplings at LEP and NLC

A. Belyaev [a,b], F. de Campos [c], S.F. Novaes [a], R. Rosenfeld [a]

[a] *Instituto de Física Teórica, Universidade Estadual Paulista, Rua Pamplona 145, 01405–900 São Paulo, Brazil*
[b] *Skobeltsyn Institute of Nuclear Physics, Moscow State University, 119899 Moscow, Russian Federation*
[c] *Depto. de Física e Química, Universidade Estadual Paulista Av. Dr. Ariberto Pereira da Cunha 333, 12500 Guaratinguetá, Brazil*

Received 17 November 1998; revised 4 December 1998
Editor: M. Cvetič

Abstract

We study the effects of new dimension-6 operators, resulting from a general $SU(3)_C \otimes SU(2)_L \otimes U(1)_Y$ invariant effective Lagrangian, on three jet production at LEP and at the Next Linear Collider. Contributions to the total event rate and to some event shape variables are analysed in order to establish bounds on these operators.

PACS: 12.60.-i; 13.87.-a

Quantum Chromodynamics (QCD), an important part of the Standard Model (SM), has been tested in the perturbative regime to a high degree of precision [1]. However, the possible existence of new physics beyond the Standard Model, involving heavy colored particles, may give rise to small effects in QCD phenomenology at present and future colliders. Certainly, one of the main goals of the future generation of colliders will be to scrutinize the several competitive models describing the physics at high energies.

On the phenomenological side, instead of concentrating on a specific model, it is in general quite instructive to make a model independent analysis of the indirect effects that an unknown high-energy theory can have at the present energy scale. This can be accomplished by the effective Lagrangian approach [2]. After the heavy fields of the high-energy theory have been integrated out, their low-energy consequences can be represented by a series of local $SU(3)_C \otimes SU(2)_L \otimes U(1)_Y$ invariant operators built from the light Standard Model fields:

$$\mathscr{L}_{\text{eff}} = \mathscr{L}_0 + \sum_{n=1\cdots} \frac{f_{(n+4)}}{\Lambda^n} O_{(n+4)}, \qquad (1)$$

where $\mathscr{L}_{\text{SM}}$ is the Standard Model Lagrangian, Λ is the characteristic scale of the new physics and $O_{(n+4)}$ are the local operators of dimension $(n+4)$. Different scenarios can generate the same kind of operator but with distinct effective couplings f_{n+4} making possible, at least in principle, to point out a specific model for the new physics.

The classification of the operators $O_{(n+4)}$ have been first done in Ref. [3] and since then the phenomenological implications have been studied in the bosonic sector of the SM [4], and for the third-family quarks [5]. There have also been many studies of the so-called purely gluonic operators [6] where the high dimension operators $O_{(n+4)}$ involves only the gluon

0370-2693/99/$ - see front matter
PII: S0370-2693(98)01595-0

field and modify the non-abelian three and four vertex.

Nevertheless, effective operators involving gluons and light quarks (and possibly the Higgs fields) can also give rise to some measurable effects in QCD processes at the present colliders. These new couplings can be generated via loops of colored objects belonging to the underlying theory [7]. In this letter we search for possible signals of the existence of these new couplings in three jet events at e^+e^- colliders. We analyze the total event rate for different values of the jet resolution variable ($y_{\rm cut}$). Event shape observables in e^+e^- colliders are important to test QCD and have been studied at PETRA [8], LEP1 [9] and LEP2 [10] energies. Therefore, we also explore the differences in the event shape distributions due to the anomalous contribution in order to establish theoretical bounds on the coefficient of the dimension-6 operators that alter the qqg interaction.

In order to study the possible deviation from the Standard Model predictions for the couplings involving quarks and gluons, we start by writing the most general dimension-6 effective Lagrangian requiring the $SU(3)_C \otimes SU(2)_L \otimes U(1)_Y$ invariance of the new operators. We assume that there are no additional new fields and we construct these operators taking into account only the usual light particles, i.e. gauge bosons and quarks. Furthermore, we do not consider here the operators that modify the couplings of the gauge bosons with fermions since they are strongly constrained by the LEP1 measurements at the Z^0 pole. Therefore the new Lagrangian can be written as [3],

$$\mathscr{L}_2 = \frac{1}{\Lambda^2} \sum_i A_i \mathscr{O}_i , \tag{2}$$

where A_i are constants and the dimension-6 operators $\mathscr{O}_i$ can either involve just quarks and vector bosons or may contain also the Higgs field. In the first case, we have,

$$\mathscr{O}_{Qg} = i\left(\overline{Q}\lambda^a\gamma^\mu\mathscr{D}^\nu Q\right) G^a_{\mu\nu} + \text{h.c.}, \tag{3a}$$

$$\mathscr{O}_{Ug} = i\left(\overline{U}\lambda^a\gamma^\mu\mathscr{D}^\nu U\right) G^a_{\mu\nu} + \text{h.c.}, \tag{3b}$$

$$\mathscr{O}_{Dg} = i\left(\overline{D}\lambda^a\gamma^\mu\mathscr{D}^\nu D\right) G^a_{\mu\nu} + \text{h.c.}, \tag{3c}$$

where Q are the left-handed quark doublets while U and D are the right-handed quark singlets. $G^a_{\mu\nu} = \partial_\mu G^a_\nu - \partial_\nu G^a_\mu + g_s f^{abc} G^b_\mu G^c_\nu$ is the usual $SU(3)_C$ strength tensors and $\mathscr{D}_\mu = \partial_\mu - ig_s(\lambda^a/2)G^a_\mu - ig(\tau^i/2)W^i_\mu - ig' Y B_\mu$ is the $SU(3)_C \otimes SU(2)_L \otimes U(1)_Y$ covariant derivative of the quarks. The operator (3a) gives rise to a new qqg vertex involving left-handed up and down quarks while (3b) and (3c) operators involve right-handed up and down quarks respectively. Therefore, if we assume that the quark–gluon coupling is blind to the quark flavors, i.e. universal, and that the new physics affects left and right-handed quarks in the same way, we should require that $A_{Qg} = A_{Ug} = A_{Dg} \equiv A_{qg}$. We should point out that the new interactions (3) also generate new couplings involving weak-vector bosons (V), like $qqgV$ and $qqggV$, and also vertex with quarks and two and three gluons.

The operators that involves also the Higgs field doublet (ϕ) can be written as

$$\mathscr{O}_{Ug\phi} = \left(\overline{Q}\sigma^{\mu\nu}\lambda^a U\right)\tilde{\phi}\, G^a_{\mu\nu} + \text{h.c.}, \tag{4a}$$

$$\mathscr{O}_{Dg\phi} = \left(\overline{Q}\sigma^{\mu\nu}\lambda^a D\right)\phi\, G^a_{\mu\nu} + \text{h.c.}, \tag{4b}$$

where $\sigma^{\mu\nu} = (i/2)[\gamma^\mu,\gamma^\nu]$. When ϕ is replaced by its vacuum expectation value, the operators (4) generate new qqg, and $qqgg$ interactions, for $q = u, d$ quarks. In order to guarantee the universality also in the magnetic type qqg coupling, we should assume that $A_{Ug\phi} = A_{Dg\phi} \equiv A_{qg\phi}$.

Therefore, we end up with the following new Lagrangians,

$$\begin{aligned}\mathscr{L}_{qg} = \frac{2A_{qg}}{\Lambda^2}\Bigg\{ & \frac{i}{2}\sum_q \left[\bar{q}\lambda^a\gamma^\mu(\partial^\nu q) - (\partial^\nu\bar{q})\lambda^a\gamma^\mu q\right] \\ & + \frac{g_s}{2}\sum_q (\bar{q}\{\lambda^a,\lambda^b\}\gamma^\mu q)G^b_\nu \\ & + e\sum_q Q_q(\bar{q}\lambda^a\gamma^\mu q)A^\nu \\ & + \frac{e}{s_W c_W}\sum_q \left[\bar{q}\lambda^a\gamma^\mu(g^q_V + g^q_A\gamma_5)q\right]Z^\nu \\ & + \frac{e}{2\sqrt{2}\,s_W}\sum_{u,d}\Big[\bar{u}\lambda^a\gamma^\mu(1-\gamma_5)d\,W^{+\nu} \\ & + \bar{d}\lambda^a\gamma^\mu(1-\gamma_5)u\,W^{-\nu}\Big]\Bigg\}G^a_{\mu\nu}, \end{aligned} \tag{5}$$

where the summation is made over all the quark flavors q and over up and down quarks (u, d). $g^q_V = T^q_3/2 - Q_q s^2_W$ and $g^q_A = -T^q_3/2$ with s_W be-

ing the sine of the Weinberg angle, T_3^q and Q_q being the quark weak isospin and electric charge respectively, and

$$\mathscr{L}_{qg\phi} = \frac{A_{qg\phi}}{\Lambda^2} \frac{(v+H)}{\sqrt{2}} \sum_q (\bar{q}\,\sigma^{\mu\nu}\lambda^a q) G^a_{\mu\nu}\,, \qquad (6)$$

We shall start by studying the sensitivity to these new higher dimensional operators at LEP1, which has accumulated a large data sample of three jet events. This analysis was performed by including the new couplings generated by the higher dimensional operators into the package CompHEP [11,12]. We found that there is no contribution of the operators $\mathscr{O}_{qg}$ when the gluon is on-shell, like in the process $e^+e^- \to q\bar{q}g$. Furthermore, for the contributions generated by the $\mathscr{L}_{qg\phi}$ Lagrangian there is no interference with the SM amplitudes.

In order to compare with LEP1 data, we used the OPAL Collaboration [13] best fit values for the relevant energy scale ($Q^2 = (6.4\,\mathrm{GeV})^2$) and for the QCD scale ($\Lambda_{\mathrm{QCD}} = 147$ MeV). In this way we effectively minimize the uncertainty due to next-to-leading order corrections. We employed the JADE jet algorithm [14] by requiring that the three final state partons obey:

$$y_{ij} \equiv \frac{M_{ij}^2}{s} > y_{\mathrm{cut}} \qquad (7)$$

for any pair of final state partons, where M_{ij} is the invariant mass of the (i,j) pair and y_{cut} is a parameter that determines the jet separation criteria used experimentally. We have checked that our result do not change in a significant way if we consider the Durham [15] or Cambridge [16] jet algorithms where $M_{ij} = 2\min(E_i^2, E_j^2)(1-\cos\theta_{ij})$.

In our analysis, we assumed $y_{\mathrm{cut}}^{\mathrm{min}} = 0.05$ and we analyzed, besides the relative production rate of three jet events as a function of y_{cut}, different event shape distributions, like thrust (T) [17]

$$T = \max_{\boldsymbol{n}} \frac{\sum_i |\boldsymbol{p}_i \cdot \boldsymbol{n}|}{\sum_i |\boldsymbol{p}_i|}\,, \qquad (8)$$

spherocity (S) [18],

$$S = \left(\frac{4}{\pi}\right)^2 \min_{\boldsymbol{n}} \left(\frac{\sum_i |\boldsymbol{p}_i \times \boldsymbol{n}|}{\sum_i |\boldsymbol{p}_i|} \right)^2\,, \qquad (9)$$

and the C-variable [19],

$$C = \frac{3}{2} \frac{\sum_{i,j} \left[|\boldsymbol{p}_i||\boldsymbol{p}_j| - (\boldsymbol{p}_i \cdot \boldsymbol{p}_j)^2 / |\boldsymbol{p}_i||\boldsymbol{p}_j| \right]}{\left(\sum_i |\boldsymbol{p}_i| \right)^2}\,. \qquad (10)$$

In order to illustrate the shape of these distributions, we present in Fig. 1, our results for y_{cut}, S, T and C normalized distributions for the Standard Model and for the pure anomalous case.

We performed a χ^2 analysis for the various distributions to estimate the sensitivity of the three jet events to the anomalous parameter. We have taken into account the statistical errors and the over-

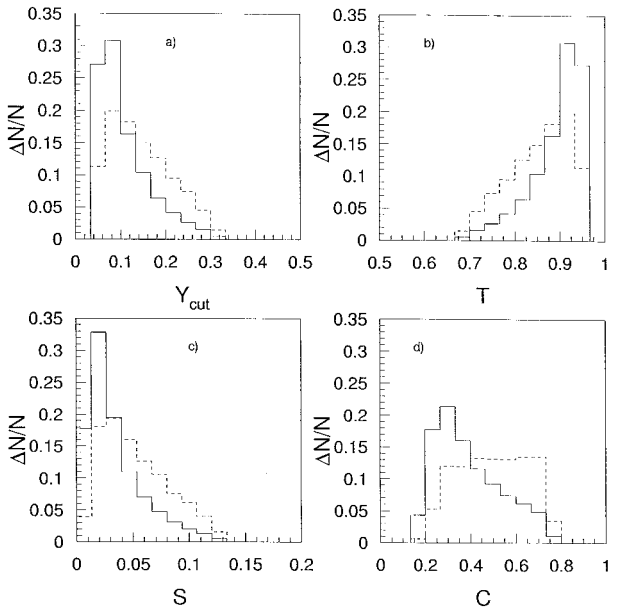

Fig. 1. Relative production rate of three jet events as a function of y_{cut} (a), and the normalized distributions for the event shape variables: thrust (b), spherocity (c) and C-parameter (d), for SM (solid line) and pure anomalous interactions (dashed line). In all cases we have considered $y_{\mathrm{cut}}^{\mathrm{min}} = 0.05$.

all normalization uncertainty of the QCD prediction. We consider,

$$\chi^2 = \sum_i \frac{\left[N_i - f N_i^{\mathrm{SM}}\right]^2}{f N_i^{\mathrm{SM}}} = \sum_i \frac{\left[N_i^{\mathrm{ANO}} + (1-f)\, N_i^{\mathrm{SM}}\right]^2}{f N_i^{\mathrm{SM}}},$$

where, N_i and N_i^{SM} are the numbers of events in the ith histogram bin in the presence of anomalous coupling and for the pure standard case, while $N_i^{\mathrm{ANO}} = N_i - N_i^{\mathrm{SM}}$ and f is a normalization parameter which parametrizes the changes in the overall QCD normalization. We have minimized χ^2 with respect to f in order to restrict χ^2 sensitivity only to the shape difference between anomalous and the Standard Model scenarios. In our analysis we assumed that the dominant errors are statistical and fragmentation and detector effects could be ignored.

Assuming a total luminosity of $220\,\mathrm{pb}^{-1}$ [20], we derived the theoretical bounds on the anomalous coupling from the various distributions, at 95% C.L.,

$$\frac{A_{qg\phi}}{\Lambda^2} < 16.3\,\mathrm{TeV}^{-2}, \quad \text{from } y_{\mathrm{cut}}, \tag{11}$$

$$\frac{A_{qg\phi}}{\Lambda^2} < 14.2\,\mathrm{TeV}^{-2}, \quad \text{from thrust}, \tag{12}$$

$$\frac{A_{qg\phi}}{\Lambda^2} < 16.0\,\mathrm{TeV}^{-2}, \quad \text{from spherocity}, \tag{13}$$

$$\frac{A_{qg\phi}}{\Lambda^2} < 16.1\,\mathrm{TeV}^{-2}, \quad \text{from } C\text{-parameter}. \tag{14}$$

It is important to notice that these bounds decrease by only $\sim 15\%$ if we assumed the value $Q^2 = M_Z^2$ for the QCD energy scale instead of the OPAL best fit value. In fact there is not a very good improvement on the bounds obtained from the event shape distribution when compared with the ones coming from the total yield: the thrust gives a slightly better bound. Therefore, we are able to establish the bound of $\Lambda \gtrsim 270$ GeV, for $A_{qg\phi} = 1$, while for $A_{qg\phi} = 4\pi$, Λ should be larger than 1 TeV.

We have also repeated the same analysis for LEP2 energies ($\sqrt{s} \simeq 200$ GeV) and 200 pb^{-1} of data and also for the Next Linear Collider assuming a center-of-mass energy of $\sqrt{s} = 500$ GeV and $\sqrt{s} = 1$ TeV with an integrated luminosity of 100 fb^{-1}.

At LEP2, since we are far from the Z^0 peak, we get a weaker bound on the scale of $\Lambda \gtrsim 140$ GeV ($A_{qg\phi} = 1$). However, at NLC with higher energies and luminosities, we can improve our bounds. The relative contribution from anomalous interaction grows with the energy while the SM cross section falls down. At $\sqrt{s} = 500$ GeV, NLC is able to establish the limit of $\Lambda \gtrsim 390$ GeV, for $A_{qg\phi} = 1$. When we further increase the energy to $\sqrt{s} = 1$ TeV the bound becomes: $\Lambda \gtrsim 480$ GeV, for $A_{qg\phi} = 1$.

In this letter, we have shown how the study of three jet production at an e^+e^- collider can provide an important test of the qqg coupling. We have made a theoretical sensitivity estimate of the values of the anomalous couplings that could be probed both at LEP and at the Next Linear Collider (NLC). In particular, we have suggested how to establish direct bounds on the anomalous couplings involving light quarks, gluons and the Higgs boson. These estimated bounds were obtained from the study of the total cross section and also from the event shape variables distributions. Similar operators to the ones studied here have been recently constrained by Gounaris, Papadamou and Renard [5] using unitarity arguments. However, these indirect bounds are important only for operators involving the top quark, and hence cannot be applied to the operators discussed in the present work. In conclusion, the comparison of anomalous contribution to the qqg vertex with the QCD predictions can be quite sensitive to new physics effect.

Acknowledgements

This work was supported by Conselho Nacional de Desenvolvimento Científico e Tecnológico (CNPq), by Fundação de Amparo à Pesquisa do Estado de São Paulo (FAPESP), and by Programa de Apoio a Núcleos de Excelência (PRONEX).

References

[1] See, for instance: S. Bethke, in: S. Marison (Ed.), Proceedings of the High-Energy Physics International Euroconference on Quantum Chromodynamics (QCD 97), Montpellier, France, 1997, Nucl. Phys. B 64 (1998) 54; D. Duchesneau, talk given at 29th International Conference on High-Energy Physics (ICHEP 98), Vancouver, Canada, 1998.

[2] See, for instance: H. Georgi, Weak Interactions and Modern Particle Theory, Benjamim/Cummings, Menlo Park, 1984; J.F. Donoghue, E. Golowich, B.R. Holstein, Dynamics of the Standard Model, Cambridge University Press, 1992.
[3] C.J.C. Burgess, H.J. Schnitzer, Nucl. Phys. B 228 (1983) 454; C.N. Leung, S.T. Love, S. Rao, Z. Phys. 31 (1986) 433; W. Buchmüller, D. Wyler, Nucl. Phys. B 268 (1986) 621.
[4] A. De Rújula, M.B. Gavela, P. Hernández, E. Massó, Nucl. Phys. B 384 (1992) 3; K. Hagiwara, S. Ishihara, R. Szalapski, D. Zeppenfeld, Phys. Lett. B 283 (1992) 353; Phys. Rev. D 48 (1993) 2182.
[5] F. Larios, C.-P. Yuan, Phys. Rev. D 55 (1997) 7218; O.J.P. Éboli, M.C. Gonzalez-Garcia, S.F. Novaes, Phys. Lett. B 415 (1997) 75; K. Whisnant, J.M. Yang, B.-L. Young, X. Zhang, Phys. Rev. D 56 (1997) 467; J.M. Yang, B.-L. Young, Phys. Rev. D 56 (1997) 5907; G.J. Gounaris, D.T. Papadamou, F.M. Renard, Z. Phys. C 76 (1997) 333.
[6] E.H. Simmons, Phys. Lett. B 226 (1989) 132; B 246 (1990) 471; H. Dreiner, A. Duff, D. Zeppenfeld, Phys. Lett. B 282 (1992) 441; A. Duff, D. Zeppenfeld, Z. Phys. 53 (1992) 529; P. Cho, E.H. Simmons, Phys. Lett. B 323 (1994) 401; Phys. Rev. D 51 (1995) 2360; L. Dixon, Y. Shadmi, Nucl. Phys. B 423 (1994) 3; B 452 (1995) 724 (E); G.J. Gounaris, D.T. Papadamou, F.M. Renard, Phys. Rev. D 57 (1998) 6752.
[7] C. Arzt, M.B. Einhorn, J. Wudka, Nucl. Phys. B 433 (1995) 41.
[8] P.A. Movilla Fernandez et al., Jade Collaboration, Eur. Phys. J. C 1 (1998) 461; P.A. Movilla Fernandez et al., Jade Collaboration, talk given at 29th International Conference on High-Energy Physics (ICHEP 98), Vancouver, Canada, 1998, and e-Print Archive hep-ex/9807007.
[9] B. Adeva et al., L3 Collaboration, Phys. Lett. B 263 (1991) 551; R. Akers et al., Opal Collaboration, Z. Phys. C 65 (1995) 31; C 68 (1995) 519.
[10] G. Alexander et al., Opal Collaboration, Z. Phys. C 72 (1996) 191; P. Abreu et al., Delphi Collaboration, Z. Phys. C 73 (1997) 229; K. Ackerstaff et al., Opal Collaboration, Z. Phys. C 75 (1997) 193.
[11] E.E. Boos, M.N. Dubinin, V.A. Ilyin, A.E. Pukhov, V.I. Savrin, preprint SNUTP–94–116 and E-print Archive hep-ph/9503280; P.A. Baikov et al., E-print Archive hep-ph/9701412.
[12] The Fortran source and the Monte Carlo CompHEP generator used in our calculations are available at http://door1.ift.unesp.br/users/belyaev/3jets.
[13] P.D. Acton et al., Z. Phys. C 55 (1992) 1; M.Z. Akrawy et al., Z. Phys. C 49 (1991) 375.
[14] JADE Collaboration, W. Bartels, Phys. Lett. B 123 (1993) 460.
[15] Yu.L. Dokshitzer, J. Phys. G 17 (1991) 1537.
[16] Yu.L. Dokshitzer, G. Leder, S. Moretti, B. Webber, JHEP 08 (1997) 001.
[17] S. Brandt, Ch. Peyrou, R. Sosnowski, A. Wroblewski, Phys. Lett. 12 (1964) 57; E. Farhi, Phys. Rev. Lett. 39 (1977) 1587.
[18] H. Georgi, M. Machacek, Phys. Rev. Lett. 39 (1977) 1237.
[19] R.K. Ellis, D.A. Ross, A.E. Terrano, Nucl. Phys. B 178 (1981) 421; R.K. Ellis, W.J. Stirling, B.R. Weber, QCD and Collider Physics, Cambridge University Press, 1996.
[20] The SLD Heavy Flavor Group, The LEP Collaborations and LEP Electroweak Working Group, CERN–PPE/97–154, 1997.

Os estudos mencionados foram publicados nas seguintes revistas: Physical Review D, Physical Review Letters e Physics Letters B. Como anexamos tais publicções, com suas referências bibliográficas, consideramos que os trabalhos mencionados também devam ser considerados referências associadas ao tema apresentado.

Todos os estudos foram realizados considerando-se os dados disponíveis na época, e utilizando algorítmos públicos. O estudo mediante o uso de software que simulasse detectores não foi possível de se realizar por não haver, como atualmente não há, acesso a este tipo de código. No entanto, uma revisão dos valores estabelecidos, à luz dos novos dados do LHC poder ser realizada, com o objetivo de se imporem novos limites sobres os acoplamentos anômalos, incluindo a possibilidade de se trabalhar na busca de efeitos reais no acoplamentos do boson de Higgs, tendo em vista sua detecção anunciada recentemente. Desse modo, poderia ser possível restringir de forma única os possíveis acoplamentos anômalos relacionados ao Higgs. Os resultaods expeíficos sobre o bóson de Higgs podem ser extemamente relevantes para se obter limites ainda mais restritivos sobre os acoplamentos anômalos associados à interação Higgs-bóson vetorial, por exemplo. Diversos trabalhos recentemente publicados ampliam os limites, embora não haja evidências de efeitos residuais de novas interações a energias mais altas.

Capítulo 4

Modelos Supersimétricos com quebra de paridade R

Outra forma de estudarmos as possíveis extensões do SM é considerarmos suas limitações e a forma de solucioná-las teoricamente, para então se verificar os indícios ou possibilidade da realização dessa solução em termos de resultados experimentais. Duas questões que exigem resposta no âmbito do SM se referem à hierarquia e à unificação das constantes de acoplamento. No primeiro caso, o problema reside no fato de correções radiativas à massa do Higgs divergirem quadraticamente a altas energias. No segundo caso, como a tentativa de se estabelecer uma teoria unificada deve levar a uma consequente unificação das constante de acoplamento das interações fundamentais, no caso do SM, considerando o modelo da forma estabelecida, a evolução no valor dessas constantes, a energias mais altas, não converge. Assim, esses problemas são a referência para a proposta de extensões, que apresentem uma possível solução.

A Supersimetria, até o momento, permanece como a solução mais aceita em

física de partículas para o problema da hierarquia, com a vantagem adicional da unificação das constantes de acoplamento a altas energias, incluindo a gravitação. Tal simetria associa férmios e bósons, de forma que na estrutura associada ao Modelo Padrão cada partícula correspondente tenha o seu parceiro supersimétrico. No entanto, pouco se sabe sobre a forma como a Supersimetria ocorre e como ela é quebrada. Sómente os resultados experimentais poderão indicar alguma possível solução para o assunto. Teoricamente a quebra da Supersimetria pode ocorrer por meio de termos associados à interação gravitacional, embora existam outras formas de se realizar a quebra. Também se considera que a paridade R seja conservada. Entretanto, não existe nenhuma indicação para que tal paridade seja imposta "a priori". Assim, vários mecanismos de quebra da Supersimetria podem ser estabelecidos e, de forma análoga, a quebra da paridade R. O número de parâmetros livres associados a modelos supersimétricos é a principal ressalva a esta classe de modelos, visto que no SM os parâmetros livres são fixados a partir dos dados experimentais, e no caso Supersimétrico permanecem livres. Apesar dessa ressalva, o estudo de tais modelos pode, em último caso, indicar que aspectos podem ser desconsiderados na referida formulação, e apontam possíveis caminhos no entendimento e desenvolvimento de novos modelos.

Nos trabalhos desenvolvidos consideramos casos distintos da quebra da Supersimetria: via termo de origem gravitacional, via termo anômalo ou termo de gauge, além da quebra da paridade R, e estudamos as conseqüências fenomenoógicas da quebra de paridade. A invariância sob a paridade R, definida por $R_P = (-1)^{3(B-L)+2S}$, é normalmente considerada em modelos supersimétricos. Essa simetria tem duas razões para ser imposta: manter a estabilidade do próton e assegurar que o LSP é o candidato à matéria escura. A primeira das condições

pode ser conseguida por diferentes simetrias que assegurem a conservação do número bariônico. Por outro lado, se introduzirmos a quebra do número leptônico podemos gerar massa para os neutrinos no cenário supersimétrico. Assim, introduzimos a quebra de paridade R por meio de termos bilineares do tipo:

$$W_{BRpV} = W_{MSSM} + \epsilon_{ab}\epsilon_i \hat{L}_i^a \hat{H}_b^u \tag{4.1}$$

na qual incluímos um parâmetro extra ϵ_i para cada geração de férmions. Para assegurarmos que os dados sobre neutrinos serão satisfeitos, o termo de acoplamento deve satisfazer a condição:$|\epsilon_i| << |\mu|$, na qual μ é o parâmetro bilinear de massa supersimétrico. Adicionamos em nosso trabalho, por consistência, termos de quebra sotf,

$$V_{soft} = V_{MSSM} - \epsilon_{ab}(B_i \epsilon_i \bar{L}_i^a H_u^b) \tag{4.2}$$

Desse modo temos novos parâmetros, relacionados à quebra de paridade R, e, consequentemente, a valores esperados no vácuo (vev) para o sneutrino, que proporciona mistura na matriz de massa de neutrinos e neutralinos. Uma vez diagonalizada a matriz de massa neutrino-neutralino, apresentam-se os auto-estados puros associados aos neutralinos, denotados por $\tilde{\chi}_k^0$. O neutralino mais leve é $\tilde{\chi}_1^0$. O mesmo ocorre com os leptons carregados e os charginos. Nesse caso os charginos são denotados por $\tilde{\chi}_1^{\pm}$.

Consideramos, em geral, o caso no qual a quebra da paridade R ocorre espontaneamente, como resultado da minimização do potencial de Higgs, de forma análoga à quebra da simetria eletrofraca. Modelos com quebra espontânea de paridade R são caracterizados pela existência de valores esperados no vácuo de dois tipos de sneutrinos: sneutrinos de mão esquerda e direita, singleto e dubleto

sob $SU(3) \otimes SU(2) \otimes U(1)$ respectivamente, satisfazendo a relação $v_L v_R \sim h_\nu m_W^2$ (mecanismo see-saw), no qual h_ν é o acoplamento tipo Yukawa, associado à quebra de paridade R. Abaixo da escala v_R, a quebra de paridade R é explícita através do termo bilinear que aparece no superpotencial e no termo de quebra soft do superpotencial. Para manter a simplicidade, sem perder o caráter geral do nosso estudo, podemos substituir o vev do sneutrino de mão direira por um acoplamento efetivo do tipo bilinear (o estudo do caso em que se mantem o termo associado ao vev do sneutrino de mão direita também foi realizado. Nesse modelo temos um bóson de goldstone, o Majoron, associado à quebra espontânea de paridade R). Referimo-nos a esse modelo como BRpV-mSUGRA, quando a quebra da supersimetria ocorrer via termo associado à gravitação, ou BRpV-AMSB, quando a quebra da supersimetria ocorrer via acoplamento anômalo.

Consideramos em nossos estudos que a partícula supersimétrica mais leve (LSP) é o neutralino em ambos os casos: mSUGRA e AMSB. Uma vantagem no estudo dos modelos mencionados é o fato de ser possível gerar as massas, misturas e acoplamentos dos neutrinos de forma a satisfazer todas as restrições experimentais conhecidas. Alem disso, já é conhecido que, independente da amplitude do termo da quebra da paridade R, associada aos dados experimentais de oscilação de neutrinos, os efeitos da quebra podem ser estudados em experimentos de aceleradores. Assim estudamos os possíveis sinais e suas implicações na busca por "nova física" em aceleradores - Tevatron, LEP e LHC. Há vários estudos sobre as buscas por supersimetria, a partir do estudo dos sinais em aceleradores. Entretanto, a absoluta maioria desses estudos sempre se pauta em modelos nos quais a paridade R é conservada. Até o momento, nenhuma evidencia sobre a SUSY em experimentos de altas energias foi encontrada. Os estudos realizados no Tevatro e

LEP (I e II) não permitiram uma conclusão definitiva sobre esse aspecto. Com a entrada em funcionamento do LHC, a busca por sinais de quebra de paridade R adquirem motivação ainda maior devido ao fato de, além da resposta à existência da supersimetria, também será possível estudar as possíveis conseqüências desse modelo no estudo de aspectos associados às oscilações de neutrinos. A diferença fundamental entre os modelos estudados e os chamados convencionais é que nos modelos propostos a partícula supersimétrica mais leve (LSP) não é estável e pode se desintegrar. Esse fenômeno pode ocorrer no interior do detector, e como conseqüência, modificar o resultado final do sinal detectado nos aceleradores. Tal fato tem as seguintes implicações: 1- O neutralino deixa de ser o candidato a matéria escura, sendo necessário responder à questão de que partícula pode ser o melhor candidato. Dentre as possibilidades aparecem o gravitino, o majoron ou uma partícula do tipo axion. Em tais modelos, o vínculo sobre a matéria escura que aparece em modelos supersimétricos sem quebra de paridade R não pode ser imposto. 2- Qualquer partícula supersimétrica pode ser a mais leve, inclusive aquelas carregadas. Consideramos em nossos estudos que o neutralino será sempre a LSP. No estudo dos sinais, o decaimento da LSP implica na redução de sinais com "transversal missing momentum" e ao correspondente aumento na multiplicidade de jatos e/ou leptons carregados no estado final. Para uma ampla margem no espaço de parâmetros associados, a LSP pode ter um tempo de vida grande o suficiente para dar origem ao que chamamos de vértice deslocado, o que sugere um sinal diferente do tipicamente estudado. Essa característica é presente em toda a classe de modelos com quebra de paridade R estudada. Estudamos os possíveis sinais no canal de multi-leptons para o caso BRpV-mSUGRA no Tevatron, utilizando os vértices deslocados como principal característica de tais sinais.

Assim, estudar a quebra da paridade R e os respectivos parâmetros de quebra de tal simetria significa também estudar a forma de quebra da Supersimetria. Do mesmo modo realizamos o estudo para o LHC, considerando modelos do tipo mSUGRA e AMSB.

4.1 Modelo BRPV–mSUGRA

Nosso objetivo aqui é descrever brevemente as características fundamentais dessa classe de modelos, nos quais a Supersimetria tem sua quebra baseada na gravidade e a quebra da paridade R em termo bilinear, como descrito anteriormente. Os novos termos que levam à violação do número leptônico e, conseqüentemente, à quebra de paridade R induzem também vev's $v_i = v_{L_i}$, para os três tipos de sneutrinos de mão esquerda. Não há uma base na qual esses termos possam ser eliminados ao mesmo tempo por efeito de transformações. Na base onde o termo bilinear do superpotencial pode ser eliminado, aparecem como resultado termos do tipo trilinear, dado por expressões do tipo:

$$\lambda_{ijk} = (\frac{\epsilon_i}{\mu})Y_{E,jk} \tag{4.3}$$

e

$$\lambda^{'}_{ijk} = (\frac{\epsilon_i}{\mu})Y_{D,jk}. \tag{4.4}$$

Consideramos em nossos estudos, no cenário de supergravidade, termos soft universais na escala de unificação. Esse modelo contém onze parâmetros livres, isto é: m_0 , $m_{1/2}$, $\tan\beta$, $\mathrm{sign}(\mu)$, A_0 , ϵ_i e Λ_i onde m_0 , $m_{1/2}$ são respectivamente a massa dos gaugino e a massa associada ao termo soft na escala de unificação,

A_0 é o termo trilinear e $\tan\beta$ a razão entre os vev's dos campos de Higgs. Por conveniência consideramos $\Lambda_i = \epsilon_i v_d + \mu v_i$, termo que está diretamente associado às propriedades neutrino-neutralino. Os termos bilineares de quebra de paridade R serão os responsáveis pela origem das misturas entre os termos associados ás partículas do Modelo Padrão e as parceiras supersimétricas. Além da geração de massa para neutrinos, termos de mistura neutralino-neutrino, também aparecem os decaimentos do LSP em partículas do Modelo Padrão. A nível árvore, apenas um neutrino adquire massa, enquanto os demais terão suas massas definidas por correções radiativas. Nesse caso, a escala de energia associada ao nível árvore é a escala atmosférica e, nessa aproximação, oscilações de neutrinos solares não ocorrem. As oscilações adquirem sentido quando as correções são incluídas. No caso dos neutralinos, o tempo de vida da LSP depende do espectro de massa e dos parâmetros de quebra de paridade R. Utilizando-se os resultados experimentais sobre neutrinos - o termo de interação associado à quebra de paridade R deve ser mínimo - se obtém um tempo de vida grande o suficiente para dar a origem a vértices deslocados. Em modelos BRpV–mSUGRA, para um dado valor dos parâmetros mSUGRA, há uma ampla margem na qual os parâmetros BRpV podem variar. Essa variação não tem efeito algum na seção de choque de produção para as partículas supersimétricas, porém afeta a largura de decaimento do LSP.

4.2 Modelo BRpV-AMSB

Modelos com quebra de supersimetria, mediada por termos anômalos, tem por característica contribuições de termos de quebra soft do setor anômalo conforme dominantes. Nesse tipo de modelo as massas das duas primeiras gerações de

escalares são automaticamente iguais e os termos de sabor fora da diagonal são dados em termos de acoplamento de Yukawa para quark. Na sua forma original, esse modelo sofre de problemas com a massa dos sleptons, que adquirem característica taquiônica, sendo necessária então a adição de termos de massa que, no caso mínimo, são universais. Podemos estudar a extensão por meio da introdução de termos bilineares que quebrem a paridade R. O modelo AMSB pode ser caracterizado pelos seguintes parâmetros: $m_{3/2}$, m_0, $\tan\beta$, sign(μ) e m_{ν_τ}. Neste caso consideramos a quebra de paridade R associada ao neutrino tau, isto é, apenas termos associados à terceira família foi considerada. Ampliar o trabalho considerando termos associados à primeira e segunda família podem completar o estudo. Consideramos a escala de energia associada à unificação neste caso $M_{GUT} \sim 10^{16} GeV$). A massa do gravitino, $m_{3/2}$, muito maior que as massas das demais partículas, é a única gerada a nível árvore. Os termos de quebra soft são proporcionais à massa do gravitino em modelos puramente AMSB. Entretanto, para evitar massas do slepton negativas, um parâmetro de massa extra universal m_0^2 é adicionado à massa de todos os sfermions e do Higgs no AMSB. A relação ente os vev's dos campos de Higgs mantem a mesma nomenclatura que no modelo discutido anteriormente, e o sinal do parâmetro de mistura Higgs-Higgsino, μ, pode ser qualquer. A convenção, nesse caso, é a de que tal parâmetro aparece no superpotencial como o termo $-\mu\hat{H}_d\hat{H}_u$. A relação completa entre os parâmetros citados acima e os parâmetros de quebra soft para o modelo AMSB pode ser encontrada nas referências indicadas nos artigos publicados, apresentados nas respectivas seções. O espectro de massa típico no cenário mediado por quebra anômala, tem o neutralino mais leve como a LSP. O stau ou o sneutrino-tau aparece como a LSP em uma região bastante reduzida considerando os parâmetros

citados anteriormente, sendo determinado pelo parâmetro $\tan\beta$. Para valores grandes de m_0, o neutralino mais leve será a LSP. O espectro de massa no modelo AMSB tem então a característica de quase degenerescência da massa da LSP (neutralino) e do chargino mais leve. Como a massa do wino é muito menor que a dos outros gauginos, ela será praticamente igual à massa da partícula associada ao estado mais leve, com o estado neutro sendo levemente menor. A natureza tipo wino do neutralino mais leve é importante, pois as interações são mais intensas e ele será produzido com maior abundancia em aceleradores. A segunda característica é a quase degenerescência entre os sleptons. Esse resultado é a conseqüência da adição do termo extra, universal, que contribui para a massa dos escalares. Apesar da quase degenerescência da massa da LSP e do chargino mais leve, consideramos sempre o cenário no qual o neutralino é a LSP.

ELSEVIER

Nuclear Physics B 623 (2002) 47–72

NUCLEAR PHYSICS B

www.elsevier.com/locate/npe

Anomaly mediated supersymmetry breaking without R-parity

F. de Campos [a], M.A. Díaz [b], O.J.P. Éboli [c], M.B. Magro [c], P.G. Mercadante [c]

[a] *Departamento de Física e Química, Universidade Estadual Paulista, Av. Dr. Ariberto Pereira da Cunha 333, Guaratinguetá, SP, Brazil*

[b] *Departamento de Física, Universidad Católica de Chile, Av. Vicuña Mackenna 4860, Santiago, Chile*

[c] *Instituto de Física, Universidade de São Paulo, CP 66.318, 05389-970, São Paulo, SP, Brazil*

Received 9 October 2001; accepted 4 December 2001

Abstract

We analyze the low energy features of a supersymmetric standard model where the anomaly-induced contributions to the soft parameters are dominant in a scenario with bilinear R-parity violation. This class of models leads to mixings between the standard model particles and supersymmetric ones which change the low energy phenomenology and searches for supersymmetry. In addition, R-parity violation interactions give rise to small neutrino masses which we show to be consistent with the present observations.

PACS: 12.60.Jv; 14.60.Pq; 14.80.Ly

1. Introduction

Supersymmetry (SUSY) is a promising candidate for physics beyond the Standard Model (SM) and there is a large ongoing search for supersymmetric partners of the SM particles. However, no positive signal has been observed so far. Therefore, if supersymmetry is a symmetry of nature, it is an experimental fact that it must be broken. The two best known classes of models for supersymmetry breaking are gravity-mediated [1] and gauge-mediated [2] SUSY breaking. In gravity-mediated models, SUSY is assumed to be broken in a hidden sector by fields which interact with the visible particles only via gravitational interactions and not via gauge or Yukawa interactions. In gauge-

E-mail address: magro@fma.if.usp.br (M.B. Magro).

0550-3213/02/$ – see front matter
PII: S0550-3213(01)00618-6

mediated models, on the contrary, SUSY is broken in a hidden sector and transmitted to the visible sector via SM gauge interactions of messenger particles.

There is a third scenario, called anomaly-mediated SUSY breaking [3], which is based on the observation that the super-Weyl anomaly gives rise to loop contribution to sparticle masses. The anomaly contributions are always present and in some cases they can dominate; this is the anomaly mediated supersymmetry breaking (AMSB) scenario. In this way, the gaugino masses are proportional to their corresponding gauge group β-functions with the lightest SUSY particle being mainly wino. Analogously, the scalar masses and trilinear couplings are functions of gauge and Yukawa β-functions. Without further contributions the slepton squared masses turn out to be negative. This tachyonic spectrum is usually cured by adding an universal non-anomaly mediated contribution $m_0^2 > 0$ to every scalar mass [4].

So far, most of the work on AMSB has been done assuming R-parity (R_P) conservation [5–7]; see [8] for an exception. R-parity violation [9] has received quite some attention lately motivated by the Super-Kamiokande Collaboration results on neutrino oscillations [10], which indicate neutrinos have mass [11]. One way of introducing mass to the neutrinos is via bilinear R-parity violation (BRpV) [12], which is a simple and predictive model for the neutrino masses and mixing angles [13,14]. In this work, we study the phenomenology of an anomaly mediated SUSY breaking model which includes bilinear R-parity violation (AMSB-BRpV), stressing its differences to the R-parity conserving case.

In BRpV-MSSM [15], bilinear R-parity and lepton number violating terms are introduced explicitly in the superpotential. These terms induce vacuum expectation values (vev's) v_i for the sneutrinos, and neutrino masses through mixing with neutralinos. At tree level, only one neutrino acquires a mass [16], which is proportional to the sneutrino vev in a basis where the bilinear R-parity violating terms are removed from the superpotential. At one-loop, three neutrinos get a non-zero mass, producing a hierarchical neutrino mass spectrum [17]. It has been shown that the atmospheric mass scale, given by the heaviest neutrino mass, is determined by tree level physics and that the solar mass scale, given by the second heaviest neutrino mass, is determined by one-loop corrections [14].

In our model, the presence of R_P violating interactions gives rise to neutrino masses which we show to be consistent with the present observations. Moreover, the low-energy phenomenology is quite distinct of the conserving R-parity AMSB scenario. For instance, the lightest supersymmetric particle (LSP) is unstable, which allows regions of the parameter space where the stau or the tau-sneutrino is the LSP. In our scenario, decays can proceed via the mixing between the standard model particles and supersymmetric ones. As an example, the mixing between the lightest neutralino $\tilde{\chi}_1^0$ (chargino $\tilde{\chi}_1^\pm$) and ν_τ ($\tau^\pm$) allows the following decays

$$\begin{aligned}
&\tilde{\chi}_1^0 \to \nu_\tau Z^*, \\
&\tilde{\chi}_1^0 \to \tau^\pm W^{\mp *}, \\
&\tilde{\chi}_1^\pm \to \tau^\pm Z^*, \\
&\tilde{\chi}_1^\pm \to \nu_\tau W^{\pm *}.
\end{aligned} \tag{49}$$

Another effect of the mixing between the standard model and supersymmetric particles is a sizeable change in the mass of the supersymmetric particles. For instance, the mixing between scalar taus and the charged Higgs can lead to an increase in the splitting between the two scalar tau mass eigenstates by a factor that can be as large as 10 with respect to the R_P conserving case.

This paper is organized as follows. We define in Section 2 our anomaly mediated SUSY breaking model which includes bilinear R-parity violation, stating explicitly our working hypotheses. This section also contains an overall view of the supersymmetric spectrum in our model. We study the properties of the CP-odd, CP-even, and charged scalar particles in Sections 3, 4, and 5, respectively, concentrating on the mixing angles that arise from the introduction of the R-parity violating terms. Section 6 contains the analysis that shows that our model can generate neutrino masses in agreement with the present knowledge. In Section 7 we provide a discussion of the general phenomenological aspects of our model while in Section 8 we draw our conclusions.

2. The AMSB-BRpV model

Our model, besides the usual R_P conserving Yukawa terms in the superpotential, includes the following bilinear terms

$$W_{\text{bilinear}} = -\varepsilon_{ab}\big(\mu \widehat{H}_d^a \widehat{H}_u^b + \epsilon_i \hat{L}_i^a \widehat{H}_u^b\big), \tag{1}$$

where the second one violates R_P and we take $|\epsilon_i| \ll |\mu|$. Analogously, the relevant soft bilinear terms are

$$\begin{aligned} V_{\text{soft}} = {} & m_{H_u}^2 H_u^{a*} H_u^a + m_{H_d}^2 H_d^{a*} H_d^a + M_{L_i}^2 \tilde{L}_i^{a*} \tilde{L}_i^a \\ & - \varepsilon_{ab}\big(B\mu H_d^a H_u^b + B_i \epsilon_i \tilde{L}_i^a H_u^b\big), \end{aligned} \tag{2}$$

where the terms proportional to B_i are the ones that violates R_P. The explicit R_P violating terms induce vacuum expectation values v_i, $i = 1, 2, 3$ for the sneutrinos, in addition to the two Higgs doublets vev's v_u and v_d. In phenomenological studies where the details of the neutrino sector are not relevant, it has been proven very useful to work in the approximation where R_P and lepton number are violated in only one generation [18]. In these cases, a determination of the mass scale of the atmospheric neutrino anomaly within a factor of two is usually enough, and that can be achieved in the approximation where R_P is violated only in the third generation.

In this work we assume that R_P violation takes place only in the third generation, and consequently the parameter space of our model is

$$m_0, m_{3/2}, \tan\beta, \text{sign}(\mu), \epsilon_3, \text{ and } m_{\nu_\tau}, \tag{3}$$

where $m_{3/2}$ is the gravitino mass and m_0^2 is the non-anomaly mediated contribution to the soft masses needed to avoid the appearance of tachyons. We characterize the BRpV sector by the ϵ_3 term in the superpotential and the tau–neutrino mass m_{ν_τ} since it is convenient to trade v_3 by m_{ν_τ}.

In AMSB models, the soft terms are fixed in a non-universal way at the unification scale which we assumed to be $M_{\rm GUT} = 2.4 \times 10^{16}$ GeV; see Appendix A for details. We considered the running of the masses and couplings to the electroweak scale, assumed to be the top mass, using the one-loop renormalization group equations (RGE) that are presented in Appendix B. In the evaluation of the gaugino masses, we included the next-to-leading order (NLO) corrections coming from α_s, the two-loop top Yukawa contributions to the beta-functions, and threshold corrections enhanced by large logarithms; for details see [4]. The NLO corrections are especially important for M_2, leading to a change in the wino mass by more than 20%.

One of the virtues of AMSB models is that the $SU(2) \otimes U(1)$ symmetry is broken radiatively by the running of the RGE from the GUT scale to the weak one. This feature is preserved by our model since the one-loop RGE are not affected by the bilinear R_P violating interactions; see Appendix B. In our model, the electroweak symmetry is broken by the vacuum expectation values of the two Higgs doublets H_d and H_u, and the neutral component of the third left slepton doublet $\tilde{L}_3$. We denote these fields as

$$H_d = \begin{pmatrix} \frac{1}{\sqrt{2}}\left[\chi_d^0 + v_d + i\varphi_d^0\right] \\ H_d^- \end{pmatrix}, \qquad H_u = \begin{pmatrix} H_u^+ \\ \frac{1}{\sqrt{2}}\left[\chi_u^0 + v_u + i\varphi_u^0\right] \end{pmatrix},$$
$$\tilde{L}_3 = \begin{pmatrix} \frac{1}{\sqrt{2}}\left[\tilde{\nu}_\tau^R + v_3 + i\tilde{\nu}_\tau^{i0}\right] \\ \tilde{\tau}^- \end{pmatrix}. \tag{4}$$

The above vev's v_i can be obtained through the minimization conditions, or tadpole equations, which in the AMSB-BRpV model are

$$\begin{aligned} t_d^0 &= \left(m_{H_d}^2 + \mu^2\right)v_d - B\mu v_u - \mu\epsilon_3 v_3 + \frac{1}{8}\left(g^2 + g'^2\right)v_d\left(v_d^2 - v_u^2 + v_3^2\right), \\ t_u^0 &= \left(m_{H_u}^2 + \mu^2 + \epsilon_3^2\right)v_u - B\mu v_d + B_3\epsilon_3 v_3 - \frac{1}{8}\left(g^2 + g'^2\right)v_u\left(v_d^2 - v_u^2 + v_3^2\right), \\ t_3^0 &= \left(m_{L_3}^2 + \epsilon_3^2\right)v_3 - \mu\epsilon_3 v_d + B_3\epsilon_3 v_u + \frac{1}{8}\left(g^2 + g'^2\right)v_3\left(v_d^2 - v_u^2 + v_3^2\right), \end{aligned} \tag{5}$$

at tree level. At the minimum we must impose $t_d^0 = t_u^0 = t_3^0 = 0$. In practice, the input parameters are the soft masses m_{H_d}, m_{H_u}, and m_{L_3}, the vev's v_u, v_d, and v_3 (obtained from m_Z, $\tan\beta$, and m_{ν_τ}), and ϵ_3. We then use the tadpole equations to determine B, B_3, and $|\mu|$.

One-loop corrections to the tadpole equations change the value of $|\mu|$ by $\mathcal{O}(20\%)$, therefore, we also included the one-loop corrections due to third generation of quarks and squarks [17]:

$$t_i = t_i^0 + \widetilde{T}_i(Q), \tag{6}$$

where t_i, with $i = d, u$, are the renormalized tadpoles, t_i^0 are given in (5), and $\widetilde{T}_i(Q)$ are the renormalized one-loop contributions at the scale Q. Here we neglected the one-loop corrections for t_3 since we are only interested in the value of μ.

Using the procedure underlined above[51], the whole mass spectrum can be calculated as a function of the input parameters m_0, $m_{3/2}$, $\tan\beta$, $\mathrm{sign}(\mu)$, ϵ_3, and m_{ν_τ}. In Fig. 1, we show a scatter plot of the mass spectrum as a function of the scalar mass m_0 for

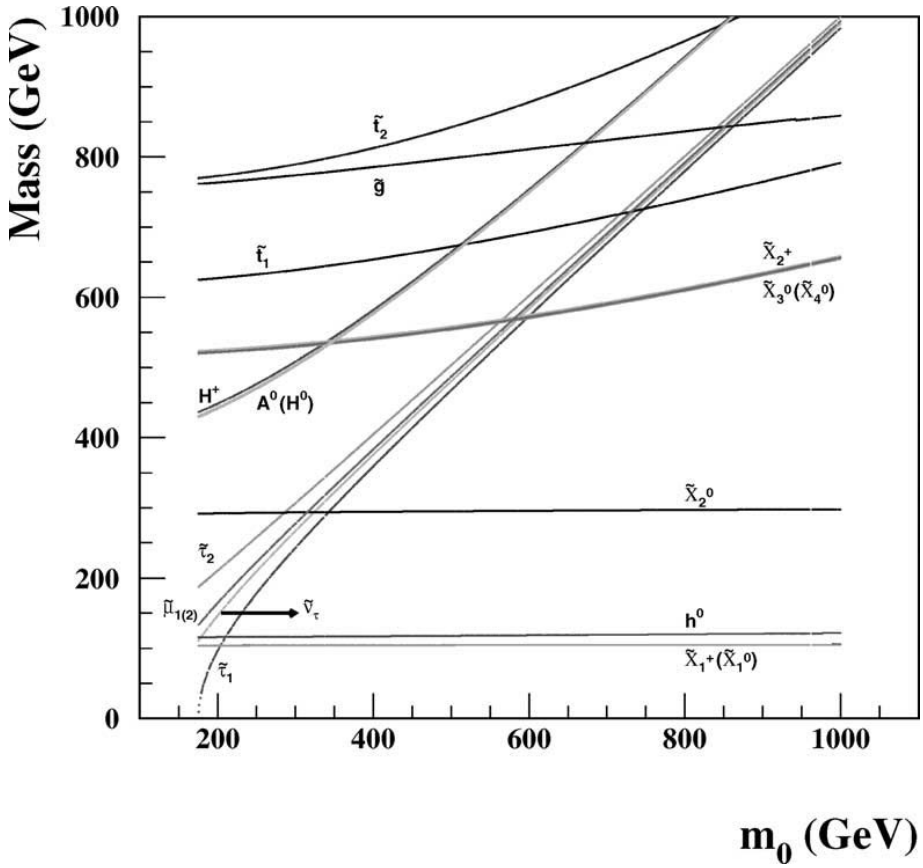

Fig. 1. Supersymmetric mass spectrum in AMSB-BRpV for $m_{3/2} = 32$ TeV, $\tan\beta = 5$, and $\mu < 0$. The values of ϵ_3 and m_{ν_τ} were randomly varied according to $10^{-5} < \epsilon_3 < 1$ GeV and $10^{-6} < m_{\nu_\tau} < 1$ eV.

$m_{3/2} = 32$ TeV, $\tan\beta = 5$, and $\mu < 0$, varying ϵ_3 and m_{ν_τ} according to $10^{-5} < \epsilon_3 < 1$ GeV and $10^{-6} < m_{\nu_\tau} < 1$ eV. The widths of the scatter plots show that the spectrum exhibits a very small dependence on ϵ_3 and m_{ν_τ}. Throughout this paper we use this range for ϵ_3 and m_{ν_τ} in all figures.

We can see from this figure that, for $m_0 \gtrsim 200$ GeV, the LSP is the lightest neutralino $\tilde{\chi}_1^0$ with the lightest chargino $\tilde{\chi}_1^+$ almost degenerated with it, as in R_P-conserving AMSB. Nevertheless, the LSP is the lightest stau $\tilde{\tau}_1^+$ for $m_0 \lesssim 200$ GeV. This last region of parameter space is forbidden in R_P-conserving AMSB, but perfectly possible in AMSB-BRpV since the stau is unstable, decaying into R_P-violating modes with sizeable branching ratios. Furthermore, the slepton masses have a strong dependence on m_0. We plotted masses of the two staus, which have an appreciable splitting, the almost degenerated smuons, and the closely degenerated tau-sneutrinos.[1] The heavy Higgs bosons have also a strong dependence on m_0 and, for the chosen parameters, they are much heavier than the sleptons. On the other hand, the gauginos show little dependence on m_0, as expected.

[1] In fact, there are two tau-sneutrinos in this model, a CP-even and a CP-odd field that are almost degenerated; see further sections for details.

Bounds on BRpV parameters depend in general on supersymmetric masses and couplings, as shown in [19]. In models with BRpV in only one generation it is possible to estimate the bound on ϵ_3 in a much simpler way: if we rotate the lepton and Higgs fields such that the bilinear term in the superpotential is eliminated [20], a trilinear term λ' is generated

$$\lambda'_{3ii} = h_{d_i} \frac{\epsilon_3}{\sqrt{\mu^2 + \epsilon_3^2}}, \tag{7}$$

where h_{d_i} is the Yukawa coupling of the down quark of the ith generation. Bounds on these couplings can be found on [9]:

$$\lambda'_{311} < 0.11 \times \frac{m_{\tilde{d}_R}}{100\ \text{GeV}}, \qquad \lambda'_{322} < 0.52 \times \frac{m_{\tilde{s}_R}}{100\ \text{GeV}}, \qquad \lambda'_{333} < 0.45, \tag{8}$$

and, considering the values of the Yukawa couplings, it is easy to see that these bounds are satisfied for our choice $\epsilon_3 < 1$ GeV.

3. CP-odd Higgs/sneutrino sector

In our model, the CP-odd Higgs sector mixes with the imaginary part of the tau-sneutrino due to the bilinear R_P violating interactions. Writing the mass terms in the form

$$V_{\text{quadratic}} = \frac{1}{2}\big[\varphi_d^0, \varphi_u^0, \tilde{\nu}_\tau^{i0}\big] \boldsymbol{M}^2_{P^0} \begin{bmatrix} \varphi_d^0 \\ \varphi_u^0 \\ \tilde{\nu}_\tau^{i0} \end{bmatrix}, \tag{9}$$

we have

$$\boldsymbol{M}^2_{P^0} = \begin{bmatrix} m_A^{2(0)} s_\beta^2 + \mu\epsilon_3 \frac{v_3}{v_d} & m_A^{2(0)} s_\beta c_\beta & -\mu\epsilon_3 \\ m_A^{2(0)} s_\beta c_\beta & m_A^{2(0)} c_\beta^2 - \mu\epsilon_3 \frac{v_3}{v_d}\frac{c_\beta^2}{s_\beta^2} + \frac{v_3^2}{v_d^2}\frac{c_\beta^2}{s_\beta^2}\bar{m}^2_{\tilde{\nu}_\tau} & -\mu\epsilon_3 \frac{c_\beta}{s_\beta} + \frac{v_3}{v_d}\frac{c_\beta}{s_\beta}\bar{m}^2_{\tilde{\nu}_\tau} \\ -\mu\epsilon_3 & -\mu\epsilon_3 \frac{c_\beta}{s_\beta} + \frac{v_3}{v_d}\frac{c_\beta}{s_\beta}\bar{m}^2_{\tilde{\nu}_\tau} & \bar{m}^2_{\tilde{\nu}_\tau} \end{bmatrix}, \tag{10}$$

with $\bar{m}^2_{\tilde{\nu}_\tau} = m^{2(0)}_{\tilde{\nu}_\tau} + \epsilon_3^2 + \frac{1}{8} g_Z^2 v_3^2$ and $g_Z^2 \equiv g^2 + g'^2$. Here,

$$m_A^{2(0)} = \frac{B\mu}{s_\beta c_\beta} \quad \text{and} \quad m^{2(0)}_{\tilde{\nu}_\tau} = M^2_{L_3} + \frac{1}{8} g_Z^2 \big(v_d^2 - v_u^2\big) \tag{11}$$

are, respectively, the CP-odd Higgs and sneutrino masses in the R_P conserving limit ($\epsilon_3 = v_3 = 0$). In order to write this mass matrix we have eliminated $m^2_{H_u}$, $m^2_{H_d}$, and B_3 using the tadpole equations (5). The mass matrix has an explicitly vanishing eigenvalue, which corresponds to the neutral Goldstone boson.

This matrix can be diagonalized with a rotation

$$\begin{bmatrix} A^0 \\ G^0 \\ \tilde{\nu}_\tau^{\text{odd}} \end{bmatrix} = \boldsymbol{R}_{P^0} \begin{bmatrix} \varphi_d^0 \\ \varphi_u^0 \\ \tilde{\nu}_\tau^{i0} \end{bmatrix}, \tag{12}$$

where G^0 is the massless neutral Goldstone boson. Between the other two eigenstates, the one with largest $\tilde{\nu}_\tau^{i0}$ component is called CP-odd tau-sneutrino $\tilde{\nu}_\tau^{\text{odd}}$ and the remaining state is called CP-odd Higgs A^0.

As an intermediate step, it is convenient to make explicit the masslessness of the Goldstone boson with the rotation

$$\widehat{\boldsymbol{R}}_{P^0} = \begin{bmatrix} s_\beta & c_\beta & 0 \\ -c_\beta r & s_\beta r & -\frac{v_3}{v_d} c_\beta r \\ -\frac{v_3}{v_d} c_\beta^2 r & \frac{v_3}{v_d} s_\beta c_\beta r & r \end{bmatrix}, \tag{13}$$

where

$$r = \frac{1}{\sqrt{1 + \frac{v_3^2}{v_d^2} c_\beta^2}}, \tag{14}$$

obtaining a rotated mass matrix $\widehat{R}_{P^0} M_{P^0}^2 \widehat{R}_{P^0}^{\text{T}}$ which has a column and a row of zeros, corresponding to G^0. This procedure simplifies the analysis since the remaining 2×2 mass matrix for $(A^0, \tilde{\nu}_\tau^{\text{odd}})$ is

$$\widehat{\boldsymbol{M}}_{P^0}^2 = \begin{bmatrix} m_A^{2(0)} + \frac{v_3^2}{v_d^2} \frac{c_\beta^4}{s_\beta^2} \bar{m}_{\tilde{\nu}_\tau}^2 + \mu \epsilon_3 \frac{v_3}{v_d} \frac{s_\beta^2 - c_\beta^2}{s_\beta^2} & \left(\frac{v_3}{v_d} \frac{c_\beta^2}{s_\beta} \bar{m}_{\tilde{\nu}_\tau}^2 - \mu \epsilon_3 \frac{1}{s_\beta} \right) r \\ \left(\frac{v_3}{v_d} \frac{c_\beta^2}{s_\beta} \bar{m}_{\tilde{\nu}_\tau}^2 - \mu \epsilon_3 \frac{1}{s_\beta} \right) r & \bar{m}_{\tilde{\nu}_\tau}^2 \frac{1}{r^2} \end{bmatrix}. \tag{15}$$

We quantify the mixing between the tau-sneutrino and the neutral Higgs bosons through

$$\sin^2 \theta_{\text{odd}} = \left| \langle \tilde{\nu}_\tau^{\text{odd}} | \varphi_u^0 \rangle \right|^2 + \left| \langle \tilde{\nu}_\tau^{\text{odd}} | \varphi_d^0 \rangle \right|^2. \tag{16}$$

If we consider the R_P violating interactions as a perturbation, we can show that

$$\sin^2 \theta_{\text{odd}} \simeq \frac{\left(\frac{v_3}{v_d} c_\beta^2 m_{\tilde{\nu}_\tau}^{2(0)} - \mu \epsilon_3 \right)^2}{s_\beta^2 \left(m_A^{2(0)} - m_{\tilde{\nu}_\tau}^{2(0)} \right)^2} + \frac{v_3^2}{v_d^2} c_\beta^2, \tag{17}$$

indicating that this mixing can be large when the CP-odd Higgs boson A^0 and the sneutrino $\tilde{\nu}_\tau$ are approximately degenerate.

Fig. 2(a) displays the full sneutrino-Higgs mixing (16), with no approximations, as a function of $\tan\beta$ for $m_{3/2} = 32$ TeV, $\mu < 0$ and $100 < m_0 < 300$ GeV. In a large fraction of the parameter space this mixing is small, since it is proportional to the BRpV parameters squared divided by MSSM mass parameters squared. However, it is possible to find a region where the mixing is sizable, e.g., for our choice of parameters this happens at $\tan\beta \approx 15$. As expected, the region of large mixing is associated to near degenerate states, as we can see from Fig. 2(b) where we present the ratio between the CP-odd Higgs mass m_A and the CP-odd tau-sneutrino mass $m_{\tilde{\nu}_\tau^{\text{odd}}}$ as a function of $\tan\beta$.

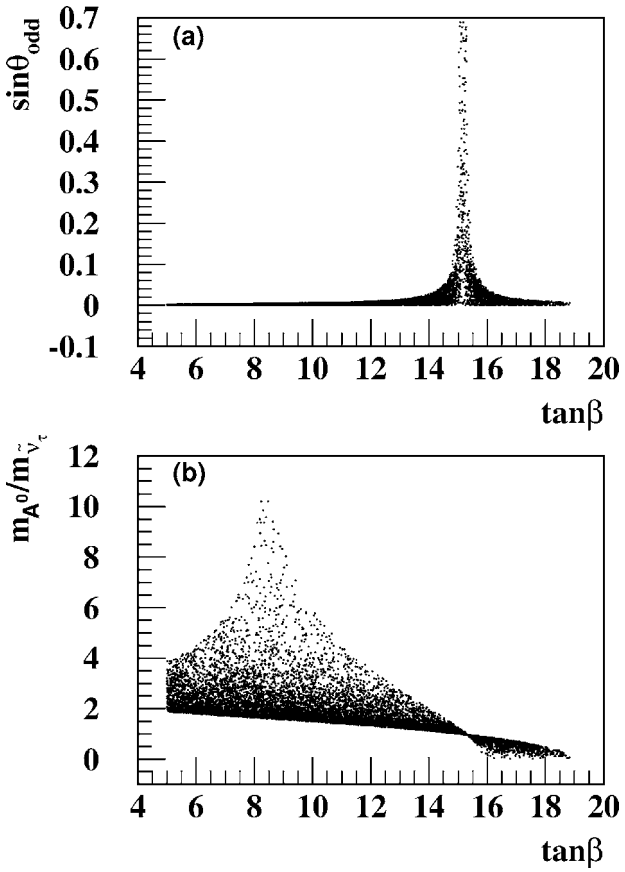

Fig. 2. (a) CP-odd Higgs–sneutrino mixing and (b) ratio between the CP-odd Higgs mass and the sneutrino mass as a function of $\tan\beta$ for $m_{3/2} = 32$ TeV, $\mu < 0$ and $100 < m_0 < 300$ GeV.

4. CP-even Higgs/sneutrino sector

The mass terms of the CP-even neutral scalar sector are

$$V_{\text{quadratic}} = \frac{1}{2}\left[\chi_d^0, \chi_u^0, \tilde{\nu}_\tau^{r0}\right] \boldsymbol{M}_{S^0}^2 \begin{bmatrix} \chi_d^0 \\ \chi_u^0 \\ \tilde{\nu}_\tau^{r0} \end{bmatrix}, \tag{18}$$

where the mass matrix can be separated into two pieces

$$\boldsymbol{M}_{S^0}^2 = \boldsymbol{M}_{S^0}^{2(0)} + \boldsymbol{M}_{S^0}^{2(1)}. \tag{19}$$

The first term due to R_P conserving interactions is

$$\boldsymbol{M}_{S^0}^{2(0)} = \begin{bmatrix} m_A^{2(0)} s_\beta^2 + \frac{1}{4} g_Z^2 v_d^2 & -m_A^{2(0)} s_\beta c_\beta - \frac{1}{4} g_Z^2 v_d v_u & 0 \\ -m_A^{2(0)} s_\beta c_\beta - \frac{1}{4} g_Z^2 v_d v_u^{55} & m_A^{2(0)} c_\beta^2 + \frac{1}{4} g_Z^2 v_u^2 & 0 \\ 0 & 0 & m_{\tilde{\nu}_\tau}^{2(0)} \end{bmatrix}, \tag{20}$$

while the one associated to the R_P violating terms is

$$M^{2(1)}_{S^0} = \begin{bmatrix} \mu\epsilon_3 \frac{v_3}{v_d} & 0 & -\mu\epsilon_3 + \frac{1}{4}g_Z^2 v_d v_3 \\ 0 & \frac{v_3^2}{v_d^2}\frac{c_\beta^2}{s_\beta^2} m^{2(0)}_{\tilde{\nu}_\tau} - \mu\epsilon_3 \frac{v_3}{v_d}\frac{c_\beta^2}{s_\beta^2} & \mu\epsilon_3 \frac{c_\beta}{s_\beta} - \frac{v_3}{v_d}\frac{c_\beta}{s_\beta} m^{2(0)}_{\tilde{\nu}_\tau} - \frac{1}{4}g_Z^2 v_u v_3 \\ -\mu\epsilon_3 + \frac{1}{4}g_Z^2 v_d v_3 & \mu\epsilon_3 \frac{c_\beta}{s_\beta} - \frac{v_3}{v_d}\frac{c_\beta}{s_\beta} m^{2(0)}_{\tilde{\nu}_\tau} - \frac{1}{4}g_Z^2 v_u v_3 & \epsilon_3^2 + \frac{3}{8}g_Z^2 v_3^2 \end{bmatrix} \tag{21}$$

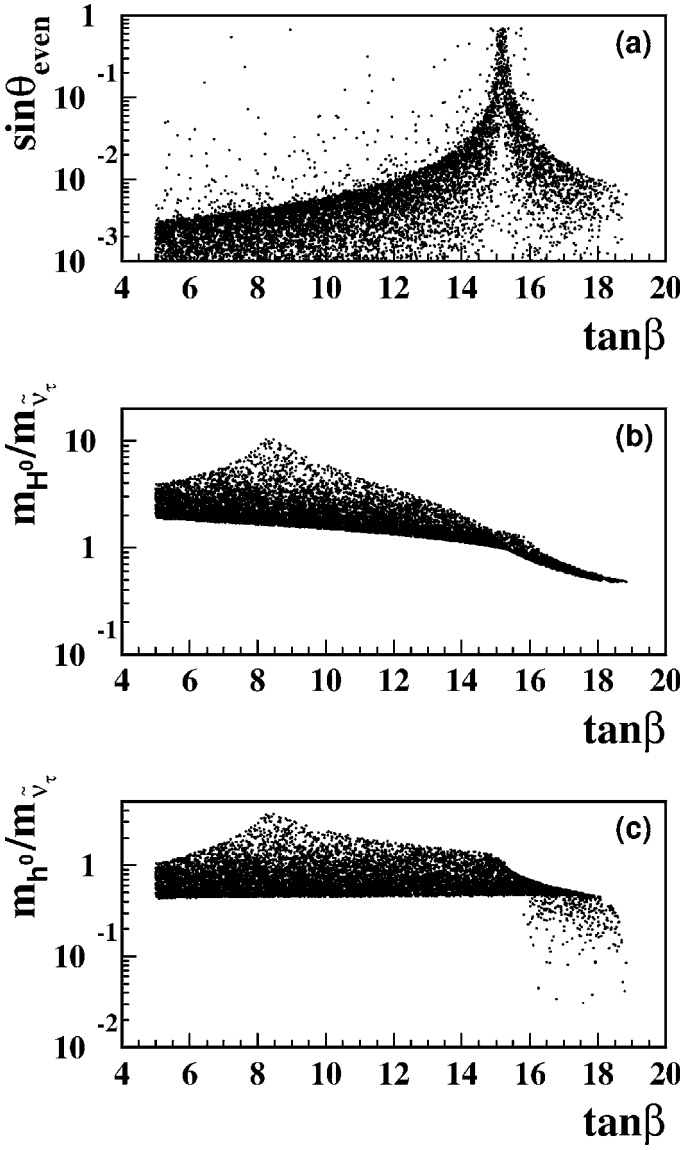

Fig. 3. (a) CP-even Higgs–sneutrino mixing; (b) ratio between heavy CP-even Higgs and tau-sneutrino masses and (c) ratio between light CP-even Higgs and tau-sneutrino masses as a function of $\tan\beta$ for $m_{3/2} = 32$ TeV, $\mu < 0$ and $100 < m_0 < 300$ GeV.

Radiative corrections can change significantly the lightest Higgs mass and, consequently, we have also introduced the leading correction to its mass

$$\Delta m_{\chi_u^0} \equiv \frac{3m_t^4}{2\pi^2 v_u^2 v'} \ln\left(\frac{m_{\tilde{t}_1} m_{\tilde{t}_2}}{m_t^2}\right), \tag{22}$$

with

$$v' = 1 - \frac{v_3^2}{v_d^2 + v_u^2 + v_3^2}, \tag{23}$$

by adding it to the element $[\boldsymbol{M}^2_{S^0}]_{22}$.

Analogously to the CP-odd sector, we define the mixing between the CP-even tau-sneutrino and the neutral Higgs bosons as

$$\sin^2\theta_{\text{even}} = \left|\left\langle \tilde{\nu}_\tau^{\text{even}} \middle| \chi_d^0 \right\rangle\right|^2 + \left|\left\langle \tilde{\nu}_\tau^{\text{even}} \middle| \chi_u^0 \right\rangle\right|^2 = \left|\left\langle H^0 \middle| \tilde{\nu}_\tau^{r0} \right\rangle\right|^2 + \left|\left\langle h^0 \middle| \tilde{\nu}_\tau^{r0} \right\rangle\right|^2. \tag{24}$$

In general, this mixing is small since it is proportional to the R_P breaking parameters squared, however, it can be large provided the sneutrino is degenerate either with h^0 or H^0.

In Fig. 3(a), we present the mixing (24) as a function of $\tan\beta$, for the input parameters as in Fig. 2. Similarly to the CP-odd scalar sector, this mixing can be very large, occurring either when $m_H \approx m_{\tilde{\nu}_\tau^{\text{even}}}$ or $m_h \approx m_{\tilde{\nu}_\tau^{\text{even}}}$. In fact, we can see from Fig. 3(b) that the peak in Fig. 3(a) for $\tan\beta \sim 15$ is mainly due to the mass degeneracy between the heavy CP-even Higgs H^0 and the CP-even tau-sneutrino $\tilde{\nu}_\tau^{\text{even}}$. On the other hand, the other scattered dots with high mixing angle values throughout Fig. 3(a) come from points in the parameter space where the light CP-even Higgs h^0 and the CP-even tau-sneutrino $\tilde{\nu}_\tau^{\text{even}}$ are degenerated. We see from Fig. 3(c) that this may occur for $5 < \tan\beta < 15$.

It is important to notice that the enhancement of the mixing between the tau-sneutrino and the CP-even Higgs bosons for almost degenerate states implies that large R_P violating effects are possible even for small R_P violating parameters ($\epsilon_3 \lesssim 1$ GeV), and for neutrino masses consistent with the solutions to the atmospheric neutrino anomaly ($m_{\nu_\tau} \lesssim 1$ eV).

5. Charged Higgs/charged slepton sector

The mass terms in the charged scalar sector are

$$V_{\text{quadratic}} = \left[H_u^-, H_d^-, \tilde{\tau}_L^-, \tilde{\tau}_R^-\right] \boldsymbol{M}^2_{S^\pm} \begin{bmatrix} H_u^+ \\ H_d^+ \\ \tilde{\tau}_L^+ \\ \tilde{\tau}_R^+ \end{bmatrix}, \tag{25}$$

where it is convenient to split the mass matrix into a R_P conserving part and a R_P violating one

$$\boldsymbol{M}^2_{S^\pm} = \boldsymbol{M}^{2(0)}_{S^\pm} + \boldsymbol{M}^{2(1)}_{S^\pm}. \tag{26}$$

The R_P conserving mass matrix has the usual MSSM form

$$\boldsymbol{M}^{2(0)}_{S^\pm} = \begin{bmatrix} m_A^{2(0)} s_\beta^2 + \frac{1}{4} g^2 v_u^2 & m_A^{2(0)} s_\beta c_\beta + \frac{1}{4} g^2 v_u v_d & 0 & 0 \\ m_A^{2(0)} s_\beta c_\beta + \frac{1}{4} g^2 v_u v_d & m_A^{2(0)} c_\beta^2 + \frac{1}{4} g^2 v_d^2 & 0 & 0 \\ 0 & 0 & \widehat{M}^2_{L_3} & \frac{1}{\sqrt{2}} h_\tau (A_\tau v_d - \mu v_u) \\ 0 & 0 & \frac{1}{\sqrt{2}} h_\tau (A_\tau v_d - \mu v_u) & \widehat{M}^2_{R_3} \end{bmatrix}, \tag{27}$$

where h_τ is the τ Yukawa coupling and

$$\widehat{M}^2_{L_3} = M^2_{L_3} - \frac{1}{8}\big(g^2 - g'^2\big)\big(v_d^2 - v_u^2\big) + \frac{1}{2} h_\tau^2 v_d^2,$$
$$\widehat{M}^2_{R_3} = M^2_{R_3} - \frac{1}{4} g'^2 \big(v_d^2 - v_u^2\big) + \frac{1}{2} h_\tau^2 v_d^2. \tag{28}$$

The contribution due to R_P violating terms is

$$\boldsymbol{M}^{2(1)}_{S^\pm} = \begin{bmatrix} \mu\epsilon_3 \frac{v_3}{v_d} - \frac{1}{4} g^2 v_3^2 + \frac{1}{2} h_\tau^2 v_3^2 & 0 & X_{uL} & X_{uR} \\ 0 & \frac{v_3^2}{v_d^2} \frac{c_\beta^2}{s_\beta^2} \bar{m}^2_{\tilde{\nu}} - \mu\epsilon_3 \frac{v_3}{v_d} \frac{c_\beta^2}{s_\beta^2} + \frac{1}{4} g^2 v_3^2 & X_{dL} & X_{dR} \\ X_{uL} & X_{dL} & \epsilon_3^2 + \frac{1}{8} g_Z^2 v_3^2 & 0 \\ X_{uR} & X_{dR} & 0 & \frac{1}{2} h_\tau^2 v_3^2 - \frac{1}{4} g'^2 v_3^2 \end{bmatrix}, \tag{29}$$

with

$$X_{uL} = \frac{1}{4} g^2 v_d v_3 - \mu\epsilon_3 - \frac{1}{2} h_\tau^2 v_d v_3, \tag{30}$$
$$X_{uR} = -\frac{1}{\sqrt{2}} h_\tau (A_\tau v_3 + \epsilon_3 v_u), \tag{31}$$
$$X_{dL} = \frac{v_3}{v_d} \frac{c_\beta}{s_\beta} \bar{m}^2_{\tilde{\nu}} - \mu\epsilon_3 \frac{c_\beta}{s_\beta} + \frac{1}{4} g^2 v_u v_3, \tag{32}$$
$$X_{dR} = -\frac{1}{\sqrt{2}} h_\tau (\mu v_3 + \epsilon_3 v_d). \tag{33}$$

The complete matrix $\boldsymbol{M}^2_{S^\pm}$ has an explicit zero eigenvalue corresponding to the charged Goldstone boson $G^\pm$, and is diagonalized by a rotation matrix $\boldsymbol{R}_{\boldsymbol{S}^\pm}$ such that

$$\begin{bmatrix} H^+ \\ G^+ \\ \tilde{\tau}_1^+ \\ \tilde{\tau}_2^+ \end{bmatrix} = \boldsymbol{R}_{S^\pm} \begin{bmatrix} H_u^+ \\ H_d^+ \\ \tilde{\tau}_L^+ \\ \tilde{\tau}_R^+ \end{bmatrix}. \tag{34}$$

In analogy with the discussion on the CP-even scalar sector, we define the mixing of the lightest (heaviest) stau $\tilde{\tau}_1^\pm$ ($\tilde{\tau}_2^\pm$) with the charged Higgs bosons as

$$\sin^2\theta_1^+ = \big|\langle \tilde{\tau}_1^+ | H_u^+ \rangle\big|^2 + \big|\langle \tilde{\tau}_1^+ | H_d^+ \rangle\big|^2, \tag{35}$$
$$\sin^2\theta_2^+ = \big|\langle \tilde{\tau}_2^+ | H_u^+ \rangle\big|^2 + \big|\langle \tilde{\tau}_2^+ | H_d^+ \rangle\big|^2. \tag{36}$$

58

Fig. 4(a), (b) contains the mixing between the lightest (heaviest) stau and the charged Higgs fields $\sin\theta^{+}_{1(2)}$ as a function of $\tan\beta$ for $m_{3/2} = 32$ TeV, $\mu < 0$, and $100 < m_0 < 300$ GeV. In this sector, the mixing can also be very large provided there is a near degeneracy between the staus $\tilde{\tau}^{\pm}_1$, $\tilde{\tau}^{\pm}_2$ and $H^{\pm}$. We can see clearly this effect in Fig. 4(c), (d), where we show the ratio between the charged Higgs mass m_{H^+} and the lightest (heaviest) stau mass $m_{\tilde{\tau}_{1(2)}}$. In Fig. 4(a) and (b) we also notice that large light stau–charged Higgs mixing occurs at slight different value of $\tan\beta$ compared with heavy stau–charged Higgs mixing. Large light stau–charged Higgs mixing is found in Fig. 4(a) as a peak at $\tan\beta \approx 16$, as opposed to large heavy stau–charged Higgs mixing, which presents a peak at $\tan\beta \approx 15$. In Fig. 4(a) we notice that the mixing angle vanishes at $\tan\beta \sim 11$. This zero occurs at the point of parameter space where the two staus are nearly degenerated, as will be explained in Section 7.

Similarly, in the last figure, the exact value of $\tan\beta$ at which the peak of the lightest stau-charged scalar mixing occurs is somewhat larger than the analogous mixing for the CP-odd sector $\sin\theta_{\rm odd}$. This can be appreciated in Fig. 5(a) where we show the ratio between $\sin\theta^{+}_1$ and $\sin\theta_{\rm odd}$ as a function of $\tan\beta$ for $m_{3/2} = 32$ TeV, $\mu < 0$ and $100 < m_0 < 300$ GeV.

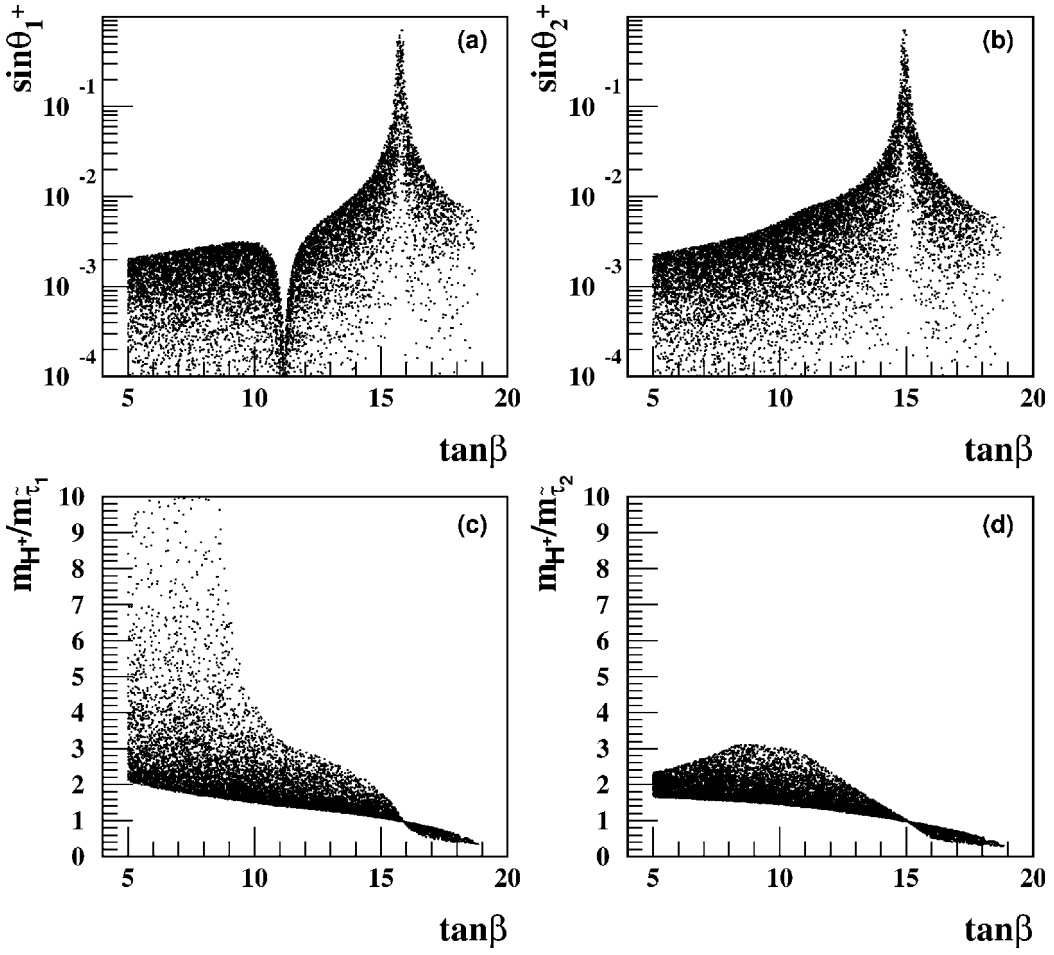

Fig. 4. (a) Charged Higgs–light stau mixing; (b) charged Higgs–heavy stau mixing; (c) charged Higgs–light stau mass ratio and (d) charged Higgs–heavy stau mass ratio as a function of $\tan\beta$ for $m_{3/2} = 32$ TeV, $\mu < 0$ and $100 < m_0 < 300$ GeV.

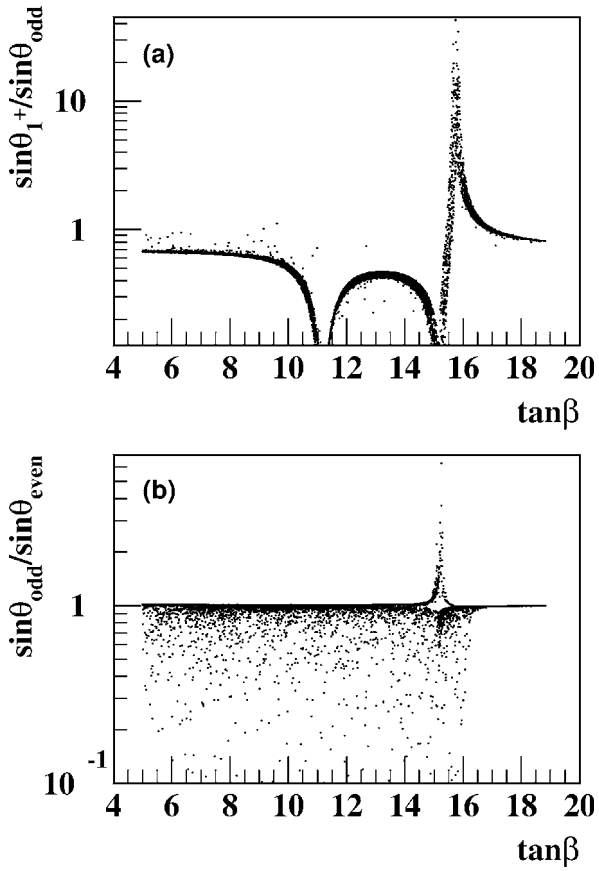

Fig. 5. (a) Ratio between the charged Higgs–stau and CP-odd Higgs–tau-sneutrino mixing angles and (b) ratio between the CP-odd Higgs–tau-sneutrino and CP-even Higgs–tau-sneutrino mixing angles as a function of $\tan\beta$ for $m_{3/2} = 32$ TeV, $\mu < 0$ and $100 < m_0 < 300$ GeV.

The peak of the charged sector mixing is located at the peak of the ratio. On the other hand, the peak for the neutral CP-odd sector is located at the nearby zero of the ratio. The other zero of the ratio near $\tan\beta \approx 11$ corresponds to a zero of the charged scalar sector mixing, as shown in Fig. 4. For the sake of comparison, we display in Fig. 5(b) the ratio between the CP-odd and CP-even mixings ($\sin\theta_{\text{odd}}/\sin\theta_{\text{even}}$) as a function of $\tan\beta$. We can see that most of the time the ratio is equal to 1 showing that the two neutral scalar sectors have similar behavior with $\tan\beta$ in contrast with the charged scalar sector. The points where this ratio is lower than 1 correspond to the case where the CP-even scalar sector mixings are dominated by the light Higgs and tau-sneutrino degeneracy which occurs for any value of $\tan\beta$ lower than 16, as shown in Fig. 3(c).

6. The neutrino mass

BRpV provides a solution to the atmospheric and solar neutrino problems due to their mixing with neutralinos, which generates neutrino masses and mixing angles. It was shown in [14] that the atmospheric mass scale is adequately described by the tree level neutrino

mass

$$m_{\nu_3}^{\text{tree}} = \frac{M_1 g^2 + M_2 g'^2}{4\Delta_0} |\vec{\Lambda}|^2, \tag{37}$$

where Δ_0 is the determinant of the neutralino sub-matrix and $\vec{\Lambda} = (\Lambda_1, \Lambda_2, \Lambda_3)$, with

$$\Lambda_i = \mu v_i + \epsilon_i v_d, \tag{38}$$

where the index i refers to the lepton family. The spectrum generated is hierarchical, and obtained typically with $\Lambda_1 \ll \Lambda_2 \approx \Lambda_3$.

As it was mentioned in the introduction, for many purposes it is enough to work with R_P violation only in the third generation. In this case, the atmospheric mass scale is well described by Eq. (37) with the replacement $|\vec{\Lambda}|^2 \to \Lambda_3^2$. In Fig. 6, we plot the neutrino mass as a function of Λ in AMSB-BRpV with the input parameters $m_{3/2} = 32$ TeV, $\mu < 0$, $5 < \tan\beta < 20$, $100 < m_0 < 1000$ GeV and $10^{-5} < \epsilon_3 < 1$ GeV. The quadratic dependence of the neutrino mass on Λ is apparent in this figure and neutrino masses smaller than 1 eV occur for $|\Lambda| \lesssim 0.6$ GeV^2. Moreover, the stars correspond to the allowed neutrino masses when the tau-sneutrino is the LSP. In general the points with a small (large) m_0 are located in the inner (outer) regions of this scattered plot.

From Fig. 6, we can see that the attainable neutrino masses are consistent with the global three-neutrino oscillation data analysis in the first reference of [10] that favors the $\nu_\tau \to \nu_\mu$ oscillation hypothesis. Although only mass squared differences are constrained by the neutrino data, our model naturally gives a hierarchical neutrino mass spectrum, therefore, we extract a naïve constraint on the actual mass coming from the analysis of the full atmospheric neutrino data, $0.04 \lesssim m_{\nu_\tau} \lesssim 0.09$ eV [10]. In addition, we notice that it

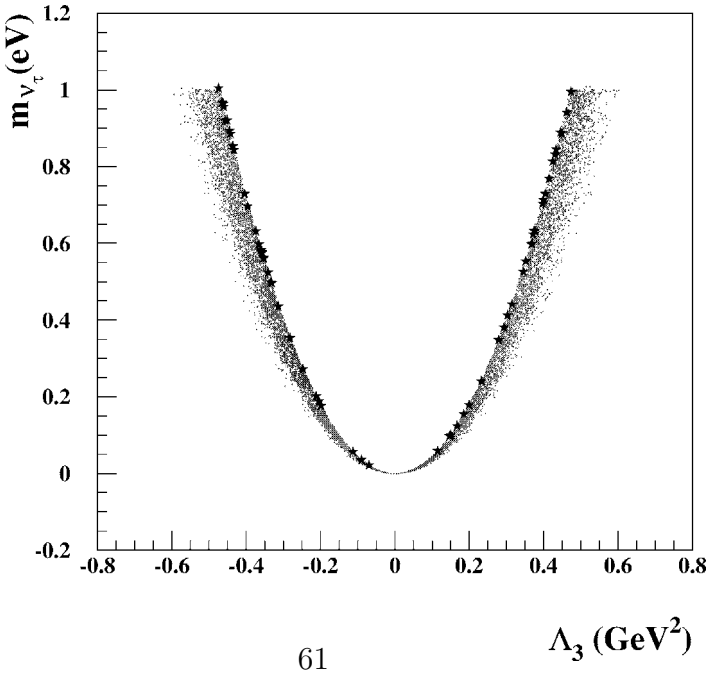

Fig. 6. Tau neutrino mass as a function of Λ_3 for $5 < \tan\beta < 20$, $100 < m_0 < 1000$ GeV, $m_{3/2} = 32$ TeV and $\mu < 0$.

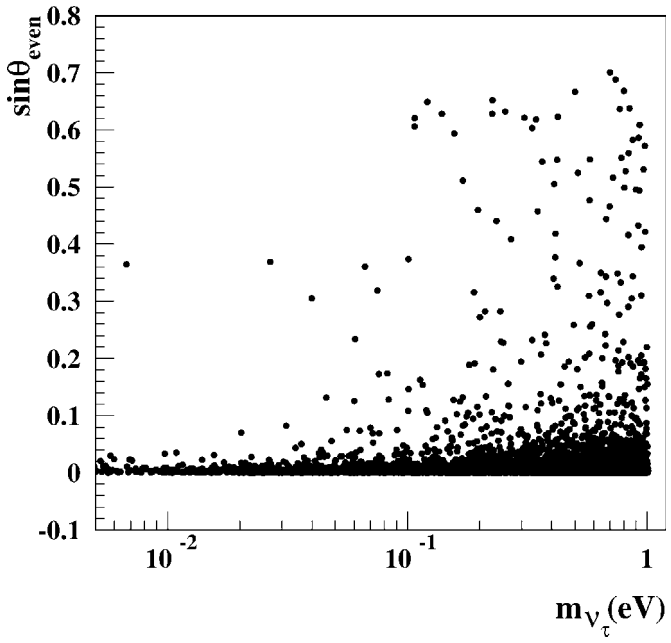

Fig. 7. Mixing between CP-even Higgses and sneutrino as a function of the tau neutrino mass.

is not possible to find an upper bound on the neutrino mass if angular dependence on the neutrino data is not included and only the total event rates are considered.

In Fig. 7 we show the correlation between the neutrino mass and mixing of the tau-sneutrino and the CP-even Higgses ($\sin\theta_{\text{even}}$) for the parameters assumed in Fig. 6. As expected, the largest mixings are associated to larger neutrino masses. Notwithstanding, it is possible to obtain large mixings for rather small neutrino masses because the mixing is proportional to the R_P violating parameters ϵ_3 and v_3, and not directly on $\Lambda_3 \propto m_{\nu_\tau}$. In any case, Fig. 7 suggests that large scalar mixings are still possible even imposing these bounds on the neutrino mass. This is extremely important for the phenomenology of the model because it indicates that non negligible R_P violating branching ratios are possible for scalars even in the case they are not the LSP.

7. Discussions

The presence of R_P violating interactions in our model render the LSP unstable, avoiding strong constraints on the possible LSP candidates. In the parameter regions where the neutralino is not the LSP, whether the light stau or the tau-sneutrino is the LSP depends crucially on the value of $\tan\beta$. This fact can be seen in Fig. 8 where we plot the ratio between the light stau and the tau-sneutrino masses as a function of $\tan\beta$ for $m_{3/2} = 32$ TeV, $100 < m_0 < 300$ GeV, and $\mu < 0$. From this figure we see that the tau-sneutrino is the LSP for $8.5 \lesssim \tan\beta \lesssim 14$, otherwise the stau is the LSP.[2]

[2] Of course, m_0 has to be small enough so that the slepton is lighter than the neutralino.

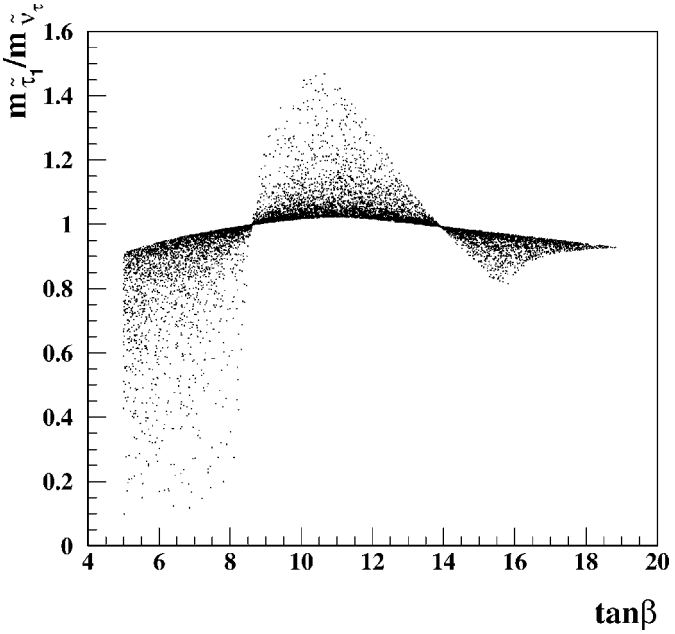

Fig. 8. Ratio between the light stau and the sneutrino masses as a function of $\tan\beta$ for $m_{3/2} = 32$ TeV, $100 < m_0 < 300$ GeV and $\mu < 0$.

When the stau is the LSP, it decays via R_P violating interactions, i.e., its decays take place through mixing with the charged Higgs, and consequently, they will mimic the charged Higgs boson ones. Therefore, it is very important to be able to distinguish between $\tilde{\tau}_1^{\pm}$ and $H^{\pm}$. This can be achieved either through precise studies of branching ratios, or via the mass spectrum, or both [21].

Measurements on the mass spectrum are also important in order to distinguish AMSB with and without conservation of R_P. In Fig. 9 we present the ratio between the stau mass splitting in AMSB-BRpV and in the AMSB, $R = (m_{\tilde{\tau}_2} - m_{\tilde{\tau}_1})_{\text{AMSB}-\text{BRpV}}/(m_{\tilde{\tau}_2} - m_{\tilde{\tau}_1})_{\text{AMSB}}$, with $\epsilon_3 = v_3 = 0$ and keeping the rest of the parameters unchanged, as a function of $\tan\beta$. In these figures, we took $100 < m_0 < 1000$ GeV, $m_{3/2} = 32$ TeV, and (a) $\mu > 0$, and (b) $\mu < 0$. For $\mu > 0$ (Fig. 9(a)), the stau mass splitting is always larger in the AMSB-BRpV than in the AMSB by a factor that increases when $\tan\beta$ decreases, and can be as large as $R \sim 10$ for $\tan\beta \sim 3$! We remind the reader that, in the absence of R_P violation, the left–right stau mixing decreases with decreasing $\tan\beta$, thus augmenting the importance of R-parity violating mixings. On the other hand, for $\mu < 0$ (Fig. 9(b)), this ratio can be as large as before at small $\tan\beta$, but in addition, the splitting can go to zero in AMSB-BRpV near $\tan\beta \approx 11$, which also constitutes a sharp difference with the AMSB. For both signs of μ the ratio goes to unity at large $\tan\beta$ because the left–right mixing in the AMSB is proportional to $\tan\beta$ and dominates over any R_P violating contribution.

The behavior of R at $\tan\beta \sim 11$ in Fig. 9(b) indicates that the two staus can be nearly degenerated in AMSB-BRpV. In Fig. 10 we plot the ratio between the light and heavy stau masses as a function of $\tan\beta$, for $m_{3/2} = 32$ TeV, $100 < m_0 < 300$ GeV and $\mu < 0$, observing clearly that the near degeneracy occurs at $\tan\beta \sim 11$. In first approximation, consider that the near degeneracy occurs when $A_\tau v_d - \mu v_u \approx 0$ as inferred from Eq. (27). In addition, the mixing X_{dR} in Eq. (33) is also very small because it is proportional to Λ_τ

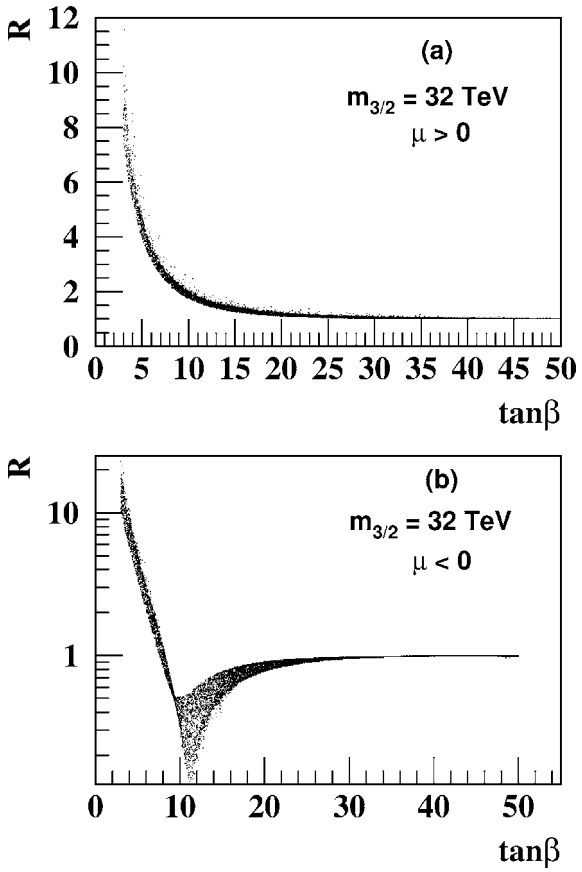

Fig. 9. Ratio (R) between the stau splitting in AMSB with and without R_P violation as a function of $\tan\beta$, for: $m_{3/2} = 32$ TeV, $100 < m_0 < 1000$ GeV and (a) $\mu > 0$ or (b) $\mu < 0$.

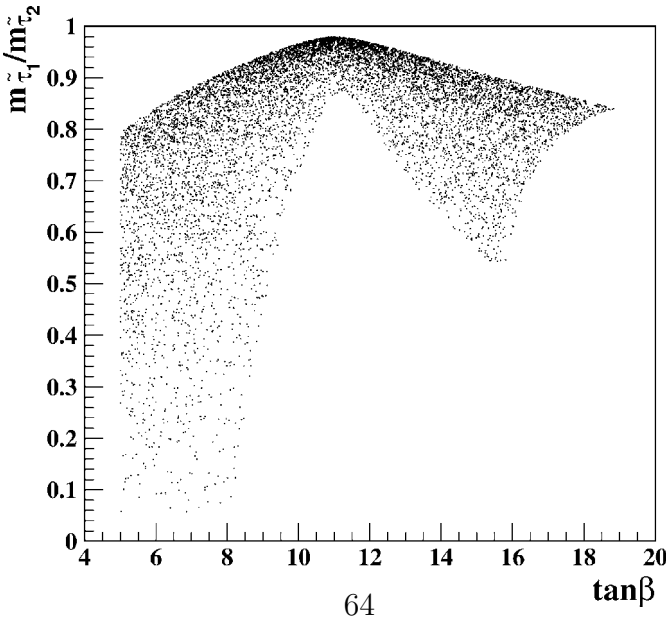

Fig. 10. Ratio between the light and heavy stau masses as a function of $\tan\beta$ for $m_{3/2} = 32$ TeV, $100 < m_0 < 300$ GeV and $\mu < 0$.

in Eq. (38), which defines the atmospheric neutrino mass, as indicated in Eq. (37). The smallness of these two quantities implies that the mixing X_{uR} in Eq. (31) is also small in this particular region of parameter space, indicating that the right stau is decoupled from the Higgs fields and thus originating the zero in the mixing angle, noted already in Figs. 4 and 5.

In order to quantify the stau mass splitting in our model, we present in Fig. 11 contours of constant splitting between the stau masses, $m_{\tilde{\tau}_2} - m_{\tilde{\tau}_1}$, in the plane $m_{3/2} \times m_0$ in GeV for $\mu < 0$ and several $\tan\beta$. We can see in Fig. 11(a) that for small $\tan\beta = 3$ the stau mass splitting in our model starts at $m_{\tilde{\tau}_2} - m_{\tilde{\tau}_1} \sim 30$ GeV, in sharp contrast with the R_P conserving case where the biggest splittings barely goes over this value [7]. This is in agreement with the results presented in Fig. 9(b). Furthermore, we can also see that there is a considerable region in the $m_{3/2} \times m_0$ plane, indicated by the grey area, where the

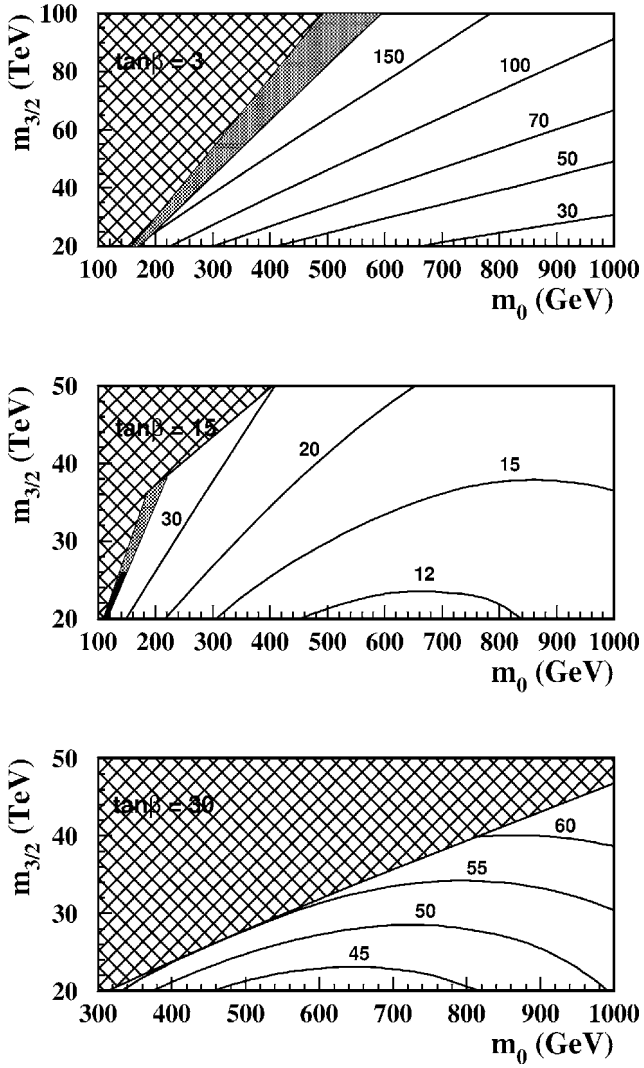

Fig. 11. Contours of constant splitting between the light stau and heavy stau masses in the plane $m_{3/2} \times m_0$ in GeV for $\mu < 0$, $\tan\beta = 3$ (a), 15 (b) and 30 (c). The hatched area is theoretically forbidden; the grey area in (a) and (b) is where the lightest stau is the LSP, while the small black area in (b) is where the tau-sneutrino is the LSP.

lightest stau is the LSP. For intermediary values of $\tan\beta \sim 15$, Fig. 11(b) shows that the stau mass splitting goes to a minimum. This is a different behavior from the MSSM which presents a mass splitting up to 10 times bigger as we have seen in Fig. 9(b). For this value of $\tan\beta$ we still have a small region where the lightest stau is the LSP (grey area) and, as a novelty, a tiny region for small values of $m_{3/2}$ and m_0 where the tau-sneutrino is the LSP (black area). For large values of $\tan\beta = 30$, the stau splitting mass shown in Fig. 11(c) is similar to the MSSM one [7].

We have made below a series of three figures fixing the value $\tan\beta = 15$ to study the dependence on m_0 of the mass spectrum and mixings in the scalar sector. This choice of $\tan\beta$ is such that we find a degeneracy among the masses, and consequently we obtain large mixings in the scalar sector. We also chose $m_{3/2} = 32$ TeV and $\mu < 0$, while the R_P violating parameters were varied according to $10^{-5} < \epsilon_3 < 1$ GeV and $10^{-6} < m_{\nu_\tau} < 1$ eV.

In Fig. 12(a) we plot tau-sneutrino mixing with the CP-odd neutral Higgs as a function of m_0 for the parameters indicated above. We find quite large mixings for $m_0 \approx 320$ GeV. In Fig. 12(b) we show the CP-odd Higgs and tau-sneutrino masses, which depend almost linearly on m_0. Moreover, the value of m_0 at which these two particles have the same mass coincides with the point of maximum mixing.

The CP-even tau-sneutrino mixing with the CP-even Higgs is presented in Fig. 13(a) as a function of m_0. There are two peaks of high mixing; the main one at $m_0 \approx 320$ GeV and

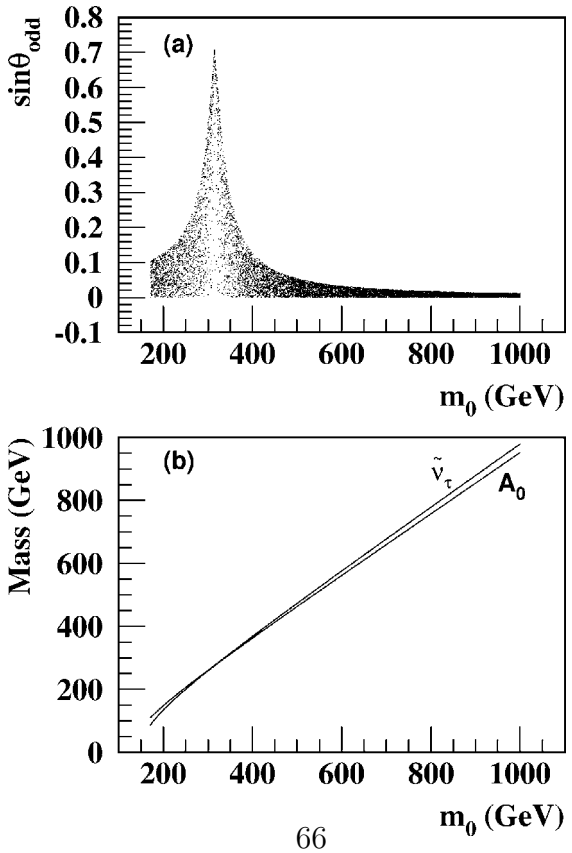

Fig. 12. (a) Mixing of the CP-odd Higgs and the sneutrino and (b) the CP-odd Higgs and sneutrino masses as a function of m_0 for $m_{3/2} = 32$ TeV, $\mu < 0$ and $\tan\beta = 15$.

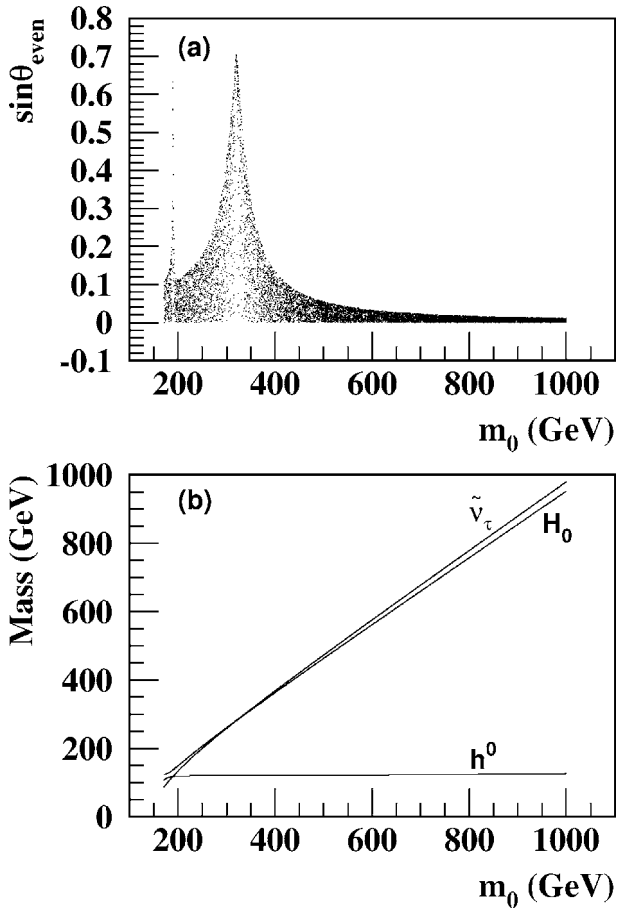

Fig. 13. (a) Mixing between the CP-even Higgs and sneutrino and (b) the light and heavy CP-even Higgs masses as well as the sneutrino one as a function of m_0 for $m_{3/2} = 32$ TeV, $\mu < 0$ and $\tan\beta = 15$.

a narrow one at $m_0 \approx 180$ GeV. These two peaks have a different origin, as indicated by Fig. 13(b), where we plot the masses of the two CP-even neutral Higgs bosons, m_h and m_H, and the mass of the CP-even tau-sneutrino $m_{\tilde{\nu}_\tau^{\text{even}}}$, as a function of m_0. We observe that the broad peak is due to a degeneracy between the tau-sneutrino and the heavy neutral Higgs boson and the narrow peak comes from a degeneracy between the tau-sneutrino and the light neutral Higgs boson. As expected, the H^0 and $\tilde{\nu}_\tau^{\text{even}}$ masses grow linearly with m_0, contrary to the h^0 mass which remains almost constant.

In Fig. 14(a) we display the light stau mixing with the charged Higgs as a function of m_0. The maximum mixing, obtained at $m_0 \approx 550$ GeV, is the result of a mass degeneracy between the charged Higgs boson and the light stau. This can be observed in Fig. 14(b) where we plot the charged Higgs mass $m_{H^\pm}$ and the light stau mass $m_{\tilde{\tau}_1}$ as a function of m_0.

In a similar way, we show the heavy stau mixing with charged Higgs as a function of m_0 in Fig. 14(c), where we observe a maximum for the mixing at $m_0 \approx 200$ GeV. This large mixing is due to a degeneracy between the charged Higgs boson and the heavy stau masses, as can be seen in Fig. 14(d). One can notice that all charged scalars show an almost linear dependency of their mass on the mass parameter m_0.

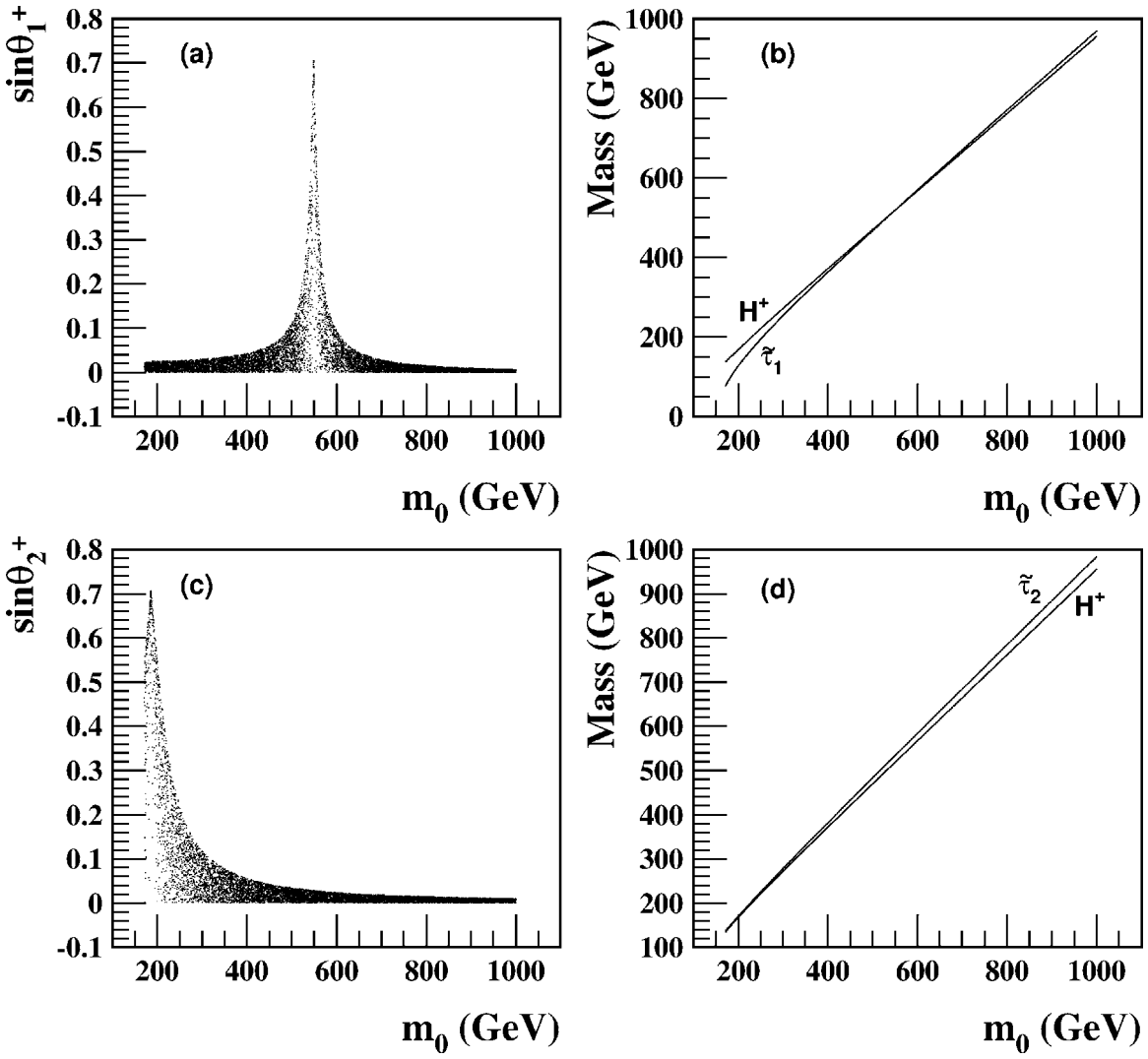

Fig. 14. (a) Mixing of the charged Higgs with the light stau, (b) charged Higgs and light stau masses, (c) mixing of the charged Higgs with the heavy stau, and (d) charged Higgs and heavy stau masses as a function of m_0 for $m_{3/2} = 32$ TeV, $\mu < 0$ and $\tan\beta = 15$.

As opposed to the scalar sector, where mixing between the Higgs bosons and sleptons can be maximum, in the chargino and neutralino sectors the mixings with leptons are controlled by the neutrino mass being very small. Despite this fact, the mixing in the neutralino sector is sufficient to generate adequate masses for the neutrinos and give rise to the neutralino decays mentioned in the introduction. Therefore, in the chargino sector the BRpV-AMSB phenomenology changes very little with respect to the R_P conserving AMSB. One of the distinctive features of AMSB that differentiates it from other scenarios of supersymmetry breaking in the chargino-neutralino sector is the near degeneracy between the lightest chargino and the lightest neutralino. This feature remains in BRpV-AMSB as was anticipated in Fig. 1. For $m_{3/2} = 32$ TeV, $\mu < 0$, and $100 < m_0 < 300$ GeV, we show in Fig. 15 the lightest chargino mass as a function of $\tan\beta$. The lightest chargino mass has a small dependence on $\tan\beta$ since its value varies only between 100 and 104 GeV. As in R_P conserving AMSB, the mass difference $m_{\tilde{\chi}_1^+} - m_{\tilde{\chi}_1^0}$ remains small.

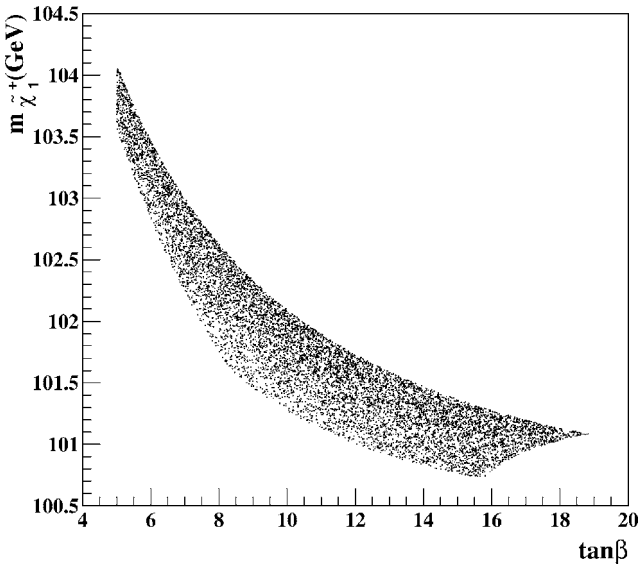

Fig. 15. Light chargino mass as a function of $\tan\beta$ for $m_{3/2} = 32$ TeV, $\mu < 0$ and $100 < m_0 < 300$ GeV.

8. Conclusions

We have shown in the previous sections that our model exhibiting anomaly mediated supersymmetry breaking and bilinear R_P violation is phenomenologically viable. In particular, the inclusion of BRpV generates neutrino masses and mixings in a natural way. Moreover, the R_P breaking terms give rise to mixing between the Higgs bosons and the sleptons, which can be rather large despite the smallness of the parameters needed to generate realistic neutrino masses. These large mixings occur in regions of the parameter space where two states are nearly degenerate. Our model also alters substantially the mass splitting between the scalar taus in a large range of $\tan\beta$.

The R_P violating interactions render the LSP unstable since it can decay via its mixing with the SM particles (leptons or scalars). Therefore, the constraints on the LSP are relaxed and forbidden regions of parameter space become allowed, where scalar particles like staus or sneutrinos are the LSP. Furthermore, the large mixing between Higgs bosons and sleptons has the potential to change the decays of these particles. These facts have a profound impact in the phenomenology of the model, changing drastically the signals at colliders [22].

Acknowledgements

This work was partially supported by a joint grant from Fundación Andes and Fundación Vitae, by DIPUC, by CONICYT grant No. 1010974, by Fundação de Amparo à Pesquisa do Estado de São Paulo (FAPESP), by Conselho Nacional de Desenvolvimento Científico e Tecnológico (CNPq) and by Programa de Apoio a Núcleos de Excelência (PRONEX).

Appendix A. AMSB boundary conditions

The AMSB boundary conditions at the GUT scale for the gaugino masses are proportional to their beta functions, resulting in

$$M_1 = \frac{33}{5}\frac{g_1^2}{16\pi^2}m_{3/2}, \tag{A.1}$$

$$M_2 = \frac{g_2^2}{16\pi^2}m_{3/2}, \tag{A.2}$$

$$M_3 = -3\frac{g_3^2}{16\pi^2}m_{3/2}, \tag{A.3}$$

while the third generation scalar masses are given by

$$m_U^2 = \left(-\frac{88}{25}g_1^4 + 8g_3^4 + 2f_t\hat{\beta}_{f_t}\right)\frac{0}{m_{3/2}^2}\left(16\pi^2\right)^2 + m_0^2, \tag{A.4}$$

$$m_D^2 = \left(-\frac{22}{25}g_1^4 + 8g_3^4 + 2f_b\hat{\beta}_{f_b}\right)\frac{m_{3/2}^2}{(16\pi^2)^2} + m_0^2, \tag{A.5}$$

$$m_Q^2 = \left(-\frac{11}{50}g_1^4 - \frac{3}{2}g_2^4 + 8g_3^4 + f_t\hat{\beta}_{f_t} + f_b\hat{\beta}_{f_b}\right)\frac{m_{3/2}^2}{(16\pi^2)^2} + m_0^2, \tag{A.6}$$

$$m_L^2 = \left(-\frac{99}{50}g_1^4 - \frac{3}{2}g_2^4 + f_\tau\hat{\beta}_{f_\tau}\right)\frac{m_{3/2}^2}{(16\pi^2)^2} + m_0^2, \tag{A.7}$$

$$m_E^2 = \left(-\frac{198}{25}g_1^4 + 2f_\tau\hat{\beta}_{f_\tau}\right)\frac{m_{3/2}^2}{(16\pi^2)^2} + m_0^2, \tag{A.8}$$

$$m_{H_u}^2 = \left(-\frac{99}{50}g_1^4 - \frac{3}{2}g_2^4 + 3f_t\hat{\beta}_{f_t}\right)\frac{m_{3/2}^2}{(16\pi^2)^2} + m_0^2, \tag{A.9}$$

$$m_{H_d}^2 = \left(-\frac{99}{50}g_1^4 - \frac{3}{2}g_2^4 + 3f_b\hat{\beta}_{f_b} + f_\tau\hat{\beta}_{f_\tau}\right)\frac{m_{3/2}^2}{(16\pi^2)^2} + m_0^2. \tag{A.10}$$

Finally, the A-parameters are given by

$$A_t = \frac{\hat{\beta}_{f_t}}{f_t}\frac{m_{3/2}}{16\pi^2}, \qquad A_b = \frac{\hat{\beta}_{f_b}}{f_b}\frac{m_{3/2}}{16\pi^2}, \qquad A_\tau = \frac{\hat{\beta}_{f_\tau}}{f_\tau}\frac{m_{3/2}}{16\pi^2}, \tag{A.11}$$

where we have defined

$$\hat{\beta}_{f_t} = 16\pi^2\beta_t = f_t\left(-\frac{13}{15}g_1^2 - 3g_2^2 - \frac{16}{3}g_3^2 + 6f_t^2 + f_b^2\right), \tag{A.12}$$

$$\hat{\beta}_{f_b} = 16\pi^2\beta_b = f_b\left(-\frac{7}{15}g_1^2 - 3g_2^2 - \frac{16}{3}g_3^2 + f_t^2 + 6f_b^2 + f_\tau^2\right), \tag{A.13}$$

$$\hat{\beta}_{f_\tau} = 16\pi^2\beta_\tau = f_\tau\left(-\frac{9}{5}g_1^2 - 3g_2^2 + 3f_b^2 + 4f_\tau^2\right). \tag{A.14}$$

Appendix B. The renormalization group equations

Here we present the one-loop renormalization group equations for our model, assuming the bilinear R_P breaking terms are restricted only to the third generation. First, we display the equations for the Yukawa couplings of the trilinear terms

$$16\pi^2\frac{dh_U}{dt} = h_U\left(6h_U^2 + h_D^2 - \frac{16}{3}g_3^2 - 3g_2^2 - \frac{13}{9}g_1^2\right), \tag{B.1}$$

$$16\pi^2\frac{dh_D}{dt} = h_D\left(6h_D^2 + h_U^2 + h_\tau^2 - \frac{16}{3}g_3^2 - 3g_2^2 - \frac{7}{9}g_1^2\right), \tag{B.2}$$

$$16\pi^2\frac{dh_\tau}{dt} = h_\tau\left(4h_\tau^2 + 3h_D^2 - 3g_2^2 - 3g_1^2\right). \tag{B.3}$$

The corresponding RGE for cubic soft supersymmetry breaking parameters are given by

$$8\pi^2\frac{dA_U}{dt} = 6h_U^2A_U + h_D^2A_D + \frac{16}{3}g_3^2M_3 + 3g_2^2M_2 + \frac{13}{9}g_1^2M_1, \tag{B.4}$$

$$8\pi^2\frac{dA_D}{dt} = 6h_D^2A_D + h_U^2A_U + h_\tau^2A_\tau + \frac{16}{3}g_3^2M_3 + 3g_2^2M_2 + \frac{7}{9}g_1^2M_1, \tag{B.5}$$

$$8\pi^2\frac{dA_\tau}{dt} = 4h_\tau^2A_\tau + 3h_D^2A_D + 3g_2^2M_2 + 3g_1^2M_1. \tag{B.6}$$

For the soft supersymmetry breaking mass parameters we have

$$8\pi^2\frac{dM_Q^2}{dt} = h_U^2\left(m_{H_2}^2 + M_Q^2 + M_U^2 + A_U^2\right) + h_D^2\left(m_{H_1}^2 + M_Q^2 + M_D^2 + A_D^2\right) - \frac{16}{3}g_3^2M_3^2 - 3g_2^2M_2^2 - \frac{1}{9}g_1^2M_1^2 + \frac{1}{6}\,g_1^2\mathcal{S}, \tag{B.7}$$

$$8\pi^2\frac{dM_U^2}{dt} = 2h_U^2\left(m_{H_2}^2 + M_Q^2 + M_U^2 + A_U^2\right) - \frac{16}{3}g_3^2M_3^2 - \frac{16}{9}g_1^2M_1^2 - \frac{2}{3}\,g_1^2\mathcal{S}, \tag{B.8}$$

$$8\pi^2\frac{dM_D^2}{dt} = 2h_D^2\left(m_{H_1}^2 + M_Q^2 + M_D^2 + A_D^2\right) - \frac{16}{3}g_3^2M_3^2 - \frac{4}{9}g_1^2M_1^2 + \frac{1}{3}\,g_1^2\mathcal{S}, \tag{B.9}$$

$$8\pi^2\frac{dM_L^2}{dt} = h_\tau^2\left(m_{H_1}^2 + M_L^2 + M_R^2 + A_\tau^2\right) - 3g_2^2M_2^2 - g_1^2M_1^2 - \frac{1}{2}\,g_1^2\mathcal{S}, \tag{B.10}$$

$$8\pi^2\frac{dM_R^2}{dt} = 2h_\tau^2\left(m_{H_1}^2 + M_L^2 + M_R^2 + A_\tau^2\right) - 4g_1^2M_1^2 + g_1^2\mathcal{S}, \tag{B.11}$$

$$8\pi^2\frac{dm_{H_2}^2}{dt} = 3h_U^2\left(m_{H_2}^2 + M_Q^2 + M_U^2 + A_U^2\right) - 3g_2^2M_2^2 - g_1^2M_1^2 + \frac{1}{2}\,g_1^2\mathcal{S}, \tag{B.12}$$

$$8\pi^2\frac{dm_{H_1}^2}{dt} = 3h_D^2\left(m_{H_1}^2 + M_Q^2 + M_D^2 + A_D^2\right) + h_\tau^2\left(m_{H_1}^2 + M_L^2 + M_R^2 + A_\tau^2\right) - 3g_2^2M_2^2 - g_1^2M_1^2 - \frac{1}{2}\,g_1^2\mathcal{S}, \tag{B.13}$$

where

$$\mathcal{S} = m_{H_2}^2 - m_{H_1}^2 + M_Q^2 - 2M_U^2 + M_D^2 - M_L^2 + M_R^2\,. \tag{B.14}$$

For the bilinear terms in the superpotential we get

$$16\pi^2\frac{d\mu}{dt} = \mu\left(3h_U^2 + 3h_D^2 + h_\tau^2 - 3g_2^2 - g_1^2\right), \tag{B.15}$$

$$16\pi^2\frac{d\epsilon_3}{dt} = \epsilon_3\left(3h_U^2 + h_\tau^2 - 3g_2^2 - g_1^2\right), \tag{B.16}$$

and for the corresponding soft breaking terms

$$8\pi^2\frac{dB}{dt} = 3h_U^2A_U + 3h_D^2A_D + h_\tau^2A_\tau + 3g_2^2M_2 + g_1^2M_1, \tag{B.17}$$

$$8\pi^2\frac{dB_2}{dt} = 3h_U^2A_U + h_\tau^2A_\tau + 3g_2^2M_2 + g_1^2M_1. \tag{B.18}$$

The g_i are the $SU(3) \times SU(2) \times U(1)$ gauge couplings and the M_i are the corresponding soft breaking gaugino masses.

References

[1] A. Chamseddine, R. Arnowitt, P. Nath, Phys. Rev. Lett. 49 (1982) 970;
R. Barbieri, S. Ferrara, C. Savoy, Phys. Lett. B 119 (1982) 343;
L.J. Hall, J. Lykken, S. Weinberg, Phys. Rev. D 27 (1983) 2359.

[2] M. Dine, A. Nelson, Phys. Rev. D 48 (1993) 1277;
M. Dine, A. Nelson, Y. Shirman, Phys. Rev. D 51 (1995) 1362;
M. Dine, A. Nelson, Y. Nir, Y. Shirman, Phys. Rev. D 53 (1996) 2658.

[3] L. Randall, R. Sundrum, Nucl. Phys. B 557 (1999) 79;
G. Giudice, M. Luty, H. Murayama, R. Rattazzi, JHEP 9812 (1998) 027.

[4] T. Gherghetta, G.F. Giudice, J.D. Wells, Nucl. Phys. B 559 (1999) 27.

[5] A. Pomarol, R. Rattazzi, JHEP 9905 (1999) 013;
Z. Chacko, M.A. Luty, I. Maksymyk, E. Ponton, JHEP 0004 (2000) 001;
E. Katz, Y. Shadmi, Y. Shirman, JHEP 9908 (1999) 015;
M.A. Luty, R. Sundrum, Phys. Rev. D 62 (2000) 035008;
J.A. Bagger, T. Moroi, E. Poppitz, JHEP 0004 (2000) 009;
I. Jack, D.R.T. Jones, Phys. Lett. B 482 (2000) 167;
M. Kawasaki, T. Watari, T. Yanagida, Phys. Rev. D 63 (2001) 083510.

[6] T. Moroi, L. Randall, Nucl. Phys. B 570 (2000) 455;
G.D. Kribs, Phys. Rev. D 62 (2000) 015008;
S. Su, Nucl. Phys. B 573 (2000) 87;
R. Rattazzi, A. Strumia, J.D. Wells, Nucl. Phys. B 576 (2000) 3;
M. Carena, K. Huitu, T. Kobayashi, Nucl. Phys. B 592 (2001) 164;
H. Baer, M.A. Díaz, P. Quintana, X. Tata, JHEP 0004 (2000) 016;
D.K. Ghosh, P. Roy, S. Roy, JHEP 0008 (2000) 031;
U. Chattopadhyay, D.K. Ghosh, S. Roy, Phys. Rev. D 62 (2000) 115001;
H. Baer, J.K. Mizukoshi, X. Tata, Phys. Lett. B 488 (2000) 367.

[7] J.L. Feng, T. Moroi, Phys. Rev. D 61 (2000) 095004.

[8] B.C. Allanach, A. Dedes, JHEP 0006 (2000) 017.

[9] B. Allanach et al., hep-ph/9906224;
B. Allanach et al., J. Phys. G 24 (1998) 421.

[10] M.C. Gonzalez-García, M. Maltoni, C. Peña-Garay, J.W.F. Valle, Phys. Rev. D 63 (2001) 033005;
J.N. Bahcall, P.I. Krastev, A.Yu. Smirnov, JHEP 0105 (2001) 015.

[11] Y. Fukuda et al., Super-Kamiokande Collaboration, Phys. Rev. Lett. 81 (1998) 1562;
Y. Fukuda et al., Super-Kamiokande Collaboration, Phys. Lett. B 433 (1998) 9;
Y. Fukuda et al., Super-Kamiokande Collaboration, Phys. Lett. B 436 (1998) 33.

[12] F. de Campos, O.J.P. Éboli, M.A. García-Jareño, J.W.F. Valle, Nucl. Phys. B 546 (1999) 33;
R. Kitano, K. Oda, Phys. Rev. D 61 (2000) 113001;
D.E. Kaplan, A.E. Nelson, JHEP 0001 (2000) 033;
C.-H. Chang, T.-F. Feng, Eur. Phys. J. C 12 (2000) 137;
M. Frank, Phys. Rev. D 62 (2000) 015006;
F. Takayama, M. Yamaguchi, Phys. Lett. B 476 (2000) 116;
K. Choi, E.J. Chun, K. Hwang, Phys. Lett. B 488 (2000) 145;
J.M. Mira, E. Nardi, D.A. Restrepo, J.W.F. Valle, Phys. Lett. B 492 (2000) 81.
[13] R. Hempfling, Nucl. Phys. B 478 (1996) 3.
[14] J.C. Romão, M.A. Díaz, M. Hirsch, W. Porod, J.W.F. Valle, Phys. Rev. D 61 (2000) 071703;
M. Hirsch, M.A. Díaz, W. Porod, J.C. Romão, J.W.F. Valle, Phys. Rev. D 62 (2000) 113008.
[15] T. Banks, Y. Grossman, E. Nardi, Y. Nir, Phys. Rev. D 52 (1995) 5319;
A.S. Joshipura, M. Nowakowski, Phys. Rev. D 51 (1995) 2421;
G. Bhattacharyya, D. Choudhury, K. Sridhar, Phys. Lett. B 349 (1995) 118;
M. Nowakowski, A. Pilaftsis, Nucl. Phys. B 461 (1996) 19;
A.Yu. Smirnov, F. Vissani, Nucl. Phys. B 460 (1996) 37;
J.C. Romão, F. de Campos, M.A. García-Jareño, M.B. Magro, J.W.F. Valle, Nucl. Phys. B 482 (1996) 3;
B. de Carlos, P.L. White, Phys. Rev. D 54 (1996) 3427;
B. de Carlos, P.L. White, Phys. Rev. D 55 (1997) 4222;
H. Nilles, N. Polonsky, Nucl. Phys. B 484 (1997) 33.
[16] A. Santamaria, J.W.F. Valle, Phys. Lett. B 195 (1987) 423;
A. Santamaria, J.W.F. Valle, Phys. Rev. Lett. 60 (1988) 397;
A. Santamaria, J.W.F. Valle, Phys. Rev. D 39 (1989) 1780.
[17] M.A. Díaz, J.C. Romão, J.W.F. Valle, Nucl. Phys. B 524 (1998) 23.
[18] A. Akeroyd, M.A. Díaz, J. Ferrandis, M.A. García-Jareño, J.W.F. Valle, Nucl. Phys. B 529 (1998) 3;
M.A. Díaz, J. Ferrandis, J.C. Romão, J.W.F. Valle, Phys. Lett. B 453 (1999) 263;
A.G. Akeroyd, M.A. Díaz, J.W.F. Valle, Phys. Lett. B 441 (1998) 224;
M.A. Díaz, E. Torrente-Lujan, J.W.F. Valle, Nucl. Phys. B 551 (1999) 78;
M.A. Díaz, J. Ferrandis, J.C. Romão, J.W.F. Valle, Nucl. Phys. B 590 (2000) 3;
M.A. Díaz, D.A. Restrepo, J.W.F. Valle, Nucl. Phys. B 583 (2000) 182;
M.A. Díaz, J. Ferrandis, J.W.F. Valle, Nucl. Phys. B 573 (2000) 75.
[19] M. Frank, K. Huitu, Phys. Rev. D 64 (2001) 095015.
[20] M.A. Díaz, hep-ph/9802407.
[21] A.G. Akeroyd, C. Liu, J. Song, hep-ph/0107218.
[22] F. de Campos et al., in preparation.

4.3 Determinação dos parâmetros associados aos modelos

Os parâmetros de quebra de paridade R são calculados nos modelos citados, da mesma forma como no caso mSUGRA. Para tanto utilizamos o código SPheno, com a expansão para o caso de quebra de paridade R no cálculo do espectro de massa e larguras de decaimento das partículas. Os parâmetros RPV são calculados a baixas energias. Os termos bilineares no superpotencial formam um sistema fechado na evolução das equações do grupo de renormalização (RGE), que dependem do valor do parâmetro μ. Os parâmetros de quebra soft SUSY também formam um sistema fechado embora tenhamos que considerar contribuições a escalas mais altas de energia, semelhante ao caso dos parâmetros de massa dos escalares. A degenerescência entre $\tilde{\chi}_1^0$ e $\tilde{\chi}_1^+$ pode aparecer em modelos BRPV–mSUGRA, bem como nos modelos BRpV-AMSB, porém nesse caso os acoplamentos associados à quebra de paridade R tem pouca influência na massa dos parceiros supersimétricos. É importante o cálculo da massa do neutralino e chargino mais leve devido a degenerescência, e devido ao fato da diferença entre esses valores ter influência direta na vida média do chargino. Para tanto consideramos correções a 1 loop nas matrizes de massa dos neutrinos-neutralinos e leptons carregados-charginos. Para simular os eventos associados aos fundos, bem como ao sinal, integramos os resultados do SPheno ao PHYTIA. Ambos os códigos são abertos e utilizados na área. As versões atualizadas desses códigos, contendo correções, não alteram os resultados apresentados.

4.4 Os modelos BRpV e a Física de Neutrinos

O setor de neutrinos em modelos de física de partículas são de extremo interesse, assim como os resultados associados aos parâmetros que caracterizam tal setor, considerando-se a possibilidade do uso de dados de aceleradores para o estudo de parâmetros associados à Física de Neutrinos. As diferenças de massa para neutrinos solares e atmosféricos assim como os ângulos de mistura são muito estudados e discutidos na área de Física de Neutrinos. Além disso, os dados recentes sobre oscilação de neutrinos em reatores e aceleradores [KamLAND e MINOS] foram utilizados para melhorar os resultados sobre as diferenças de massa para neutrinos solares e atmosféricos. Essa diferença se reflete na ambigüidade no sinal da diferença de massa para neutrinos atmosféricos que permite duas possibilidades de hierarquia na sua massa, a normal ou a inversa. Consideramos o mecanismo conhecido para a geração de massa dos neutrinos, cuja característica é a pequena massa dos neutrinos quando comparada com a dos férmions carregados, chamado mecanismo see-saw. Entretanto, como a escala de energia associada a tal mecanismo é extremamente elevada, não é possível testá-lo. Por outro lado, como nesta classe de modelos a origem de massa dos neutrinos está associada a parâmetros cuja ordem de grandeza está na escala TeV, podem ser testados nos aceleradores em funcionamento. A quebra de paridade R em modelos supersimétricos na escala TeV terá como conseqüência, a geração de massa para os neutrinos e podem ser considerados como modelos efetivos. Alguns parâmetros do modelo podem ser determinados com a ajuda de resultados de estudos sobre neutrinos. As massas e as misturas de neutrinos podem ser expressas de forma adequada ao modelo se considerarmos as grandezas $\Lambda_i = \epsilon_i v_d + \mu v_i$ e ϵ_i está relacionado

com a matriz de mistura para a massa dos neutrinos a nível árvore. Dessa forma podemos utilizar resultados experimentais para estudar e buscar limites sobre a diferença de massa no caso de neutrinos solares e atmosféricos. Da mesma forma que em modelos mSUGRA com quebra de paridade R , em modelos BRpV-AMSB também podemos estudar as massas e misturas de neutrinos, assegurando que satisfazem as condições derivadas dos dados experimentais sobre neutrinos, assim como acomodam a relação de hierarquia nas massas. Em geral a diferença de massa e o ângulo de mistura para neutrinos atmosféricos estão associadas aos cálculos a nível árvore enquanto a diferença de massa e ângulo de mistura para neutrinos solares às correções radiativas. Nesses modelos, os acoplamentos que dão origem às massas dos neutrinos também são os responsáveis pelas propriedades de decaimento do neutralino. Isso significa que há uma conexão entre a física dos neutralinos e os parâmetros de mistura dos neutrinos. Nesse caso, as taxas de decaimento dos neutralinos estão relacionadas com os ângulos de mistura dos neutrinos. Especificamente, há relações bem conhecidas entre o ângulo de mistura para neutrinos atmosféricos, a taxa de decaimento do neutralino em W e tau e em W e muons. Desse modo, medir as taxas de decaimento do neutralino, como se espera que seja possível no LHC, será útil para se impor restrições sobre modelos tais como os discutidos acima. Do mesmo modo que em modelos mSUGRA, a intensidade do acoplamento do termo de quebra de paridade R é pequena, porém suficientemente grande para se manifestar nos decaimentos que podem ser observados no LHC. Uma característica diferente dos modelos do tipo mSUGRA é a quase degenerescência entre o neutralino mais leve e o chargino mais leve. Assim, o chargino também terá uma vida media grande porém, ele se desintegrará antes de deixar o detector. Tanto o chargino quanto o neutralino apresentam como

característica de observação os vértices deslocados. A diferença entre os dois modelos considerados é que em mSUGRA apenas os neutralinos apresentam tais vértices. Um problema estudado relaciona a precisão com a qual é possível medir as taxas de decaimento do neutralino (quando o neutralino for a LSP) e como correlacionar tais resultados com os ângulos de mistura para neutrinos. Cabe ressaltar que não é apenas em modelos com quebra de paridade R que o sinal de vértice deslocado é a característica principal. Modelos em Física de Neutrinos, como o See-saw tipo III também apresenta a mesma característica e é possível realizar o estudo de tais modelos em face aos resultados experimentais. Uma vez realizado o referido estudo, à luz da descoberta do bóson de Higgs e conhecidos os resultados para os limites sobre a massa e ângulos de mistura dos neutrinos, é importante estabelecer o limite inverso, isto é, qual o limite no valor da taxa de decaimento para os neutralinos, que possibilitariam entender um pouco mais sobre a hierarquia normal ou inversa na massa dos neutrinos. Tal trabalho ainda está por ser realizado.

PHYSICAL REVIEW D **82,** 075002 (2010)

Probing neutrino oscillations in supersymmetric models at the Large Hadron Collider

F. de Campos,[1,*] O. J. P. Éboli,[2,†] M. Hirsch,[3,‡] M. B. Magro,[2,4,§] W. Porod,[5,3,‖] D. Restrepo,[6,¶] and J. W. F. Valle[3,**]

[1]*Departamento de Física e Química, Universidade Estadual Paulista, Guaratinguetá, SP, Brazil*
[2]*Instituto de Física, Universidade de São Paulo, São Paulo, SP, Brazil*
[3]*AHEP Group, Instituto de Física Corpuscular—C.S.I.C./Universitat de València, Edificio Institutos de Paterna, Apartado Postal 22085, E–46071 Valencia, Spain*
[4]*Centro Universitário Fundação Santo André, Santo André, SP, Brazil*
[5]*Institut für Theoretische Physik und Astronomie, Universität Würzburg, Germany*
[6]*Instituto de Física, Universidad de Antioquia, Colombia*

(Received 13 July 2010; published 6 October 2010)

The lightest supersymmetric particle may decay with branching ratios that correlate with neutrino oscillation parameters. In this case the CERN Large Hadron Collider (LHC) has the potential to probe the atmospheric neutrino mixing angle with sensitivity competitive to its low-energy determination by underground experiments. Under realistic detection assumptions, we identify the necessary conditions for the experiments at CERN's LHC to probe the simplest scenario for neutrino masses induced by minimal supergravity with bilinear R parity violation.

DOI: 10.1103/PhysRevD.82.075002 PACS numbers: 11.30.Pb, 12.60.Jv, 14.60.Pq, 95.30.Cq

I. INTRODUCTION

The CERN Large Hadron Collider (LHC) will provide high enough center-of-mass energy to probe directly the weak scale and the origin of mass [1–6]. In addition to its designed potential, here we show how LHC searches for new physics at the TeV region may provide an unexpected opportunity to probe neutrino properties, currently determined only in neutrino oscillation experiments [7], shedding light on some of the key issues in neutrino physics. We illustrate how this works in a class of supersymmetric models where the lepton number is broken, together with the so-called R parity symmetry [8]. Even when the latter holds as a symmetry at the Lagrangian level, as in some SO(10) unification schemes, R parity breaking may be driven spontaneously by a nonzero vacuum expectation value of an $SU(3) \otimes SU(2) \otimes U(1)$ singlet sneutrino [9–12]. In this case the low-energy theory is no longer described by the minimal supersymmetric standard model, but contains new R parity violating interactions [13–15]. The simplest realization of this scenario leads to an effective model with bilinear violation of R parity [16–20]. The latter constitutes the minimal way to break R parity in the minimal supersymmetric standard model and provides the simplest intrinsically supersymmetric way to induce neutrino masses [21–24]. Its main feature is that it relates lightest supersymmetric particle (LSP) decay properties and neutrino mixing angles [25–27].

Here we demonstrate that indeed, under realistic assumptions, the simplest scenario for neutrino masses in supersymmetry (SUSY) with bilinear violation of R parity can be tested at the LHC in a crucial way and potentially falsified. We identify the regions of minimal supergravity (mSUGRA) parameters, event reconstruction efficiencies, and luminosities where the LHC will be able to probe the atmospheric neutrino mixing angle with sensitivity competitive to its low-energy determination by underground experiments, both for 7 and 14 TeV center-of-mass energies.

For the sake of definiteness, we consider the minimal supergravity model supplemented with bilinear R parity breaking [22–24] added at the electroweak scale; we refer to this scenario as RmSUGRA. In this effective model one typically finds that the atmospheric scale is generated at tree level by a weak-scale neutralino-exchange seesaw, while the solar scale is induced radiatively [22]. The LSP lacks a symmetry to render it stable and, given the neutrino mass scales indicated by oscillation experiments, typically decays inside the LHC detectors [22,23,25].[1] As an illustration we depict the neutralino LSP decay length in Fig. 1. We can see from Fig. 1 that the expected decay lengths are large enough to be experimentally resolved, leading to displaced vertex events [33,34].

More strikingly, one finds that in such a RmSUGRA model one has a strict correlation between neutralino decay properties measurable at high-energy collider experiments and neutrino mixing angles determined in low-energy neutrino oscillation experiments, that is,

*camposc@feg.unesp.br
†eboli@fma.if.usp.br
‡hirsch@ific.uv.es
§magro@fma.if.usp.br
‖porod@physik.uni-wuerzburg.de
¶restrepo@uv.es
**valle@ific.uv.es

[1]We may add, parenthetically, that such schemes require a different type of dark matter particle, such as the axion [28]. Variants with other forms of supersymmetric dark matter, such as the gravitino [29–32], are also possible.

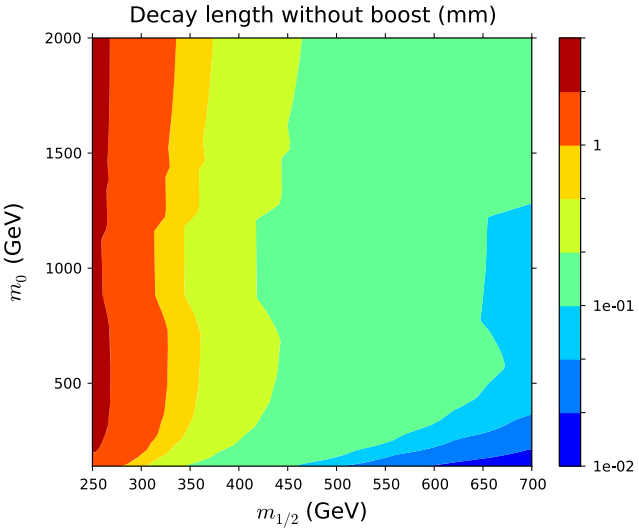

FIG. 1 (color online). $\tilde{\chi}_1^0$ decay length in the plane m_0, $m_{1/2}$ for $A_0 = -100$ GeV, $\tan\beta = 10$, and $\mu > 0$.

$$\tan^2\theta_{\rm atm} \simeq \frac{\mathrm{BR}(\tilde{\chi}_1^0 \to \mu^\pm W^\mp)}{\mathrm{BR}(\tilde{\chi}_1^0 \to \tau^\pm W^\mp)}. \quad (1)$$

The derivation of Eq. (1) can be found in [25]. In short, the relation between the neutralino decay branching ratio and the low-energy neutrino angle in the bilinear model can be understood in the following way. At tree-level in RmSUGRA the neutrino mass matrix is given by [22]

$$m_{\rm eff} = \frac{M_1 g^2 + M_2 g'^2}{4\det(\mathcal{M}_{\chi^0})} \begin{pmatrix} \Lambda_e^2 & \Lambda_e\Lambda_\mu & \Lambda_e\Lambda_\tau \\ \Lambda_e\Lambda_\mu & \Lambda_\mu^2 & \Lambda_\mu\Lambda_\tau \\ \Lambda_e\Lambda_\tau & \Lambda_\mu\Lambda_\tau & \Lambda_\tau^2 \end{pmatrix}, \quad (2)$$

where $\Lambda_i = \mu v_i + v_D \epsilon_i$ and ϵ_i and v_i are the bilinear superpotential parameters and scalar neutrino vacuum expectation values, respectively. Equation (2) is diagonalized by two angles; the relevant one for this discussion is the angle $\tan\theta_{23} = -\frac{\Lambda_\mu}{\Lambda_\tau}$. One can understand this tree-level mass as a seesaw-type neutrino mass with the right-handed neutrino and the Yukawa couplings of the ordinary seesaw replaced by the neutralinos of the minimal supersymmetric standard model and couplings of the form $c\Lambda_i$, where c is some combination of (generation independent) parameters. These couplings, which determine (the generation structure of) the neutrino mass matrix, also determine the couplings $\chi_i^0 - l_i^\pm - W^\mp$ and $\chi_i^\pm - \nu_i - W^\mp$ [25]. Taking the ratio of decays to different generations the prefactors c drop out and one finds Eq. (1), when the angle $\tan\theta_{23}$ is identified with the atmospheric neutrino angle. One-loop corrections tend to modify this relation, but as long as the loop corrections are smaller than the tree-level neutrino mass, Eq. (1) is a good approximation [25].

In other words, as seen in Fig. 2, the LSP decay pattern is predicted by the low-energy measurement of the atmospheric angle [21,25], currently determined by underground low-energy neutrino experiments [7], as

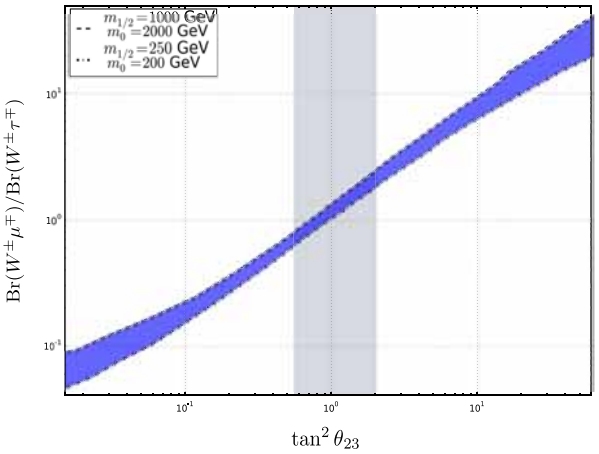

FIG. 2 (color online). Ratio of $\tilde{\chi}_1^0$ decay branching ratios, $\mathrm{Br}(\tilde{\chi}_1^0 \to \mu q'\bar{q})$ over $\mathrm{Br}(\tilde{\chi}_1^0 \to \tau q'\bar{q})$, in terms of the atmospheric angle in bilinear R parity violation [25]. The shaded bands include the variation of the model parameters in such a way that the neutrino masses and mixing angles fit the required values within 3σ.

$$\sin^2\theta_{\rm atm} = 0.50^{+0.07}_{-0.06},$$

the 2 and 3 σ ranges being 0.39–0.63 and 0.36–0.67, respectively.

In this paper we show how a high-energy measurement of LSP decay branching ratios at the LHC allows for a redetermination of $\theta_{\rm atm}$ and hence a clear test of the model. We provide quantitative estimates of how well this ratio of branchings should be measured at LHC in order to be competitive with current oscillation measurements. This issue has already been addressed but only at the parton level, using some semirealistic acceptance and reconstruction cuts, and for just one specific mSUGRA point [35].

II. FRAMEWORK OF OUR ANALYSIS

Our goal is to present a more detailed analysis of the LHC potential to measure the LSP branching ratios required to test the relation shown in Eq. (1), going beyond the approximations made in the previous work of Ref. [35]. The generation of the supersymmetric spectrum and decays in the scope of the RmSUGRA model was carried out using the SPHENO package [36].[2] The event generation was done employing PYTHIA [37] with the RmSUGRA particle properties being passed into it in the SUSY Les Houches accord format [38,39]. Jets were defined using the subroutine PYCELL with a cone size of $\Delta R = 0.4$.

A striking property of RmSUGRA models is the existence of displaced vertices associated to the LSP decay [34]. We use the detached vertices to probe the LSP

[2]An updated version including bilinear R parity violation can be obtained at http://www.physik.uni-wuerzburg.de/~porod/SPheno.html.

branching ratio relation Eq. (1). In order to mimic the LHC potential to study displaced vertices we use a toy detector based on the ATLAS technical proposal [3].

We begin our analysis demanding that the events pass some basic requirements to guarantee that they will be triggered by the experimental collaborations. This is done because the LHC experiments have not defined so far any specific strategy to trigger displaced vertices with such high invariant mass; therefore, we restricted our analysis to events that would be accepted by the ongoing analyses. We accept events passing at least one of the following requirements, denoted as cut **C1**:

(1) the event has one isolated electron or a photon with $p_T > 20$ GeV;
(2) the event has one isolated muon with $p_T > 6$ GeV;
(3) the event has two isolated electrons or photons with $p_T > 15$ GeV;
(4) the event has one jet with $p_T > 100$ GeV;
(5) the event has missing transversal energy in excess of 100 GeV.

Next, in cut **C2**, we require that at least one of the neutralinos in the event decays beyond the primary vertex point, that is, outside an ellipsoid [34]

$$\left(\frac{x}{5\delta_{xy}}\right)^2 + \left(\frac{y}{5\delta_{xy}}\right)^2 + \left(\frac{z}{5\delta_z}\right)^2 = 1, \tag{3}$$

where the z axis is taken along the beam direction. We made a conservative assumption, since we are not performing a detailed detector simulation, that the ellipsoid dimensions are 5 times the ATLAS expected resolutions in the transverse plane ($\delta_{xy} = 20\mu$m) and in the beam direction ($\delta_z = 500\mu$m), in order to ensure that the neutralino displaced vertex is distant of the primary vertex. We also demand that all tracks must be initiated inside the pixel inner detector within a radius of 550 mm and z axis length of 800 mm. A detached vertex complying with these requirements we called *signal vertex*.

In order to check relation Eq. (1) we looked for detached vertices presenting a W associated to them and we must isolate the LSP decays into $W\mu$ and $W\tau$. Moreover we consider only hadronic final states of the W as a necessary condition for the identification of the lepton flavor. In cut **C3**, which is designed for the W reconstruction, we require two jets with charged tracks intersecting the neutralino resolution ellipsoid, and invariant mass between 60 and 100 GeV. In order to be sure that the W reconstruction is clean, we further impose that the axes of other jets of the event to be outside of a cone $\Delta R = 0.8$ of the W jets' axes. Note that this cut should eliminate standard model backgrounds coming from displaced vertices associated to b's or τ's. To guarantee a high quality in the reconstruction of the displaced vertices we impose that the W decay jets must be central, having pseudorapidities $|\eta| < 2.5$; this constitutes our cut **C4**. The events passing the above requirements most probably originate from LSP decay, having basically no sizable standard model background, except for instrumental backgrounds and beam-gas interactions.

A signal vertex is classified as originating from the LSP decay into a μW pair if it presents a $\mu^{\pm}$ and a hadronically decaying W stemming from the displaced vertex with transverse momentum $p_T > 6$ GeV and $|\eta| < 2.5$. In the $\tau^{\pm}$ case we demanded that the $\tau^{\pm}$ associated to a detached W possesses $p_T > 20$ GeV and $|\eta| < 2.5$. These requirements are called **C5**.

Detecting taus is somewhat more complicated than detecting muons, so one needs to be more careful in reconstructing the τW pair displaced vertex. The following criteria, denoted **C6**, are used to separate the detached vertices exhibiting a $\tau^{\pm}$ through its 1- and 3-prong decay modes. We check also that the secondary displaced vertex from tau decay does not spoil the signal vertex; i.e., we verify that the tau decay products point towards the LSP decay vertex within the experimental resolution. We define the neutralino resolution ellipsoid as the ellipsoid centered at the displaced vertex position of neutralino, v_1, with axes $\delta_{xy} = 12\mu$m and $\delta_z = 77\mu$m based on Ref. [3]. Let $\mathbf{p}_{\text{prong}}$ be the momentum of either 1-prong tau decay or the sum of momenta of the 3-prong decays. Let also v_2 be the position of the secondary vertex coming from τ. We verify whether the line along $\mathbf{p}_{\text{prong}}$, crossing v_2 intersects the neutralino resolution ellipsoid. For this we require that for each τ the discriminant of quadratic equation for parameter t

$$\sum_i^2 \left(\frac{p^i_{\text{prong}} t + v^i_2 - v^i_1}{\delta_{xy}}\right)^2 + \left(\frac{p^3_{\text{prong}} t + v^3_2 - v^3_1}{\delta_z}\right)^2 - 1 = 0 \tag{4}$$

be equal to or greater than zero. In previous [35] analysis only 3-prong tau decays modes were considered.

An additional cut **C7** was applied to 3-prong tau events i.e., we also require that one of the prongs has a transverse momentum $p_T > 9$ GeV, while the other two have $p_T > 2$ GeV. In addition we check if all prongs lie within a cone radius of $\Delta R < 0.2$ around the tau direction obtained from the prongs' tracks.

Finally we require that the signal lepton (μ or τ) be isolated: cut **C8**. μ isolation demands that there are no other tracks whose total transverse energy satisfies $E_T > 5$ GeV within a cone $\Delta R > 0.3$. The τ was required to be isolated using the same criteria as for the muon, but for an annulus of outer radius $\Delta R = 0.4$ and inner radius $\Delta R = 0.1$. Isolation of the leptons is a needed requirement to eliminate events presenting leptons generated inside jets and constitutes an important cut to reduce potential backgrounds.

III. RESULTS AND DISCUSSION

In order to access the effects of the above defined cuts **C1**–**C8** we present detailed information on their effects for the mSUGRA SPS1a benchmark point [40] characterized

by $m_{1/2} = 250$ GeV, $m_0 = 100$ GeV, $A_0 = -100$ GeV, $\tan\beta = 10$, and $\mathrm{sgn}(\mu) = +1$. This allows us to compare our results with the one previously obtained in [35]. For the default solution of SPHENO to the neutrino masses and mixings, the relevant neutralino branching ratios are

$$\begin{aligned}
\mathrm{BR}(\tilde{\chi}_1^0 \to W^\pm \mu^\mp) &= 5.4\%, \\
\mathrm{BR}(\tilde{\chi}_1^0 \to W^\pm \tau^\mp) &= 6.2\%, \\
\mathrm{BR}(\tilde{\chi}_1^0 \to Z\nu) &= 1.2\%, \\
\mathrm{BR}(\tilde{\chi}_1^0 \to e^\pm \tau^\mp \nu) &= 11.5\%, \\
\mathrm{BR}(\tilde{\chi}_1^0 \to \mu^\pm \tau^\mp \nu) &= 24.3\%, \\
\mathrm{BR}(\tilde{\chi}_1^0 \to \tau^\pm \tau^\mp \nu) &= 36.4\%, \\
\mathrm{BR}(\tilde{\chi}_1^0 \to b\bar{b}\nu) &= 14.7\%,
\end{aligned} \tag{5}$$

with the R parity parameters being

$$\begin{aligned}
\epsilon_1 &= 0.0405 \text{ GeV}, & \epsilon_2 &= -0.0590 \text{ GeV}, \\
\epsilon_3 &= 0.0506 \text{ GeV}, & \upsilon_1 &= -0.0027 \text{ GeV}, \\
\upsilon_2 &= 0.0042 \text{ GeV}, & \upsilon_3 &= -0.0033 \text{ GeV}.
\end{aligned}$$

Furthermore, for this choice of parameters the neutralino decay length is $c\tau = 1.1$ mm, and it travels an average of 4.4 mm in the laboratory.

From Table I we see that the vast majority of the events pass the trigger requirements **C1**, as expected. For the SPS1a SUSY point, the LSP decay length is sufficiently long to guarantee that a sizeable fraction of its decays take place away from the primary vertex; this reflects as a high efficiency for passing the cut **C2**. We have focused our attention to events presenting a $W^\pm$ decaying into two jets through **C3**. It is interesting to notice that 63% of the W hadronic decays are in the form of two jets. Additional suppression of the signal by **C3** comes from the matching of the sum of momenta of the charged tracks pointing to the detached vertex and the jets reconstructed using PYTHIA. To further illustrate the W decay, we present in Fig. 3 the jet-jet invariant mass distribution. As we can see, this distribution is clearly peaked around the W mass and a good fraction of the two jets reconstructed as associated to the LSP decay pass the cut **C3**. The observed high efficiency of cut **C4** shows that the W's produced in the LSP decay are rather central.

TABLE I. Fraction of events passing the successive cuts **C1–C8** used for the event reconstruction at the SPS1a mSUGRA point.

Cut	N_μ	N_τ	$N_{\tau\to\mathrm{all}}^{1-\mathrm{prong}}$	$N_{\tau\to\mathrm{hadron}}^{1-\mathrm{prong}}$	$N_\tau^{3-\mathrm{prong}}$
C1	0.996	0.968	0.816	0.475	0.058
C2	0.923	0.898	0.757	0.440	0.055
C3	0.391	0.407	0.344	0.199	0.025
C4	0.369	0.385	0.325	0.188	0.024
C5	0.230	0.248	0.211	0.121	0.024
C6 + **C7**	0.230	0.078	0.057	0.033	0.014
C8	0.102	0.015	0.014	0.009	0.001

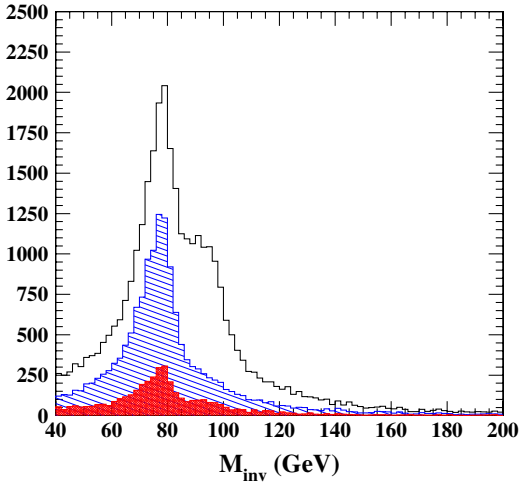

FIG. 3 (color online). From top to bottom: $\tilde{\chi}_1^0 \to jjX$ without cuts, with cut on lepton isolation (μ or τ), and with all other cuts leaving free the invariant mass range.

We also learn from Table I that detached vertices presenting a W possess around 60% of the time an energetic $\mu^\pm$ or $\tau^\pm$ complying with **C5**. Moreover the cuts **C6** and **C7**, which ensure the quality of the τ reconstruction, reduce significantly the number of $W^\pm\tau^\mp$ events. Finally the isolation cut **C8** turns out to be quite important, significantly reducing the signal.

For the parameter point SPS1a, the expected efficiencies for the reconstruction of μW and τW decays are 0.107 and 0.0098, respectively, where in the last we have added 1- and 3-prong hadronic decays. When the τ decays into a μ and neutrinos, the event was computed as being a μW decay if the μ passes the cuts. This was included appropriately in our calculations. Taking into account the total SUSY production cross section (41 pb) at 14 TeV, an integrated luminosity of 100 fb^{-1}, and these efficiencies, we anticipate that the number of observed μW and τW events after cuts to be

$$N_\mu = 32\,000 \qquad N_\tau^{\mathrm{hadron}} = 3382,$$

where $N_\tau^{\mathrm{hadron}} = N_{\tau\to\mathrm{hadron}}^{1-\mathrm{prong}} + N_\tau^{3-\mathrm{prong}}$. Therefore, the statistical accuracy of the ratio $R = \mathrm{BR}(\tilde{\chi}_1^0 \to \mu^\pm W^\mp)/\mathrm{BR}(\tilde{\chi}_1^0 \to \tau^\pm W^\mp)$ is expected to be $\sigma(R)/R = \sqrt{1/N_\mu + 1/N_\tau} \approx 0.015$. In the case one takes into account only the three-prong decays of the taus, as done in Ref. [35], the statistical error of this ratio increases to ≈ 0.053. Moreover, as expected, there is a degradation of the accuracy in the determination of this ratio of branching ratios in a more realistic analysis; the result obtained in [35] is $\simeq 0.028$.

In the evaluation of the above efficiencies we have not taken into account multiple interactions at the LHC as

needed for the high luminosity run. Therefore, we reevaluated the detection efficiencies for muons and taus with multiple interactions switched on in PYTHIA. We found that these efficiencies were only slightly degraded by the occurrence of pileup; that is, we obtained that the efficiencies for muon reconstruction are reduced to 0.102 and for tau are 0.008 68 in hadronic mode and 0.000 94 in the 3-prong mode. In our analyses we took into account the effect of multiple interactions.

For the sake of comparison, we present a detailed analysis for a different mSUGRA point that is $m_{1/2} = 500$ GeV, $m_0 = 500$ GeV, $A_0 = -100$ GeV, $\tan\beta = 10$, and $\mathrm{sgn}(\mu) = +1$. Once again using SPHENO, we obtain that the neutralino branching ratios larger than 1% are

$$\begin{aligned}
\mathrm{BR}(\tilde{\chi}_1^0 \to W^{\pm}\mu^{\mp}) &= 22.9\%, \\
\mathrm{BR}(\tilde{\chi}_1^0 \to W^{\pm}\tau^{\mp}) &= 25.2\%, \\
\mathrm{BR}(\tilde{\chi}_1^0 \to Z\nu) &= 25.1\%, \\
\mathrm{BR}(\tilde{\chi}_1^0 \to \nu h^0) &= 16.9\%, \\
\mathrm{BR}(\tilde{\chi}_1^0 \to \tau^{\pm}\tau^{\mp}\nu) &= 3.4\%, \\
\mathrm{BR}(\tilde{\chi}_1^0 \to b\bar{b}\nu) &= 2.9\%,
\end{aligned}$$

and the corresponding R parity parameters are

$$\begin{aligned}
\epsilon_1 &= 0.1507 \text{ GeV}, & \epsilon_2 &= -0.1507 \text{ GeV}, \\
\epsilon_3 &= 0.1507 \text{ GeV}, & \upsilon_1 &= -0.0056 \text{ GeV}, \\
\upsilon_2 &= 0.0058 \text{ GeV}, & \upsilon_3 &= -0.0054 \text{ GeV}.
\end{aligned}$$

As we can see, the neutralino LSP decays are dominated by the two-body ones, in contrast with the SPS1a point where the three-body decays mediated by light scalars are dominant. Because of its heavier spectrum, the total SUSY production for this parameter point is smaller than the SPS1a one; however, the cross section loss is partially compensated by the higher branching ratios into μW and τW.

The total cross section for this case is 832.0 fb and our analyses indicate that the reconstruction efficiency for μW decays is 0.203 while the τW decays are reconstructed with an efficiency of 0.035, where we did not take into account pileup. The inclusion of this effect leads to a tiny reduction of the reconstruction efficiencies that become 0.199 for μW and 0.033 for τW. On the other hand the efficiency for reconstructing a τW event in the 3-prong mode is 0.012. Notice that these efficiencies are larger for this mSUGRA point than for the SPS1a because the neutralino is heavier and, consequently, its decay products are more energetic and pass the cuts more easily. The expected total number of reconstructed events after cuts for this SUSY point is $N_{\mu} = 5171$ and $N_{\tau}^{\mathrm{hadron}} = 933$ where we have included the pileup effects. Therefore, the expected statistical error on the ratio R becomes ≈ 0.036, or ≈ 0.056 when we only use 3-prong taus as in [35]. As we can see, the statistical error on the ratio R increases as $m_{1/2}$ (LSP mass) increases due to the reduction of the SUSY production cross section despite the increase in the detection efficiencies.

We evaluated the reconstruction efficiencies as a function of $m_0 \otimes m_{1/2}$ for $A_0 = -100$ GeV, $\tan\beta = 10$, and $\mathrm{sgn}(\mu) = +1$ and our results are depicted in Fig. 4. As we can see from the left panel of this figure, the μW decays exhibit a high reconstruction efficiency, i.e., between 10% and 20%, in a large area of the parameter space, degrading only at large $m_{1/2}$. On the other hand, the τW reconstruction (see right panel of Fig. 4) is at most 3.5%, indicating that the statistical error on the ratio R is going to be dominated by these events.

We present in Fig. 5 the attainable precision $\sigma(R)/R$ with which the correlation R can be measured as a function of $m_0 \otimes m_{1/2}$ for $A_0 = -100$ GeV, $\tan\beta = 10$, and $\mathrm{sgn}(\mu) = +1$ for an integrated luminosity of 100 fb^{-1} and a

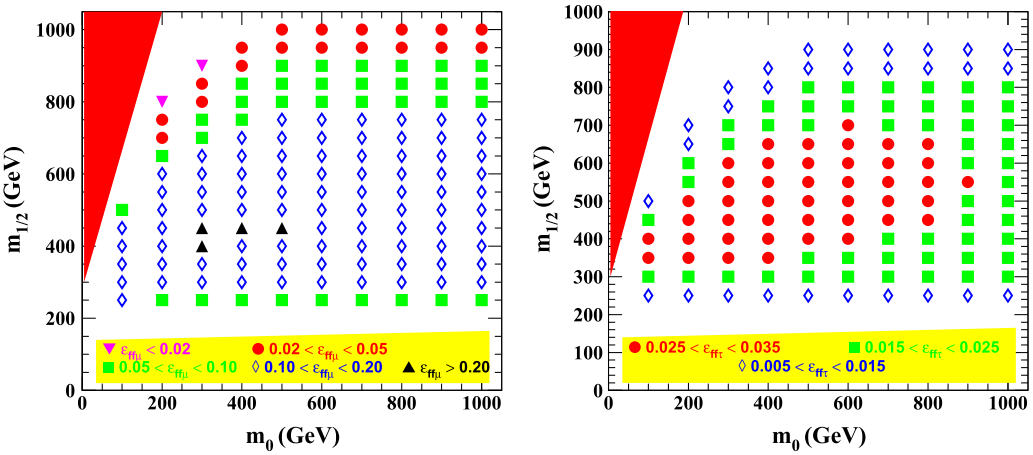

FIG. 4 (color online). Reconstruction efficiencies of μW (left panel) and τW events (right panel) as a function of $m_0 \otimes m_{1/2}$ for $A_0 = -100$ GeV, $\tan\beta = 10$, and $\mathrm{sgn}(\mu) = +1$ including the effect of pileup. The red (dark shaded) area corresponds to the region where stau is the LSP, while the yellow (light shaded) area represents the region excluded by LEP.

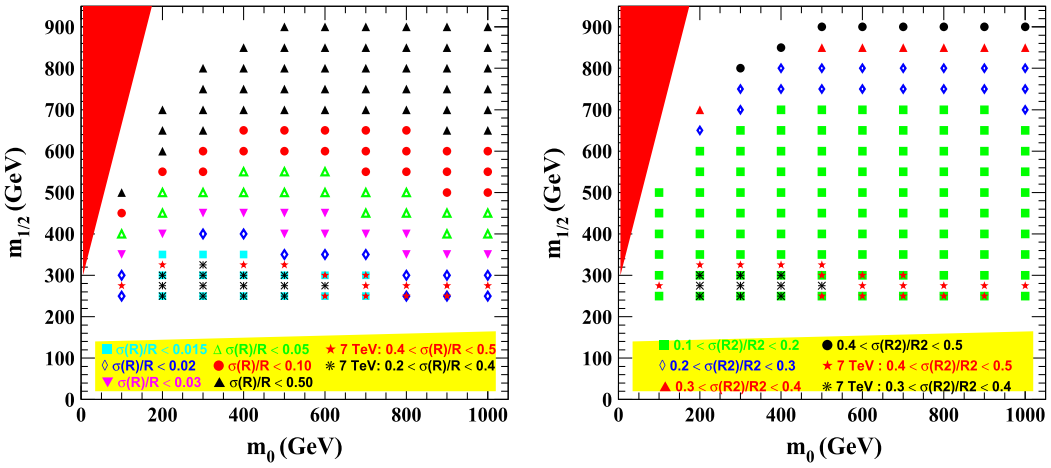

FIG. 5 (color online). Precision in the determination of the ratio R in the plane $m_{1/2} \times m_0$ for a luminosity of 100 fb^{-1}, center-of-mass energy of 14 TeV, $A_0 = -100$ GeV, $\tan\beta = 10$, and $\mathrm{sgn}(\mu) = +1$. In the right (left) panel we did (not) include a possible systematic uncertainty in the extraction of the efficiencies for the channels μW and τW. The stars in the right panel represent the results for the 7 TeV run with an integrated luminosity of 1 fb^{-1}. The shaded areas represent the same as in Fig. 4.

center-of-mass energy of 14 TeV. We require in all plots that at least 5 events of reconstructed taus are observed. In the left panel of this figure we present the expected statistical error on the ratio R assuming no systematic errors on the determination of the reconstruction efficiencies, while in the right panel we consider a more conservative scenario, where we anticipate a systematic error of 10% in each of the reconstruction efficiencies. One can see from this panel that the precision drops as $m_{1/2}$ grows since the neutralino production rates from squark/gluino cascade decays also decrease with increasing $m_{1/2}$ values. Therefore, if the systematic errors of the efficiency determination are negligible, the LHC collaborations should be able to probe with a very good precision ($\lesssim 10\%$) the ratio R for $m_{1/2} \lesssim 650$ GeV, which corresponds to an LSP mass up to $\simeq 270$ GeV. The inclusion of systematic errors at the level assumed in the right panel of Fig. 5 increases the uncertainty in R; however, it is still possible to perform an accurate test of the RmSUGRA scenario.

Note that in Fig. 5 we also present results for the 7 TeV run of the LHC. For this case one can see that the LHC has a much more limited capability of probing the ratio R, since the reach of this run covers only up to $m_{1/2} \lesssim 300$ GeV. Still, although large, the statistical errors in this region $[0.3 \lesssim \sigma(R)/R \lesssim 0.5]$, due mainly to the small anticipated integrated luminosity, which we have taken to be 1 fb^{-1}, allow a determination of the atmospheric angle comparable to that obtained at low energies.

In the left panel of Fig. 6 we show the dependence of the attained precision as a function of the neutralino mass for

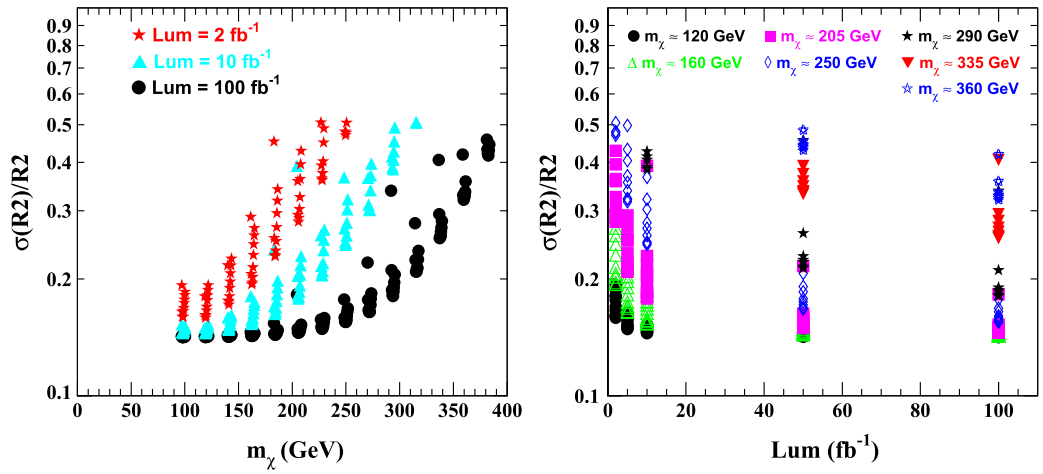

FIG. 6 (color online). The left panel displays the achievable precision in the ratio R as a function of the neutralino mass $m_{\tilde{\chi}_1^0}$ for luminosities of 2, 10, and 100 fb^{-1} at 14 TeV, whereas the right panel contains the foreseen statistical error on R as a function of the integrated luminosity for several LSP masses.

luminosities of 2, 10, and 100 fb^{-1}. For small neutralino masses the SUSY production cross section is large enough to guarantee that the statistical errors are small; therefore, the uncertainty on the ratio R is dominated by the assumed systematic errors on the reconstruction efficiencies, even for an integrated luminosity of 2 fb^{-1}. As the accumulated luminosity increases the LHC experiments will be able to probe higher neutralino masses; however, the precision worsens due to the increase of statistical errors. We can also see clearly that increasing the luminosity allows a more precise measurement of R as expected. Moreover, one can probe LSP masses up to 250 (320 or 370) GeV for an integrated luminosity of 2(10 or 100) fb^{-1}.

From the right panel of Fig. 6 we estimate the luminosity needed to measure R with a given precision for several LSP masses. For instance, let us consider $m_{\tilde{\chi}_1^0} = 250$ GeV. In this case R can only be measured with a precision $\sigma(R)/R \simeq 50\%$ with 2 fb^{-1}, while this error can be brought down to 20%, i.e., close to the limit set by the systematic uncertainties, with 50 fb^{-1}.

IV. CONCLUSIONS

We have demonstrated how the LHC may have the potential of probing neutrino mixing angles with sensitivity competitive to their low-energy determination by oscillation experiments. This analysis was carried out, for the sake of concreteness, in the simplest scenario for neutrino masses induced by minimal supergravity with R parity violation as framework. In this class of models, the smoking gun for the neutrino mass generation mechanism is the ratio of branching fractions of neutralino decaying into μW and τW, as this fraction is related to the atmospheric neutrino mixing angle in RmSUGRA models.

Under realistic detection assumptions we have made a detailed analysis of the reconstruction of neutralino decays, as well as of the cuts needed to characterize the signal. After that we determined the attainable precision on the measurements of the ratio R given in Eq. (1). Comparing with a previous parton level study, we improved the reconstruction efficiencies of muons as well as taus.

We showed that the 7 TeV run of the LHC will have a somewhat weak potential for probing the RmSUGRA model, since it is statistics limited. Still, precisions comparable to the low-energy determination should be reached. In contrast, a 14 TeV run with 100 fb^{-1} integrated luminosity will be able to probe a large fraction of the parameter space with a good precision, as seen in Fig. 5. In fact, our analyses suggest that the error on R will be dominated by the systematic ones on the reconstruction efficiencies of the decay μW and τW, with the statistical errors being under control.

In short, we find that in this case the atmospheric mixing angle may be probed relatively neatly. In fact, a determination of R within a given error translates into a prediction of the atmospheric mixing angle with an error of very similar size. Needless to say, what we have presented is only one example of a class of LSPs. There are other variant schemes based on alternative supersymmetry and/or R parity breaking, where other states emerge as LSP and similar correlations to other neutrino mixing angles appear [41–43]. These would, however, require separate dedicated studies. We encourage the particle detector groups ATLAS and CMS to add the test of such possibilities to their physics agenda, as this might lead to a tantalizing synergy between high-energy accelerator and low-energy nonaccelerator searches for new physics. Studies with the real LHC data may also make it possible to probe, at some level, the mass scale characterizing atmospheric neutrino oscillations, as well as the angle characterizing solar neutrino oscillations, an issue to be taken up separately.

ACKNOWLEDGMENTS

Work supported in part by Spanish grants FPA2008-00319/FPA, MULTIDARK Consolider CSD2009-00064, and PROMETEO/2009/091, by European network UNILHC, PITN-GA-2009-237920, by Conselho Nacional de Desenvolvimento Científico e Tecnológico (CNPq), and by Fundação de Amparo à Pesquisa do Estado de São Paulo (FAPESP). F. de Campos thanks USP and IFIC/C.S.I.C. for hospitality. M. B. M. thanks IFIC/C.S.I.C. for hospitality. W. P. is supported by the DFG, Project No. PO-1337/1-1, and by the Alexander von Humboldt Foundation. D. R. is partly supported by Sostenibilidad-UdeA/2009 grant.

[1] P. Nath *et al.*, Nucl. Phys. B, Proc. Suppl. **200-202**, 185 (2010).
[2] S. P. Martin, arXiv:hep-ph/9709356.
[3] ATLAS Collaboration, ATLAS inner detector: Technical design report. Report No. CERN-LHCC-97-16, Vol. 1.
[4] J. A. Aguilar-Saavedra *et al.*, Eur. Phys. J. C **46**, 43 (2006).
[5] G. L. Bayatian *et al.*, J. Phys. G **34**, 995 (2007).
[6] G. Aad *et al.* (ATLAS Collaboration), arXiv:0901.0512.
[7] T. Schwetz, M. Tortola, and J. W. F. Valle, New J. Phys. **10**, 113011 (2008); for a review see M. Maltoni *et al.*, New J. Phys. **6**, 122 (2004).
[8] R. Barbier *et al.*, Phys. Rep. **420**, 1 (2005).
[9] A. Masiero and J. W. F. Valle, Phys. Lett. B **251**, 273 (1990).
[10] J. C. Romao, C. A. Santos, and J. W. F. Valle, Phys. Lett. B **288**, 311 (1992).

[11] J. C. Romao, A. Ioannissyan, and J. W. F. Valle, Phys. Rev. D **55**, 427 (1997).
[12] For a recent review see G. Bhattacharyya and P. B. Pal, Phys. Rev. D **82** 055013 (2010).
[13] L. J. Hall and M. Suzuki, Nucl. Phys. **B231**, 419 (1984).
[14] G. G. Ross and J. W. F. Valle, Phys. Lett. **151B**, 375 (1985).
[15] J. R. Ellis *et al.*, Phys. Lett. **150B**, 142 (1985).
[16] M. A. Diaz, J. C. Romao, and J. W. F. Valle, Nucl. Phys. **B524**, 23 (1998).
[17] E. J. Chun, S. K. Kang, C. W. Kim, and U. W. Lee, Nucl. Phys. **B544**, 89 (1999).
[18] D. E. Kaplan and A. E. Nelson, J. High Energy Phys. 01 (2000) 033.
[19] F. Takayama and M. Yamaguchi, Phys. Lett. B **476**, 116 (2000).
[20] T. Banks, Y. Grossman, E. Nardi, and Y. Nir, Phys. Rev. D **52**, 5319 (1995).
[21] J. C. Romao, M. A. Diaz, M. Hirsch, W. Porod, and J. W. F. Valle, Phys. Rev. D **61**, 071703 (2000).
[22] M. Hirsch, M. A. Diaz, W. Porod, J. C. Romao, and J. W. F. Valle, Phys. Rev. D **62**, 113008 (2000); **65**, 119901 (2002).
[23] M. A. Diaz, M. Hirsch, W. Porod, J. C. Romao, and J. W. F. Valle, Phys. Rev. D **68**, 013009 (2003).
[24] M. Hirsch and J. W. F. Valle, New J. Phys. **6**, 76 (2004).
[25] W. Porod, M. Hirsch, J. C. Romao, and J. W. F. Valle, Phys. Rev. D **63**, 115004 (2001).
[26] S. Y. Choi, E. J. Chun, S. K. Kang, and J. S. Lee, Phys. Rev. D **60**, 075002 (1999).
[27] B. Mukhopadhyaya, S. Roy, and F. Vissani, Phys. Lett. B **443**, 191 (1998).
[28] E. J. Chun and H. B. Kim, Phys. Rev. D **60**, 095006 (1999).
[29] S. Borgani, A. Masiero, and M. Yamaguchi, Phys. Lett. B **386**, 189 (1996).
[30] F. Takayama and M. Yamaguchi, Phys. Lett. B **485**, 388 (2000).
[31] M. Hirsch, W. Porod, and D. Restrepo, J. High Energy Phys. 03 (2005) 062.
[32] F. Staub, W. Porod, and J. Niemeyer, J. High Energy Phys. 01 (2010) 058.
[33] F. de Campos *et al.*, Phys. Rev. D **71**, 075001 (2005).
[34] F. de Campos *et al.*, J. High Energy Phys. 05 (2008) 048.
[35] W. Porod and P. Skands, arXiv:hep-ph/0401077.
[36] W. Porod, Comput. Phys. Commun. **153**, 275 (2003).
[37] T. Sjostrand, S. Mrenna, and P. Skands, J. High Energy Phys. 05 (2006) 026.
[38] P. Skands *et al.*, J. High Energy Phys. 07 (2004) 036.
[39] B. Allanach *et al.*, Comput. Phys. Commun. **180**, 8 (2009).
[40] B. C. Allanach *et al.*, Eur. Phys. J. C **25**, 113 (2002).
[41] D. Restrepo, W. Porod, and J. W. F. Valle, Phys. Rev. D **64**, 055011 (2001).
[42] M. Hirsch, W. Porod, J. C. Romao, and J. W. F. Valle, Phys. Rev. D **66**, 095006 (2002).
[43] M. Hirsch and W. Porod, Phys. Rev. D **68**, 115007 (2003).

Published by Institute of Physics Publishing for SISSA/ISAS
Received: *April 25, 2003*
Revised: *September 22, 2003*
Accepted: *September 29, 2003*

Probing neutrino mass with multilepton production at the Tevatron in the simplest R-parity violation model

Mauricio Bernardino Magro,[a] **Fernando de Campos,**[b] **Oscar J.P. Éboli,**[a] **Werner Porod,**[c] **Diego Restrepo,**[d] **José W.F. Valle**[e]

[a] *Instituto de Física, Universidade de São Paulo, São Paulo, SP, Brazil*
[b] *Departamento de Física e Química, Universidade Estadual Paulista, Brazil*
[c] *Institut für Theoretische Physik, Universität Zürich, Zürich, Switzerland*
[d] *Instituto de Física, Universidad de Antioquia, Colombia*
[e] *Instituto de Física Corpuscular, C.S.I.C./Universitat de València Edificio Institutos de Paterna, Apt 22085, E-46071 València, Spain*
E-mail: magro@fma.if.usp.br, fernando@ift.unesp.br, eboli@fma.if.usp.br, porod@physik.unizh.ch, restrepo@uv.es, valle@ific.uv.es

Abstract: We analyse the production of multileptons in the simplest supergravity model with bilinear violation of R parity at the Fermilab Tevatron. Despite the small R-parity violating couplings needed to generate the neutrino masses indicated by current atmospheric neutrino data, the lightest supersymmetric particle is unstable and can decay inside the detector. This leads to a phenomenology quite distinct from that of the R-parity conserving scenario. We quantify by how much the supersymmetric multilepton signals differ from the R-parity conserving expectations, displaying our results in the $m_0 \otimes m_{1/2}$ plane. We show that the presence of bilinear R-parity violating interactions enhances the supersymmetric multilepton signals over most of the parameter space, specially at moderate and large m_0.

Keywords: Supersymmetry Phenomenology, Solar and Atmospheric Neutrinos, Beyond Standard Model.

http://jhep.sissa.it/archive/papers/jhep092003071/jhep092003071.pdf

JHEP09(2003)071

Contents

1. Introduction **1**

2. Main features of our BRpV model **2**

3. Signal, backgrounds, and selection cuts **6**

4. Conclusion **12**

1. Introduction

Supersymmetry (SUSY) provides a promising candidate for physics beyond the Standard Model (SM). The search for supersymmetric partners of the SM particles constitutes an important item in the agenda of current high energy colliders like the Tevatron, and future colliders like the CERN Large Hadron Collider or a linear e^+e^- collider. So far most of the effort in searching for supersymmetric signatures has been confined to the framework of R-parity conserving realizations [1]; see, however, ref. [2] and references therein.

Recent data on solar and atmospheric neutrinos give a robust evidence for neutrino conversions [3], probably the most profound discovery in particle physics in the recent years. It has been suggested long ago that neutrino masses and supersymmetry may be deeply tied together [4]. Indeed, SUSY models exhibiting R-parity violation can lead to neutrino masses and mixings [5] in agreement with the current solar and atmospheric neutrino data. Furthermore, the simplest possibility is bilinear R-parity violation [6, 7] which may arise as an effective description of a spontaneous R-parity violation scenario [8], or from some suitable *ab initio* symmetries [9].

It is interesting to notice that neutrino mass models based on R-parity violation can be tested at colliders [10, 11, 12]. In this work, we study the production of multileptons ($\geq 3\ell$ with $\ell = e$ or μ) at the Fermilab Tevatron within the framework of the simplest supergravity (SUGRA) model without R-parity conservation [7]. We show that the presence of bilinear R-parity violating (BRpV) interactions enhances the supersymmetric multilepton signals over most of the parameter space, specially at moderate and large m_0. In order to make the comparison with the R-parity conserving case easier, we performed our detailed study of the signal and SM backgrounds, adopting the same cuts (soft cuts SC2) proposed in ref. [13].

In SUGRA with universal soft breaking terms at unification, the masses of the sleptons, the lighter chargino ($\tilde{\chi}_1^{\pm}$), and the lighter neutralinos ($\tilde{\chi}_1^0$ and $\tilde{\chi}_2^0$) are considerably smaller than the gluino and squark ones over a large range of the parameter space [13]. Therefore, the production of charginos and neutralinos provides the largest reach at the

Tevatron. In R-parity conserving scenarios, a promising signal for SUGRA at the Tevatron is the production of $\tilde{\chi}_2^0\tilde{\chi}_1^\pm$ pairs and their subsequent decay into three charged leptons in association with missing energy due to the undetected lightest supersymmetric particle (LSP), which turns out to be $\tilde{\chi}_1^0$. In the presence of R-parity violation, the LSP is no longer stable, giving rise to events containing more particles, and it can be electrically charged since it decays. Interesting signals for such scenarios have been worked out for staus [12], stops [14], gluinos [15] and also for supersymmtric Higgs bosons [16]. The larger activity in the detector can either enhance the signal, via the production of additional leptons or suppress it due to the hadronic activity that spoils the isolation of the leptons. Therefore, a careful reanalysis of the trilepton signal is necessary.

In this work, we consider a SUGRA model that includes the following bilinear terms in the superpotential [6, 7, 17]

$$W_{\rm BRpV} = W_{\rm MSSM} - \varepsilon_{ab}\epsilon_i \widehat{L}_i^a \widehat{H}_u^b \,, \tag{1.1}$$

where the last term violates R parity. In order to reproduce the values of neutrino masses indicated by current neutrino data [18] we must have $|\epsilon_i| \ll |\mu|$, where μ denotes the SUSY bilinear mass parameter [5]. The relevant bilinear terms in the soft supersymmetry breaking sector are

$$V_{\rm soft} = m_{H_u}^2 H_u^{a*} H_u^a + m_{H_d}^2 H_d^{a*} H_d^a + M_{L_i}^2 \widetilde{L}_i^{a*} \widetilde{L}_i^a - \varepsilon_{ab}\left(B\mu H_d^a H_u^b + B_i \epsilon_i \widetilde{L}_i^a H_u^b\right), \tag{1.2}$$

where the terms proportional to B_i are the ones that violate R parity. The explicit R-parity violating terms induce vacuum expectation values (vev) v_i, $i = 1, 2, 3$ for the sneutrinos, in addition to the two Higgs vev's v_u and v_d.

Our goal is to determine the impact of R-parity violation on SUSY multilepton signals, for example in the production of three or more electrons or muons, taking into account the magnitude of the mass scale indicated by the current atmospheric neutrino experiments. In phenomenological studies where the details of the neutrino sector are not relevant, it has been proven very useful to work in the approximation where R parity and lepton number are violated in only one generation [16, 19]. Thus, the first step to achieve our goal is to assume the approximation where R parity is violated only in the third generation (of course all gauge interactions are treated in the full three-generation scheme). This is the theoretically natural choice to make, since the third generation forms the basis for the radiative breaking of the electroweak symmetry, driven by the top quark Yukawa coupling. From the point of view of the analysis presented below, the breaking of R parity only in the third generation also corresponds to the worst-case-scenario: the breaking of R parity in the muon channel would produce muons directly, not just as tau decay products, leading to an enhanced multilepton (multi-muon) signal.

2. Main features of our BRpV model

The parameter space of our SUGRA model, which exhibits R-parity violation only in the third generation, is

$$m_0\,, \qquad m_{1/2}\,, \qquad \tan\beta\,, \qquad \mathrm{sign}(\mu)\,, \qquad A_0\,, \qquad \epsilon_\tau \qquad \text{and} \quad m_{\nu_3}\,, \tag{2.1}$$

where $m_{1/2}$ and m_0 characterise the common gaugino mass and scalar soft SUSY breaking masses at the unification scale, A_0 is the common trilinear term, and $\tan\beta$ is the ratio between the Higgs field vev's. Although many parameterisations are possible, it is convenient to characterise the BRpV sector by the bilinear superpotential term ϵ_τ and the neutrino mass m_{ν_3}.

We considered the running of the masses and couplings to the electroweak scale, assumed to be the top mass, using the one-loop renormalization group equations. In the evaluation of the gaugino masses, we included the next-to-leading order (NLO) corrections coming from α_s, the two-loop top Yukawa contributions to the beta-functions, and threshold corrections enhanced by large logarithms; for details see [20]. The NLO corrections are especially important for M_2, leading to a change in the wino mass up to 20%. We then input the soft terms into PYTHIA that was used to evaluated the masses and decay rates of all particles, except the first and second neutralinos.

Present neutrino oscillation data fix the mass splittings among the three neutrinos, leaving arbitrary the overall scale of neutrino masses. The latter could be as large as an electron volt or so without conflicting with cosmology, beta decays and neutrinoless double beta decays, given current uncertainties in nuclear matrix element calculations [21]. However, in the BRpV model, neutrino masses are strongly hierarchical [5], specially the lightest neutrino mass. As a result the possibility of quasi-degenerate neutrinos is not realized in this model and, correspondingly, we will not discuss it any further. In what follows, whenever we fix the BRpV parameters, we take the tree level neutrino mass as $m_{\nu_3} = 0.05\,\text{eV}$, the current atmospheric best fit value from ref. [18, 22], and fix the value of the remaining BRpV parameter ϵ_τ at representative values $0.22\,\text{GeV}$ and $7\times10^{-4}\,\text{GeV}$.

The presence of BRpV induces a mixing between the neutrinos and neutralinos, giving rise to R-parity violating decays of the LSP. In our model, the lightest neutralino presents leptonic decays $\tilde\chi_1^0 \to \nu\ell^+\ell'^-$, semi-leptonic ones $\tilde\chi_1^0 \to \nu q\bar q$ or $\ell q\bar q$, and the invisible mode $\tilde\chi_1^0 \to \nu\nu\nu$ [11]. The expected $\tilde\chi_1^0$ lifetime and decay lengths depend both on the magnitude of R-parity breaking parameters and the chosen values of the SUGRA parameters.

Figure 4*a* shows the lightest neutralino decay length as a function of its mass for $A_0 = 0$, $\mu > 0$, $\tan\beta = 3$, and $\epsilon_\tau = 0.22\,\text{GeV}$. In this figure, the solid lines stand for the tree-level neutrino mass $m_{\nu_3} = 0.05\,\text{eV}$, corresponding to the best fit atmospheric scale as given in ref. [18], and we chose $m_0 = 200$ and $700\,\text{GeV}$. The bands in these figures were obtained by taking m_{ν_3} within the 3σ allowed atmospheric mass splitting of ref. [18]. Figure 4*b* presents the LSP decay length as a function of the neutrino mass, for different lightest neutralino masses and the parameters used in figure 4*a*.

From figures 4 we can see clearly that the LSP decay length is shorter for larger neutrino and LSP masses, as expected. Furthermore, irrespective of the smallness of the neutrino mass indicated by the atmospheric oscillation data, the LSP ($\tilde\chi_1^0$) decays inside the detector in a large portion of the parameter space, specially for small m_0. It is interesting to notice that the kinks in figure 4 are associated to the opening of the LSP decays into on-shell gauge bosons.

Figure 1 contains the $\tilde\chi_1^0$ branching ratios as a function of $m_{1/2}$ for $\epsilon_\tau = 0.22\,\text{GeV}$, $m_{\nu_3} = 0.05\,\text{eV}$, $A_0 = 0$, and $\mu > 0$. As can be seen from this figure, the decay $\tilde\chi_1^0 \to \nu b\bar b$

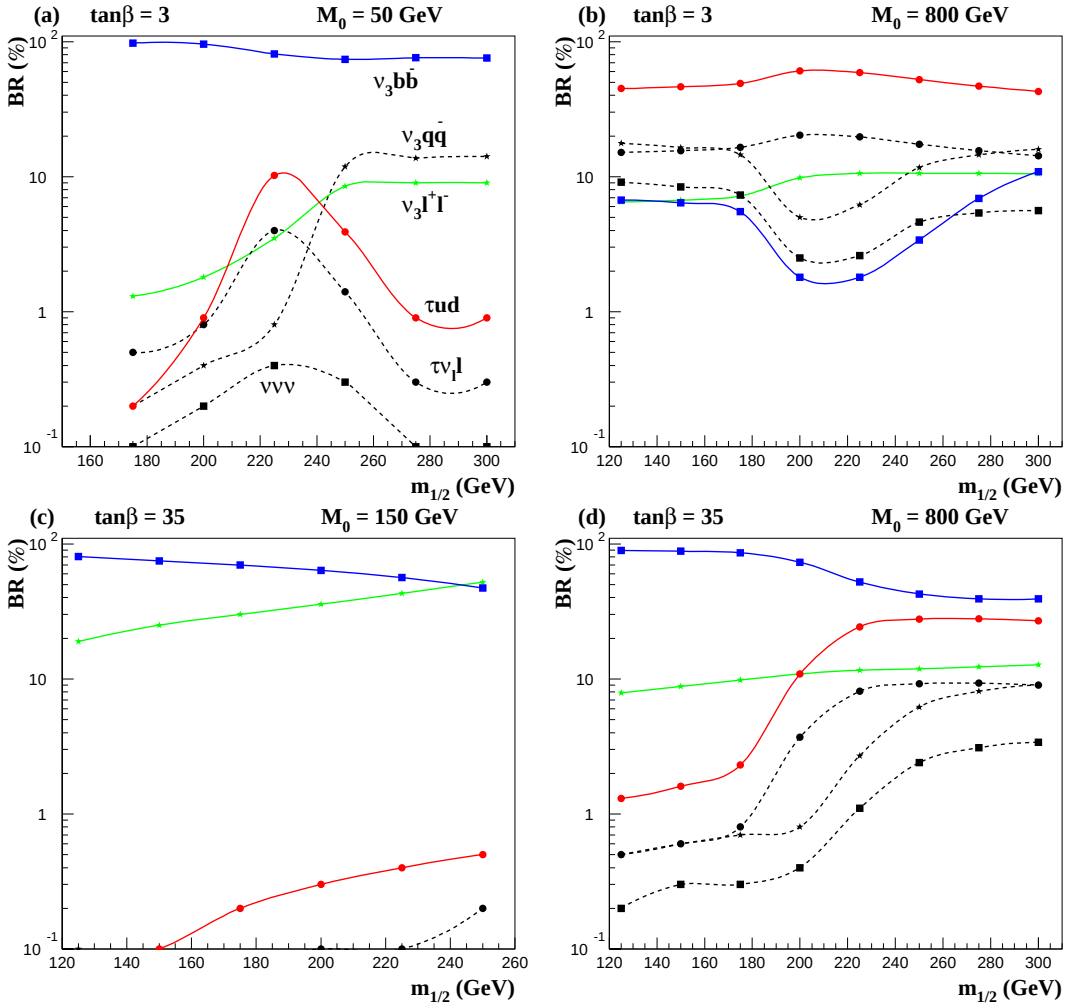

Figure 1: $\tilde{\chi}_1^0$ branching ratios as a function of $m_{1/2}$ for $A_0 = 0$, $\mu > 0$, $\epsilon_\tau = 0.22\,\mathrm{GeV}$, and $m_{\nu_3} = 0.05\,\mathrm{eV}$. The solid lines denote $\tilde{\chi}_1^0 \to \nu_3 b\bar{b}$ (squares); $\tilde{\chi}_1^0 \to \tau u\bar{d}$ (circles); and $\tilde{\chi}_1^0 \to \nu_3 \ell^+\ell^-$ (stars). The dashed lines denote $\tilde{\chi}_1^0 \to$ invisible (squares); $\tilde{\chi}_1^0 \to \tau\nu_\ell\ell$ (circles); and $\tilde{\chi}_1^0 \to \nu_3 q\bar{q}$ (stars).

dominates at small m_0 and large $\tan\beta$. This decay channel arises from an effective coupling λ'_{333}, induced by the neutrino-neutralino mixing, which is proportional both to the bottom Yukawa coupling and to the bilinear parameter ϵ_τ in our model. Therefore, this decay is enhanced at small m_0 due to the lightness of the scalars that mediate it and at large $\tan\beta$ due to enhanced Yukawa couplings. Both features are apparent in the panels of this figure. Moreover, whenever $\tilde{\chi}_1^0 \to \nu b\bar{b}$ is not the leading channel, the LSP decays mostly to $\tau u\bar{d}$, with a sizable branching fraction $\tilde{\chi}_1^0 \to \tau\nu_\ell\bar{\ell}$.

In figure 2, we present the dependence of the $\tilde{\chi}_1^0$ branching ratios with respect to the R-parity violating parameter ϵ_τ. The importance of the $\nu b\bar{b}$ decay mode increases for large ϵ_τ, since the effective coupling λ'_{333} is proportional to ϵ_τ. Moreover, figure 3 shows that the LSP branching ratio into $\nu b\bar{b}$ decreases with increasing m_{ν_3} in the parameter regions where this mode is sizeable.

JHEP09(2003)071

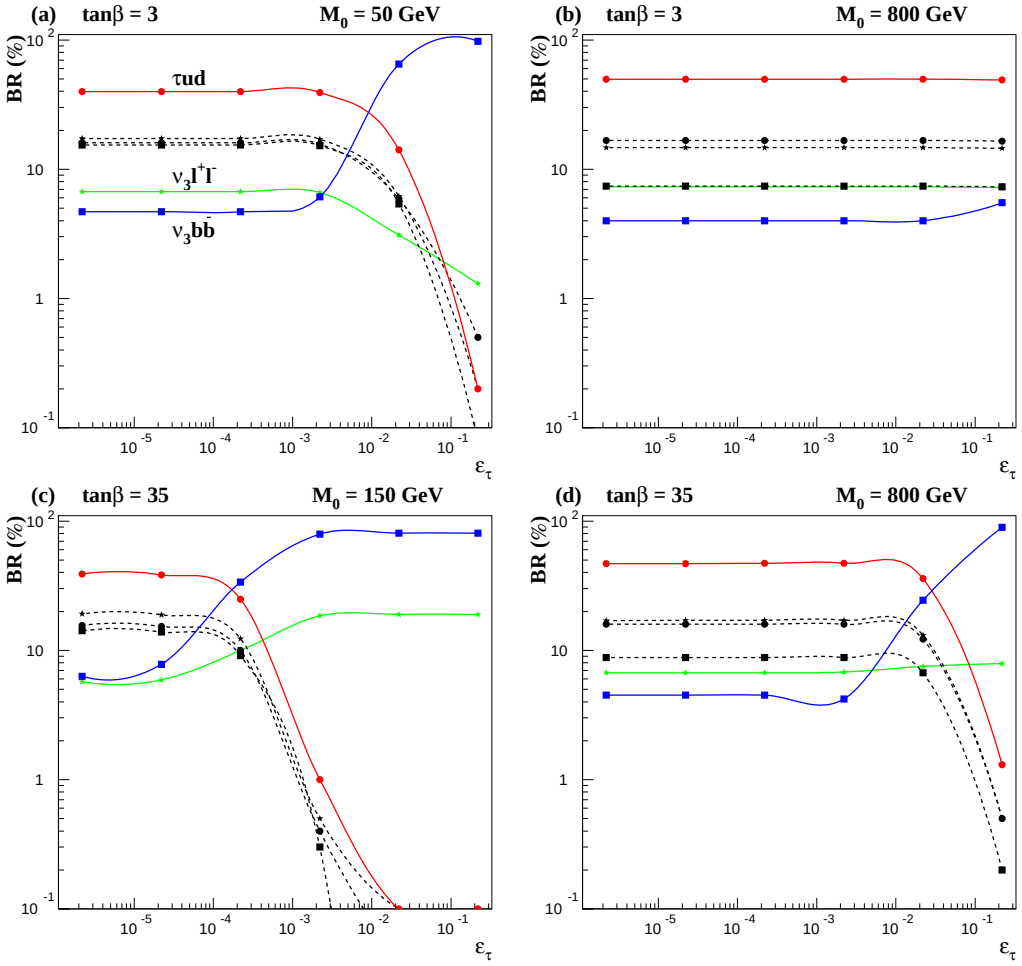

Figure 2: $\tilde{\chi}_1^0$ branching ratios as a function of ϵ_τ for $A_0 = 0$, $\mu > 0$, and $m_{\nu_3} = 0.05\,\text{eV}$. We fixed $m_{1/2} = 175\,\text{GeV}$ in the case of $\tan\beta = 3$ and $m_{1/2} = 125\,\text{GeV}$ for $\tan\beta = 35$. The lines are as in figure 1.

One comment is in order here, concerning the naturalness of the above branching ratio predictions. This issue depends somewhat on the assumptions about the supersymmetry soft breaking terms. We are tacitly assuming them to be universal at some unification scale. This is the usual practice and is adopted here to ensure simple comparison with the SUGRA R-parity conserving results for the trilepton signal obtained in ref. [13]. In the BRpV model universality plays another important role, namely, it ensures "calculability" of the neutrino mass m_{ν_3}, by the renormalization group evolution. One finds in this case that the smallness of m_{ν_3} required by experiment follows naturally from the approximate "alignment" of BRpV parameters discussed, for example, in ref. [19, 9]. In such scenario one has that the short LSP decay path is indeed technically natural, despite the small neutrino mass. However one should stress that strictly universal boundary conditions are not at all essential for the consistency of the results presented here.

Summing up, we can say that in the BRpV model the $\tilde{\chi}_1^0$ decays mainly into τud for large m_0 or small ϵ_τ, while its decays are dominated by $\nu b\bar{b}$ at small m_0 and large ϵ_τ ($\tan\beta$). As we will see in what follows this has important implications for the trilepton signal.

JHEP09(2003)071

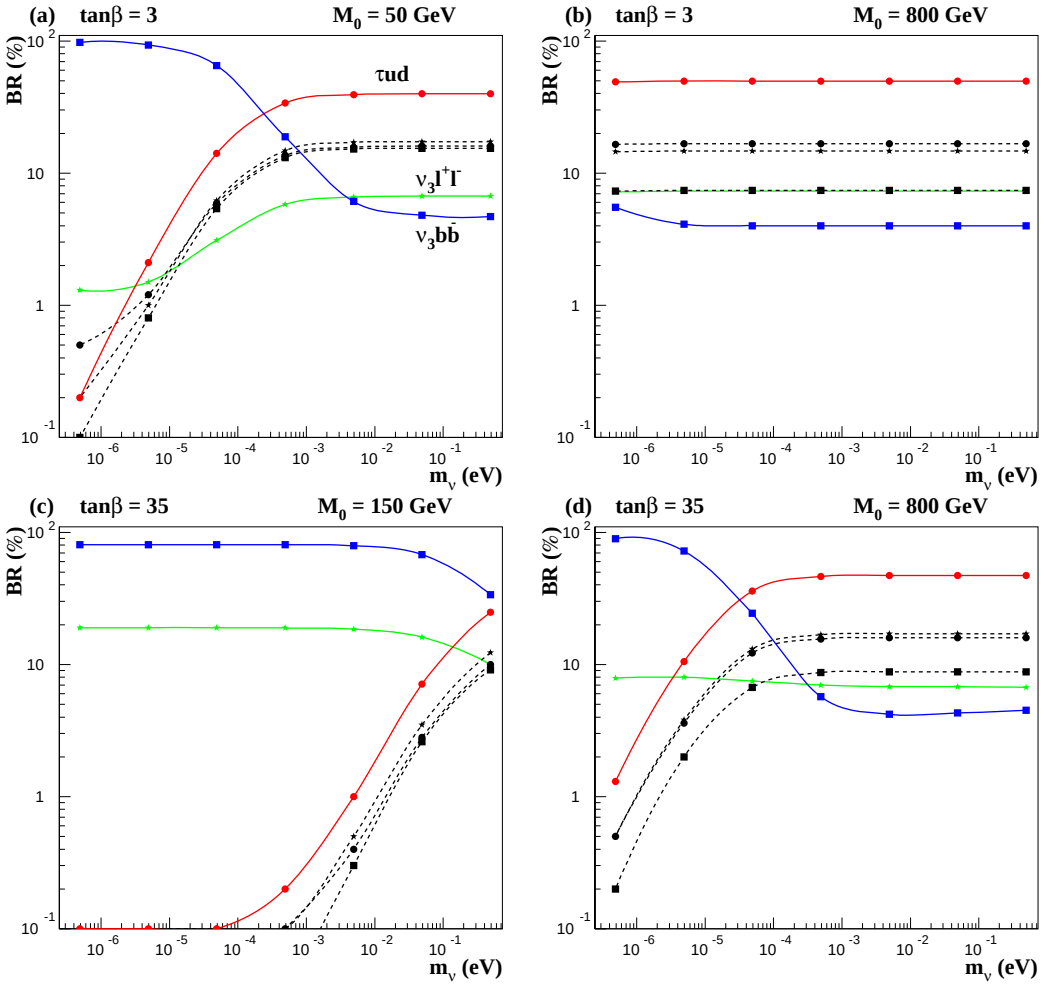

Figure 3: $\tilde{\chi}_1^0$ branching ratios as a function of m_{ν_3} for $A_0 = 0$, $\mu > 0$, and $\epsilon_\tau = 7 \times 10^{-4}$ GeV. We fixed $m_{1/2} = 175$ GeV in the case of $\tan\beta = 3$ and $m_{1/2} = 125$ GeV when $\tan\beta = 35$. The lines are as in figure 1.

3. Signal, backgrounds, and selection cuts

In R-parity conserving scenarios, trilepton production at the Tevatron proceeds via $p\bar{p} \to \tilde{\chi}_2^0 \tilde{\chi}_1^\pm$ with $\tilde{\chi}_1^\pm \to \ell\nu\tilde{\chi}_1^0$, $\tilde{\chi}_2^0 \to \ell^+\ell^-\tilde{\chi}_1^0$, and the LSP ($\tilde{\chi}_1^0$) leaving the detector undetected. The main SM backgrounds for trilepton production are displayed in table 1. In order to suppress these backgrounds, we have imposed the soft cuts SC2 defined in ref. [13], which were tailored for scenarios containing soft signal leptons coming from τ decays [23]:

C1: We required the presence of three isolated leptons (e or μ) with a hadronic E_T smaller that 2 GeV in a cone of size $\Delta R = 0.4$ around the lepton;[1]

C2: We required the most energetic lepton to satisfy $|\eta_{\ell_1}| < 1.0$ and $p_T(\ell_1) > 11$ GeV;

[1] In the trilepton analysis, we reject events presenting more than three isolated charged leptons. In the R-parity conserving case, this procedure makes no difference.

C3: The second (third) most energetic lepton must satisfy $|\eta_{\ell_{2/3}}| < 2.0$ and $p_T(\ell_{2(3)}) > 7$ (5) GeV;

C4: We required the missing transverse energy to be larger than 25 GeV;

C5: We vetoed events exhibiting a $\ell^+\ell^-$ pair with an invariant mass smaller than 20 GeV and larger than 81 GeV (this avoids both Z boson and QED contributions);

C6: We vetoed events with a transverse mass of a charged lepton and missing transverse energy between 60 GeV and 85 GeV in order to suppress W decays.

In our analysis, the signal and backgrounds were generated using PYTHIA [24], except for the $WZ^\star(\gamma^\star)$ which was computed using the complete matrix elements [25]. Furthermore, we also simulate experimental resolutions by smearing the energies, but not directions, of all final state particles with a gaussian error given by $\Delta E/E = 0.7/\sqrt{E}$ (E in GeV) for hadrons and $\Delta E/E = 0.15/\sqrt{E}$ for charged leptons.

BG (fb)	σ (fb)
WZ (Z $\to \tau\tau$)	0.17
W*Z*,W*$\gamma \to ll\bar{l}$	0.12
W*Z*,W*$\gamma \to ll'l'$	0.15
$t\bar{t}$	1.15
Z*Z*	0.05
total	1.64

Table 1: Background cross sections in fb for the trilepton signal at the Tevatron Run II after kinematical cuts discussed in the text.

The cross section for the SM backgrounds after cuts are shown in table 1. Notice that our results differ slightly from the ones in ref. [13] because the hadronization procedures used in PYTHIA and ISAJET are different. Moreover, we can see that the most important background is the $t\bar{t}$ production, accounting for 70% of the total background. We further tested our code by verifying that our results for the R-parity conserving signal agree with the ones in ref. [13].

In our BRpV model there are more SUSY reactions that can contribute to the trilepton signal than in the R-parity conserving case, since the $\tilde{\chi}_1^0$ decays can give rise to charged leptons. In the parameter range interesting for neutrino physics R-parity violating decay modes are only important for the LSP decays and can safely be neglected for the other SUSY particles. We have used the branching ratios generated by PYTHIA except for the the lightest and second-to-lightest neutralinos. In the case of the second neutralino, the branching fractions generated by PYTHIA are in disagreement with the expectations at large $\tan(\beta)$ and low and moderate m_0 [26]. For instance, the ISAJET branching ratio for $\tilde{\chi}_0^2 \to \tau^+\tau^-\tilde{\chi}_1^0$ is 52% for $m_0 = 150$ GeV, $m_{1/2} = 125$ GeV and $\tan(\beta) = 35$, while the PYTHIA prediction for this point is 14%. We have evaluated the second neutralino branching ratios taking into account the large $\tan(\beta)$ effects and used this information as an input of PYTHIA. Our results agree with the predictions of ISAJET within a few percent; *e.g.* for the choice of parameters above our result for the same branching fraction is 48%.

Assuming that gluinos and squarks are too heavy to be produced at the Tevatron, we considered the following processes:

$$p\bar{p} \to \tilde{\ell}\tilde{\ell}^\star\,, \qquad \tilde{\nu}\tilde{\ell}\,, \qquad \tilde{\chi}_i^0\tilde{\chi}_j^0\ (i(j) = 1,2)\,, \qquad \tilde{\chi}_1^+\tilde{\chi}_1^-\,, \qquad \text{and} \quad \tilde{\chi}_i^0\tilde{\chi}_1^\pm (i = 1,2)\,.$$

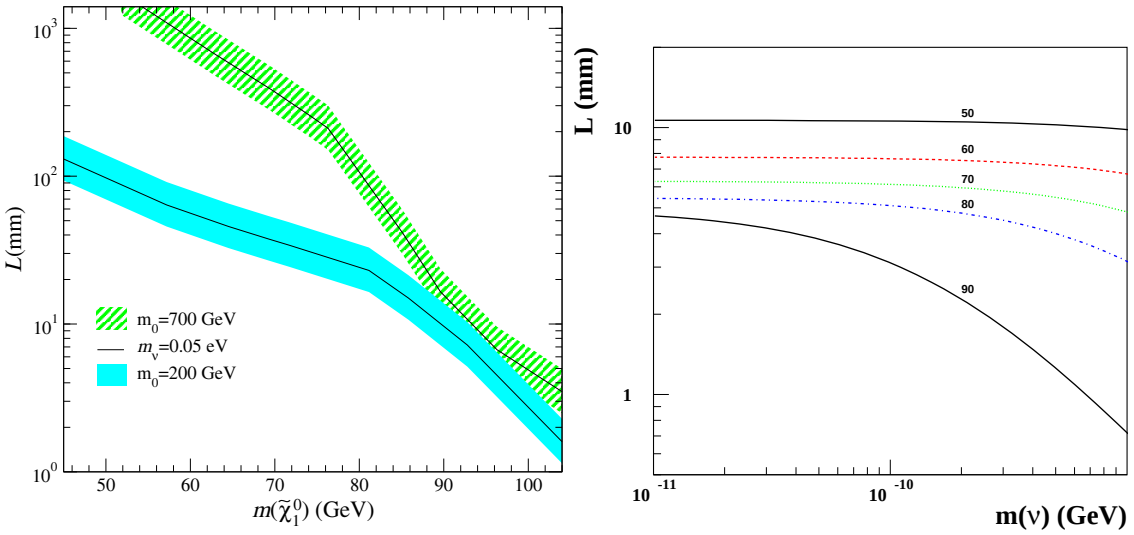

Figure 4: $\tilde{\chi}_1^0$ decay length versus LSP mass for $A_0 = 0$, $\mu > 0$ and $\tan\beta = 3$ for (a) fixed BRpV parameters: $\epsilon_\tau = 0.22\,\text{GeV}$, $m_{\nu_3} = 0.05\,\text{eV}$ (solid lines) and current atmospheric 3σ band (shaded bands); (b) as a function of the neutrino mass m_{ν_3} for $m_0 = 100\,\text{GeV}$ and several values of $\tilde{\chi}_1^0$ masses.

The $\tilde{\chi}_1^0$ decays can contain charged leptons, and therefore, we should also analyse multilepton ($\geq 4\ell$) production. In order to extract this signal, we applied the cuts C1, C3, C5, and C2 but accepting leptons with $|\eta(\ell)| < 3$. We also required the presence of an additional isolated lepton with $p_T > 5\,\text{GeV}$ and demanded the missing transverse energy to be larger than 20 GeV. The main SM backgrounds for this process are $t\bar{t}$, WZ, and ZZ productions whose cross sections after cuts are shown in table 2.

BG (fb)	σ (fb)
WZ	0.01
Z*Z*	0.10
$t\bar{t}$	0.16
total	0.27

Table 2: Background cross sections in fb for the multilepton signal at the Fermilab Tevatron Run II after kinematical cuts discussed in the text.

We can see from figure 4 that the lightest neutralino might not decay inside the detector depending on the point of the parameter space. If it decays inside the tracking system, it can give rise to spectacular events exhibiting displaced vertices without an incoming track associated to it. In our analyses, we did not look for displaced vertices since the corresponding backgrounds depend upon details of the detector. This possibly is a conservative hypothesis since this kind of events should present a small background, leading to a larger reach of the Tevatron. Nevertheless, we kept track of the position of the neutralino decay and accepted events where the neutralino decays inside the tracking system, rejecting all events where one of the neutralinos decays outside a cylinder around the beam pipe of radius 0.5 m and length 2.0 m; we named this requirement C7. Again, this is another conservative estimate of the expected BRpV signal.

We investigated the regions of the $m_0 \otimes m_{1/2}$ plane where the trilepton and multilepton signals can be established at the Tevatron for integrated luminosities of $2\,\text{fb}^{-1}$ and $25\,\text{fb}^{-1}$ and fixed values of A_0 (=0), $\tan\beta$, sign(μ) (> 0), ϵ_τ, and m_{ν_3} ($= 0.05\,\text{eV}$). We evolved the renormalization group equations starting at the unification scale (few $\times 10^{16}\,\text{GeV}$) for the

JHEP09(2003)071

soft parameters, rejecting the points where either the electroweak symmetry is not correctly broken, or which exhibit particles with mass excluded by present experimental data [27]. In our analysis, we have employed the Poisson statistics, except when the expected number of signal events is large enough to justify the use of the gaussian distribution.[2] We exhibit our results in the $m_0 \otimes m_{1/2}$ plane, denoting by black circles the theoretically excluded points, and by white circles the experimentally excluded by sparticle and Higgs boson searches at LEP2 [27]. The black squares represent points accessible to Tevatron experiments at 5σ level with $2\,\mathrm{fb}^{-1}$ of integrated luminosity, while the white squares are accessible with $25\,\mathrm{fb}^{-1}$. Points denoted by diamonds are accessible only at the 3σ level with $25\,\mathrm{fb}^{-1}$, while the stars correspond to the region not accessible to the Tevatron.

The trilepton cross section is always dominated by the $\tilde{\chi}_1^+\tilde{\chi}_1^-$ and $\tilde{\chi}_2^0\tilde{\chi}_1^\pm$ productions, with the second process being about 20% to 50% larger than the first. For example, these reactions are responsible for approximately 99% of the cross section at large m_0. Note that the first process can contribute to the trilepton signal only in R-parity violating scenarios. Moreover, at small and moderate m_0 ($\lesssim 400\,\mathrm{GeV}$), the $\tilde{\chi}_1^0\tilde{\chi}_1^\pm$ production is responsible for approximately 5–10% of the signal cross section and the production of sleptons also gives a sizable contribution.

To study the multilepton signal we choose three representative parameter regions. The best scenario corresponds to the case where $\tan\beta$ and ϵ_τ are small. We subsequently relax this optimistic assumption by considering separately the cases where either (but not both, since in this case the signal is too small) ϵ_τ or $\tan\beta$ are large.

In figure 5, we present the region of the $m_0 \otimes m_{1/2}$ plane that can be probed at the Tevatron for $\tan\beta = 3$ and BRpV parameters $\epsilon_\tau = 7 \times 10^{-4}\,\mathrm{GeV}$ and $m_{\nu_3} = 0.05\,\mathrm{eV}$. For these values of the parameters, the signal cross section is dominated by $\tilde{\chi}_1^+\tilde{\chi}_2^0$ production followed by $\tilde{\chi}_1^+ \to \tilde{\chi}_1^0 l^+\nu$, $\tilde{\chi}_2^0 \to \tilde{\chi}_1^0 qq$ and the LSP $\tilde{\chi}_1^0$ decays mainly into $\tau u\bar{d}$. As expected, the long lifetime of the neutralino reduces considerably the signal in the shaded area of figure 5 after we apply the cut C7. Therefore, we might be able to further probe this region by looking for displaced vertices, and consequently enhance the Tevatron reach.

It is interesting to compare our results presented in figure 5 with the ones in ref. [13]. First of all, the presence of BRpV interactions reduces the Tevatron reach in the trilepton channel for small values of m_0. This happens because there are some competing effects in this region of parameters: on the one hand there are new contributions to the trilepton process due to LSP decay and on the other hand, the decay of the neutralinos produce a larger hadronic activity, worsening the lepton isolation, and reducing the missing E_T compared with the MSSM case. Besides that, the leptons from the $\tilde{\chi}_1^0$ decay can give rise to additional isolated leptons which can contribute to the trilepton signal or, alternatively, can suppress it due to the presence of more than three isolated leptons. The last effect and the larger hadronic activity reduce the trilepton signal at small m_0 in the BRpV model. In contrast, as can be seen from figure 5, the trilepton reach at large m_0 always tends to increase with respect to the MSSM expectation. This follows from the fact that the

[2] This procedure differs from the one used in ref. [13], which used only gaussian statistics. The use of Poisson statistics leads to more restrictive bounds.

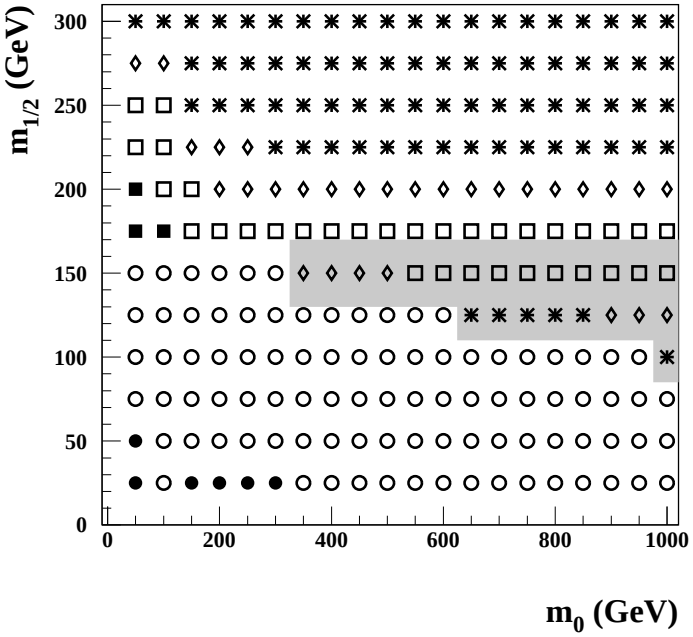

Figure 5: Reach of Fermilab Tevatron Run II using the trilepton signal in the $m_0 \otimes m_{1/2}$ plane for $A_0 = 0$, $\tan\beta = 3$, $\mu > 0$, $\epsilon_\tau = 7 \times 10^{-4}$ GeV, and $m_{\nu_3} = 0.05$ eV. The black circles are theoretically excluded, while the white circles are experimentally excluded by sparticle and Higgs boson searches at LEP2. The black squares denote points accessible to Tevatron experiments at 5σ level with $2\,\text{fb}^{-1}$ of integrated luminosity, while the white squares are accessible with $25\ \text{fb}^{-1}$. Points denoted by diamonds are accessible at the 3σ level with $25\,\text{fb}^{-1}$, while the stars correspond to the region not accessible to Tevatron. The long lifetime of the neutralino reduces considerably the signal in the shaded area, however, it suggests that the sensitivity can be improved by looking for displaced vertices.

drastic reduction of the $\tilde{\chi}_2^0$ branching ratio into leptons at large m_0 is compensated by the additional production of charged leptons in $\tilde{\chi}_1^0$ decays. Since these extra leptons come from tau decays, it is important to adopt cuts which increase the acceptance of soft leptons. The cuts we used satisfy this requirement.

In figure 6*a* we present the Tevatron reach in the multilepton (four leptons or more) channel for the same parameters adopted in figure 5. As we can see, the multilepton reach is larger than the trilepton one, increasing the discovery potential at large values of $m_{1/2}$. For instance, the Tevatron reach at large m_0 is $\simeq 225$ GeV in our BRpV model while it is of the order of 150 GeV in the MSSM. Moreover, unlike the trilepton signal, the discovery potential at small m_0 is also increased with respect to that of the MSSM. In this region it is clear that the reduction of the trilepton signal is largely due to the presence of additional isolated leptons. As in figure 5, the shaded area represent the region where displaced vertices could be used to further increase the sensitivity to BRpV. In figure 6*b* we present the combined results for the trilepton and multilepton searches using the chi-square criteria. It is interesting to notice that the presence of R-parity violating interactions leads to a 5σ SUSY discovery even at large m_0, a region where the usual R-parity conserving SUGRA model has no discovery potential at all. Notice the importance of combining trilepton and multilepton signals to achieve this conclusion. 96

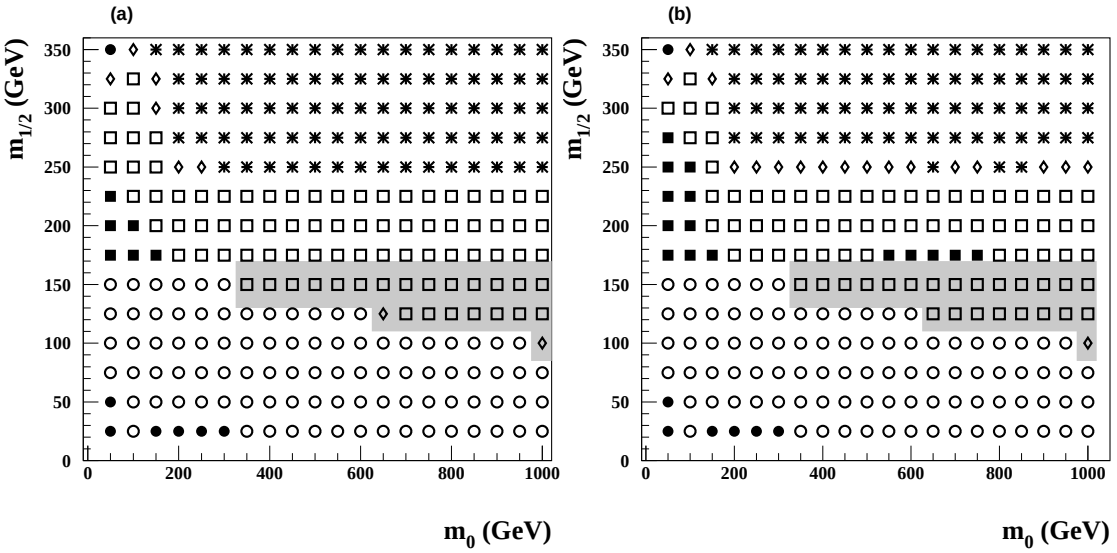

Figure 6: (a) Reach of Fermilab Tevatron Run II in the 4 or more lepton channel. (b) Combined trilepton and multilepton results. All parameters and conventions were chosen as in figure 5.

Let us now consider a second scenario where the $\tilde{\chi}_1^0$ decays predominantly into $\nu_3 b\bar{b}$ at low m_0. As seen in figure 2, the dominance of this decay channel happens for large ϵ_τ values since the LSP decay is scalar mediated. The $\nu_3 b\bar{b}$ decay mode spoils lepton isolation, without producing any additional charged leptons and may be regarded, in a sense, as a worse case scenario in comparison with the case of small ϵ_τ and m_0. In order to illustrate this case we fixed $\epsilon_\tau = 0.22\,\text{GeV}$ and the remaining parameters as before; $A_0 = 0$, $\tan\beta = 3$, $\mu > 0$, and $m_{\nu_3} = 0.05\,\text{eV}$. From figure 7 we can see that the trilepton reach is indeed further reduced at small and medium m_0, as expected. The same happens for the multilepton signal; see figure 8. Nevertheless, combining these signals still leads to a reach that is better than the MSSM one for all m_0 and $m_{1/2}$ values.

Finally, we consider the case of small ϵ_τ and large $\tan\beta$, say $\epsilon_\tau = 7 \times 10^{-4}\,\text{GeV}$ and $\tan\beta = 35$. Figure 9 displays the Tevatron reach in the trilepton channel for this case, keeping the remaining parameters as before; $A_0 = 0$, $\mu > 0$, and $m_{\nu_3} = 0.05\,\text{eV}$. For these parameters, the main $\tilde{\chi}_1^0$ decay mode is $\tau u\bar{d}$. However, there is a sizable contribution of the $\nu b\bar{b}$ channel at small m_0. As expected, the SUSY reach decreases at small m_0, specially as we increase $\tan\beta$. In contrast, there is a slight gain for $m_0 \gtrsim 200\,\text{GeV}$; see figure 9. The similarity between the results in figure 5 and figure 9 at large m_0 can be ascribed to the τud dominance of the LSP decay; see figure 3b and figure 3d. In contrast the situation is more complicated at smaller m_0 as seen in figure 5 and figure 9.

For the last choice of parameters, the Tevatron discovery potential in the multilepton channel is larger in our BRpV model than in the MSSM except at small m_0, however, it is similar to the first case we analyzed; see figure 10a and figure 6a. This feature survives the combination of three and multilepton signals, as can be seen from figure 6b and figure 10b. In contrast, the combined analysis does make a difference in the small m_0 region. In all cases, however, the reach of the BRpV model is larger than the MSSM one.

JHEP09(2003)071

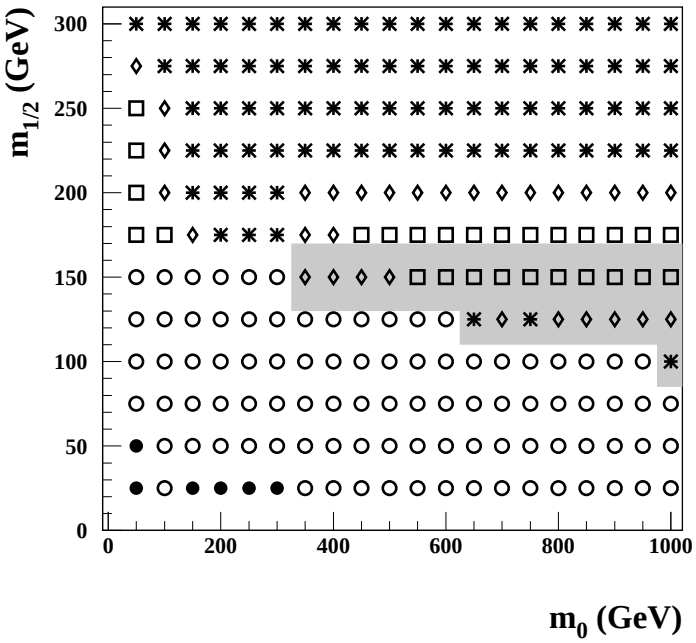

Figure 7: Reach of Fermilab Tevatron Run II using the trilepton signal in the $m_0 \otimes m_{1/2}$ plane for $A_0 = 0$, $\tan\beta = 3$, $\mu > 0$, $\epsilon_\tau = 0.22\,\text{GeV}$, and $m_{\nu_3} = 0.05\,\text{eV}$. The conventions are the ones in figure 5.

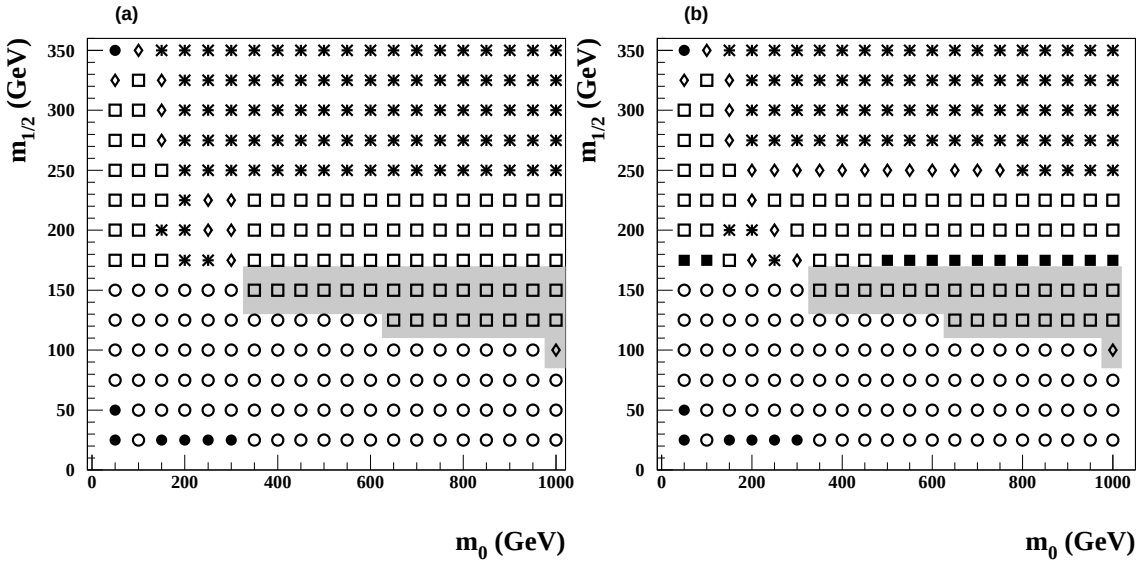

Figure 8: (*a*) Reach of Fermilab Tevatron Run II in the 4 or more lepton channel. (*b*) Combined trilepton and multilepton results. All parameters were chosen as in figure 7.

4. Conclusion

We have analyzed the production of multileptons ($\geq 3\ell$ with $\ell = e$ or μ) in the simplest supergravity model with violation of R parity at the Fermilab Tevatron. In this model, an effective bilinear term in the superpotential parameterizes the explicit breaking of R

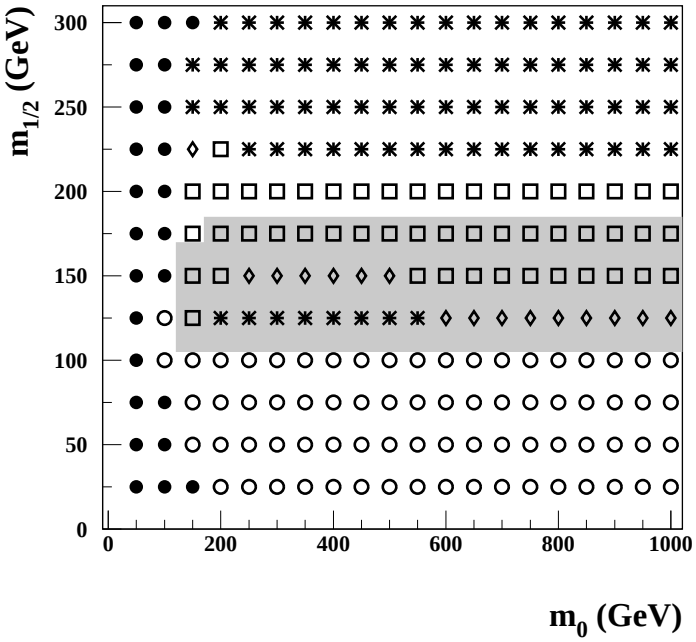

Figure 9: Reach of Fermilab Tevatron Run II using the trilepton signal in the $m_0 \otimes m_{1/2}$ plane for $A_0 = 0$, $\tan\beta = 35$, $\mu > 0$, $\epsilon_\tau = 7 \times 10^{-4}\,\mathrm{GeV}$, and $m_{\nu_3} = 0.05\,\mathrm{eV}$. The conventions are as in figure 5.

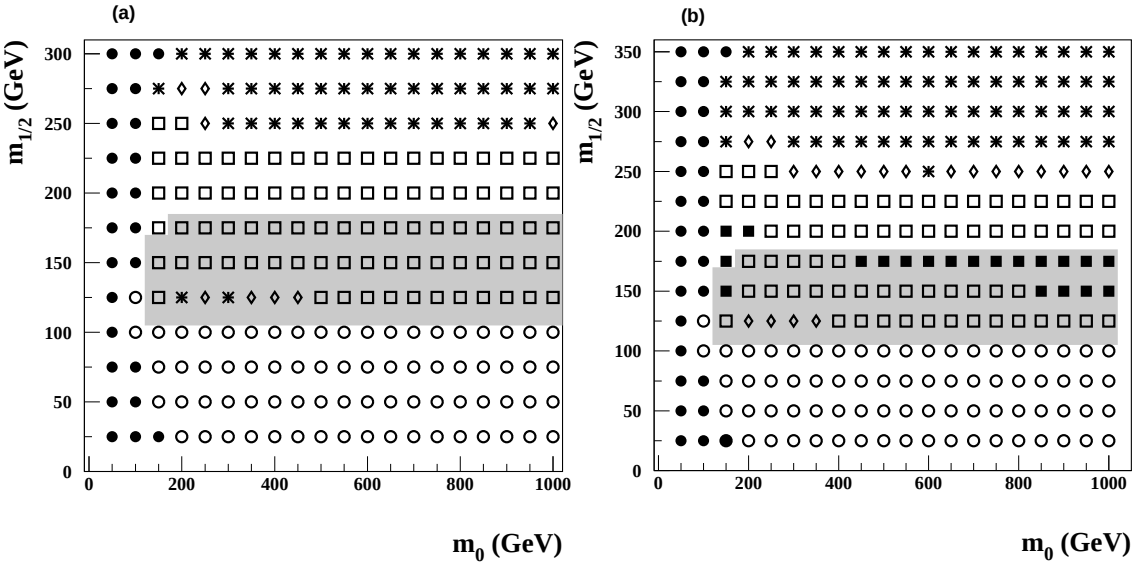

Figure 10: (a) Reach of Fermilab Tevatron Run II in the 4 or more lepton channel. (b) Combined trilepton and multilepton results. All parameters were chosen as in figure 9.

parity. Despite the small R-parity violating couplings needed to generate the neutrino masses indicated by current atmospheric neutrino data, the lightest supersymmetric particle is unstable and can decay inside the detector. This leads to a phenomenology quite distinct from that of the R-parity conserving scenario. We have quantified by how much the supersymmetric multilepton signals differ from the R-parity conserving expectations,

displaying our results in the $m_0 \otimes m_{1/2}$ plane. We have shown that the presence of bilinear R-parity violating interactions enhances the supersymmetric multilepton signals over most of the parameter space, specially at moderate and large m_0. These topologies are useful not only for discovery, but also to verify whether R parity is conserved or not.

Adopting the hadronization procedures used in PYTHIA, we have first reproduced the results for the trilepton signal expected in the conventional R-parity conserving supergravity model. We have found good agreement with the results of ref. [13] which adopts the ISAJET event generator. We have then shown how the presence of BRpV interactions leads to a small suppression of the trilepton signal at small values of m_0 irrespective of the value of BRpV parameter ϵ_τ. This is due to the $\tilde{\chi}_1^0$ decay into $\nu b\bar{b}$. However, the $\tilde{\chi}_1^0$ decays lead to a drastically extended reach at large m_0 as a result of the LSP decay into $\tau u\bar{d}$. Moreover, the presence of additional isolated leptons in the signal allows us to look for multilepton events.

We have demonstrated that combining the trilepton and multilepton searches increases the Tevatron Run II sensitivity for most of SUGRA and R-parity breaking parameters. Note, however, that for neutrino masses in the range indicated by current atmospheric data one has a gap between the $\tilde{\chi}_1^0$ masses that can be probed at LEP2 (up to 40 GeV or so) and those that can be studied at the Tevatron (above 70 GeV or so): within this range the $\tilde{\chi}_1^0$ decay length is rather large, requiring the study of other topologies, like the presence of displaced vertices in the tracking system. It is interesting to notice that we can search for SUSY signals also in the low m_0 region by looking for events exhibiting multi jets + lepton + missing transverse momentum [28, 29].

In the present paper we have confined ourselves to the case in which the lightest neutralino is also the lightest supersymmetric particle,[3] the most likely possibility if we adopt the simplest set of supersymmetry soft breaking terms, universal at some unification scale. We also have focused on the case where we have only one generation and this is chosen to be the third. This is done first for simplicity. Second we adopt this choice as a worse-case scenario. In other words, in those parameter regions where our multi-lepton signal can be discovered in the present one-generation approximation, the inclusion of additional generations can only improve our result. In contrast, in those regions where our results are negative, the situation is totally inconclusive in the sense that a full fledged analysis including all generations might reveal that the signal can also be detected in part of those regions. Therefore our results are robust, in the sense that the inclusion of additional generations would imply new sources of leptons, specially muons. The analysis is substantially more involved, however, than the one considered here and will be taken up elsewhere.

Acknowledgments

Research supported by Fundação de Amparo à Pesquisa do Estado de São Paulo (FAPESP), by Conselho Nacional de Desenvolvimento Científico e Tecnológico (CNPq), by Programa de Apoio a Núcleos de Excelência (PRONEX), by Spanish MCyT grant BFM2002-00345

[3] In our model, any supersymmetric particle is a possible LSP candidate, since it is unstable and thus is not a cosmological relic. However, only the lightest neutralino leads to a signal cross section which can be large enough to be measurable at the Tevatron.

and by the European Commission RTN network HPRN-CT-2000-00148. W.P. has been supported by the 'Erwin Schrödinger fellowship' No. J2272 of the 'Fonds zur Förderung der wissenschaftlichen Forschung' of Austria and partly by the Swiss 'Nationalfonds'. D.R. has been partially supported by UdeA-CODI Grant No. 381-8-10-02.

References

[1] Proc. of the Workshop on Physics at LEP2, CERN 96-01, Vol. I, p. 463, G. Altarelli, T. Sjöstrand, and F. Zwirner eds.;
G.F. Giudice et al., *Searches for new physics*, hep-ph/9602207;
J. Amundson *et al.*, Proceedings of the 1996 DPF/DPB Summer Study on High-Energy Physics, Snowmass, Colorado, 1996, edited by D.G. Cassel, L. Trindle Gennari, R.H. Siemann, p. 655;
A. Bartl *et al.*, *ibid.*, p. 693;
S. Mrenna *et al.*, *ibid.*, p. 681;
M. Carena, R.L. Culbertson, S. Eno, H.J. Frisch and S. Mrenna, *The search for supersymmetry at the Tevatron collider*, hep-ex/9802006;
M. Carena, R.L. Culbertson, S. Eno, H.J. Frisch and S. Mrenna, *The search for supersymmetry at the Tevatron collider*, *Rev. Mod. Phys.* **71** (1999) 937 [hep-ex/9712022];
ECFA/DESY LC Physics Working Group collaboration, E. Accomando et al., *Physics with e^+e^- linear colliders*, *Phys. Rept.* **299** (1998) 1 [hep-ph/9705442].

[2] R parity Working Group collaboration, B. Allanach et al., *Searching for R-parity violation at Run-II of the Tevatron*, hep-ph/9906224;
A. Datta, B. Mukhopadhyaya and F. Vissani, *Tevatron signatures of an R-parity violating supersymmetric theory*, *Phys. Lett.* **B 492** (2000) 324 [hep-ph/9910296];
B. Mukhopadhyaya, S. Roy and F. Vissani, *Correlation between neutrino oscillations and collider signals of supersymmetry in an R-parity violating model*, *Phys. Lett.* **B 443** (1998) 191 [hep-ph/9808265];
F. de Campos, O.J.P. Eboli, M.A. Garcia-Jareno and J.W.F. Valle, *R-parity violating signals for chargino production at LEP II*, *Nucl. Phys.* **B 546** (1999) 33 [hep-ph/9710545].

[3] SNO collaboration, Q.R. Ahmad et al., *Measurement of day and night neutrino energy spectra at SNO and constraints on neutrino mixing parameters*, *Phys. Rev. Lett.* **89** (2002) 011302 [nucl-ex/0204009];
Super-Kamiokande collaboration, S. Fukuda et al., *Determination of solar neutrino oscillation parameters using 1496 days of Super-Kamiokande-I data*, *Phys. Lett.* **B 539** (2002) 179 [hep-ex/0205075];
Super-Kamiokande collaboration, Y. Fukuda et al., *Evidence for oscillation of atmospheric neutrinos*, *Phys. Rev. Lett.* **81** (1998) 1562 [hep-ex/9807003];
see also talks by T. Kirsten, V. Gavrin, K. Lande and M. Smy at Neutrino 2002.

[4] C.S. Aulakh and R. N. Mohapatra, *Phys. Lett.* **B 119** (1982) 13;
L.J. Hall and M. Suzuki, *Explicit R parity breaking in supersymmetric models*, *Nucl. Phys.* **B 231** (1984) 41;
G.G. Ross and J.W.F. Valle, *Supersymmetric models without R-parity*, *Phys. Lett.* **B 151** (1985) 375;
J.R. Ellis, G. Gelmini, C. Jarlskog, G.G. Ross and J.W.F. Valle, *Phenomenology of supersymmetry with broken R-parity*, *Phys. Lett.* **B 150** (1985) 142.

[5] M. Hirsch, M.A. Díaz, W. Porod, J.C. Romão and J.W.F. Valle, *Neutrino masses and mixings from supersymmetry with bilinear r-parity violation: a theory for solar and atmospheric neutrino oscillations*, *Phys. Rev.* **D 62** (2000) 113008 [hep-ph/0004115];
J.C. Romão, M.A. Díaz, M. Hirsch, W. Porod and J.W.F. Valle, *A supersymmetric solution to the solar and atmospheric neutrino problems*, *Phys. Rev.* **D 61** (2000) 071703 [hep-ph/9907499];
M.A. Díaz, M. Hirsch, W. Porod, J.C. Romão and J.W.F. Valle, *Solar neutrino masses and mixing from bilinear R-parity broken supersymmetry: analytical versus numerical results*, *Phys. Rev.* **D 68** (2003) 013009 [hep-ph/0302021].

[6] S.Y. Choi, E.J. Chun, S.K. Kang and J.S. Lee, *Neutrino oscillations and R-parity violating collider signals*, *Phys. Rev.* **D 60** (1999) 075002 [hep-ph/9903465];
D.E. Kaplan and A.E. Nelson, *Solar and atmospheric neutrino oscillations from bilinear R-parity violation*, *J. High Energy Phys.* **01** (2000) 033 [hep-ph/9901254];
C.-H. Chang and T.-F. Feng, *The supersymmetric extension of the standard model with bilinear R-parity violation*, *Eur. Phys. J.* **C 12** (2000) 137 [hep-ph/9901260];
F. Takayama and M. Yamaguchi, *Pattern of neutrino oscillations in supersymmetry with bilinear R-parity violation*, *Phys. Lett.* **B 476** (2000) 116 [hep-ph/9910320].

[7] M.A. Díaz, J.C. Romão and J.W.F. Valle, *Minimal supergravity with R-parity breaking*, *Nucl. Phys.* **B 524** (1998) 23 [hep-ph/9706315];
for a brief review see, e. g. J.W.F. Valle, *Super-gravity unification with bilinear R-parity violation*, Proc. of International Symposium on Particles, Strings and Cosmology (PASCOS 98), pp. 502–512, [hep-ph/9808292].

[8] A. Masiero and J.W.F. Valle, *A model for spontaneous R-parity breaking*, *Phys. Lett.* **B 251** (1990) 273;
J.C. Romão, C.A. Santos and J.W.F. Valle, *How to spontaneously break R-parity*, *Phys. Lett.* **B 288** (1992) 311;
J.C. Romão and J.W.F. Valle, *Neutrino masses in supersymmetry with spontaneously broken R-parity*, *Nucl. Phys.* **B 381** (1992) 87;
K. Huitu, J. Maalampi and K. Puolamaki, *Signals of spontaneous R-parity breaking at lep and at a linear collider*, *Eur. Phys. J.* **C 6** (1999) 159 [hep-ph/9705406];
R. Kitano and K.-y. Oda, *Neutrino masses in the supersymmetric standard model with right-handed neutrinos and spontaneous R-parity violation*, *Phys. Rev.* **D 61** (2000) 113001 [hep-ph/9911327].

[9] J.M. Mira, E. Nardi, D.A. Restrepo and J.W.F. Valle, *Bilinear R-parity violation and small neutrino masses: a self-consistent framework*, *Phys. Lett.* **B 492** (2000) 81 [hep-ph/0007266].

[10] A. Bartl, W. Porod, D. Restrepo, J. Romão and J.W.F. Valle, *Neutralino phenomenology at LEP2 in supersymmetry with bilinear breaking of R-parity*, *Nucl. Phys.* **B 600** (2001) 39 [hep-ph/0007157], and references therein.

[11] W. Porod, M. Hirsch, J. Romão and J.W.F. Valle, *Testing neutrino mixing at future collider experiments*, *Phys. Rev.* **D 63** (2001) 115004 [hep-ph/0011248], and references therein.

[12] M. Hirsch, W. Porod, J.C. Romão and J.W.F. Valle, *Probing neutrino properties with charged scalar lepton decays*, *Phys. Rev.* **D 66** (2002) 095006 [hep-ph/0207334].

[13] H. Baer, M. Drees, F. Paige, P. Quintana and X. Tata, *Trilepton signal for supersymmetry at the Fermilab Tevatron revisited*, *Phys. Rev.* **D 61** (2000) 095007 [hep-ph/9906233].

JHEP09(2003)071

[14] A. Bartl et al., *New signatures for a light stop at LEP2 in SUSY models with spontaneously broken R-parity*, *Phys. Lett.* **B 384** (1996) 151 [hep-ph/9606256];
M.A. Díaz, D.A. Restrepo and J.W.F. Valle, *Two-body decays of the lightest stop in supergravity with and without R-parity*, *Nucl. Phys.* **B 583** (2000) 182 [hep-ph/9908286];
D. Restrepo, W. Porod and J.W.F. Valle, *Broken R-parity, stop decays and neutrino physics*, *Phys. Rev.* **D 64** (2001) 055011 [hep-ph/0104040].

[15] A. Bartl et al., *Signatures of spontaneous breaking of R-parity in gluino cascade decays at LHC*, *Nucl. Phys.* **B 502** (1997) 19 [hep-ph/9612436].

[16] A.G. Akeroyd, M.A. Díaz, J. Ferrandis, M.A. Garcia-Jareno and J.W.F. Valle, *Charged Higgs boson and stau phenomenology in the simplest R-parity breaking model*, *Nucl. Phys.* **B 529** (1998) 3 [hep-ph/9707395];
F. de Campos, M.A. Garcia-Jareno, A.S. Joshipura, J. Rosiek and J.W.F. Valle, *Novel scalar boson decays in SUSY with broken R-parity*, *Nucl. Phys.* **B 451** (1995) 3 [hep-ph/9502237].

[17] T. Banks, Y. Grossman, E. Nardi and Y. Nir, *Supersymmetry without R-parity and without lepton number*, *Phys. Rev.* **D 52** (1995) 531;
J.C. Romão, F. de Campos, M.A. Garcia-Jareno, M.B. Magro and J.W.F. Valle, *LEP sensitivities to spontaneous R-parity violating signals*, *Nucl. Phys.* **B 482** (1996) 3 [hep-ph/9604244];
M. Nowakowski and A. Pilaftsis, *W and Z boson interactions in supersymmetric models with explicit R-parity violation*, *Nucl. Phys.* **B 461** (1996) 19 [hep-ph/9508271];
G. Bhattacharyya, D. Choudhury and K. Sridhar, *New LEP bounds on b violating scalar couplings: R-parity violating supersymmetry or diquarks*, *Phys. Lett.* **B 355** (1995) 193 [hep-ph/9504314];
H.-P. Nilles and N. Polonsky, *Supersymmetric neutrino masses, R-symmetries and the generalized mu problem*, *Nucl. Phys.* **B 484** (1997) 33 [hep-ph/9606388];
A.Y. Smirnov and F. Vissani, *Large R-parity violating couplings and grand unification*, *Nucl. Phys.* **B 460** (1996) 37 [hep-ph/9506416];
B. de Carlos and P.L. White, *R-parity violation and quark flavour violation*, *Phys. Rev.* **D 55** (1997) 4222 [hep-ph/9609443].

[18] M. Maltoni, T. Schwetz, M.A. Tortola and J.W.F. Valle, *Constraining neutrino oscillation parameters with current solar and atmospheric data*, *Phys. Rev.* **D 67** (2003) 013011 [hep-ph/0207227], and references therein. The e-Print Archive version of this paper has been updated to include the results of KamLAND.

[19] M.A. Díaz, J. Ferrandis, J.C. Romão and J.W.F. Valle, *Unification of gauge couplings and the tau neutrino mass in supergravity without R-parity*, *Nucl. Phys.* **B 590** (2000) 3 [hep-ph/9906343];
M.A. Díaz, J. Ferrandis, J.C. Romão and J.W.F. Valle, *Gauge and Yukawa unification with broken R-parity*, *Phys. Lett.* **B 453** (1999) 263 [hep-ph/9801391];
A.G. Akeroyd, M.A. Díaz and J.W.F. Valle, *Tau lepton mixing with charginos and its effects on chargino searches at e^+e^- colliders*, *Phys. Lett.* **B 441** (1998) 224 [hep-ph/9806382];
M.A. Díaz, E. Torrente-Lujan and J.W.F. Valle, *Charged Higgs mass bounds from $b \to s\gamma$ in a bilinear R-parity violating model*, *Nucl. Phys.* **B 551** (1999) 78 [hep-ph/9808412];
M.A. Díaz, J. Ferrandis and J.W.F. Valle, *Supersymmetry unification predictions for m(top), V(cb) and* $\tan\beta$, *Nucl. Phys.* **B 573** (2003) 75 [hep-ph/9909212].

JHEP09(2003)071

[20] T. Gherghetta, G.F. Giudice and J.D. Wells, *Phenomenological consequences of supersymmetry with anomaly-induced masses*, *Nucl. Phys.* **B 559** (1999) 27 [hep-ph/9904378].

[21] J.W.F. Valle, *Standard and non-standard neutrino properties*, Proc. of 20th International Conference on Neutrino Physics and Astrophysics (Neutrino 2002), Munich, Germany, 25–30 May 2002, [hep-ph/0209047];

[22] M.C. Gonzalez-Garcia and Y. Nir, *Developments in neutrino physics*, *Rev. Mod. Phys.* **75** (2003) 345 [hep-ph/0202058];
For an updated review of neutrino properties after KamLAND, including also atmospheric data see S. Pakvasa and J.W.F. Valle, *Neutrino properties before and after kamland*, hep-ph/0301061; invited contribution to the INSA special issue on Neutrinos.

[23] V.D. Barger, C. Kao and T.-j. Li, *Trilepton signal of minimal supergravity at the Tevatron including tau-lepton contributions*, *Phys. Lett.* **B 433** (1998) 328 [hep-ph/9804451];
V.D. Barger and C. Kao, *Trilepton signature of minimal supergravity at the upgraded Tevatron*, *Phys. Rev.* **D 60** (1999) 115015 [hep-ph/9811489].

[24] T. Söstrand, *High-energy physics event generation with PYTHIA 5.7 and JETSET 7.4*, *Comput. Phys. Commun.* **82** (1994) 74;

[25] T. Stelzer and W.F. Long, *Automatic generation of tree level helicity amplitudes*, *Comput. Phys. Commun.* **81** (1994) 357 [hep-ph/9401258].

[26] H. Baer, C.-h. Chen, M. Drees, F. Paige and X. Tata, *Collider phenomenology for supersymmetry with large* $\tan\beta$, *Phys. Rev. Lett.* **79** (1997) 986 [hep-ph/9704457];
Supersymmetry reach of Tevatron upgrades: the large $\tan\beta$ *case*, *Phys. Rev.* **D 58** (1998) 075008 [hep-ph/9802441].

[27] Particle Data Group collaboration, K. Hagiwara et al., *Review of particle physics*, *Phys. Rev.* **D 66** (2002) 010001.

[28] V.D. Barger, T. Han, S. Hesselbach and D. Marfatia, *Testing radiative neutrino mass generation via R-parity violation at the Tevatron*, *Phys. Lett.* **B 538** (2002) 346 [hep-ph/0108261].

[29] K.T. Matchev and D.M. Pierce, *Supersymmetry reach of the Tevatron via trilepton, like-sign dilepton and dilepton plus tau jet signatures*, *Phys. Rev.* **D 60** (1999) 075004 [hep-ph/9904282].

JHEP09(2003)071

4.5 Sinais em aceleradores: o Tevatron, LEP II e o LHC

O objetivo do estudo dos sinais nos LHC é estabelecer os possíveis limites para modelos do tipo BRpV-AMSB e BRpV-mSUGRA, a partir da análise dos canais cujo sinal formado por jatos e "missing energy", multileptons, e vértices deslocados. Sinal e fundo são gerados por meio da utilização do código PYTHIA, última versão disponível. Com relação aos sinais canônicos em SUSY, as topologias no LHC são identificadas a seguir:

1- Jatos inclusivos e "missing energy", 2- Jatos, "missing energy" sem leptons isolados, 3- Jatos, "missing energy" e um lepton isolado, 4- Jatos, "missing energy", par de leptons isolados de sinais opostos, 5- Jatos, "missing energy" e multileptons (três ou mais leptons isolados)

Como vínculos sobre os modelos, consideramos alguns resultados conhecidos sobre parâmetros a baixas energias. Além dos resultados sobre neutrinos, consideramos dados do LEP, processos raros como $b \to s\gamma$ e o resultado para o momento magnético anômalo do muon, assim como resultados experimentais para o limite na massa e mistura de neutrinos, a 90%C.L.

De acordo com os resultados do LEP, também são conhecidos os limites inferiores para a massa dos parceiros supersimétricos, também considerados em nossa análise. Nos modelos discutidos anteriormente, tanto o neutralino como a LSP no modelo BRpV-mSUGRA como o neutralino e o chargino no modelo BRpV-AMSB podem viajar por uma distancia microscópica antes de decair. Desse modo, a vida media longa dessas partículas pode dar origem aos vértices deslocados. Entretanto esse decaimento deve estar localizado numa região do detector cujo sinal e

trajetória possa ser reconstruída. Como já estudado, as partículas supersimétricas decaem em região interna do detector, mesmo quando considerada a respectiva correção relativística. Partimos do pressuposto de que o sinal pode ser reconstruído tanto para o neutralino como para o chargino, e consideramos os cenários nos quais a LSP é o neutralino. É importante mencionar que escalares e bósons de gauge participam dos processos que levam aos estados finais citados acima. De acordo com o espectro de massa, alguns desses estados apresentam sinais que podem ser calculados como decaimentos a dois corpos. O decaimento invisível do neutralino a neutrinos não pode ser reconstruído e por tal razão não é utilizado em nossa análise. Consideramos um "toy model" para os detectores do LHC (não é possível incluir as informações sobre os detectores) para a identificação dos eventos contendo vértices deslocados em nossas simulações, bem como estudamos os fundos e os cortes associados aos sinais decorrentes do Modelo Padrão.

ELSEVIER

Nuclear Physics B 546 (1999) 33–51

NUCLEAR PHYSICS B

R-parity-violating signals for chargino production at LEP II

F. de Campos [a,1], O.J.P. Éboli [b,2], M.A. García-Jareño [c,3], J.W.F. Valle [c,4]

[a] *Universidade Estadual Paulista, Campus de Guaratinguetá, Av. Dr. Ariberto Pereira da Cunha, 333, 12500-000, Guaratinguetá, S.P., Brazil*

[b] *Instituto de Física, Universidade de São Paulo, C.P. 66.318, CEP 05315-970 São Paulo, Brazil*

[c] *Instituto de Física Corpuscular – C.S.I.C., Departament de Física Teòrica, Universitat de València, 46100 Burjassot, València, Spain*

Received 3 November 1998; revised 14 January 1999; accepted 15 January 1999

Abstract

We study chargino pair production at LEP II in supersymmetric models with spontaneously broken *R*-parity. We perform signal and background analyses, showing that a large region of the parameter space of these models can be probed through chargino searches at LEP II. In particular, we determine the attainable limits on the chargino mass as a function of the magnitude of the effective bilinear *R*-parity violation parameter ϵ, demonstrating that LEP II is able to unravel the existence of charginos with masses almost up to their kinematical limit even in the case of *R*-parity violation. This requires the study of several final state topologies since the usual MSSM chargino signature is recovered as $\epsilon \to 0$. Moreover, for sufficiently large ϵ values, for which the chargino decay mode $\chi^{\pm} \to \tau^{\pm} J$ dominates, we find through a dedicated Monte Carlo analysis that the $\chi^{\pm}$ mass bounds are again very close to the kinematic limit. Our results establish the robustness of the chargino mass limit, in the sense that it is basically model-independent. They also show that LEP II can establish the existence of spontaneous *R*-parity violation in a large region of parameter space should charginos be produced.

PACS: 12.60.Jv; 14.80.Ly; 04.65.+e; 12.60.J

[1] E-mail: fernando@feg.unesp.br

[2] Present address: Instituto de Física Teórica (UNESP), Rua Pamplona 145, São Paulo, SP, 01405, Brazil. E-mail: eboli@fma.if.usp.br

[3] E-mail: miguel@flamenco.ific.uv.es

[4] E-mail: valle@flamenco.ific.uv.es

0550-3213/99/$ - see frontmatter
PII S0550-3213(99)00032-2

1. Introduction

In the *Minimal Supersymmetric Standard Model* (MSSM) the conservation of a discrete symmetry called R-parity is imposed [1]. R-parity is related to the particle spin (S), lepton number (L), and baryon number (B) through $R = (-1)^{(3B+L+2S)}$, being all the standard model particles R-even while their superpartners are R-odd. From this it follows that supersymmetric particles must be produced only in pairs, with the lightest one being stable. So far, most searches for supersymmetric particles have assumed conservation of R-parity, however, neither gauge invariance nor supersymmetry (SUSY) require its conservation. In general, we can build models exhibiting R-parity violation which may be explicit [2] or spontaneous [3], or even the residual effect of a more fundamental unified theory [4].

One possible scenario for spontaneous R-parity breaking is that it takes place through non-zero vacuum expectation values (VEVs) of scalar neutrinos [5]. In this case there are two distinct possibilities depending whether lepton number is a gauge symmetry or not. If lepton number is part of the gauge symmetry there is an additional gauge boson which acquires mass via the Higgs mechanism. Therefore, there is no physical Goldstone boson and the scale of R-parity violation, in the TeV range, also characterizes the new gauge interaction [6,7]. In this work, we consider the alternative scenario where spontaneous R-parity violation occurs in the absence of an additional gauge symmetry, so that there is a physical massless Nambu–Goldstone boson, called Majoron [8–13].[5] In this model, the Majoron remains massless and stable in the absence of further explicit R-parity-violating terms that might arise, for instance from gravitational effects [15,16]. Thus, it will lead to a missing energy signal at high energy accelerators.

In Majoron models, the neutralino is unstable and for moderate strengths of the R-parity-violating interactions, it will decay inside the detector, either via

$$\begin{aligned} &\chi^0 \to \nu_\tau Z^\star \to \nu_\tau \nu\nu,\ \nu_\tau \ell^+\ell^-,\ \nu_\tau q\bar{q};\\ &\chi^0 \to \tau W^\star \to \tau \nu_i \ell_i,\ \tau q\bar{q}', \end{aligned} \tag{1}$$

or through Majoron emission,

$$\chi^0 \to \nu J\,. \tag{2}$$

Note that this decay mode is R-parity conserving, since the Majoron is mainly R-odd (see Eq. (6)).

In the first case the neutralino gives rise to visible signals, except for the 3ν decay mode. In the case of Eq. (2) the neutralino decay leads to a missing energy signature, exactly as the stable MSSM neutralino.

[5] There are many models where neutrinos get mass from spontaneous breaking of lepton number [14]. In the present context the Majoron appears also because the (tau) neutrino mass arises as a result of the spontaneous violation of lepton number implied by the non-zero sneutrino VEVs.

In this work, we study the implications of R-parity-breaking SUSY models with a Majoron for chargino searches at LEP II. In this case, in addition to the conventional MSSM chargino decay mode

$$\chi^+ \to W^+\chi^0, \tag{3}$$

where the W can be real or virtual depending on the chargino and neutralino masses, there is a new R-parity conserving two-body decay mode

$$\chi^\pm \to \tau^\pm J, \tag{4}$$

As in Eq. (2) the decay in Eq. (4) is R-parity conserving and therefore it can be quite sizeable.

Note that R-parity-violating decays $\chi^+ \to W^+\nu_\tau$ and $\chi^\pm \to Z\tau^\pm$ are typically negligible compared to the above decay modes, as shown explicitly in Ref. [17]. As we will see in Section 3, we have assumed that all sfermions are sufficiently heavy not to influence the physics at LEP II.

We evaluate the LEP II potential for probing the R-parity-violating SUSY parameter space through the study of new signatures arising from chargino pair production and its corresponding cascade decay. We determine the limits on the chargino mass (m_{χ^1}) for different values of the R-parity-violating interactions. In our analyses, we recover the MSSM chargino mass limit, which is close to the kinematic limit, for sufficiently small strengths of the R-parity-violating interactions. As the magnitude of R-parity violation becomes larger, new final state topologies become available. By performing a Monte Carlo analysis we show that these new topologies also lead to bounds on the chargino mass close to the kinematical limit. Assuming unification of the gaugino mass parameters we also determine the corresponding neutralino mass limit.

2. Basic framework

We adopted the conceptually simplest model for the spontaneous violation of R proposed in Ref. [8] in which, by construction, neutrinos are massless before breaking of R-parity. As a result, all R-parity-violating observables are directly correlated to the mass of the tau neutrino with the magnitude of this correlation depending upon the choice of the R-parity SUSY parameters. Apart from the theoretical attractive idea of giving a dynamical origin for the violation of R-parity and neutrino mass, these models offer the possibility of realizing a radiative scenario for the breaking of R-parity, similar to that of electroweak breaking [18].

In order to set up our notation, we first recall some basic ingredients. The superpotential, which conserves *total* lepton number and R, is given by

$$h_u Q H_u u^c + h_d H_d Q d^c + h_e \ell H_d e^c + (h_0 H_u H_d - \epsilon'^2)\Phi + h_\nu \ell H_u \nu^c + h\Phi S\nu^c + \text{h.c.}, \tag{5}$$

where the couplings h_u, h_d, h_e, h_ν, h are arbitrary matrices in generation space. The additional chiral superfields (Φ, $\nu^c{}_i$, S_i) are singlets under $SU(2) \otimes U(1)$ and carry a conserved lepton number assigned as $(0, -1, 1)$ respectively. Note that terms such as Φ^2 and Φ^3 are in principle allowed and have been discussed in earlier papers. For example, a Φ^2 term was included in Ref. [13] and a Φ^3 has been included in a recent formulation of the theory with radiative symmetry breaking [18]. However, the presence of the Φ field is not essential in the formulation of the theory. In schemes with radiative breaking one may simply add bare mass terms $\mu H_u H_d$ and $MS\nu^c$ without adding the Φ field. From the point of view of our analysis the presence of Φ has basically no effect, as it relies mainly on the chargino sector.

The superfields ν^c, S [19] and Φ [20] are required to drive the spontaneous violation of R-parity in an acceptable way, so that the Majoron is mostly a singlet, that is given by the imaginary part of [8]

$$\frac{v_L^2}{Vv^2}(v_u H_u - v_d H_d) + \frac{v_L}{V}\tilde{\nu}_\tau - \frac{v_R}{V}\tilde{\nu^c}_\tau + \frac{v_S}{V}\tilde{S}_\tau\,, \tag{6}$$

where the isosinglet VEVs

$$v_R = \langle \tilde{\nu}_{R\tau} \rangle\,, \qquad v_S = \langle \tilde{S}_\tau \rangle\,, \tag{7}$$

and $V = \sqrt{v_R^2 + v_S^2}$ characterizes R or lepton number breaking. The isodoublet VEVs

$$v_u = \langle H_u \rangle\,, \qquad v_d = \langle H_d \rangle \tag{8}$$

are responsible for the breaking of the electroweak symmetry and the generation of fermion masses with the combination $v^2 = v_u^2 + v_d^2$ being fixed by the W, Z masses. Finally, there is a small seed of R-parity breaking in the doublet sector, i.e.

$$v_L = \langle \tilde{\nu}_{L\tau} \rangle\,, \tag{9}$$

whose magnitude is now related to the Yukawa coupling h_ν. Since this vanishes as $h_\nu \to 0$, we can naturally satisfy the limits originating from stellar energy loss [21]. Note that, unlike the standard seesaw model, the neutral leptons members of the singlet superfields $\nu^c{}_i$ and S_i are given only Dirac-type masses.

Notice that we have assumed R-parity-violating VEVs only for the third generation. This is the theoretically well-motivated choice if one has in mind a radiatively induced symmetry-breaking mechanism [18,22], since the largest Yukawa couplings are those of the third generation.[6] For future use we define an effective parameter $\epsilon_i \equiv h_{\nu ij} v_{Rj}$, which measures the violation of R-parity now expressed as an effective bilinear superpotential term which breaks R-parity explicitly. Together with the standard MSSM μ parameter it will affect the fermion mass matrices given below.

[6] Some of the effects in such a complete dynamical scheme get communicated through mixing to the lightest generations. See, example, Ref. [12].

The form of the chargino mass matrix is common to a wide class of $SU(2) \otimes U(1)$ SUSY models with spontaneously broken R-parity and is given by

	e_j^+	$\tilde{H}_u^+$	$-i\tilde{W}^+$
e_i	$h_{eij}v_d$	$-h_{\nu ij}v_{Rj}$	$\sqrt{2}g_2 v_{Li}$
$\tilde{H}_d^-$	$-h_{eij}v_{Li}$	μ	$\sqrt{2}g_2 v_d$
$-i\tilde{W}^-$	0	$\sqrt{2}g_2 v_u$	M_2

(10)

Two matrices U and V are needed to diagonalize the 5×5 (non-symmetric) chargino mass matrix

$$\chi_i^+ = V_{ij}\psi_j^+ , \tag{11}$$

$$\chi_i^- = U_{ij}\psi_j^- , \tag{12}$$

where the indices i and j run from 1 to 5, $\psi_j^+ = (e_1^+, e_2^+, e_3^+, \tilde{H}_u^+, -i\tilde{W}^+)$ and $\psi_j^- = (e_1^-, e_2^-, e_3^-, \tilde{H}_d^-, -i\tilde{W}^-)$.

If the singlet superfield mass terms are large one can truncate the neutralino mass matrix so as to obtain an effective 7×7 matrix of the following form [8]:

	ν_i	$\tilde{H}_u$	$\tilde{H}_d$	$-i\tilde{W}_3$	$-i\tilde{B}$
ν_i	0	$h_{\nu ij}v_{Rj}$	0	$g_2 v_{Li}$	$-g_1 v_{Li}$
$\tilde{H}_u$	$h_{\nu ij}v_{Rj}$	0	$-\mu$	$-g_2 v_u$	$g_1 v_u$
$\tilde{H}_d$	0	$-\mu$	0	$g_2 v_d$	$-g_1 v_d$
$-i\tilde{W}_3$	$g_2 v_{Li}$	$-g_2 v_u$	$g_2 v_d$	M_2	0
$-i\tilde{B}$	$-g_1 v_{Li}$	$g_1 v_u$	$-g_1 v_d$	0	M_1

(13)

where $M_{1(2)}$ denote the supersymmetry-breaking gaugino mass parameters and $g_{1(2)}$ are the $SU(2) \otimes U(1)$ gauge couplings divided by $\sqrt{2}$. Moreover, we assumed the canonical GUT relation $M_1/M_2 = \frac{5}{3}\tan^2\theta_W$. We have however included the full neutral mass matrix, including the singlet sector, and diagonalized it numerically in order to determine, for example, the ν_τ mass and to identify the physical mass eigenstates. In any case the singlets are hardly relevant for our present analysis, as they appear in the chargino mass matrix only through the effective bilinear parameters$\epsilon_i \equiv h_{\nu ij}v_{Rj}$, which measures the violation of R-parity and the usual MSSM μ parameter.

The matrix (13) is diagonalized by a 7×7 unitary matrix N,

$$\chi_i^o = N_{ij}\psi_j^o , \tag{14}$$

where $\psi_j^0 = (\nu_i, \tilde{H}_u, \tilde{H}_d, -i\tilde{W}_3, -i\tilde{B})$, with ν_i denoting the three weak-eigenstate neutrinos.

In our analyses, we considered typical values for the SUSY parameters μ, M_2 that can be covered by chargino production at LEP II,

$$-200 \leqslant \mu \leqslant 200 \text{ [GeV]} , \qquad 111$$

$$40 \leqslant M_2 \leqslant 400 \text{ [GeV]} . \tag{15}$$

We also varied $\tan\beta$ in the range

$$2 \leqslant \tan\beta = \frac{v_u}{v_d} \leqslant 40. \tag{16}$$

This is a standard choice for the ranges of the SUSY parameters which generously accounts for chargino masses within the kinematical reach of LEP I. This range has only been used in order to have an overview of parameter space in the first two figures of our paper (see below). Note that we have explicitly limited $\tan\beta$ to values that are consistent with supergravity versions with perturbative Yukawa couplings up to the GUT scale, excluding, for example $\tan\beta = 1$. No essential change would result if lower $\tan\beta$ values were included. In the analysis of the signals we have simply fixed $\tan\beta$ at the two illustrative values used by the DELPHI collaboration.

As we can see from the neutralino and chargino mass matrices, the ϵ parameter gives the main contribution to the mixing between charged (neutral) leptons and the charginos (neutralinos) and also leads to R-violating gauge couplings.

We have required the parameters $h_{\nu i,3}$ and the expectation values lie in the ranges

$$h_{\nu 13} = h_{\nu 23} = 0, \qquad 10^{-5} \leqslant h_{\nu 33} \leqslant 10^{-1}, \tag{17}$$

$$v_L = v_{L3} = 100 \text{ MeV},$$

$$50 \text{ GeV} \leqslant v_R = v_{R3} \leqslant 1000 \text{ GeV},$$

$$50 \text{ GeV} \leqslant v_S = v_{S3} = v_R \leqslant 1000 \text{ GeV}. \tag{18}$$

For definiteness we have set $v_{L1} = v_{L2} = 0$ and $v_{R1} = v_{R2} = 0$.

The above range for the R-parity-breaking parameters is quite reasonable and generous, and has been used widely in previous papers, e.g., Refs. [7,13]. There are many restrictions on the parameters in broken R models which follow from laboratory experiments related to neutrino physics, weak interactions, cosmology, and astrophysics [5,14]. The most relevant constraints come from neutrino-less double beta decay and neutrino oscillation searches, direct searches for anomalous peaks at π and K-meson decays, the limit on the tau neutrino mass [23], and cosmological limits on the ν_τ lifetime and mass, as well as limits on muon and tau lifetimes, on lepton-flavour-violating decays, and universality violation. These constraints have been taken into account in several previous papers [12,13]. Here we improved these constraints including the most recent experimental results as, for example, the new tau neutrino mass bound [23]).

The model described above constitutes a very useful way to parametrize the physics of R violation, due to the strict correlation between the magnitude of R-violating phenomena and the resulting ν_τ mass. In other words, neutrinos are strictly massless before breaking R, therefore all R-violating observables, such as the lightest neutralino decay rate Γ_χ, are directly correlated to the mass of the tau neutrino. In fact, the τ neutrino mass may be written schematically as $m_{\nu_\tau} \sim \xi\epsilon^2/m_{\chi^+}$, where ξ is some effective parameter given as a function of M_2, μ, $\tan\beta$, etc.[7] This establishes a correlation between

[7] For a more complete discussion see the second paper in Ref. [18,22]

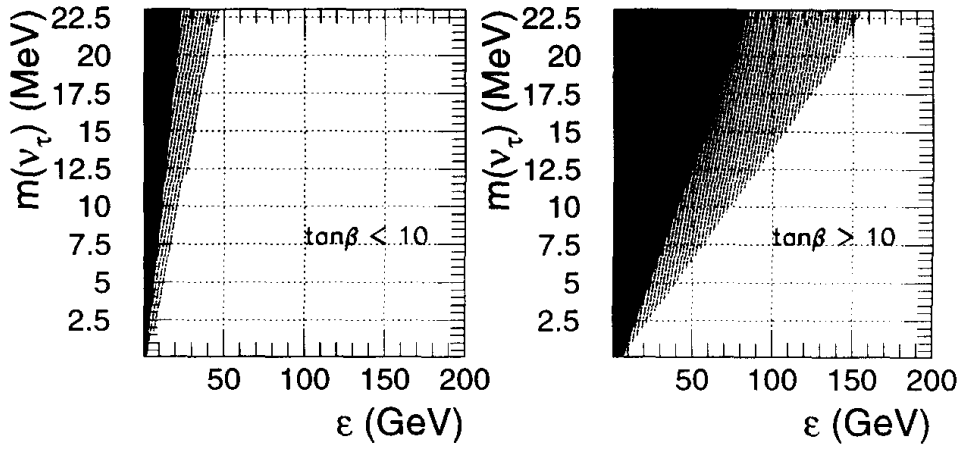

Fig. 1. The value of the predicted tau neutrino mass in our model is compatible with the LEP experimental limits in the light shaded area. Within the dark shaded area, chargino masses are such that they can be produced at $\sqrt{s} = 172$ GeV.

the violation of R and the ν_τ mass showing explicitly how the broken R-model provides an interesting mechanism to understand the origin of neutrino mass without invoking physics at very high energy scales [24].

In Fig. 1, we exhibit the tau neutrino mass as a function of ϵ, showing in light grey the region in the (m_{ν_τ}, ϵ) plane which is compatible with the tau neutrino mass limit from LEP. We also present in this figure the region in which the charginos can be pair produced at LEP, which corresponds to a smaller range of ϵ values (dark zone). As we can see, for $\tan\beta < 10$, the maximum value of ϵ that can be probed through chargino pair production at LEP II is around 20 GeV and it increases for larger $\tan\beta$. For definiteness we fixed the value of ϵ in our analysis.

In the following section we describe the most relevant chargino and neutralino decay modes for this work. A complete list of the decay widths and couplings can be found in Ref. [17] or Ref. [25].

3. Signals and backgrounds

3.1. Chargino production

At LEP II the lightest chargino may be pair produced via

$$e^+e^- \to \gamma, Z, \tilde{\nu} \to \chi^+\chi^- . \tag{19}$$

In this work we assumed that the sneutrinos are so heavy that only the γ and Z s-channels contribute to the cross section; see, for instance, Refs. [26,27]. In fact, the contribution of the t-channel to the total cross section is completely negligible for sneutrinos heavier than 500 GeV. Fig. 2 shows a scatter plot of the allowed values of the $e^+e^- \to \chi^+\chi^-$ total cross section versus the chargino mass for $\sqrt{s} = 172$ GeV, when the parameters are varied as in Eq. (15) and Eq. (16). As one can see, this

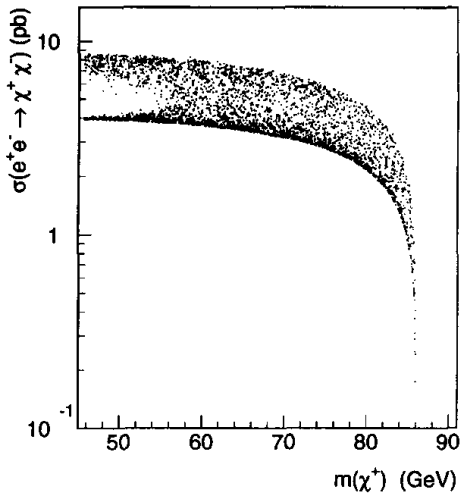

Fig. 2. $e^+e^- \to \chi^+\chi^-$ cross section, in the large $m_{\tilde{\nu}}$ limit, versus chargino mass for the parameter region defined in Eqs. (17) and (18) and $\sqrt{s}$ = 172 GeV. The upper and lower limiting curves of this plot define the range of LEP II chargino pair production cross section for our parameter space.

cross section varies between 2 and 10 pb for almost all kinematically allowed chargino masses.

Although, our model allows for the single R-parity-violating chargino production

$$e^+e^- \to \chi^\pm \tau^\mp , \tag{20}$$

we only considered in this paper the pair production of charginos, as in the MSSM, since the cross section for the single chargino production at LEP II is too small to be observed [28].

3.2. Neutralino and chargino decays

The breaking of R-parity not only opens new decay channels for the chargino but also allows the lightest neutralino to decay. Therefore, there are new signatures for SUSY, some of them being very striking. As said in the Introduction, we assumed that all the sfermions are heavy and therefore we neglected their effects in the chargino production as well as in their decays. In the present model, the lightest neutralino (χ^0) can decay invisibly $\chi^0 \to \nu J$, as in Eq. (2), as well as into R-parity-violating channels

$$\chi^0 \to \nu_\tau Z^\star \to \nu_\tau \nu\nu,\ \nu_\tau \ell^+\ell^-,\ \nu_\tau q\bar{q}; \tag{21}$$

$$\chi^0 \to \tau W^\star \to \tau \nu_i \ell_i,\ \tau q\bar{q}' . \tag{22}$$

For the chargino masses accessible at LEP II, the above W and Z are off-shell and the neutralino has only two-body Majoron decays and the above three-body modes. A complete description of neutralino decay modes as a function of the model parameters and masses can be found in Ref. [17].

It is interesting to notice that all three-body decay channels of the lightest neutralino are *visible*, except for the neutral current one leading to three neutrinos. In the parameter space regions where most of neutralino decays are *visible*, the strategies to search for

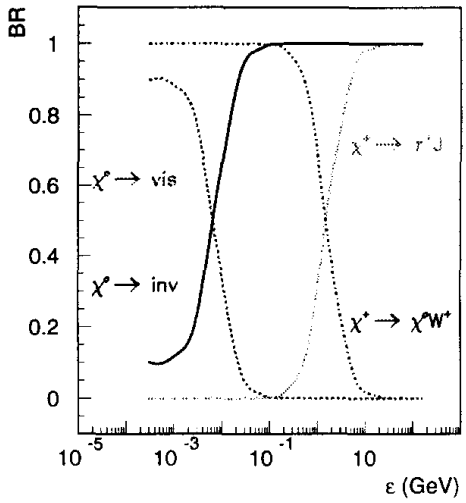

Fig. 3. Typical neutralino and chargino decay branching ratios as a function of ϵ for μ = 150 GeV, M_2 = 100 GeV, and $\tan\beta$ = 35.

SUSY particles are considerably modified with respect to the ones used in the MSSM. The MSSM is recovered as a special limit of this class of models, when the lightest neutralino decays outside the detector because R-parity violation is not strong enough. Notwithstanding, χ^0 decays can also lead to missing momentum due to the presence of neutrinos or Majorons. It is important to notice that, the neutralino of a spontaneously broken R-parity model fakes the MSSM one when the invisible decay given in Eq. (2) dominates since its decay products escape undetected.

In R-parity-breaking models, the decays of the lightest chargino, denoted by $\chi^\pm$, are modified by the existence of new channels. In models with a Majoron, the lightest chargino ($\chi^\pm$) exhibits the two-body decay mode $\chi^\pm \to \tau^\pm J$ of Eq. (4), in addition to the channels[8]

$$\chi^\pm \to \nu_\tau W^\star \to \nu_\tau q\bar{q}', \ \nu_\tau \ell_i^\pm \nu_i, \tag{23}$$

$$\chi^\pm \to \tau^\pm Z^\star \to \tau^\pm q\bar{q}, \ \tau^\pm \ell^+\ell^-, \ \tau^\pm \nu\bar{\nu}, \tag{24}$$

$$\chi^\pm \to \chi^0 W^\star \to \chi^0 q\bar{q}', \ \chi^0 \ell_i^\pm \nu_i, \tag{25}$$

where we again assumed that the sfermions are heavy. In the framework of the MSSM only the last decay channel is present, however, with the χ^0 being stable. Therefore, the breaking of R-parity can modify substantially the signature of charginos.

For the sake of illustration we show in Fig. 3 typical values of the branching ratios of charginos and neutralinos, when we vary ϵ for μ = 150 GeV, M_2 = 100 GeV, and $\tan\beta$ = 35. For neutralinos we show its total visible and invisible branching ratios, where we included in the invisible width the contributions coming from the neutrino plus Majoron channel ($\chi^0 \to \nu$J), as well as from the neutral current channel when the Z decays into a pair of neutrinos ($\chi^0 \to 3\nu$).

[8] Notice that there is the possibility of a chargino decaying into the second lightest neutralino plus a W^+, which conserves R-parity. However, for the parameter range considered, the second lightest neutralino mass is around the chargino mass, so that this decay is forbidden or kinematically suppressed.

For small ϵ values (up to 10^{-4} GeV) the neutralino will decay outside the detector (since its lifetime is longer than 10^{-6} s) so that it leaves no visible track. In this case it is effectively stable and the MSSM limit is restored. In this region the invisible component of the neutralino decay is associated only to the $\chi^0 \to 3\nu$ channel. When the ϵ parameter grows to the order of 1 GeV the decay channels get mixed and both neutralinos as well as charginos have R-parity-violating decays at the same level as the standard MSSM ones. As expected, above $\epsilon \sim 1$ GeV or so $\chi^\pm$ and χ^0 decay predominantly into Majorons, that is, the invisible channel dominates the decay of the neutralino and the main chargino decay mode is $\tau^+ J$.

3.3. *Signatures for chargino pair production*

At LEP II there is a variety of topologies associated to the production of lightest chargino pairs. We classified the possible signatures into four categories which contain almost all the final states allowed in R-parity-violating models.

- *MSSM topologies:* This class includes the following topologies

$$\chi^+\chi^- \to 4 \text{ jets } + \not{p}_T ,$$
$$\chi^+\chi^- \to 2 \text{ jets } + \ell^\pm + \not{p}_T ,$$
$$\chi^+\chi^- \to \ell^+\ell^- + \not{p}_T ,$$

where $\ell^\pm$ stands for $e^\pm$ or $\mu^\pm$. These are the channels used in the chargino searches within the framework of the MSSM. In Majoron models, such topologies are obtained by charged-current decays into $\nu_\tau W^*$ or $\chi^0 W^*$, with the χ^0 decaying invisibly. As we can see from Fig. 3, these topologies are expected to be important for very small values of ϵ since this is the region where $\chi^\pm$ decays predominantly into $W^*\chi^0$ and the neutralino has such a long life-time and it is not observed in the detector. These topologies also play an important rôle for moderate values of ϵ (e.g. $\simeq 0.1$) where the invisible decay of the neutralino is dominant and the chargino still decays into a $\chi^0 W^*$.

- *Multi-fermion (exotic) topologies:* When the neutralino decays visibly, almost all the three-body channels of the chargino lead to at least three charged leptons or jets. Again, this occurs for small values of ϵ, where the chargino decays predominantly into $\chi^0 W^*$. Therefore, the pair production of charginos can give rise to events with a large multiplicity of leptons and/or jets in this region of the parameter space. This is a striking signature of new physics. We focused our attention on final states with five or more charged leptons and/or jets that also present missing energy.

- $\tau^\pm$ *with 2 jets topology:* For moderate values of ϵ the neutralino decays invisibly and the chargino either into $\tau^\pm J$ or into $\chi^0 W^*$. An important topology to analyze for this range of parameters is

$$\chi^+\chi^- \to \tau^\pm + 2 \text{ jets} + \not{p}_T , \tag{26}$$

which arises when one of the charginos decays to $\tau^\pm J$ while the other one decays to $\chi^0 W^*$.

• $\tau^+\tau^-\not{p}_T$: For large values of ϵ, the chargino decay is dominated by $\chi^\pm \to \tau^\pm J$, therefore, the signal arising from its pair production is

$$\chi^+\chi^- \to \tau^+\tau^-\not{p}_T . \tag{27}$$

In this case the signal for charginos in Majoron models is the same of stau production in the MSSM framework.[9]

3.4. Standard model backgrounds and respective cuts

Our goal is to evaluate the potential of LEP II to unravel the existence of supersymmetry with spontaneous R-parity violation. In order to do so, we studied the signals and backgrounds, choosing the cuts to enhance the former. The main background for the above topologies are:

• *MSSM topologies:* The background for these signals has been studied at length by several groups, including the experimental collaborations [27]. The main sources of background for these topologies are $e^+e^- \to f\bar{f}\ (n\gamma)$ ($f = q$ or $\ell^\pm$), W^+W^-, $(Z/\gamma)^*(Z/\gamma)^*$, $We\nu_e$, and Ze^+e^-. The total cross sections of the backgrounds and respective cuts for the three MSSM topologies, after the cuts imposed by DELPHI in their analysis, are given in Ref. [27]. Moreover, we can easily obtain the signal cross sections in models with R-parity violation by evaluating the cross section for chargino pair production and multiplying it by the appropriate branching ratios and experimental detection efficiencies – that is, we basically re-scale the DELPHI analysis to our scenario. These efficiencies are a function of the mass difference between the chargino and the lightest neutralino, with a small fluctuation due to the statistical error in the simulation as well as an intrinsic dependence on the chargino mass. To be conservative, we have considered the lowest value of these efficiencies for each mass difference.

• *Multi-fermion (exotic) topologies:* At the parton level, these events exhibit five or more fermions. For instance, we can have final states $\ell_i^+\ell_i^- q\bar{q}'\ell^\pm + \not{p}_T$, or six charged leptons and missing p_T, or 8 jets and missing p_T. The Standard Model (SM) contributions to these events originate only from higher orders in perturbation theory, and consequently they have negligible cross sections. In our analysis, we assumed that there is no SM background and a conservative detection efficiency of 30%.

• $\tau^\pm$ plus 2 jets topology: The SM processes that can give rise to this topology are $e^+e^- \to W^+W^-$, $(Z/\gamma)^*(Z/\gamma)^*$, which also contribute to the $jj\ell$ MSSM topology background. At the parton level the cross sections of these process are the same for $\ell^\pm = e^\pm$, $\mu^\pm$, or $\tau^\pm$. Therefore, we evaluated the size of this background by multiplying the DELPHI's result for $\sigma_{SM}(jj\mu^\pm + \not{p}_T)$ by a τ identification efficiency, which we have taken as 80% [29].

• $\tau^+\tau^- + \not{p}_T$: This is the main signal of R-parity violation models over a large ϵ range. It happens to be the same signal which would arise from the pair production of staus in the MSSM framework. We have constructed an event generator to simulate

[9] We would like to thank F. Richard for calling our attention to this point.

the pair production of charginos as well as their decays within the framework of R-parity-violating models. The SM backgrounds were studied using the event generator PYTHIA [30]. We considered the following SM processes, taking into account the QED (QCD) initial and final state radiation, as well as fragmentation and τ decay:

$$e^+e^- \to W^+W^- \to \ell^+\ell^-\not{p}_T\,, \tag{28}$$

$$e^+e^- \to (Z/\gamma)^*(Z/\gamma)^* \to \ell^+\ell^-\not{p}_T\,, \tag{29}$$

$$e^+e^- \to (Z/\gamma)^* \to \ell^+\ell^-\not{p}_T\,, \tag{30}$$

$$e^+e^- \to [e^+e^-]\gamma\gamma \to \ell^+\ell^-\not{p}_T\,. \tag{31}$$

where ℓ denotes e, μ or τ.

In order to reduce these backgrounds, we applied a series of cuts similar to the ones used by DELPHI and ALEPHI for the stau search [31]. Initially we kept only the events presenting "two jets", which might be leptons, with a visible mass larger than 6 GeV. We also vetoed events exhibiting photons with more than 4 GeV whose angle with each jet is greater than 10° and whose invariant mass with the jets is greater than 2 GeV. The two-photon background is eliminated efficiently by requiring the missing transverse momentum to be larger than 6% of the centre-of-mass energy in events with a visible mass smaller than 30 GeV. We also imposed that the polar angle of the missing momentum lies between 30° and 150°.

A very useful variable is defined by the following procedure [31]: first, we projected the jet momenta into the plane perpendicular to the beam axis. Then we evaluated the thrust from the projected momenta, and defined δ as the scalar sum of the transverse components of the projected momenta with respect to this thrust axis. We also defined the acoplanarity A as the angle in the plane perpendicular to the beam between the two jets. With these quantities we can reduce considerably the fermion pair background ($Z^*/\gamma^* \to \ell^+\ell^-$) by rejecting the events that lead to $17.1\delta + 120 - A < 0$. This cut eliminates a large fraction of the fermion pair events since these tend to exhibit back-to-back jets with a rather small δ.

The WW background is similar to the signal. However, we can discard a large fraction of the $W^\pm \to \nu e^\pm$ or $\nu\mu^\pm$ events remembering that the $e^\pm$ or $\mu^\pm$ originating from W's are more energetic than the ones coming from $\tau^\pm$ decays. This is accomplished by requiring the largest lepton momentum to be smaller than 22 GeV. If both W's decay leptonically, we also demanded the second lepton to have a momentum smaller than 15 GeV.

After applying the above cuts and for centre-of-mass energy of 172 GeV, the $\gamma\gamma$ background is completely eliminated. On the other hand, the cross section for fermion pair production is reduced to 13 fb, while the ZZ background has a cross section of 4 fb. Most of the background events originate from WW pairs whose cross section is 60 fb. These results are compatible with the ones obtained by the ALEPH collaboration in Ref. [31]. Nevertheless, the signal possesses an efficiency of 30–40% depending on the chargino mass.

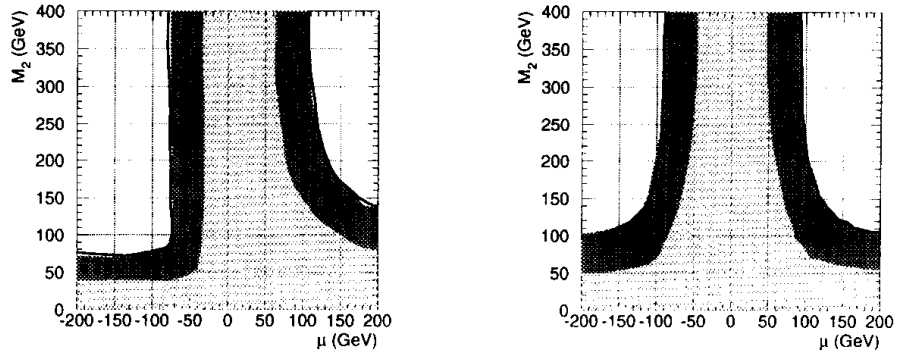

Fig. 4. 95% CL excluded region in the (μ, M_2) plane (dark shaded area) in the MSSM limit $\epsilon = v_L = 0$ for (a) $\tan\beta = 2$ and (b) $\tan\beta = 35$, $\sqrt{s} = 172$ GeV, and an integrated luminosity of 300 pb^{-1}. The light shaded zone is excluded in the MSSM limit by LEP I while the solid curve denotes the LEP II kinematical limit.

4. Results

For the sake of definiteness we considered a centre-of-mass energy of 172 GeV and a total integrated luminosity of 300 pb^{-1}, according to LEP II design expectations [32]. However, our results should be a conservative estimate of the LEP II potentiality even for actual energies and luminosities. We leave to the experimentalist the task of doing a complete analysis. In analogy to the usual analyses performed for the MSSM, we present the 95% CL excluded regions of the (μ, M_2) SUSY parameter space for different values of $\tan\beta$ and ϵ, assuming that the number of observed events is equal to the expected one for the background [32]. First of all, we obtained bounds for $\epsilon = v_R = v_L = 0$, which should reproduce the MSSM results. We show in Fig. 4 that we indeed obtain exactly the same limits found in the MSSM analyses [27], for both $\tan\beta = 2$ and 35. This shows that we are consistent.

For relatively small values of the R-parity violation parameter ϵ the most important topologies are the MSSM and the exotic multi-fermion ($\tau^{\pm}$ plus 2 jets) one for small (large) values of $\tan\beta$. We can see from Fig. 5, for $\epsilon = 0.1$ GeV and $\tan\beta = 2$, that the main constraints still come from the MSSM final states while the exotic multi-fermion channels are irrelevant to the final limits. This result can be understood by looking at Fig. 3, since for this choice of parameters the neutralino decays mostly to νJ, remaining undetected and thus giving the conventional MSSM missing momentum signal. As $\tan\beta$ increases the importance of the multi-fermion channel diminishes while the channel $\tau^{\pm}$ plus 2 jets starts to become important. We present in Fig. 6 the 95% CL excluded regions in the plane (μ, M_2) for $\epsilon = 0.1$ GeV and $\tan\beta = 35$, which clearly shows that the MSSM and $\tau^{\pm}$ plus 2 jets topologies lead to similar bounds.

For larger values of ϵ, the neutralino decays mostly invisibly while the chargino presents a sizeable τJ branching ratio, see Fig. 3. Therefore, we expect that the 2 jets$+\tau$ and $\tau\tau JJ$ signatures contribute significantly to the chargino mass bound, while the importance of the MSSM topologies becomes smaller. In fact, Fig. 7 shows for $\tan\beta = 2$ and $\epsilon = 1$ GeV that the most important channel for these parameters is 2 jets $+ \tau$ in

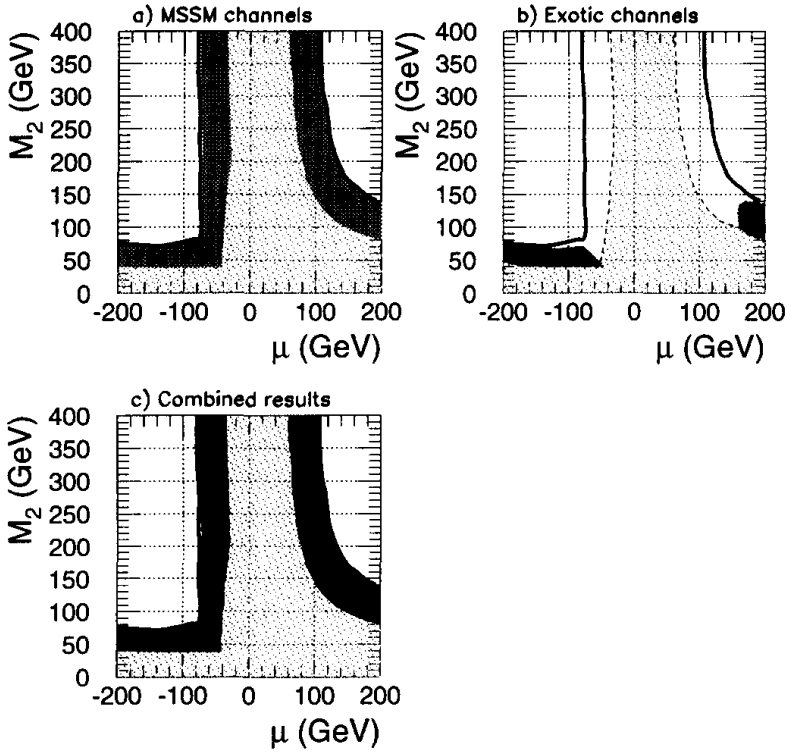

Fig. 5. 95% CL excluded region in the (μ, M_2) plane (dark shaded areas) by the analyses of (a) the MSSM and (b) exotic channels, as well as the combined excluded region (c). We assumed $\tan\beta = 2$, $\epsilon = 0.1$ GeV, $\sqrt{s} = 172$ GeV, and an integrated luminosity of 300 pb^{-1}.

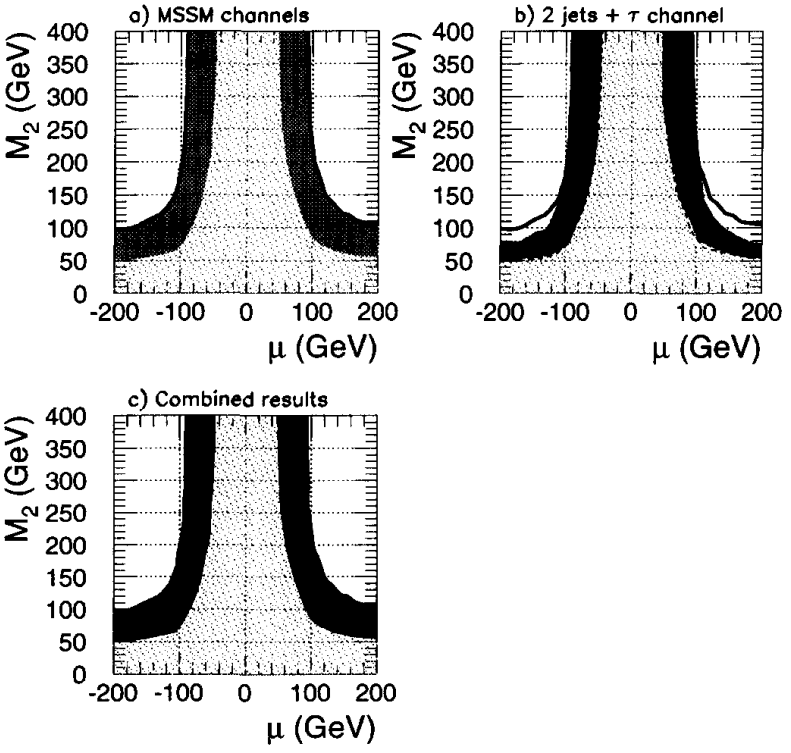

Fig. 6. 95% CL excluded region in the (μ, M_2) plane (dark shaded areas) by the analyses of (a) the MSSM and (b) 2 jets $+\tau$ channels, as well as the combined excluded region (c). We assumed $\tan\beta = 35$, $\epsilon = 0.1$ GeV, $\sqrt{s} = 172$ GeV, and an integrated luminosity of 300 pb^{-1}.

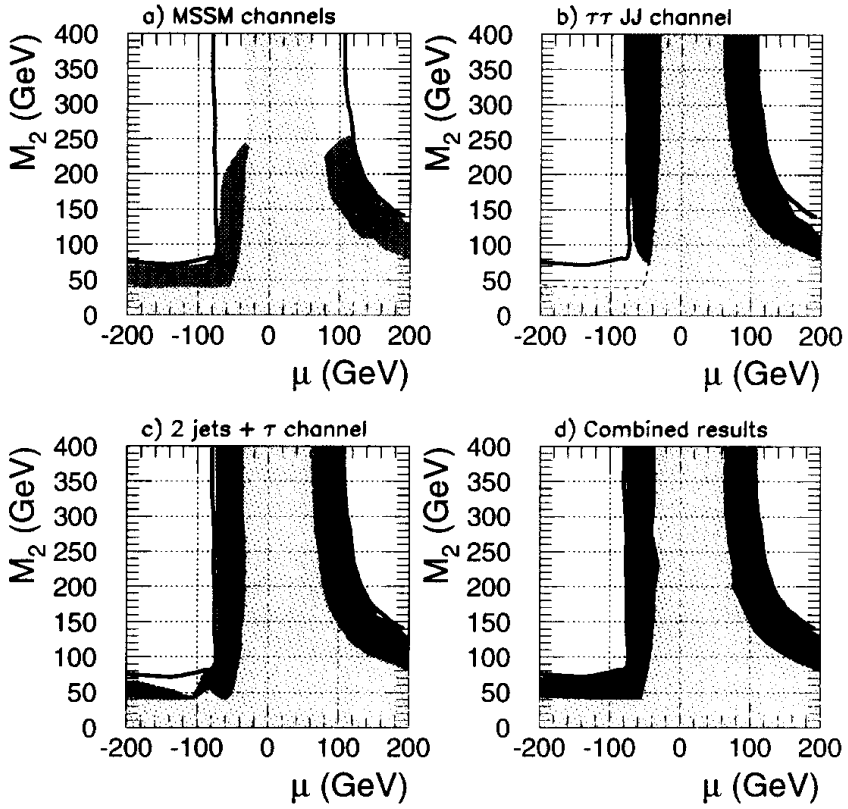

Fig. 7. 95% CL excluded region in the (μ, M_2) plane (dark shaded areas) by the analyses of (a) the MSSM, (b) $\tau\tau JJ$, and (c) 2 jets $+\tau$ channels, as well as the combined excluded region (d). We assumed $\tan\beta = 2$, $\epsilon = 1$ GeV, $\sqrt{s} = 172$ GeV, and an integrated luminosity of 300 pb^{-1}.

a large fraction of the parameter space. However, for this value of $\tan\beta$, the MSSM final states still lead to important bounds for small values of M_2. Moreover, for larger values of $\tan\beta$ the 2 jets + τ mode dominates in all points in SUSY parameter space; see Fig. 8.

Finally, for $\tan\beta = 35$ and $\epsilon = 10$ GeV, only the channels involving chargino to tau–Majoron play a significant rôle, and consequently the MSSM topologies cannot give any information. In other words, in this case the main contributions to the chargino mass constraints, as seen from Fig. 9, come from $\tau\tau\not{p}_T$ and 2 jets + τ topologies. In this range of parameters, LEP II is also able to probe chargino masses almost up to the kinematical limit despite the presence of the irreducible WW background, see Section 3.4. Furthermore, for such a large value of ϵ and smaller values of $\tan\beta$, the chargino masses compatible with the limits on the ν_τ mass are not accessible at LEP II energies, as can be seen in Fig. 1.

We summarize our results in Table 1, where we show the 95% CL chargino mass limits, that can be obtained in the absence of any signal at LEP II, for different values of the effective bilinear R-parity violation parameter ϵ and two representative values of $\tan\beta$.

These bounds are the weakest constraints that can be obtained when we vary the parameters in the ranges given by Eqs. (17) and (18), and they resulted from the

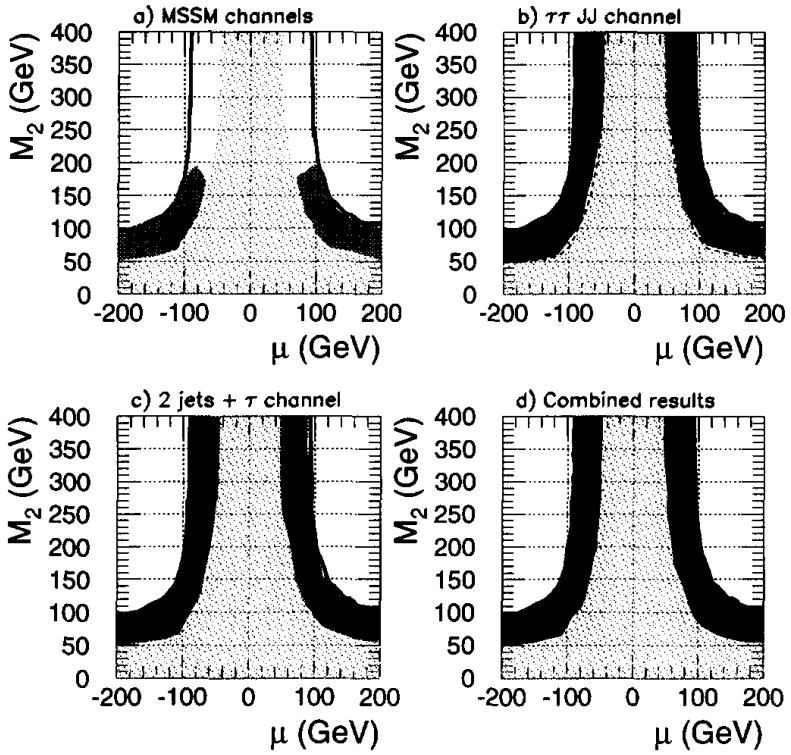

Fig. 8. 95% CL excluded region in the (μ, M_2) plane (dark shaded areas) by the analyses of (a) the MSSM, (b) $\tau\tau JJ$, and (c) 2 jets $+\tau$ channels, as well as the combined excluded region (d). We assumed $\tan\beta = 35$, $\epsilon = 1$ GeV, $\sqrt{s} = 172$ GeV, and an integrated luminosity of 300 pb^{-1}.

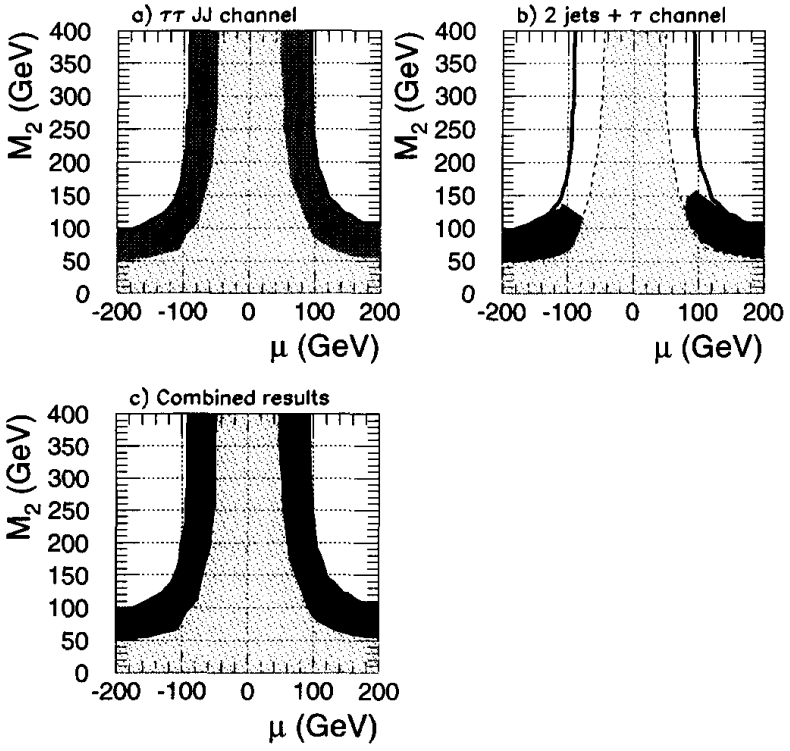

Fig. 9. 95% CL excluded region in the (μ, M_2) plane (dark shaded areas) by the analyses of (a) the $\tau\tau JJ$ and (b) 2 jets $+\tau$ (b) channels, as well as the combined excluded region (c). We assumed $\tan\beta = 35$, $\epsilon = 10$ GeV, $\sqrt{s} = 172$ GeV, and an integrated luminosity of 300 pb^{-1}.

Table 1
95% CL chargino mass limits in GeV that can be derived from negative searches at LEP II

ϵ (GeV)	$\tan\beta$	MSSM channels	$\tau\tau + \not{p}_T$	Exotic channels	Dijet $+\tau + \not{p}_T$	Combined results
0	2	86	–	–	–	86
	35	86	–	–	–	86
0.1	2	84.6	–	–	–	86
	35	84	–	–	61	86
1	2	–	60	–	63.7	84.2
	35	–	80	–	77	86
10	35	–	86	–	–	86

analysis of each topology separately, as well as from the combined results. In the case where no limit was quoted in Table 1, the bound obtained was lower than 45 GeV, the kinematical limit for LEP I, although the corresponding result was used in the combined bound. As we can see, the *combined* constraints are almost independent of $\tan\beta$, and of the R-parity-breaking parameter ϵ. For small values of ϵ, as expected, the chargino mass bounds reach up to the kinematical limit, recovering exactly the MSSM results for vanishing ϵ and v_L. For large ϵ, they come solely from $\tau\tau JJ$. For intermediate values, $\epsilon \approx 1$ GeV or so, the combination of channels is necessary, mainly $\tau\tau\not{p}_T$ and 2 jets $+ \tau$ topologies.

Assuming unification of the gaugino mass parameters, we can derive bounds on the neutralino mass from the limits on the chargino mass. We obtained a neutralino mass limit of 38 GeV for $\tan\beta = 2$ and 48 GeV for $\tan\beta = 35$, when ϵ has the values given in Table 1.

5. Comments and conclusions

We studied chargino pair production and decay at LEP II ($\sqrt{s}$ = 172 GeV) in SUSY models with spontaneously broken R-parity, characterized by the existence of the Majoron. We performed detailed signal and background analysis in order to determine the LEP II potential in probing physical parameters such as chargino or neutralino masses, m_{χ^+} or m_{χ^0}. We found that for most of the R-parity-violating SUSY parameter space the chargino signal can be seen up to chargino masses close to the kinematical limit. We explicitly verified that, as $\epsilon \to 0$ one recovers the MSSM chargino mass limit. Moreover, in analogy with standard practice, we assumed unification of the gaugino mass parameters in order to determine the corresponding neutralino mass limit. To improve this limit it is important to realize that a dedicated neutralino analysis is really needed, more so than in the corresponding MSSM case since the neutralino may exhibit visible decays.

Our analysis show that LEP II is able to discriminate between the MSSM and a model presenting spontaneous R-parity breaking in a large region of the SUSY parameter space, if charginos are indeed observed! For small values of $\epsilon(\simeq 0.1$ GeV) and $\tan\beta(\simeq 2)$, the exotic multi-fermion channel can be seen and therefore used to look for R-parity

violation when the MSSM topology is the dominant one, see Fig. 5. For larger of ϵ and $\tan\beta$, the chargino decay into τJ becomes important, and consequently, the 2 jets + τ and $\tau\tau\not{p}_T$ topologies should provide an undeniable signal for spontaneous breaking of R-parity, see Figs. 6–9.

As a final remark, we have assumed in our calculations that the whole integrated luminosity was collected at 172 GeV. Nevertheless, LEP II has already started running at 183 GeV. This increase in energy will enlarge the excluded area shown in our exclusion plots. However, we leave for the experimentalists the task of doing a more detailed analysis.

Acknowledgements

We thank M. Gandelman, J.J. Hernandez and S. Navas, for useful discussions. We also thank T. Sjostrand for valuable discussions and technical support in the preparation of our Monte Carlo for the study of the $\tau\tau JJ$ signature. This work was supported by DGICYT under grant PB95-1077, by the TMR network grant ERBFMRXCT960090 of the European Union, by Conselho Nacional de Desenvolvimento Científico e Tecnológico (CNPq), and by Fundacão de Amparo à Pesquisa do Estado de São Paulo (FAPESP). M.A.G.-J. was supported by Spanish MEC FPI fellowships.

References

[1] H.P. Nilles, Phys. Rep. 110 (1984) 1;
H. Haber and G. Kane, Phys. Rep. 117 (1985) 75.
[2] S. Dimopoulos and L.J. Hall, Phys. Lett. B 207 (1988) 210;
E. Ma and D. Ng, Phys. Rev. D 41 (1990) 1005;
V. Barger, G.F. Giudice and T. Han, Phys. Rev. D 40 (1989) 2987;
T. Banks, Y. Grossman, E. Nardi and Y. Nir, Phys. Rev. D 52 (1995) 5319;
M. Nowakowski and A. Pilaftsis, Nucl. Phys. B 461 (1996) 19;
B. de Carlos and P.L. White, Phys. Rev. D 55 (1997) 4222;
G. Bhattacharyya, Nucl. Phys. B (Proc. Suppl.) A 52 (1997) 83;
H. Dreiner, Perspectives on Supersymmetry, ed. G.L. Kane (World Scientific, Singapore) p. 462;
D. Ghosh et al., Z. Phys. C 75 (1995) 357;
A. Joshipura, hep-ph/9804346;
K. Huitu et al., Eur. Phys.J. C 6 (1999) 159;
P. Roy, hep-ph/9712520;
E.A. Baltz and P. Gondolo, Phys. Rev. D 57 (1998) 2969;
G. Bhattacharyya et al.,hep-ph/9708491;
J. Kalinosky, hep-ph/9708490;
L. Feng, hep-ph/9801248;
S. Lola, hep-ph/9706519.
[3] C.S. Aulakh and R.N. Mohapatra, Phys. Lett. B 119 (1982) 136;
G.G. Ross and J.W.F. Valle, Phys. Lett. B 151 (1985) 375;
J. Ellis, G. Gelmini, C. Jarlskog, G.G. Ross and J.W.F. Valle, Phys. Lett. B 150 (1985) 142;
A. Santamaria and J.W.F. Valle, Phys. Lett. B 195 (1987) 423; Phys. Rev. D 39 (1989) 1780;
Phys. Rev. Lett. 60 (1988) 397.
[4] L. Hall and M. Suzuki, Nucl. Phys. B 231 (1984) 419.

[5] For a recent review see J.W.F. Valle, *in* Physics Beyond the Standard Model, Lectures given at the VIII Jorge Andre Swieca Summer School (Rio de Janeiro, February 1995) and at V Taller Latinoamericano de Fenomenologia de las Interacciones Fundamentales (Puebla, Mexico, October 1995) [hep-ph/9603307].
[6] J.W.F. Valle, Phys. Lett. B 196 (1987) 157.
[7] M.C. Gonzalez-Garcia and J W F Valle, Nucl. Phys. B 355 (1991) 330.
[8] A Masiero and J.W.F. Valle, Phys. Lett. B 251 (1990) 273;
J.C. Romão, C.A. Santos and J.W.F. Valle, Phys. Lett. B 288 (1992) 311.
[9] G. Giudice, A. Masiero, M. Pietroni and A. Riotto, Nucl. Phys. B 396 (1993) 243;
M. Shiraishi, I. Umemura and K. Yamamoto, Phys. Lett. B 313 (1993) 89;
see also I. Umemura and K. Yamamoto, Nucl. Phys. B 423 (1994) 405.
[10] P. Nogueira, J.C. Romão and J.W.F. Valle, Phys. Lett. B 251 (1990) 142;
R. Barbieri and L. Hall, Phys. Lett. B 238 (1990) 86.
[11] J. Romão, J. Rosiek and J.W.F. Valle, Phys. Lett. B 351 (1995) 497.
[12] J.C. Romão, N. Rius and J.W.F. Valle, Nucl. Phys. B 363 (1991) 369.
[13] J.C. Romão and J.W.F. Valle. Phys. Lett. B 272 (1991) 436; Nucl. Phys. B 381 (1992) 87.
[14] For recent reviews see J.W.F. Valle, Gauge Theories and the Physics of Neutrino Mass, Prog. Part. Nucl. Phys. 26 (1991) 91 (ed. A. Faessler);
G. Gelmini and S. Roulet, UCLA/94/TEP/36, and references therein.
[15] V. Berezinsky, Anjan S. Joshipura and J.W.F. Valle, Phys. Rev. D 57 (1998) 147.
[16] V. Berezinskii and J.W.F. Valle, Phys. Lett. B 318 (1993) 360.
[17] A. Bartl, W. Porod, F. de Campos, M.A. García-Jareño, M.B. Magro, J.W.F. Valle and W. Majerotto, Nucl. Phys. B 502 (1997) 19 [hep-ph/9612436].
[18] J.C. Romao, A. Ioannissyan, J.W.F. Valle, Phys. Rev. D 55 (1997) 427
[19] R. Mohapatra and J.W.F. Valle, Phys. Rev. D 34 (1986) 1642;
J.W.F. Valle, Theory and Implications of Neutrino Mass, Nucl. Phys. B (Proc. Suppl.) 11 (1989) 118, and references therein.
[20] R. Barbieri, S. Ferrara and C. Savoy, Phys. Lett. B 119 (1982) 343.
[21] J.E. Kim, Phys. Rep. 150 (1987) 1;
D. Dearborn, et al., Phys. Rev. Lett. 56 (1986) 26;
M. Fukugita et al., Phys. Rev. Lett. 48 (1982) 1522; Phys. Rev. D 26 (1982) 1841;
J. Ellis and K. Olive, Nucl. Phys. B 223 (1983) 252.
[22] Marco A. Diaz, Jorge C. Romao, Jose W.F. Valle, Nucl. Phys. B 524 (1998) 23 [hep-ph/9706315].
[23] ALEPH Collaboration, Nucl. Phys. Proc. Suppl. 66 (1998) 214.
[24] F. de Campos, M.A. García-Jareño, A.S. Joshipura, J. Rosiek and J.W.F. Valle Nucl. Phys. B 451 (1995) 3.
[25] F. de Campos, M.A. García-Jareño, M.B. Magro, J. Romão and J.W.F. Valle, Nucl. Phys. B 482 (1996) 3.
[26] A. Bartl et al., Z. Phys. C 30 (1986) 441; Z. Phys. C 41 (1988) 475.
[27] F. Richard, talk at CERN, Feb. 25, 1997. For details see S. Navas PhD thesis, DELPHI, Univ. of Valencia, 1997.
[28] A.G. Akeroyd, M.A. Diaz and J.W.F. Valle, hep-ph/9806382, Phys. Lett. B 441 (1998) 224.
[29] R. Adhikari and B. Mukhopadhyaya, Phys. Lett. B 378 (1996) 342; B 384 (1996) 492 (E);
G. Ganis, talk presented at the 29th Int. Conf. on High Energy Physics, Vancouver, Canada, July 23–29, 1998, MPI-PhE/98-14.
[30] T. Sjöstrand, Comp. Phys. Commun. 82 (1994) 74.
[31] ALEPH Collaboration, R. Barate et al., preprint CERN-PPE/97-056 [hep-ex/9706006];
M. Berggren, M. Gandelman and J.H. Lopes, preprint DELPHI 97-156 PHYS 735.
[32] G. Altarelli et al., eds., Physics at LEPII, CERN 96-01.

PHYSICAL REVIEW D **80,** 015002 (2009)

Finding the Higgs boson through supersymmetry

F. de Campos,[1,*] O. J. P. Éboli,[2,†] M. B. Magro,[2,3,‡] D. Restrepo,[4,5,§] and J. W. F. Valle[4,‖]

[1]*Departamento de Física e Química, Universidade Estadual Paulista, Guaratinguetá–SP, Brazil*
[2]*Instituto de Física, Universidade de São Paulo, São Paulo–SP, Brazil.*
[3]*Centro Universitário Fundação Santo André, Santo André–SP, Brazil.*
[4]*AHEP Group, Instituto de Física Corpuscular–C.S.I.C./Universitat de València, Edificio Institutos de Paterna, Apt 22085, E–46071 Valencia, Spain*
[5]*Instituto de Física, Universidad de Antioquia, Colombia*

(Received 10 September 2008; published 6 July 2009)

The study of displaced vertices containing two b-jets may provide a double discovery at the Large Hadron Collider (LHC): we show how it may not only reveal evidence for supersymmetry, but also provide a way to uncover the Higgs boson necessary in the formulation of the electroweak theory in a large region of the parameter space. We quantify this explicitly using the simplest minimal supergravity model with bilinear breaking of R-parity, which accounts for the observed pattern of neutrino masses and mixings seen in neutrino oscillation experiments.

DOI: 10.1103/PhysRevD.80.015002 PACS numbers: 12.60.Jv, 13.85.Ni, 14.60.Pq, 14.80.Cp

I. INTRODUCTION

By opening the exploration of the new territory of physics at the terascale, the CERN Large Hadron Collider (LHC) is likely to shed light upon the main open puzzle in particle physics, namely, the origin of mass and the nature of electroweak symmetry breaking. Supersymmetry (SUSY) provides an elegant way of justifying the electroweak symmetry breaking mechanism in terms of an elementary Higgs particle, alleviating the so called hierarchy problem [1]. The Higgs boson and the existence of supersymmetry therefore stand out as the main missing pieces in our understanding of fundamental forces, and a lot of effort has been put into their direct observation. Indeed the search for the Higgs boson and for supersymmetry constitutes the main topic in the agenda of the LHC.

In contrast, so far the only established evidence for physics beyond the standard model (SM) has been the discovery of neutrino masses and oscillations [2], which has culminated decades of painstaking efforts.

Here we stress that these two issues may be closely related. Indeed, low-energy supersymmetry with broken R-parity [3] provides a plausible mechanism for the origin for neutrino masses and mixings. Indeed, as the bilinear model best illustrates [4], in contrast to the simplest seesaw schemes [5], these may be tested at particle accelerators like the LHC.[1]

Here we consider the simplest ansatz to introduce R-parity breaking in supersymmetry, characterized by an additional bilinear violating (BRpV) term in the superpotential [9]. It provides the simplest effective description of a more complete picture containing additional neutral heavy lepton [10] superfields whose scalars drive the spontaneous breaking of R-parity [11].

Our focus here is on the specific case of a minimal gravity mediated supersymmetry breaking model with bilinear R-parity violation: BRpV-mSUGRA model for short. In this model, the lightest supersymmetric particle (LSP) is no longer stable. Current neutrino oscillation data indicate that the strength of the BRpV term is small [9], hence the LSP decay length is expected to be long enough to provide a displaced vertex at the LHC [12,13]. For a low Higgs mass the dominant decay is into $b\bar{b}$, however at the LHC the overwhelming QCD background makes this signal irrelevant when the Higgs is produced in the standard way. In supersymmetry the Higgs can be produced after the decay chains of the next-to-lightest supersymmetric particle. In the R-parity conserving case for specific spectrum and supersymmetric production, the additional jets and the missing energy can allow the discovery of the Higgs in the b channel [14]. The same features also hold in our case, but in addition now the Higgs can be produced from the lightest neutralino, leading to events with a displaced vertex with two large invariant mass b-jets. The signal of a neutralino into a Higgs and a neutrino is therefore free of SM backgrounds if the neutralino decays inside the pixel detector and well outside the interaction point. Here we show explicitly that this is the case.[2]

In this work we analyze the potential of the LHC to survey the existence of the Higgs boson using a novel

*camposc@feg.unesp.br
†eboli@fma.if.usp.br
‡magro@fma.if.usp.br
§restrepo@uv.es
‖valle@ific.uv.es

[1]Such a model has no conventional neutralino dark matter, though other possible dark matter candidates may be envisaged such as the axion [6], the majoron [7], the axino, or the gravitino [8].

[2]In fact the LHCb Collaboration is considering the possibility of searching for b's originating outside the interaction point [15].

signal: a b-jet pair coming from displaced vertices generated by the lightest neutralino decays within the BRpV-mSUGRA model. We demonstrate that the LHC reach is capable of uncovering a supersymmetric Higgs in a fair region of the $M_{1/2} \otimes M_0$ parameter plane.

II. MODEL DESCRIPTION

The BRpV model is described by the superpotential

$$W_{\rm BRpV} = W_{\rm MSSM} + \varepsilon_{ab}\epsilon_i \hat{L}_i^a \hat{H}_u^b, \tag{1}$$

in which the standard minimal supersymmetric model (MSSM) is supplemented by three extra bilinear terms characterized by three new parameters (ϵ_i), one for each fermion generation. In addition to these we must also include new soft supersymmetry breaking terms (B_i) in whose presence the bilinears become physical parameters that cannot be rotated away [16],

$$V_{\rm soft} = V_{\rm MSSM} - \varepsilon_{ab} B_i \epsilon_i \tilde{L}_i^a H_u^b. \tag{2}$$

The new terms in the BRpV Lagrangian (ϵ_i, B_i) lead to the explicit violation of lepton number as well as R-parity. Furthermore, the sneutrino fields acquire a vacuum expectation value (VEV) when we minimize the scalar potential.

In BRpV models the terms presenting explicit lepton number violation, as well as the sneutrino vacuum expectation values, generate mixing among neutrinos and neutralinos giving rise to one tree-level neutrino mass. The other two neutrino masses are generated through loop diagrams [9]. One can show that, indeed, the resulting neutrino masses and mixings provide a good description of all current neutrino oscillation data [2].

For the sake of definiteness, we assume mSUGRA as the model of supersymmetry breaking, implying universality of the soft breaking terms at unification. In this case, our model depends upon 11 free parameters, namely

$$M_0, M_{1/2}, \tan\beta, \text{sign}(\mu), A_0, \epsilon_i, \quad \text{and} \quad \Lambda_i, \tag{3}$$

where $M_{1/2}$ and M_0 are the common gaugino mass and scalar soft SUSY breaking masses at the unification scale, A_0 is the common trilinear term, and $\tan\beta$ is the ratio between the Higgs field VEV's. For convenience, we trade the soft parameters B_i by $\Lambda_i = \epsilon_i v_d + \mu v_i$, where v_i is the vacuum expectation value of the sneutrino fields, since the Λ_i's are more directly related to the neutrino masses; for further details see [9].

The bilinear R-parity violating interaction gives rise to mixings between SM and SUSY particles that lead to decay of the LSP into SM particles. In a large fraction of the parameter space the lightest neutralino is the LSP and it can decay into leptonic final states $\nu\ell^+\ell'^-$, where $\ell = e$, μ, or τ, as well as into semileptonic final states $\ell q'\bar{q}$ or $\nu q\bar{q}$. For sufficiently heavy neutralinos these decays are dominated by two-body channels like νZ, $\ell^\pm W^\mp$, and νh with h being the lightest CP-even Higgs boson; for further details see [13,17,18]. In the region where the stau is the LSP the detached vertex signal disappears completely since the stau possesses a very small decay length.

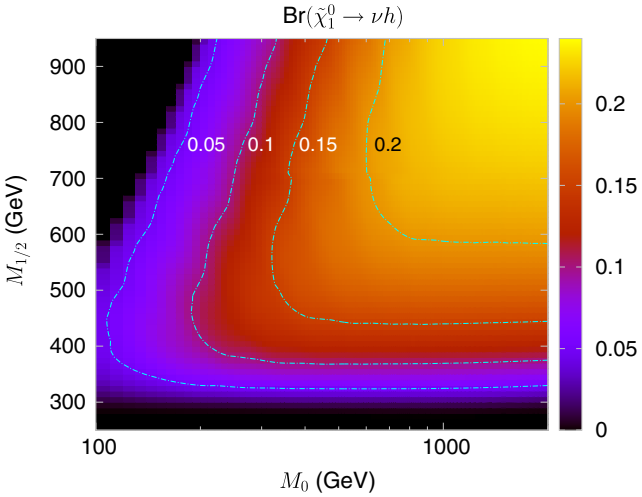

FIG. 1 (color online). Br($\tilde{\chi}_1^0 \to h\nu$) as a function of $M_{1/2} \otimes M_0$ for $\tan\beta = 10$, $A_0 = -100$ GeV, and $\mu > 0$.

In contrast, a salient feature of our BRpV model is that neutralino LSP's exhibit a rather large decay length, ranging from a few millimeters to tenths of millimeters for $M_{1/2}$ varying from 200 GeV to 1 TeV. Such large decay lengths lead to the production of detached vertices at the LHC which constitute a smoking gun of this kind of model.

In this work, we analyze the two-body lightest neutralino decay into the lightest Higgs boson h^0 as a Higgs discovery channel

$$\tilde{\chi}_1^0 \to h\nu. \tag{4}$$

If the lightest neutralino lives long enough it will be detached from the primary interaction point leaving a displaced vertex as signal at the LHC. Since the Higgs boson h decays mostly into a b-quark pair we expect a displaced vertex with two b-jets as a characteristic signature for Higgs production.

We present, in Fig. 1, the lightest neutralino branching ratio to $h\nu$ as a function of $M_{1/2} \otimes M_0$ for $\tan\beta = 10$, $A_0 = -100$ GeV, and $\mu > 0$.[3] Here we focus on the situation where the lightest neutralino is heavier then h, so the neutralino Higgs decay channel opens for $M_{1/2} \gtrsim \mathcal{O}(300)$ GeV for our choice of parameters. The maximum value of the branching ratio for this channel is about 22%; for an illustration of the full behavior of neutralino decays see, for example, Refs. [13,17,18]. This figure tells us that, for fixed values of $M_{1/2}$, the LSP branching ratio into Higgs-neutrino pairs initially grows with increasing M_0, stabilizing for M_0 in excess of a few hundred GeV. On the

[3]We note that in the upper left dark region the stau is the LSP and in what follows we will not consider this region.

other hand, the importance of this decay increases with $M_{1/2}$ for moderate and large values of M_0.

III. SIGNAL AND BACKGROUNDS

In order to simulate the Higgs production we calculate all R-parity violating branching ratios and SUSY spectra using the package SPHENO [19]. We used PYTHIA version 6.408 [20] to generate events, using the SPHENO output in the SLHA format [21]. In order to have a rough simulation of the detector response we smeared the track energies, but not their directions, with a Gaussian error given by $\Delta E/E = 0.10/\sqrt{E} + 0.01$ (E in GeV) for leptonic tracks and $\Delta E/E = 0.5/\sqrt{E} + 0.03$ for all hadronic tracks.

Displaced vertices at the LHC were identified requiring that the neutralino decays away from the primary vertex point, that is, outside an ellipsoid centered at the primary vertex

$$\left(\frac{x}{5\delta_{xy}}\right)^2 + \left(\frac{y}{5\delta_{xy}}\right)^2 + \left(\frac{z}{5\delta_z}\right)^2 = 1, \tag{5}$$

where the z axis is along the beam direction. To be conservative we assumed the ellipsoid size to be 5 times the ATLAS experiment's expected precision in both directions for the semiconductor tracker [22] which are $\delta_{xy} = 20\ \mu$m and $\delta_z = 500\ \mu$m. To reconstruct the vertices we required that visible tracks coming from neutralino decays must have an intersection inside a sphere determined by the tracking detector resolution which we assumed to be 10 μm [22]. Furthermore, we considered only the charged tracks inside the pseudorapidity region of $|\eta| < 2.5$.

Since the Higgs production in the LSP decay is characterized by the presence of two b-tagged jets we looked for events with at least one displaced vertex containing at least one jet tagged as a b-jet. In our analyses we considered a b-tagging efficiency up to 50%.

In order to ensure that the detached vertex events are properly recorded we accepted only events that pass very simple trigger requirements. We further required the events to present an isolated electron (muon) with $p_T >$ 20(6) GeV, or the presence of a jet with $p_T > 100$ GeV, or missing transverse energy in excess of 100 GeV.

For our analysis we have fixed $\tan\beta = 10$, $A_0 = -100$ GeV, and $\mu > 0$. For this choice of parameters, the Higgs mass lies in the range 110 GeV $\lesssim M_h \lesssim$ 120 GeV when we vary M_0 and $M_{1/2}$. Since we are only interested in detached jets coming from Higgs decays, we have further required that the jet-jet invariant mass is around the Higgs mass value.

Within the SM framework displaced vertices originate from decays of long lived particles like B's and τ's, and consequently its visible decay products exhibit a rather small invariant mass. In contrast, in our BRpV model, the displaced vertices are associated with the LSP decay and will have in general a large invariant mass associated with them. Therefore, physical SM processes do not lead to sizable backgrounds to the detached Higgs searches due to large difference in the invariant mass of the visible products. However, BRpV LSP decays into νZ are a potential source of background for the Higgs signal.

As an illustration we show in Fig. 2 the jet-jet invariant mass distribution of all displaced vertices exhibiting jets. As we can see, a cut on the invariant mass outside the range 100 GeV $< M_{\rm inv} <$ 125 GeV eliminates a good fraction of supersymmetric backgrounds coming, for instance, from the neutralino decay into W and Z bosons as well as the three-body $b\bar{b}\nu$ channel. The physical background can be further suppressed by requiring that at least one of the jets associated with the displaced vertex is tagged as a b-jet. Moreover, these requirements ensure that SM backgrounds coming from the decay of long lived particles are also efficiently eliminated. There remain instrumental backgrounds [23] which require a full detector simulation along the lines we have described above; this simulation is beyond the scope of the present work.

In Fig. 3 we show that almost all vertices containing b-jets come from neutralino decay via Higgs and that our invariant mass cut will eliminate the νZ background, while keeping a large fraction of the signal events. We checked that the events passing the LHC triggers and all the above cuts come from the signal events $\tilde{\chi}_1^0 \to \nu h$ with the physics background being negligible.

In order to estimate the LHC reach for Higgs search coming from displaced vertex signal in BRpV-mSUGRA

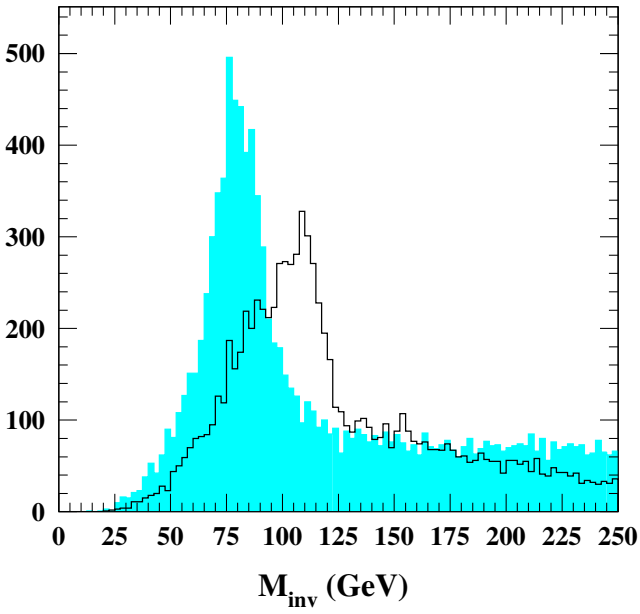

FIG. 2 (color online). Jet pair invariant mass distribution in GeV. The light blue (grayish) histogram stands for the background where the lightest neutralino decays via W and Z bosons and the other histogram stands for the channels where the lightest neutralino decays into $b\bar{b}$ pairs.

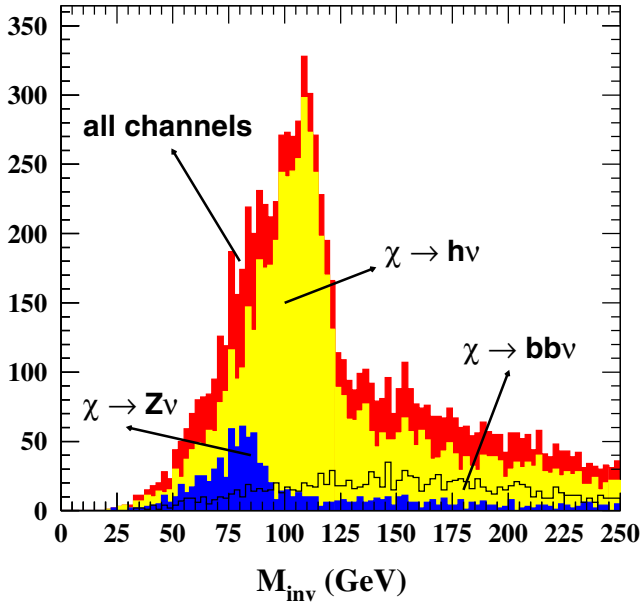

FIG. 3 (color online). Invariant mass distribution in GeV of the neutralino decaying into b-jet pairs separated into its several channels.

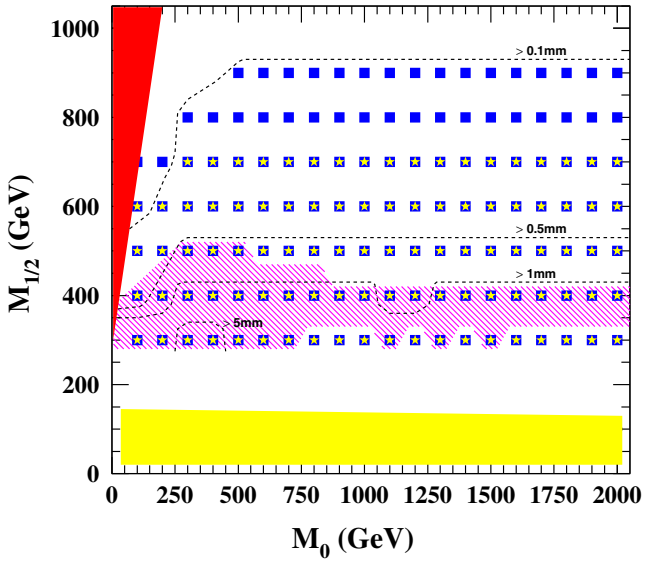

FIG. 4 (color online). LHC reach for Higgs search in displaced vertices for the BRpV-mSUGRA model in the plane $M_{1/2} \otimes M_0$ assuming $\tan\beta = 10$, $A_0 = -100$ GeV, and $\mu > 0$. The yellow stars (blue squares) represent the reach for an integrated luminosity of 10(100) fb^{-1} while the crosshatched region corresponds to the reach of the LHCb experiment for an integrated luminosity of 10 fb^{-1}. The (yellow) shaded region at the bottom stands for points excluded by direct LEP searches, while the (red) upper left area represents a region where the stau is the LSP. Note that the black lines delimit different regimes of LSP decay length.

models we considered a few scenarios. In the optimistic analysis we assumed that there is no event coming from instrumental backgrounds or overlapping events and took the b-tagging efficiency to be 50%. In this case we required that the signal must have more than five events since no background is expected and present our result in the $M_{1/2} \otimes M_0$ plane for integrated luminosities of 10 and 100 fb^{-1}. We also considered three additional scenarios. In the first one we studied the impact of a lower b-tagging efficiency (30%) but we still assumed that the process is background free. In the second case we assumed that there are five backgrounds events originating from instrumental errors and overlapping events and required a 5σ signal for a 50% b-tagging efficiency. Finally, in the last scenario we assumed the same background as in the last case, lowering however the b-tagging efficiency down to 30%.

IV. RESULTS

In Fig. 4 we depict the LHC discovery reach for the Higgs displaced vertex signal in our most optimistic scenario. The shaded (yellow) region at the bottom stands for points already excluded by direct LEP searches while the upper left corner of the $M_{1/2} \otimes M_0$ plane, the (red) shaded area has staus as LSP [13], and hence is not covered by the present analysis. The region around $M_{1/2} = 200$ GeV has no signal due to the fact that the neutralino mass is smaller than the Higgs mass in it, therefore, being forbidden the two-body LSP decays into Higgs-neutrino pairs.

From Fig. 4 one can see that the ATLAS and CMS experiments will be able to look for the signal up to $M_{1/2}$ 700(900) GeV for a LHC integrated luminosity of 10(100) fb^{-1}. Notice that the LHC Higgs discovery potential is almost independent of M_0. For a fixed value of $M_{1/2}$ the LSP total production cross section decreases as M_0 increases, however, the LSP branching ratio into Higgs-neutrino pairs increases with M_0, therefore, both effects tend to cancel and produce the observed behavior. Moreover, this figure also exhibits the average decay length of the neutralino, demonstrating that its decay takes place inside the vertex detector, ensuring a good vertex reconstruction.

We have also estimated the reach expected at LHCb for our Higgs search proposal. The crosshatched region in Fig. 4 indicates the LHCb reach for 10 fb^{-1}. Because of the strong cut on the pseudorapidity required by this experiment, the reach for 2 fb^{-1} is severely depleted and only a small region of the parameter space is covered, i.e., $300\ \text{GeV} \leq M_{1/2} \leq 350\ \text{GeV}$ and $200\ \text{GeV} \leq M_0 \leq 500\ \text{GeV}$.

Tagging b-jets emanating from a detached vertex is certainly a more intricate procedure, therefore, we also considered a lower b-tagging efficiency in our analyses. Figure 5 contains the reach of LHC for Higgs search using a b-jet reconstruction efficiency of 30%, instead of 50% used of Fig. 4, however, we still assumed that the search is background free. Comparing Figs. 4 and 5, one can see that

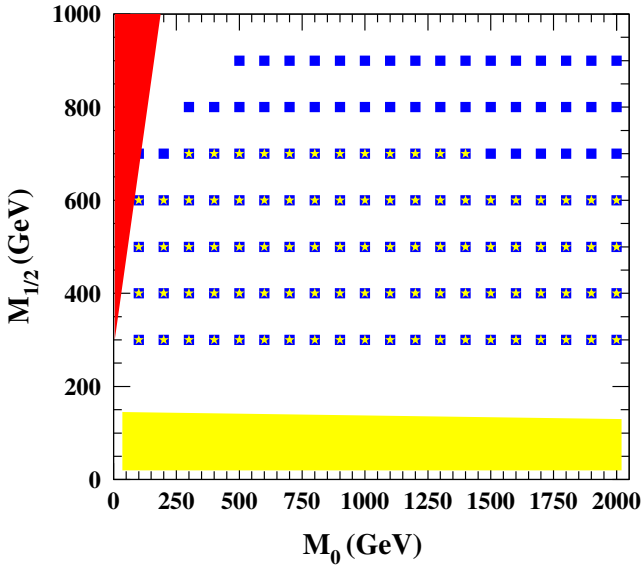

FIG. 5 (color online). Same as Fig. 4 using a b-jet reconstruction efficiency of 30% with no background events.

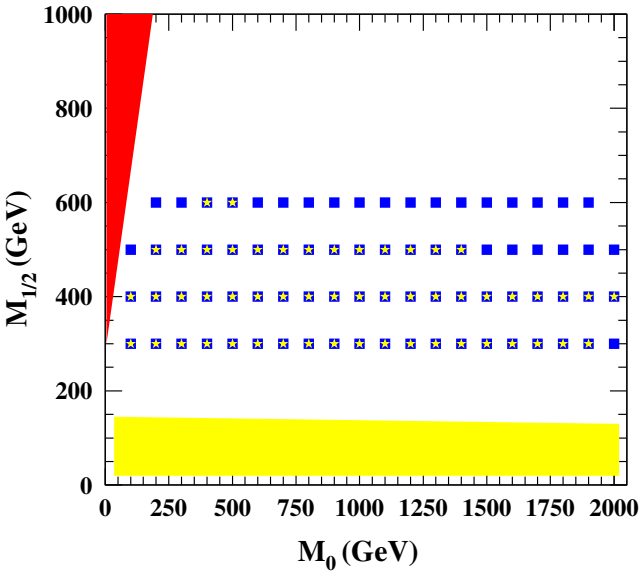

FIG. 7 (color online). Same as Fig. 4 using a b-jet reconstruction efficiency of 30% and five background events.

the LHC reach in this second case is mildly affected by this change for an integrated luminosity of 10 fb^{-1}, while the changes are minute at higher integrated luminosities.

A study of the instrumental backgrounds and the effect of overlapping events does require a full detector simulation, which is beyond the scope of this work. In order to assess the impact of existence of nonphysical backgrounds we considered that these backgrounds give rise to five background events for both integrated luminosities used in our studies. In Fig. 6 we present the 5σ LHC Higgs discovery potential assuming a b-jet reconstruction efficiency of 50% and five background events. We can see from this figure that the existence of background events does lead to a substantial reduction of the LHC reach for Higgs in displaced vertices.

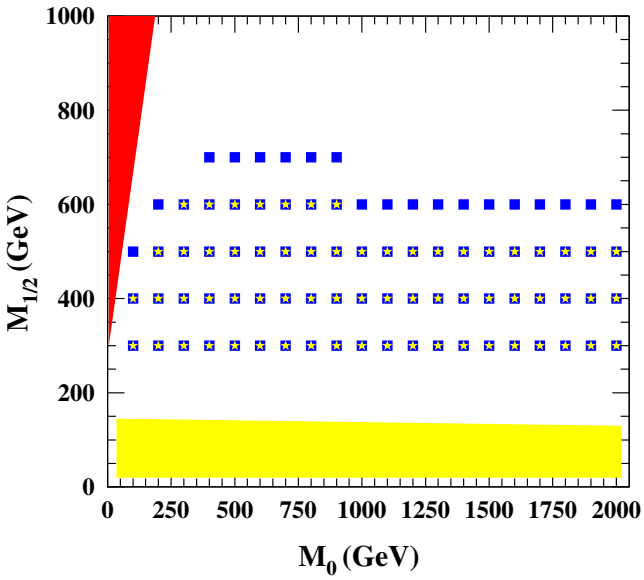

FIG. 6 (color online). Same as Fig. 4 using a b-jet reconstruction efficiency of 50% and assuming the existence five background events for both integrated luminosities.

In Fig. 7 we present the reach of LHC for Higgs search in a very pessimistic scenario that exhibits a lower b-jet reconstruction efficiency of 30%, as well as the presence of five background events. In this case we observe a more severe reduction of the LHC reach that is reduced to $M_{1/2} = 600$ GeV at most. This large depletion of the LHC search potential follows from the need of a large number of signal events to establish the signal given the fast decrease of the SUSY production cross section with increasing $M_{1/2}$. In this sense, the 100 fb^{-1} case is more affected since the production cross section exhibits a steep decrease for $M_{1/2} \gtrsim 700$ GeV.

V. CONCLUSIONS

In summary we have seen how the search for displaced vertices containing b-tagged jets at the LHC may not only provide evidence for supersymmetric particles but also lead to the discovery of the Higgs boson of the electroweak theory. We have given a quantitative analysis within the simplest minimal supergravity model with bilinear breaking of R-parity, which accounts for the observed pattern of neutrino masses and mixings observed in current neutrino oscillation experiments. Similar variant schemes can be envisaged where, for example, supersymmetry and/or electroweak breaking is realized differently.

In an optimistic background free scenario, the Higgs search in LSP decays can be carried out for LSP masses

up to 300 (380) GeV for an integrated luminosity of 10(100) fb^{-1}. We showed that this result is robust against variations of the assumed b-tagging efficiencies. Notwithstanding, the results change drastically if instrumental backgrounds are present. Assuming the existence of five background events reduces the LHC reach to LSP masses of 210 (250) GeV at the low (high) luminosity run.

ACKNOWLEDGMENTS

We thank A. Bartl for careful reading the manuscript. This work was supported by MEC Grant No. FPA2005-01269, by EC Contracts RTN network MRTN-CT-2004-503369, by Conselho Nacional de Desenvolvimento Científico e Tecnológico (CNPq) and by Fundação de Amparo à Pesquisa do Estado de São Paulo (FAPESP) and by Colciencias in Colombia under Contract No. 1115-333-18740.

[1] S. Dimopoulos, S. Raby, and F. Wilczek, Phys. Rev. D **24**, 1681 (1981).

[2] For a review of neutrino oscillations see M. Maltoni *et al.*, New J. Phys. **6**, 122 (2004). An updated three-flavor neutrino oscillation analysis is given by T. Schwetz, M. Tortola, and J. W. F. Valle, New J. Phys. **10**, 113011 (2008).

[3] For early references see L. J. Hall and M. Suzuki, Nucl. Phys. **B231**, 419 (1984); G. G. Ross and J. W. F. Valle, Phys. Lett. **151B**, 375 (1985); J. R. Ellis *et al.*, Phys. Lett. **150B**, 142 (1985).

[4] For a recent review see M. Hirsch and J. W. F. Valle, New J. Phys. **6**, 76 (2004).

[5] H. Nunokawa, S. J. Parke, and J. W. F. Valle, Prog. Part. Nucl. Phys. **60**, 338 (2008); this review gives an updated discussion of the standard seesaw mechanism and its variants.

[6] R. D. Peccei and H. R. Quinn, Phys. Rev. Lett. **38**, 1440 (1977); for a review see R. D. Peccei, Lect. Notes Phys. **741**, 3 (2008).

[7] V. Berezinsky and J. W. F. Valle, Phys. Lett. B **318**, 360 (1993); E. K. Akhmedov, Z. G. Berezhiani, R. N. Mohapatra, and G. Senjanovic, Phys. Lett. B **299**, 90 (1993); M. Lattanzi and J. W. F. Valle, Phys. Rev. Lett. **99**, 121301 (2007); F. Bazzocchi, M. Lattanzi, S. Riemer-Sorensen, and J. W. F. Valle, J. Cosmol. Astropart. Phys. 08 (2008) 013.

[8] C. Muñoz, Int. J. Mod. Phys. A **19**, 3093 (2004); M. Hirsch, W. Porod, and D. Restrepo, J. High Energy Phys. 03 (2005) 062.

[9] M. Hirsch *et al.*, Phys. Rev. D **62**, 113008 (2000); **65**, 119901(E) (2002); J. C. Romão *et al.*, Phys. Rev. D **61**, 071703 (2000); M. A. Díaz *et al.*, Phys. Rev. D **68**, 013009 (2003); **71**, 059904(E) (2005); D. E. Kaplan and A. E. Nelson, J. High Energy Phys. 01 (2000) 033; C. H. Huang and T. F. Feng, Eur. Phys. J. C **12**, 137 (2000); Y. Grossman and H. E. Haber, arXiv:hep-ph/9906310.

[10] M. Dittmar, A. Santamaria, M. C. Gonzalez-Garcia, and J. W. F. Valle, Nucl. Phys. **B332**, 1 (1990); M. C. Gonzalez-Garcia, A. Santamaria, and J. W. F. Valle, Nucl. Phys. **B342**, 108 (1990); P. Abreu *et al.*, Z. Phys. C **74**, 57 (1997); **75**, 580(E) (1997).

[11] A. Masiero and J. W. F. Valle, Phys. Lett. B **251**, 273 (1990).

[12] M. B. Magro, F. de Campos, O. J. P. Éboli, W. Porod, D. Restrepo, and J. W. F. Valle, J. High Energy Phys. 09 (2003) 071; F. de Campos, O. J. P. Éboli, M. B. Magro, W. Porod, D. Restrepo, and J. W. F. Valle, Phys. Rev. D **71**, 075001 (2005).

[13] F. de Campos, O. J. P. Éboli, M. B. Magro, W. Porod, D. Restrepo, M. Hirsch, and J. W. F. Valle, J. High Energy Phys. 05 (2008) 048.

[14] M. Consonni, Nucl. Phys. B, Proc. Suppl. **177-178**, 271 (2008).

[15] Higgs and Exotica, https://twiki.cern.ch/twiki//bin/view/LHCb/HiggsExotica.

[16] M. A. Díaz, J. C. Romão and J. W. Valle, Nucl. Phys. **B524**, 23 (1998); S. Y. Choi, E. J. Chun, S. K. Kang, and J. S. Lee, Phys. Rev. D **60**, 075002 (1999); D. E. Kaplan and A. E. Nelson, J. High Energy Phys. 01 (2000) 033; C. H. Chang and T. F. Feng, Eur. Phys. J. C **12**, 137 (2000); F. Takayama and M. Yamaguchi, Phys. Lett. B **476**, 116 (2000); T. Banks, Y. Grossman, E. Nardi, and Y. Nir, Phys. Rev. D **52**, 5319 (1995); J. C. Romão *et al.*, Nucl. Phys. **B482**, 3 (1996); M. Nowakowski and A. Pilaftsis, Nucl. Phys. **B461**, 19 (1996); G. Bhattacharyya, D. Choudhury, and K. Sridhar, Phys. Lett. B **355**, 193 (1995); H. P. Nilles and N. Polonsky, Nucl. Phys. **B484**, 33 (1997); B. de Carlos and P. L. White, Phys. Rev. D **55**, 4222 (1997).

[17] W. Porod, M. Hirsch, J. Romão, and J. W. F. Valle, Phys. Rev. D **63**, 115004 (2001).

[18] F. de Campos, O. J. P. Eboli, M. B. Magro, and D. Restrepo, Phys. Rev. D **79**, 055008 (2009).

[19] W. Porod, Comput. Phys. Commun. **153**, 275 (2003).

[20] T. Sjöstrand, Comput. Phys. Commun. **82**, 74 (1994); T. Sjöstrand, P. Eden, C. Friberg, L. Lonnblad, G. Miu, S. Mrenna, and E. Norrbin, Comput. Phys. Commun. **135**, 238 (2001).

[21] P. Skands *et al.*, J. High Energy Phys. 07 (2004) 036; B. Allanach *et al.*, Comput. Phys. Commun. **180**, 8 (2009).

[22] G. Aad *et al.* (ATLAS Collaboration), JINST **3**, P07007 (2008).

[23] M. J. Strassler, arXiv:0806.2385.

PHYSICAL REVIEW D **86,** 075001 (2012)

Probing neutralino properties in minimal supergravity with bilinear *R*-parity violation

F. de Campos[*]
Departamento de Física e Química, Universidade Estadual Paulista, Av. Dr. Ariberto Pereira da Cunha, 333, 12516-410 Guaratinguetá, São Paulo, Brazil

O. J. P. Éboli[†]
Instituto de Física, Universidade de São Paulo, C.P. 66318, 05315-970 São Paulo, São Paulo, Brazil and Institut de Physique Théorique, CEA-Saclay Orme des Merisiers, 91191 Gif-sur-Yvette, France

M. B. Magro[‡]
Instituto de Física, Universidade de São Paulo, C.P. 66318, 05315-970 São Paulo, São Paulo, Brazil and Centro Universitário Fundação Santo André, Av. Príncipe de Gales, 821, 09060-650 Santo André, São Paulo, Brazil

W. Porod[§]
Institut für Theoretische Physik und Astronomie, Universität Würzburg, Campus Hubland Nord, Emil-Hilb-Weg 22, 97074 Würzburg, Germany

D. Restrepo[‖]
Instituto de Física, Universidad de Antioquia, A.A. 1226 Medellin, Colombia

S. P. Das,[¶] M. Hirsch,[**] and J. W. F. Valle[††]
AHEP Group, Instituto de Física Corpuscular-C.S.I.C./Universitat de València, Edificio Institutos de Paterna, Apt 22085, E-46071 Valencia, Spain
(Received 18 July 2012; published 1 October 2012)

Supersymmetric models with bilinear *R*-parity violation can account for the observed neutrino masses and mixing parameters indicated by neutrino oscillation data. We consider minimal supergravity versions of bilinear *R*-parity violation where the lightest supersymmetric particle is a neutralino. This is unstable, with a large enough decay length to be detected at the CERN Large Hadron Collider. We analyze the Large Hadron Collider potential to determine the lightest supersymmetric particle properties, such as mass, lifetime and branching ratios, and discuss their relation to neutrino properties.

DOI: 10.1103/PhysRevD.86.075001 PACS numbers: 12.60.Jv, 14.60.Pq, 14.60.St, 14.80.Nb

I. INTRODUCTION

Elucidating the electroweak breaking sector of the Standard Model constitutes a major challenge for the Large Hadron Collider (LHC) at CERN. Supersymmetry provides an elegant way to stabilize the Higgs boson scalar mass against quantum corrections provided supersymmetric states are not too heavy, with some of them expected within reach for the LHC. Searches for supersymmetric particles constitute a major item in the LHC agenda [1–10], as many expect signs of supersymmetry (SUSY) to be just around the corner. However, the first searches up to ~ 5 fb^{-1} at the LHC interpreted within specific frameworks, such as constrained minimal supersymmetric Standard Model or minimal supergravity (mSUGRA), indicate that squark and gluino masses are in excess of ~ 1 TeV [11].

Despite intense efforts over more than thirty years, little is known from first principles about how exactly to realize or break supersymmetry. As a result, one should keep an open mind as to which theoretical framework is realized in nature, if any. Supersymmetry search strategies must be correspondingly redesigned if, for example, supersymmetry is realized in the absence of a conserved *R* parity [3,12].

Another major drawback of the Standard Model is its failure to account for neutrino oscillations [13,14], whose discovery constitutes one of the major advances in particle physics of the last decade. An important observation is that, if supersymmetry is realized without a conserved *R* parity, the origin of neutrino masses and mixing may be intrinsically supersymmetric [15–18].

Indeed, an attractive dynamical way to generate neutrino mass at the weak scale is through nonzero vacuum expectation values of SU(3) ⊗ SU(2) ⊗ U(1) singlet scalar neutrinos [19–21]. This leads to the minimal effective description of *R* parity violation, namely bilinear *R*-parity violation (BRPV) [22]. In contrast to the simplest variants

[*]camposc@feg.unesp.br
[†]eboli@fma.if.usp.br
[‡]magro@fma.if.usp.br
[§]porod@physik.uni-wuerzburg.de
[‖]restrepo@uv.es
[¶]spdas@ific.uv.es
[**]hirsch@ific.uv.es
[††]valle@ific.uv.es

of the seesaw mechanism [23], such supersymmetric alternative has the merit of being testable in collider experiments, like the LHC [24–27]. Here, we analyze the LHC potential to determine the lightest neutralino properties such as mass, decay length and branching ratios, and discuss their relation to neutrino properties.

II. BILINEAR *R*-PARITY VIOLATING SUSY MODELS

The bilinear R-parity violating models are characterized by two properties: first, the usual minimal supersymmetric Standard Model (MSSM) R-conserving superpotential is enlarged according to [28]

$$W_{\rm BRPV} = W_{\rm MSSM} + \varepsilon_{ab}\epsilon_i \hat{L}_i^a \hat{H}_u^b, \tag{1}$$

where there are 3 new superpotential parameters (ϵ_i), one for each fermion generation.[1] The second modification is the addition of an extra soft term

$$V_{\rm soft} = V_{\rm MSSM} - \varepsilon_{ab} B_i \epsilon_i \tilde{L}_i^a H_u^b \tag{2}$$

which depends on three soft mass parameters B_i. For the sake of simplicity, we considered the R-conserving soft terms as in mSUGRA. Field redefinitions can, in principle, be used to rewrite the bilinear terms from Eq. (1) to trilinear ones. Notwithstanding, the bilinear soft terms in Eq. (2) are not rotated away simultaneously [28].

The new bilinear terms break explicitly R parity as well as lepton number and induce nonzero vacuum expectation values v_i for the sneutrinos. As a result, neutrinos and neutralinos mix at tree level giving rise to one tree-level neutrino mass scale, which we identify with the atmospheric scale. The other two neutrino masses are generated through loop diagrams [31,32]. This model provides a good description of the observed neutrino oscillation data [14].

The BRPV-mSUGRA model is defined by eleven parameters

$$m_0, \quad m_{1/2}, \quad \tan\beta, \quad \text{sign}(\mu), \quad A_0, \quad \epsilon_i, \text{ and } B_i, \tag{3}$$

where $m_{1/2}$ and m_0 are the common gaugino mass and scalar soft SUSY breaking masses at the unification scale, A_0 is the common trilinear term, and $\tan\beta$ is the ratio between the Higgs field vacuum expectation values. In our analyses, the new parameters (ϵ_i and B_i) are determined by the neutrino masses and mixings. Therefore, we have only to vary the usual mSUGRA parameters. For the sake of simplicity in what follows, we fix $A_0 = -100$ GeV, $\tan\beta = 10$ and $\text{sign}(\mu) > 0$ and present our results in the plane $m_0 \otimes m_{1/2}$.

Due to the smallness of the neutrino masses, the BRPV interactions turn out to be rather feeble; consequently, the lightest supersymmetrical particle (LSP) has a lifetime long enough that its decay appears as a displaced vertex. We show in Fig. 1 the LSP decay length as a function of m_0 and $m_{1/2}$, when the remaining values for $\text{sign}(\mu)$, A and $\tan\beta$ are taken as mentioned above. Therefore, we can anticipate that the LSP decay vertex can be observed at the LHC within a large fraction of the parameter space.

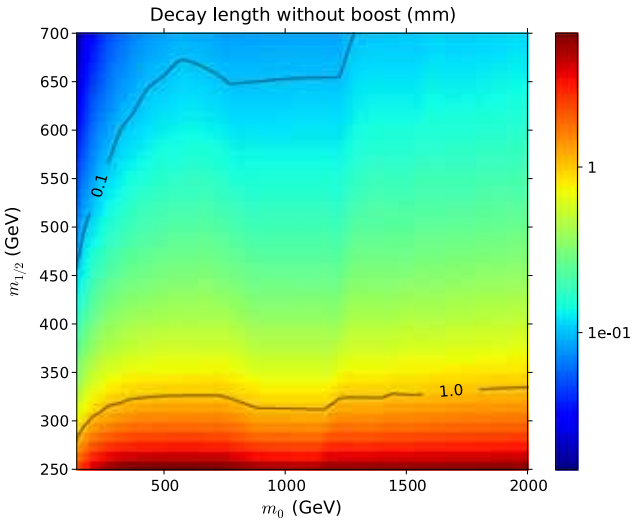

FIG. 1 (color online). Lightest neutralino decay length as a function of mSUGRA parameters m_0 and $m_{1/2}$, for $A_0 = -100$ GeV, $\tan\beta = 10$ and $\text{sign}(\mu) > 0$.

Depending on the SUSY spectrum, the lightest neutralino decay channels include fully leptonic decays

$$\tilde{\chi}_1^0 \to \nu\ell^+\ell^-, \qquad \tilde{\chi}_1^0 \to \nu\tau^+\tau^- \quad \text{and} \quad \tilde{\chi}_1^0 \to \nu\tau^\pm\ell^\mp$$

with $\ell = e$ or μ; as well as semileptonic decay modes

$$\tilde{\chi}_1^0 \to \nu q\bar{q}, \qquad \tilde{\chi}_1^0 \to \tau q'\bar{q},$$
$$\tilde{\chi}_1^0 \to \ell q'\bar{q} \quad \text{and} \quad \tilde{\chi}_1^0 \to \nu b\bar{b}.$$

If kinematically allowed, some of these modes take place via two-body decays, like $\tilde{\chi}_1^0 \to W^\mp\mu^\pm$, $\tilde{\chi}_1^0 \to W^\mp\tau^\pm$, $\tilde{\chi}_1^0 \to Z\nu$, or $\tilde{\chi}_1^0 \to h\nu$, followed by the Z, $W^\pm$ or h decay; for further details, see Refs. [25,33]. In addition to these channels, there is also the possibility of the neutralino decaying invisibly into three neutrinos; however, this channel reaches at most a few percent [33].[2]

Neutrino masses and mixings as well as LSP decay properties are determined by the same interactions; therefore, there are connections between high energy LSP physics at the LHC and neutrino oscillation physics. For instance, the ratio between charged current decays

$$\frac{\text{Br}(\tilde{\chi}_1^0 \to W^\pm\mu^\mp)}{\text{Br}(\tilde{\chi}_1^0 \to W^\pm\tau^\mp)} \tag{4}$$

[1] In a way similar to the μ term in the MSSM superpotential, the required smallness of the bilinear parameters ϵ_i could arise dynamically, through a nonzero vacuum expectation value, as in Refs. [19–21,29] and/or be generated radiatively [30].

[2] However, in models where a Majoron is present, it can be dominant [34–37].

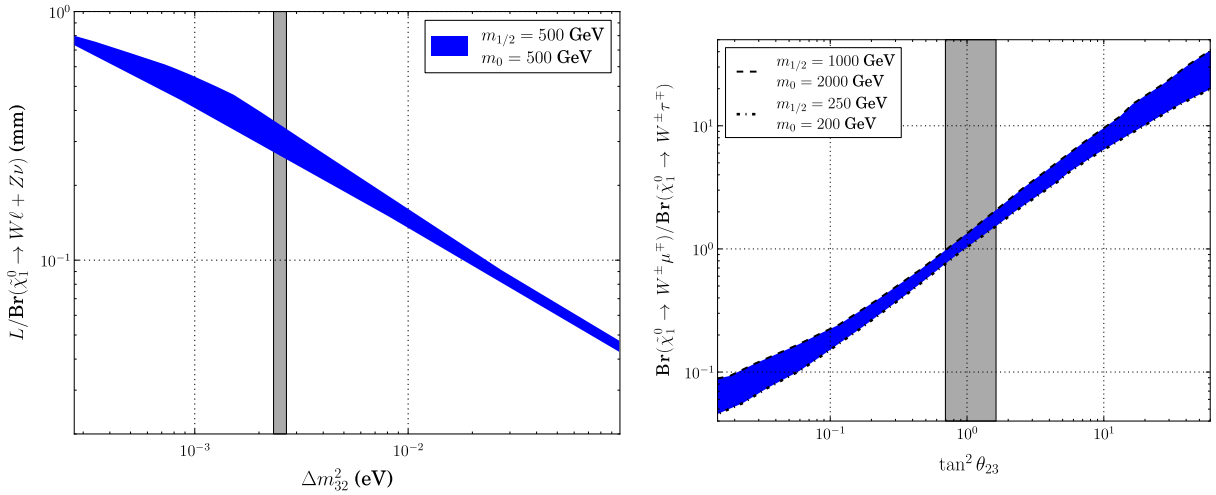

FIG. 2 (color online). Correlating LSP decay properties with neutrino oscillation parameters. The left panel shows the connection between the displayed LSP decay length parameter and the atmospheric squared mass scale Δm^2_{32}. The right panel depicts the relation between $\mathrm{Br}(\tilde{\chi}_1^0 \to W^\pm\mu^\mp)/\mathrm{Br}(\tilde{\chi}_1^0 \to W^\pm\tau^\mp)$ and the atmospheric mixing angle. The vertical shaded bands indicate the 2σ allowed values of the corresponding neutrino oscillation parameters [39].

is directly related to the atmospheric mixing angle [38], as illustrated in the right panel of Fig. 2; this relation was already considered in Ref. [27]. The vertical bands in Fig. 2 correspond to the latest 2σ precision in the determination of θ_{23} and Δm^2_{32} from Ref. [39].

Another interesting interconnection between LSP properties and neutrino properties is the direct relation between neutrino mass squared difference Δm^2_{32} and the ratio

$$R_{32} = \frac{L_0}{\mathrm{Br}(\tilde{\chi}_1^0 \to W\ell + Z\nu)} \tag{5}$$

as is illustrated in the left panel of Fig. 2. Here, L_0 is the LSP decay length, and one has to sum over all leptons and neutrinos in the final states. One can understand this relation in the following way. In the BRPV model, the tree-level neutrino mass is proportional to $m_\nu^{\mathrm{Tree}} \propto |\Lambda|^2$, where $|\Lambda|^2 = \sum_i \Lambda_i^2$, with $\Lambda_i = \epsilon v_d + \mu v_i$, is the so-called alignment vector. Couplings between the gauginos and gauge bosons plus leptons/neutrinos are proportional to Λ_i as well [33]. Thus, one expects that after summing over the lepton generations, the partial width of the neutralino into gauge bosons is also proportional to $|\Lambda|^2$. The decay length is the inverse width and dividing by the branching ratio into gauge boson final states picks out the partial width of the neutralino into gauge bosons. This leads to the correlation of R_{32} with the atmospheric neutrino mass scale, since m_{Atm} is identified mostly with m_ν^{Tree}, apart from some minor 1-loop corrections.

III. ANALYSES FRAMEWORK AND BASIC CUTS

Our analyses aim to study the LHC potential to probe the LSP properties exploring its detached vertex signature. We simulated the SUSY particle production using PYTHIA version 6.408 [40,41] where all the properties of our BRPV-mSUGRA model were included using the Supersymmetry Les Houches Accord format [42]. The relevant masses, mixings, branching ratios and decay lengths were generated using the SPHENO code [43,44].

In our studies, we used a toy calorimeter roughly inspired by the actual LHC detectors. We assumed that the calorimeter coverage is $|\eta| < 5$ and that its segmentation is $\Delta\eta \otimes \Delta\varphi = 0.10 \times 0.098$. The calorimeter resolution was included by smearing the jet energies with an error

$$\frac{\Delta E}{E} = \frac{0.50}{\sqrt{E}} \oplus 0.03.$$

Jets were reconstructed using the cone algorithm in the subroutine PYCELL with $\Delta R = 0.4$ and jet seed with a minimum transverse energy $E_{T,\mathrm{min}}^{\mathrm{cell}} = 2$ GeV.

Our analyses start by selecting events which pass some typical triggers employed by the ATLAS/CMS collaborations, i.e., an event to be accepted should fulfill at least one of the following requirements:

(i) the event contains one electron or photon with $p_T > 20$ GeV;
(ii) the event has an isolated muon with $p_T > 6$ GeV;
(iii) the event exhibits two isolated electrons or photons with $p_T > 15$ GeV;
(iv) the event has one jet with transverse momentum in excess of 100 GeV;
(v) the events possesses missing transverse energy greater than 100 GeV.

We then require the existence of, at least, one displaced vertex which is more than 5σ away from the primary vertex [25]—that is, the detached vertex is outside the ellipsoid

$$\left(\frac{x}{5\delta_{xy}}\right)^2 + \left(\frac{y}{5\delta_{xy}}\right)^2 + \left(\frac{z}{5\delta_z}\right)^2 = 1, \tag{6}$$

where the z axis is along the beam direction. We used the ATLAS expected resolutions in the transverse plane ($\delta_{xy} = 20\ \mu$m) and in the beam direction ($\delta_z = 500\ \mu$m). To ensure a good reconstruction of the displaced vertex, we further required that the LSP decays within the tracking system, i.e., within a radius of 550 mm and z axis length of 3000 mm. In our model, the decay lengths are such that this last requirement is almost automatically satisfied; see Fig. 1.

IV. LSP MASS MEASUREMENT

In order to accurately measure the LSP mass from its decay products, we focused our attention on events where the LSP decays into a charged lepton ($e^{\pm}$ or $\mu^{\pm}$) and a W which subsequently decays into a pair of jets. In addition to the basic cuts described above, we further required charged leptons to have

$$p_T^{\ell} > 20\ \text{GeV} \quad \text{and} \quad |\eta_{\ell}| < 2.5. \tag{7}$$

We demanded the charged lepton to be isolated, i.e., the sum of the transverse energy of the particles in a cone $\Delta R = 0.3$ around the lepton direction should satisfy

$$\sum_{\Delta R<0.3} E_T < 5\ \text{GeV}. \tag{8}$$

We identified the hadronically decaying W requiring that its decay jets are central

$$p_T^{j} > 20\ \text{GeV}, \qquad |\eta_j| < 2.5, \tag{9}$$

and that their invariant mass is compatible with the W mass:

$$|\eta_j| < 2.5 \quad \text{and} \quad |M_{jj} - M_W| < 20\ \text{GeV}. \tag{10}$$

In order to obtain the LSP mass, we considered points in the $m_0 \otimes m_{1/2}$ plane with more than 10 expected events for an integrated luminosity of 100 fb^{-1}. We have performed a Gaussian fit to the lepton-jet-jet invariant mass; as an illustration of the lepton-jet-jet invariant mass spectrum, see Fig. 3. As we can see from this figure, the actual LSP mass (101 GeV) is with 1% of its fitted value (100.4 GeV).

In order to better appreciate the precision with which the LSP mass can be determined for other choices of mSUGRA parameters, we have repeated the analysis for a wide grid of values in the $m_0 \otimes m_{1/2}$ plane. The left panel of Fig. 4 depicts the achievable precision in the LSP mass measurement for an integrated luminosity of 100 fb^{-1} as a function of $m_0 \otimes m_{1/2}$ for $A_0 = -100$ GeV, $\tan\beta = 10$ and $\text{sgn}(\mu) > 0$. As one can see, the LSP mass can be

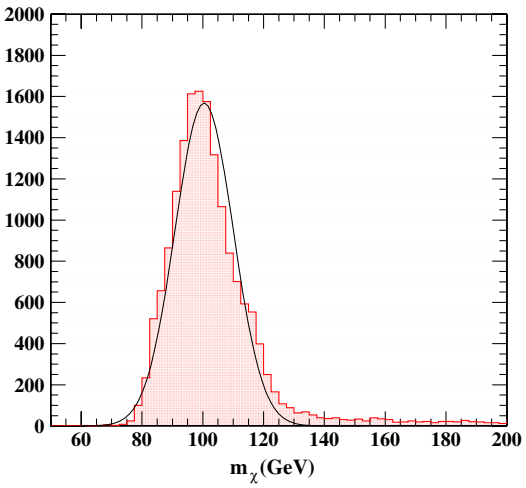

FIG. 3 (color online). Illustration of the lepton-jet-jet invariant mass spectrum fitted to obtain the LSP mass. In this figure, we considered $m_0 = 250$ GeV, $m_{1/2} = 250$ GeV, $\tan\beta = 10$, $A_0 = -100$ GeV, and $\text{sgn}(\mu) > 0$ which leads to a LSP mass of 101 GeV.

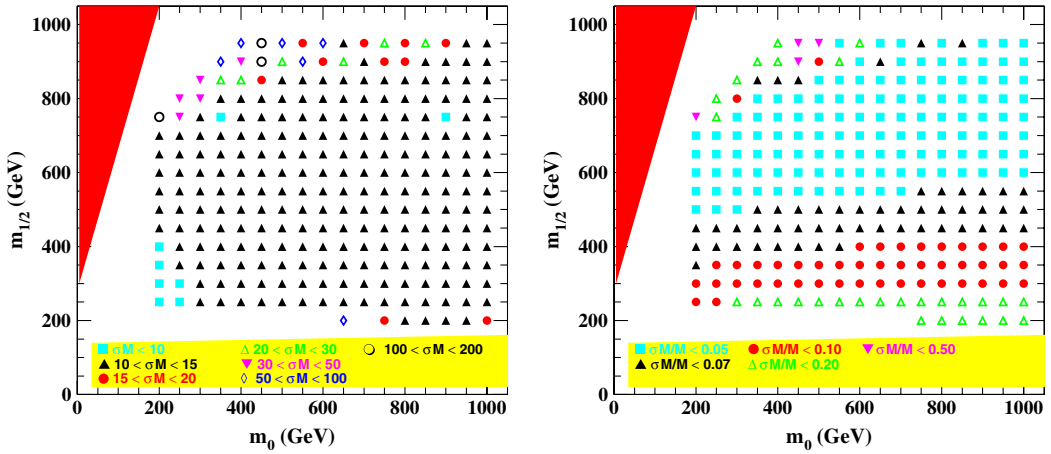

FIG. 4 (color online). The left panel presents the error (σ_M) on the LSP mass as a function of the $m_0 \otimes m_{1/2}$ point for $A_0 = -100$ GeV, $\tan\beta = 10$, $\text{sgn}\mu > 0$ and an integrated luminosity of 100 fb^{-1}, while the right panel displays the relative error in the LSP mass determination $\sigma_M / M_{\tilde{\chi}_1^0}$.

measured with an error between 10 and 15 GeV within a sizeable fraction of the $(m_0 \otimes m_{1/2})$ plane. Only at high $m_{1/2}$, there is a degradation of the precision due to poor statistics. The right panel in Fig. 4 shows that indeed this is enough to determine the LSP mass to within 5 to 10% in a relatively wide chunk of parameter space.

V. LSP DECAY LENGTH MEASUREMENT

Another important feature of the LSP in our BRPV-mSUGRA model is its decay length (lifetime). Within the simplest mSUGRA bilinear R-parity violating scheme, this is directly related to the squared mass splitting Δm^2_{32}, well measured in neutrino oscillation experiments [39]. In this analysis, we considered events where the LSP decay contains at least three charged tracks, i.e., the LSP decays into ℓjj, with $\ell = e$ or μ. Here, we sum over all jets as well as over $\tilde{\chi}^0_1 \to \ell W \to \ell jj$ and all three body decays leading to the same final state.

In Fig. 5, we depict the average distance traveled by the LSP as observed in the laboratory frame. As we can see, a substantial fraction of the LSP decays takes place within the pixel detector, except for very low $m_{1/2}$ values. It is interesting to notice that the pattern shown in the figure is similar to the one in Fig. 1, as we could easily expect. Since most of the LSP decays occur inside the beam pipe, we can anticipate a small background associated to particles scattering in the detector material.

In order to obtain the LSP decay length (L_0) from the distance traveled in the laboratory frame (d), we considered the $m_{\rm obs} d/p_{\rm obs}$ distribution, with $m_{\rm obs}$ ($p_{\rm obs}$) being the measured invariant mass (momentum) associated to the displaced vertex, and then we fitted it with an exponential

$$e^{-\frac{m_{\rm obs} d}{p_{\rm obs} L_0}},$$

where the fitting parameter (L_0) is the LSP decay length.

In order to disentangle the energy and momentum uncertainties and the statistical errors from the intrinsic limitation associated to the tracking, we first neglect the latter one. In the left panel of Fig. 6, we present the expected precision in the decay length determination in the plane $m_0 \otimes m_{1/2}$ for an assumed integrated luminosity of 100 fb^{-1}. As one can see, these sources of error have a small impact in the determination of the decay length, except for heavier LSP masses where we run out of statistics. In fact, the contribution of these sources of uncertainty is smaller than 5% for neutralino masses up to 280 GeV ($m_{1/2} \simeq 700$ GeV).

Clearly, the actual achievable precision of LSP lifetime determination at the LHC experiments depends on the ability to measure the LSP traveled distance in the laboratory. We present in the right panel of Fig. 6 the attainable

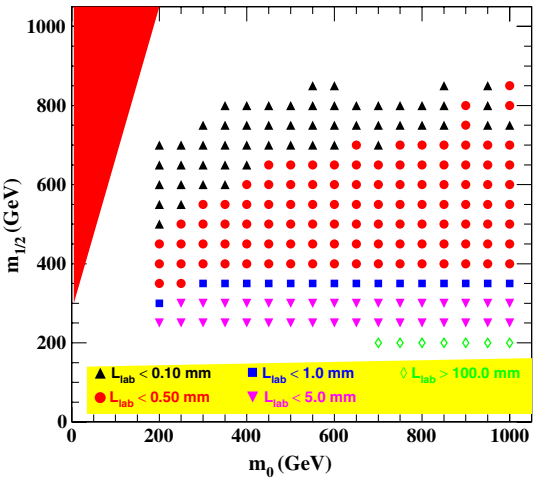

FIG. 5 (color online). Average distance traveled by the LSP in the laboratory frame as a function of the $m_0 \otimes m_{1/2}$ point for $A_0 = -100$ GeV, $\tan\beta = 10$ and $\mathrm{sgn}\mu > 0$.

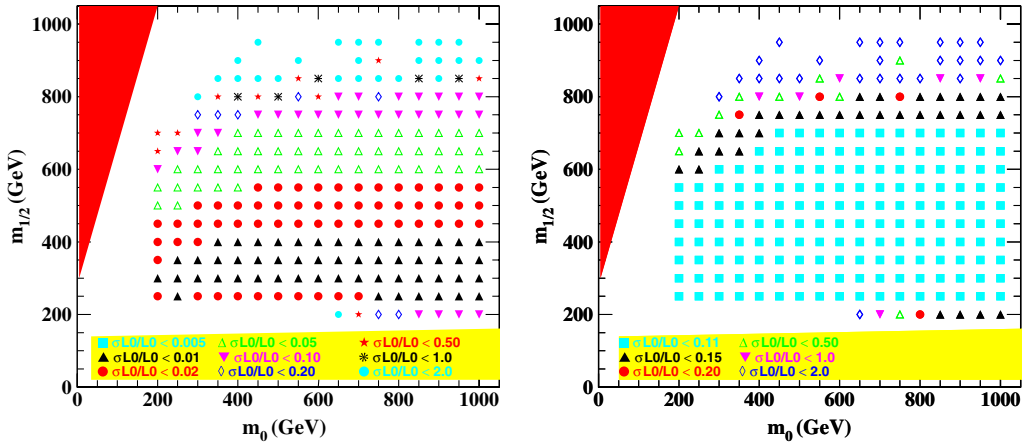

FIG. 6 (color online). Relative error (σ_{L_0}/L_0) in the determination of the LSP decay length as a function of the $m_0 \otimes m_{1/2}$ for $A_0 = -100$ GeV, $\tan\beta = 10$, $\mathrm{sgn}\mu > 0$ and an integrated luminosity of 100 fb^{-1}. The left (right) panel assumes no error (10% error) in the measurement of distance traveled by the LSP.

precision on the decay length assuming a 10% tracking error [45] in the LSP flight distance to get a rough idea. Clearly, the precision in the decay length gets deteriorated; however, it is still better than 15% within a relatively large fraction of the parameter space under this assumption but would get correspondingly worse if this uncertainty were larger.

VI. LSP BRANCHING RATIO MEASUREMENTS

As we have already mentioned, the neutrino mass squared difference Δm^2_{32} controls the ratio given in Eq. (5); therefore, we should also study how well the neutralino LSP decay ratio into ℓW and νZ can be determined. In order to illustrate the LHC capabilities in probing LSP properties at high energies, we present the reconstruction efficiency for the benchmark scenario

$$m_{1/2} = 250 \text{ GeV} \quad \text{and} \quad m_0 = 250 \text{ GeV},$$

which yields a rather light LSP ($m_{\text{LSP}} \simeq 101$ GeV) and heavy scalars. For this point in parameter space, the LSP possesses a decay length $c\tau = 30$ μm, and its dominant decay modes have the following branching ratios:

$$\begin{aligned}
&\text{BR}(\tilde{\chi}^0_1 \to W^\pm e^\mp) = 0.2\%,\\
&\text{BR}(\tilde{\chi}^0_1 \to W^\pm \mu^\mp) = 27.6\%,\\
&\text{BR}(\tilde{\chi}^0_1 \to W^\pm \tau^\mp) = 31.3\%,\\
&\text{BR}(\tilde{\chi}^0_1 \to b\bar{b}\nu) = 7.1\%,\\
&\text{BR}(\tilde{\chi}^0_1 \to Z\nu) = 11.9\%,\\
&\text{BR}(\tilde{\chi}^0_1 \to e^\pm \tau^\mp \nu) = 5.5\%,\\
&\text{BR}(\tilde{\chi}^0_1 \to \mu^\pm \tau^\mp \nu) = 5.5\%,\\
&\text{BR}(\tilde{\chi}^0_1 \to \tau^\pm \tau^\mp \nu) = 9.5\%
\end{aligned}$$

We present in Table I the reconstruction efficiencies of the LSP decay modes for our chosen benchmark point. The reconstruction efficiencies for final states containing τ's are much smaller, as expected, leading to a loss of statistics in these final states. For an exhaustive study of the reconstruction efficiencies, see Ref. [27].

We present in Fig. 7 the expected error on the LSP branching ratio $\text{Br}(\tilde{\chi}^0_1 \to \ell W + \nu Z)$ as a function $m_0 \otimes m_{1/2}$ for an integrated luminosity of 100 fb^{-1}. In order to evaluate this error, we studied the reconstruction efficiency for this final state and simulated 100 fb^{-1} of data for several points in the $m_0 \otimes m_{1/2}$ plane. As one can see, this branching ratio can be well determined in the regions of large production cross section, i.e., small m_0 and $m_{1/2}$. Although for heavier neutralinos, the precision diminishes, still this branching ratio can be determined to within 20% in a large portion of the parameter space. In order to study the possibility of LHC to probe the atmospheric mass, we have evaluated $\text{Br}(\tilde{\chi}^0_1 \to W\ell) + \text{Br}(\tilde{\chi}^0_1 \to Z\nu)$ appearing in Eq. (5). The $W\ell$ channel is obtained by first reconstructing displaced vertices with hadronic W decays, $jj\ell$, in the final state. Beside the cuts described in Secs. III and IV, we have applied an invariant mass cut on the jet pair: $|M_W - M_{jj}| < 20$ GeV to disentangle the W contribution to this final state. Afterward, we get the branching ratio for $W\ell$ using

$$\text{Br}\,(\tilde{\chi}^0_1 \to W\ell) = \frac{\text{Br}(\tilde{\chi}^0_1 \to jj\ell)}{N_{lqq'}} \times \left(1 + \frac{\text{Br}(W \to \ell\nu)}{\text{Br}(W \to qq\prime)}\right). \tag{11}$$

The $Z\nu$ channel was calculated similarly by reconstructing the displaced vertices with hadronic Z decays, $jj\nu$, in the final state and properly rescaling it. Also, here, we have applied an invariant mass cut on the jet pair: $|M_Z - M_{jj}| < 20$ GeV.

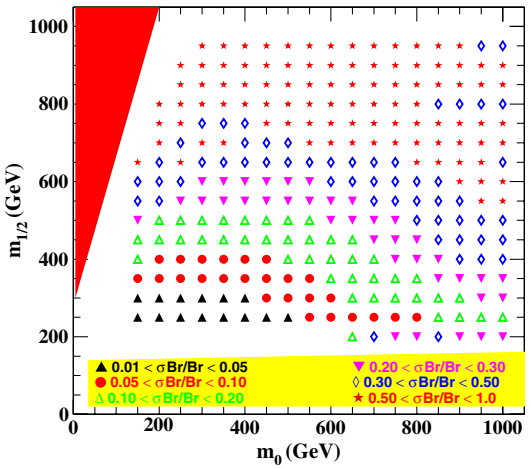

FIG. 7 (color online). Expected error on the $\text{Br}(\tilde{\chi}^0_1 \to \ell W + \nu Z)$ as a function $m_0 \otimes m_{1/2}$ for an integrated luminosity of 100 fb^{-1}.

TABLE I. Reconstruction efficiencies for neutralino LSP decays for our benchmark point. For the τ lepton, only hadronic final states have been considered while the τ decays into electrons and muons were included in the first two entries.

$N_{eqq'}$	$N_{\mu qq'}$	$N_{\tau qq'}$	$N_{e\tau\nu}$	$N_{\mu\tau\nu}$	$N_{\tau\tau\nu}$
0.291	0.106	0.011	0.087	0.126	0.061

VII. LSP PROPERTIES AND ATMOSPHERIC NEUTRINO OSCILLATIONS

As seen in Sec. II, the MSSM augmented with bilinear R-parity violation exhibits correlations between LSP decay properties and the neutrino oscillation parameters [31,32], which are by now well measured in neutrino oscillation experiments [39]. In particular, the squared mass difference Δm^2_{32} is connected to the ratio R_{32} between the LSP decay length and its branching ratio into ℓW and νZ; see

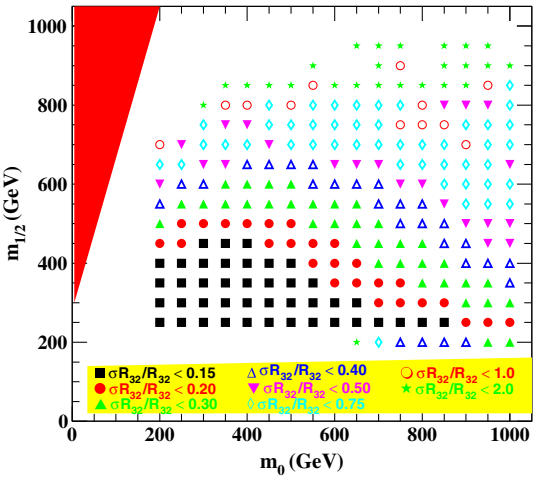

FIG. 8 (color online). Expected accuracy on the ratio R_{32} as a function of $m_0 \otimes m_{1/2}$ for an integrated luminosity of 100 fb^{-1}.

the right panel of Fig. 2. In Fig. 8, we display the expected accuracy on the ratio R_{32} as a function of $m_0 \otimes m_{1/2}$ for an integrated luminosity of 100 fb^{-1} and assuming 10% precision in the determination of the LSP traveled distance. As we can see, R_{32} can be determined with a precision 20–30% in a large fraction of the $m_0 \otimes m_{1/2}$ plane, and, as expected, the precision is lost for heavy LSPs. For small LSP masses, the error on R_{32} is dominated by the uncertainty on the decay length, while for heavier LSPs, the dominant contribution comes from the branching ratio determination due to the limited statistics.

It is interesting to notice from the right panel of Fig. 2 that a measurement of R_{32} with 20–30% precision is enough to determine the correct magnitude of Δm^2_{32} using the BRPV-mSUGRA framework. Nevertheless, a much higher precision is needed to obtain uncertainties similar to the neutrino experiments such as MINOS/T2K [39]. On the other hand, the relation between the atmospheric mixing angle and the ratio of the LSP branching ratios into τW and μW can lead to more stringent tests of the BRPV-mSUGRA model. In Ref. [27], it was shown that this ratio can be determined at the LHC with a precision better than 20% in a large fraction of the $m_0 \otimes m_{1/2}$ plane. From Fig. 2, we can see that this precision is enough to have a determination for $\tan^2\theta_{23}$ with an error similar to the low energy neutrino oscillation measurements. Looking from a different point of view, the collider data can be combined with neutrino data to determine the underlying parameters of the model. In this case, collider and neutrino data give "orthogonal" information as has been shown in Ref. [46].

VIII. CONCLUSIONS

We have analyzed the LHC potential to determine the LSP properties, such as mass, lifetime and branching ratios, within minimal supergravity with bilinear R-parity violation. We saw that the LSP mass determination is rather precise, while the LSP lifetime and branching ratios can be determined with a 20% error in a large fraction of the parameter space. This is enough to allow for qualitative test of the BRPV-mSUGRA model using the R_{32}-Δm^2_{32} correlation. On the other hand, semileptonic LSP decays to muons and taus correlate extremely well with neutrino oscillation measurements of θ_{23}.

In the BRPV model for low values of $M_{1/2}$, one can have sizeable branching ratios into the final states $e\tau\nu$ and $\mu\tau\nu$. These decays are potentially interesting for testing another aspects of the model associated with solar neutrino physics. As shown in Ref. [32], in regions of parameter space where the scalar taus are not very heavy, usually the loop with taus-staus in the diagram dominates the 1-loop neutrino mass. In this case, the solar angle is predicted to be proportional to $(\tilde{\epsilon}_1/\tilde{\epsilon}_2)^2 \propto \tan^2\theta_\odot$. Here, $\tilde{\epsilon} = V_\nu^{T,\mathrm{tree}}\vec{\epsilon}$, with $V_\nu^{T,\mathrm{tree}}$ being the matrix which diagonalizes the tree-level neutrino mass. Note that $V_\nu^{T,\mathrm{tree}}$ is entirely determined in terms of the Λ_i. In the BRPV model, R-parity violation couplings of the scalar tau are proportional to the superpotential parameters ϵ_i. Ratios of the decays $\mathrm{Br}(\chi_1^0 \to e\tau\nu)/\mathrm{Br}(\chi_1^0 \to \mu\tau\nu)$ are then given, to a very good approximation, by $\mathrm{Br}(\chi_1^0 \to e\tau\nu)/\mathrm{Br}(\chi_1^0 \to \mu\tau\nu) \propto (\epsilon_1/\epsilon_2)^2$. If the Λ_i where known, this could be turned into a test of the prediction for the solar angle. Note that in the limit where the reactor angle is exactly zero and the atmospheric angle exactly maximal, one obtains $(\tilde{\epsilon}_1/\tilde{\epsilon}_2)^2 = 2(\epsilon_1/\epsilon_2)^2$. However, the Λ_i are currently not well fixed, due to the comparatively large uncertainty in the atmospheric angle. Thus, the correlation between three-body leptonic decays of the neutralino with tau final states and the solar angle has a rather large uncertainty. This prevents a stringent consistency test of the model using these decays.

All in all, we have shown that neutralino decays can be used to extract some of their properties rather well in models with bilinear R-parity violation. Properties such as the decay length and the ratio of semileptonic decay branching ratios to muons and taus correlate rather well with atmospheric neutrino oscillation parameters. These features should also apply to schemes where the gravitino is the LSP, and the neutralino is the next to lightest SUSY particle [47,48]. For gravitino masses in the allowed range where it plays the role of cold dark matter, its R-parity conserving decays are negligible compared to its R-parity violating decays. The latter follows the same pattern studied in the present paper, so that the results derived here should also hold.

ACKNOWLEDGMENTS

We thank Susana Cabrera, Vasiliki Mitsou and Andreas Redelbach for useful discussions on the ATLAS experiment. W. P. thanks the IFIC for hospitality during an extended stay. Work supported by the Spanish MINECO under Grants No. FPA2011-22975 and MULTIDARK No. CSD2009-00064 (Consolider-Ingenio 2010 Programme), by Prometeo/

2009/091 (Generalitat Valenciana), by the EU ITN UNILHC PITN-GA-2009-237920. O. J. P. E. is supported in part by Conselho Nacional de Desenvolvimento Científico e Tecnológico (CNPq), by Fundação de Amparo à Pesquisa do Estado de São Paulo (FAPESP) and in part by the European Union FP7 ITN INVISIBLES (Marie Curie Actions, PITN-GA-2011-289442) network. W. P. has been supported by the Alexander von Humboldt foundation and in part by the DFG, project No. PO-1337/2-1.

[1] S. Chatrchyan *et al.* (CMS Collaboration), Phys. Rev. Lett. **107**, 221804 (2011).
[2] G. Aad *et al.* (ATLAS Collaboration), Phys. Lett. B **701**, 186 (2011).
[3] G. Aad *et al.* (ATLAS Collaboration), Phys. Rev. D **85**, 012006 (2012).
[4] G. Aad *et al.* (ATLAS Collaboration), J. High Energy Phys. 11 (2011) 099.
[5] G. Aad *et al.* (ATLAS Collaboration), Phys. Lett. B **709**, 137 (2012).
[6] G. Aad *et al.* (ATLAS Collaboration), Phys. Lett. B **710**, 519 (2012).
[7] V. Khachatryan *et al.* (CMS Collaboration), Phys. Lett. B **698**, 196 (2011).
[8] S. Chatrchyan *et al.* (CMS Collaboration), J. High Energy Phys. 06 (2011) 026.
[9] S. Chatrchyan *et al.* (CMS Collaboration), J. High Energy Phys. 06 (2011) 077.
[10] S. Chatrchyan *et al.* (CMS Collaboration), Phys. Lett. B **704**, 411 (2011).
[11] P. Bechtle *et al.*, J. High Energy Phys. 06 (2012) 098.
[12] G. Aad *et al.* (ATLAS Collaboration), Phys. Lett. B **707**, 478 (2012).
[13] K. Nakamura *et al.*, J. Phys. G **37**, 075021 (2010).
[14] M. Maltoni, T. Schwetz, M. A. Tortola, and J. W. F. Valle, New J. Phys. **6**, 122 (2004).
[15] C. S. Aulakh and R. N. Mohapatra, Phys. Lett. B **119**, 136 (1982).
[16] L. J. Hall and M. Suzuki, Nucl. Phys. **B231**, 419 (1984).
[17] G. G. Ross and J. W. F. Valle, Phys. Lett. B **151**, 375 (1985).
[18] J. R. Ellis, G. Gelmini, C. Jarlskog, G. G. Ross, and J. W. F. Valle, Phys. Lett. B **150**, 142 (1985).
[19] A. Masiero and J. W. F. Valle, Phys. Lett. B **251**, 273 (1990).
[20] J. C. Romao, C. A. Santos, and J. W. F. Valle, Phys. Lett. B **288**, 311 (1992).
[21] J. C. Romao, A. Ioannissyan, and J. W. F. Valle, Phys. Rev. D **55**, 427 (1997).
[22] M. Hirsch and J. W. F. Valle, New J. Phys. **6**, 76 (2004).
[23] J. W. F. Valle, J. Phys. Conf. Ser. **53**, 473 (2006).
[24] F. de Campos, O. J. P. Éboli, M. B. Magro, W. Porod, D. Restrepo, and J. W. F. Valle, Phys. Rev. D **71**, 075001 (2005).
[25] F. de Campos, O. J. P. Éboli, M. B. Magro, W. Porod, D. Restrepo, M. Hirsch, and J. W. F. Valle, J. High Energy Phys. 05 (2008) 048.
[26] F. de Campos, O. J. P. Eboli, M. B. Magro, and D. Restrepo, Phys. Rev. D **79**, 055008 (2009).
[27] F. de Campos, O. J. P. Éboli, M. Hirsch, M. B. Magro, W. Porod, D. Restrepo, and J. W. F. Valle, Phys. Rev. D **82**, 075002 (2010).
[28] M. A. Diaz, J. C. Romao, and J. W. F. Valle, Nucl. Phys. **B524**, 23 (1998).
[29] H.-P. Nilles and N. Polonsky, Nucl. Phys. **B484**, 33 (1997).
[30] G. F. Giudice and A. Masiero, Phys. Lett. B **206**, 480 (1988).
[31] M. Hirsch, M. A. Diaz, W. Porod, J. C. Romão, and J. W. F. Valle, Phys. Rev. D **62**, 113008 (2000); **65**, 119901(E) (2002).
[32] M. A. Diaz, M. Hirsch, W. Porod, J. C. Romão, and J. W. F. Valle, Phys. Rev. D **68**, 013009 (2003).
[33] W. Porod, M. Hirsch, J. Romão, and J. W. F. Valle, Phys. Rev. D **63**, 115004 (2001).
[34] M. Gonzalez-Garcia, J. Romao, and J. Valle, Nucl. Phys. **B391**, 100 (1993).
[35] A. Bartl, W. Porod, F. de Campos, M. A. García-Jareño, M. B. Magro, J. W. F. Valle , and W. Majerotto, Nucl. Phys. **B502**, 19 (1997).
[36] M. Hirsch and W. Porod, Phys. Rev. D **74**, 055003 (2006).
[37] M. Hirsch, A. Vicente, and W. Porod, Phys. Rev. D **77**, 075005 (2008).
[38] A. Datta, B. Mukhopadhyaya, and F. Vissani, Phys. Lett. B **492**, 324 (2000); B. Mukhopadhyaya, S. Roy, and F. Vissani, Phys. Lett. B **443**, 191 (1998).
[39] D. Forero, M. Tortola, and J. Valle, arXiv:1205.4018.
[40] T. Sjostrand, P. Edén, C. Friberg, L. Lönnblad, G. Miu, S. Mrenna, and E. Norrbin, Comput. Phys. Commun. **135**, 238 (2001).
[41] T. Sjostrand, Comput. Phys. Commun. **82**, 74 (1994).
[42] P. Skands *et al.*, J. High Energy Phys. 07 (2004) 036.
[43] W. Porod, Comput. Phys. Commun. **153**, 275 (2003).
[44] W. Porod and F. Staub, Comput. Phys. Commun. **183**, 2458 (2012).
[45] E. Ross (private communication).
[46] F. Thomas and W. Porod, J. High Energy Phys. 10 (2011) 089.
[47] M. Hirsch, W. Porod, and D. Restrepo, J. High Energy Phys. 03 (2005) 062.
[48] D. Restrepo, M. Taoso, J. W. F. Valle, and O. Zapata, Phys. Rev. D **85**, 023523 (2012).

Todos os trabalhos realizados, apresentados anteriormente, foram realizados considerando-se os dados publicados das colaborações associadas aos experimentos - CDF e D0 (Tevatron), DELPHI, ALEPH e L3 (LEP I e LEP II). CMS e ATLAS (LHC). Nossos resultados indicam limites possíveis a serem impostos sobre os parâmetros dos modelos estudados sugerindo, em situações nas quais tais limites sejam extremamente restritivos, a exclusão do modelo. No entando, para o caso de modelos supersimétricos com quebra de paridade R, existe uma janela, ainda que pequena, que motiva a continuidade do estudo deste tipo de modelos. Com a publicação dos resultados experimentais sobre a massa do bóson de Higgs, é necessário nova análise dos sinais estudados, e a conseqüente definição dos novos limites sobre os parâmetros já estabelecidos.As técnicas referentes à simulação e estudo de sinais e fundo permanecem inalteradas. No entanto, a restrição sobre os parâmetros dos modelos podem nos levar a valores tais que os referidos modelos possam ser excluidos. Os dados do LHC são extremamente importantes para se definir tal possibilidade, ainda que não se tenha resultado para a detecção de qualquer partícula que possa estar realcionada ao espectro supersimétrico.

Capítulo 5

Quebra de simetria de Lorentz

Recentemente participamos de estudos de sinais em aceleradores devido ao acoplamento do bóson de Higgs com partículas de espín semi-inteiro e dimensão de massa 1, o chamado Elko - *Eigenspinoren des Ladungskonjugationsoperators*. Sabendo que termos de dimensão superior a 4 devem estar suprimidos na Lagrangeana por uma escala de massa fundamental e a renormalizabilidade da teoria deve ser mantido, o espinor Elko pode ter auto acoplamento quártico ou se acoplar com o bóson de Higgs, aparecendo como candidado para a matéria escura. Uma característicasdo Elko é a não localidade, derivada da quebra de simetria de Lorentz associada a uma direção preferencial. Tal caracteística pode estar associada a propriedades da matéria escura, como indicado no trabalho realizado. Estudamos preliminarmente a não localidade do Elko quando consideradas as correções radiativas, bem como um processo no qual a fusão de bosons de Higgs pode proporcionar Elkos no estado final, tendo dois muons e *missing energy* como sinal final, no qual a energia ausente está associada ao Elko, no LHC. O estudo preliminar teve continuidade à luz dos resultados para a massa do bóson de Higgs,

assim como a simulação detalhada. Esta proposta de quebra de simetria é recente, razão pela qual apresenta váriso questionamentos. No entanto, o estudo dtalhado deste tipo de modelo é importante e merece atenção, A quebra de simetria de Lorentz já foi discutida do ponto de vista teórico, porém um estudo do ponto de vista fenomenológico não havia sido realizado.

Physics Letters B 706 (2012) 352–359

Contents lists available at SciVerse ScienceDirect

Physics Letters B

www.elsevier.com/locate/physletb

Exploring Elko typical signature

M. Dias [a,*], F. de Campos [b], J.M. Hoff da Silva [b]

[a] Departamento de Ciências Exatas e da Terra, Universidade Federal de São Paulo, Diadema, SP, Brazil
[b] Departamento de Física e Química, Universidade Estadual Paulista, Guaratinguetá, SP, Brazil

ARTICLE INFO

Article history:
Received 9 September 2011
Received in revised form 10 November 2011
Accepted 15 November 2011
Available online 20 November 2011
Editor: S. Dodelson

ABSTRACT

We study the prospects of observing the presence of a relatively light Elko particle as a possible dark matter candidate, by pointing out a typical signature for the process encompassing the Elko non-locality, exploring some consequences of the unusual Elko propagator behavior when analyzed outside the Elko axis of propagation. We also consider the production of a light Elko associated to missing energy and isolated leptons at the LHC, with center of mass energy of 7 and 14 TeV and total luminosity from 1 fb^{-1} to 10 fb^{-1}. Basically, the Elko non-locality engenders a peculiar signal in the missing energy turning it sensible to the angle of detection.

1. Introduction

Elko spinor fields are unexpected spin one-half matter fields endowed with mass dimension 1 [1,2]. Since its recent theoretical discovery, it has attracted much attention, in part by the wide range of possibility opened by such peculiar matter fields in cosmology and physics [3] and in part from the mathematical point of view [4]. The word Elko is the acronym for *Eigenspinoren des Ladungskonjugationsoperators* or Dual-helicity eigenspinors of the charge conjugation operator (see Eq. (2)).

The two aforementioned characteristics of Elko (namely, spin one-half and mass dimension 1) makes quite reduced the possible coupling to the Standard Model fields. In fact, keeping in mind that interaction terms with mass dimension greater than four should be severely suppressed by some fundamental mass scale and focusing in simple power counting renormalizable arguments, it turns out that Elko spinor fields may have quartic self-interaction and an Elko–Higgs (doublet) interaction.[1] In this vein, such spinor field may act as a dark matter candidate.

Another interesting feature about Elko is its non-locality. Elko spinor fields do not belong to a standard Wigner's class [5]. It was demonstrated, however, that Elko breaks Lorentz symmetry (in a subtle way) by containing a preferred direction [6]. It is worth to note that the existence of a preferred direction – the so-called 'axis of evil' – (as well as a self-interaction) is believed to be a property of dark matter [7]. We also remark, for completeness, that the quantum field associated to the Elko spinor is now better understood in the scope of Very Special Relativity (VSR) framework [8]. In fact, it is possible to describe, or construct, Elko spinor fields as the spinor representation of $SIM(2)$ subgroup of VSR [9]. In this vein, since $SIM(2)$ is the largest subgroup of VSR encompassing all the necessary physical symmetries except some (violated) discrete symmetry, the tension between Elko and Lorentz symmetries disappears.

On the other hand, it is well known that accelerators will test, in an incontestable way, theories in the scope of physics beyond the Standard Model as well as shed some light to the mass generation problem [10–13]. Candidates of dark matter predicted in particle physics theories, like supersymmetry, are on the focus of such studies and the answers will provide additional information for a deeper level of our understanding on astrophysics and cosmology. In such a way, the CERN Large Hadron Collider (LHC) results are fundamental for any study connecting high energy physics and astrophysics/cosmology. The LHC will provide center-of-mass energy enough to probe directly the weak scale and the origin of mass. Therefore, since we still have the open question of the dark matter nature, it is possible the study of the origin of mass as well as the candidate to the dark matter in the search of Elko. In considering some specific process for Elko production, radiative corrections must be taken into account. In this case, as we will see, the Elko non-locality is manifest leading to an exclusive output in the final signature. At phenomenological grounds, such a behavior suggests a different analysis for the search of Elko at accelerators. So, we consider in some detail a tree level process (where the non-locality is absent) concerning to the Elko production at the LHC, whose signature is $\mu^+ + \mu^- + 2\not{\varsigma}$. Such process includes the quartic self-interaction and a coupling with the Higgs scalar field.

This Letter is organized as follows: In the next section we introduce some formal aspects of the Elko spinor fields calling attention to the main characteristics that will be relevant in the subsequent

* Corresponding author.
E-mail addresses: mafd@cern.ch (M. Dias), camposc@feg.unesp.br (F. de Campos), hoff@feg.unesp.br, hoff@ift.unesp.br (J.M. Hoff da Silva).

[1] We shall emphasize that Elko does not carry standard $U(1)$ gauge invariance [1].

0370-2693/$ – see front matter
doi:10.1016/j.physletb.2011.11.030

analysis. In Section 3 we explore the Elko non-locality, when considering radiative corrections. In Section 4 we analyze the tree level case of a viable cross-section for Elko production at the LHC. Then, we move forward investigating some peculiar aspects of our signal. In the last section we conclude.

2. Elko spinor fields

In this section we briefly introduce the main aspects concerning the construction of Elko spinor fields. Its formal structure may be outlined as follows. Let C be the charge conjugation operator given, in Weyl realization, by

$$C = \begin{pmatrix} 0 & \sigma_2 \\ -\sigma_2 & 0 \end{pmatrix} K, \tag{1}$$

being K the operator that complex conjugate a spinor which appears on its right and σ_2 the usual Pauli matrix. The Elko spinor, $\lambda(\mathbf{p})$, is defined by

$$C\lambda(\mathbf{p}) = \pm\lambda(\mathbf{p}), \tag{2}$$

where plus sign yields self-conjugate spinors ($\lambda^S(\mathbf{p})$) and minus anti self-conjugate spinors ($\lambda^A(\mathbf{p})$)

$$\lambda(\mathbf{p}) = \begin{pmatrix} \pm\sigma_2\phi_L^*(\mathbf{p}) \\ \phi_L(\mathbf{p}) \end{pmatrix}. \tag{3}$$

In the above equation $\phi_L(\mathbf{p})$ transforms as a left-handed (Weyl) spinor, hence $\sigma_2\phi_L^*(\mathbf{p})$ transforms as a right-handed spinor. In this vein, Elko spinor belongs to the $(\frac{1}{2},0)\oplus(0,\frac{1}{2})$ representation space. Now, let us set the explicit form of Elko, in the rest frame[2] ($\mathbf{p}=\mathbf{0}$). In order achieve the formal profile of Elko, one may look at the helicity equation $(\sigma\cdot\hat{\mathbf{p}})\phi^{\pm}(\mathbf{0}) = \pm\phi^{\pm}(\mathbf{0})$. Taking $\hat{\mathbf{p}} = (\sin\theta\cos\phi, \sin\theta\sin\phi, \cos\theta)$ we arrive at four spinors, following the standard notation, given by

$$\begin{aligned}
\lambda^S_{\{+,-\}}(\mathbf{0}) &= \begin{pmatrix} +\sigma_2[\phi_L^-(\mathbf{0})]^* \\ \phi_L^-(\mathbf{0}) \end{pmatrix}, \\
\lambda^S_{\{-,+\}}(\mathbf{0}) &= \begin{pmatrix} +\sigma_2[\phi_L^+(\mathbf{0})]^* \\ \phi_L^+(\mathbf{0}) \end{pmatrix}, \\
\lambda^A_{\{+,-\}}(\mathbf{0}) &= \begin{pmatrix} -\sigma_2[\phi_L^-(\mathbf{0})]^* \\ \phi_L^-(\mathbf{0}) \end{pmatrix}, \\
\lambda^A_{\{-,+\}}(\mathbf{0}) &= \begin{pmatrix} -\sigma_2[\phi_L^+(\mathbf{0})]^* \\ \phi_L^+(\mathbf{0}) \end{pmatrix},
\end{aligned} \tag{4}$$

with phases adopted such that

$$\phi_L^+(\mathbf{0}) = \sqrt{m_\varsigma}\begin{pmatrix} \cos(\theta/2)e^{-i\phi/2} \\ \sin(\theta/2)e^{i\phi/2} \end{pmatrix} \tag{5}$$

and

$$\phi_L^-(\mathbf{0}) = \sqrt{m_\varsigma}\begin{pmatrix} -\sin(\theta/2)e^{-i\phi/2} \\ \cos(\theta/2)e^{i\phi/2} \end{pmatrix}. \tag{6}$$

We remark that $-i\sigma_2[\phi_L^{\pm}(\mathbf{0})]^*$ and $\phi_L^{\pm}(\mathbf{0})$ present opposite helicities and, hence, Elko carries *both* helicities. Another important formal aspect of Elko spinor fields is its dual spinor. In order to guarantee an invariant real norm, being positive definite for two Elko spinor fields and negative definite norm for the other two, the dual for Elko is defined by

$$\overline{\lambda}^{S/A}_{\{\mp,\pm\}}(\mathbf{p}) = \pm i\big[\lambda^{S/A}_{\{\pm,\mp\}}((\mathbf{0}))\big]^\dagger\gamma^0. \tag{7}$$

With such a definition for the Elko dual, one arrives at the following spin sums [1]

$$\begin{aligned}
\sum_\kappa \lambda^S_\kappa\overline{\lambda}^S_\kappa &= +m_\varsigma\big[\mathbb{I}+\mathcal{G}(\phi)\big], \\
\sum_\kappa \lambda^A_\kappa\overline{\lambda}^A_\kappa &= -m_\varsigma\big[\mathbb{I}-\mathcal{G}(\phi)\big],
\end{aligned} \tag{8}$$

where $\mathcal{G}(\phi)$ is given by [6]

$$\mathcal{G}(\phi) = \gamma^5(\gamma_1\sin\phi - \gamma_2\cos\phi), \tag{9}$$

and the gamma matrices are

$$\gamma^0 = \begin{pmatrix} 0 & 1 \\ 1 & 0 \end{pmatrix}, \qquad \gamma^i = \begin{pmatrix} 0 & -\sigma^i \\ \sigma^i & 0 \end{pmatrix}, \tag{10}$$

being $\gamma^5 = -i\gamma^0\gamma^1\gamma^2\gamma^3$. Spin sums entering in a profound level into the local structure, as well as the statistic, of the theory. It is important to note that the right-hand side of Eqs. (8) is not proportional (or unitary connected) to the momentum operators.[3] Therefore the relations (8) are responsible for the peculiar characteristics of Elko locality structure, as well as its breaking of Lorentz invariance. Such peculiarity, obviously, brings important modifications in the S-matrix calculations (see next section).

After studying the formal structure of Elko spinor fields, we shall examine the quantum field associated to such spinor. It is possible to define an Elko-based quantum field, respecting its formal properties, by

$$\begin{aligned}
\eta(x) = \int \frac{d^3p}{(2\pi)^3}\frac{1}{\sqrt{2mE(\mathbf{p})}} \\
\times\sum_\alpha\big[c_\alpha(\mathbf{p})\lambda^S_\alpha(\mathbf{p})e^{-ip_\mu x^\mu} + c^\dagger_\alpha(\mathbf{p})\lambda^A_\alpha e^{+ip_\mu x^\mu}\big],
\end{aligned} \tag{11}$$

being $c^\dagger_\alpha(\mathbf{p})$ and $c_\alpha(\mathbf{p})$ the creation and annihilation operators, respectively, satisfying the fermionic anticommutation relations

$$\big\{c_\alpha(\mathbf{p}), c^\dagger_{\alpha'}(\mathbf{p}')\big\} = (2\pi)^3\delta^3(\mathbf{p}-\mathbf{p}')\delta_{\alpha\alpha'}, \tag{12}$$

$$\big\{c^\dagger_\alpha(\mathbf{p}), c^\dagger_{\alpha'}(\mathbf{p}')\big\} = \big\{c_\alpha(\mathbf{p}), c_{\alpha'}(\mathbf{p}')\big\} = 0. \tag{13}$$

The Elko dual $\overline{\eta}$ is obtained by replacing λ by its dual, c by $c^\dagger$ and $ip_\mu x^\mu$ by $-ip_\mu x^\mu$ (and vice versa). There is a crucial identity obeyed by Elko, given by the application of the $\gamma_\mu p^\mu$ operator to $\lambda^{S/A}(\mathbf{p})$:

$$\big(\gamma_\mu p^\mu\delta^\beta_\alpha \pm im\mathbb{I}\varepsilon^\beta_\alpha\big)\lambda^{S/A}_\beta(\mathbf{p}) = 0, \tag{14}$$

where $\varepsilon^{\{-,+\}}_{\{+,-\}} := -1$ and δ^β_α is the usual Kronecker symbol. In view of (the simply algebraic) Eq. (14) it turns out that Elko satisfies the Klein–Gordon (not Dirac) equation and, therefore, it must be associated to a Klein–Gordon-like Lagrangian:

$$\mathcal{L}^{free} = \partial^\mu\overline{\eta}(x)\partial_\mu\eta(x) - m_\varsigma^2\overline{\eta}(x)\eta(x). \tag{15}$$

As already mentioned in the Introduction, we shall study the coupling between Elko and Higgs fields, since it is the unique

[2] Of course, the explicit form for any momentum is obtained by performing a boost in $\lambda(\mathbf{p})$.

[3] In acute contrast with the usual Dirac case.

renormalizable (perturbatively) Elko coupling. Therefore, in the next section we shall explore the features of the (15) Lagrangian, plus the interaction given by

$$\mathcal{L}^{int} = \lambda_\varsigma \phi^2(x)\overline{\eta}(x)\eta(x). \tag{16}$$

In this work, and consequently to obtain the Feynman rules relevant to it (see Ref. [15]), our object of study is (15) and (16) added with the usual kinetic and interaction terms for the Higgs boson, the Z vector field and summing over all the quarks in the theory, as they appear in the Standard Model after symmetry breaking.

As the last remark we emphasize that, in general, Eqs. (8) and (9) suggest that there is a preferred axis for Elko. In fact, it is possible to show that Elko enjoys locality in the direction perpendicular to its plane [6], or, equivalently, along the preferred axis $\hat{z}_e$. Let us give an example coming from the canonical structure of Elko fields in order to clarify this point. The canonical conjugate momenta to the Elko fields are given by

$$\Pi(x) = \frac{\partial \mathcal{L}_{KG}}{\partial \dot{\eta}} = \frac{\partial \overline{\eta}}{\partial t}, \tag{17}$$

where $\mathcal{L}_{KG}$ stands for a Klein–Gordon-like Lagrangian. The equal time anticommutator for $\eta(x)$ and its conjugate momentum is

$$\begin{aligned}\left\{\eta(\mathbf{x},t), \Pi\left(\mathbf{x}',t\right)\right\} = i\int \frac{d^3p}{(2\pi)^3}\frac{1}{2m}e^{i\mathbf{p}\cdot(\mathbf{x}-\mathbf{x}')} \\ \times \sum_\alpha \left[\lambda^S_\alpha(\mathbf{p})\overline{\lambda}^S_\alpha(\mathbf{p}) - \lambda^A_\alpha(-\mathbf{p})\overline{\lambda}^A_\alpha(-\mathbf{p})\right],\end{aligned} \tag{18}$$

which, in the light of the spin sums, may be recast in the following form

$$\left\{\eta(\mathbf{x},t), \Pi\left(\mathbf{x}',t\right)\right\} = i\delta^3\left(\mathbf{x}-\mathbf{x}'\right)\mathbb{I} + i\int \frac{d^3p}{(2\pi)^3 e^{i\mathbf{p}\cdot(\mathbf{x}-\mathbf{x}')}}\mathcal{G}. \tag{19}$$

The existence of a preferred axis is now evident, since the second integral in the right-hand side of Eq. (19) vanishes along the $\hat{z}_e$. So, this preferred axis may be understood as an axis of locality.

3. Exploring Elko non-locality

According to its typical Lagrangian Elko spinor fields couple only to the Higgs boson and, hence, any production mechanism of such particle must occur via Higgs production or decay process. A very specific feature of Elko production is its non-locality, encoded in the propagator behavior which has a different form (the $\mathcal{G}(\phi)$ term appears explicitly) when computed outside its axis of propagation. In order to explore a little further this effect, let us consider for instance the first graph of a cascade production of Elko particles (Fig. 1).

If one chooses to compute (or measure) such a higher order process in the same plane where the intermediary Elko is propagating, the amplitude reads

$$\begin{aligned}i\mathcal{M} = \lambda_\varsigma^3 \frac{\lambda^A_\alpha(p_3)\lambda^A_\rho(q_1)\overline{\lambda}^S_\beta(p_4)\overline{\lambda}^S_\sigma(q_2)}{(p_4+q_1+q_2)^2 - m_\varsigma^2} \\ \times \int \frac{d^4k}{(2\pi)^4}\frac{1}{[k^2-m_H^2][(k-q_1-q_2)^2-m_H^2]}.\end{aligned}$$

Otherwise, there is also in the amplitude the presence of the $\mathcal{G}(\phi)$ term

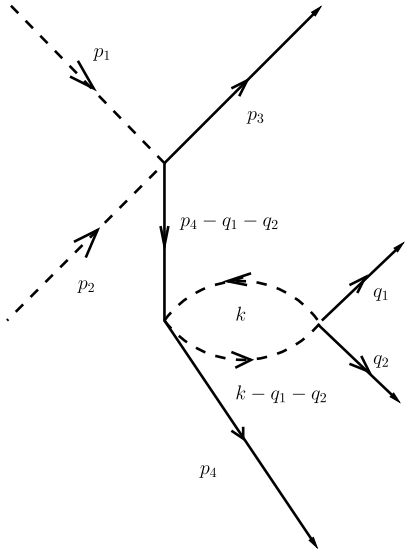

Fig. 1. Example of higher order graphic relevant to Elko production and its non-locality. Dotted lines stand for Higgs boson and continuous lines for Elko.

$$\begin{aligned}i\mathcal{M} = \lambda_\varsigma^3 \frac{\lambda^A_\alpha(p_3)\lambda^A_\rho(q_1)[1+\mathcal{G}(\phi)]\overline{\lambda}^S_\beta(p_4)\overline{\lambda}^S_\sigma(q_2)}{(p_4+q_1+q_2)^2 - m_\varsigma^2} \\ \times \int \frac{d^4k}{(2\pi)^4}\frac{1}{[k^2-m_H^2][(k-q_1-q_2)^2-m_H^2]}.\end{aligned}$$

The divergence appearing in the above amplitude was treated via Pauli–Villars regularization, subtracted this amplitude from its value at $q_1 = q_2 = 0$. The result is given by

$$\begin{aligned}i\mathcal{M}_{RG} = \lambda_\varsigma^3 \frac{\lambda^A_\alpha(p_3)\lambda^A_\rho(q_1)[\mathbb{I}+\mathcal{G}(\phi)]\overline{\lambda}^S_\beta(p_4)\overline{\lambda}^S_\sigma(q_2)}{(p_4+q_1+q_2)^2 - m_\varsigma^2} \\ \times \int_0^1 \ln\left(\frac{(q_1+q_2)^2x(x-1)+m_H^2}{m_H^2}\right).\end{aligned} \tag{20}$$

Computing the traces (where E_1 and E_2 are, respectively q_1 and q_2 particle energies) the average spin squared sum is

$$\begin{aligned}&\frac{1}{16}\sum_{spins}|\mathcal{M}_{RG}|^2 \\ &= \frac{E_2E_4(E_3+p_3)(E_1+q_1)trace[(\mathbb{I}-\mathcal{G}(\phi))(\mathbb{I}+\mathcal{G}(\phi))(\mathbb{I}+\mathcal{G}(\phi))]trace[\mathbb{I}-\mathcal{G}(\phi)]}{[(p_4+q_1+q_2)^2-m_\varsigma^2]^2} \\ &\quad\times\left[\int_0^1 \ln\left(\frac{(q_1+q_2)^2x(x-1)+m_H^2}{m_H^2}\right)\right]^2\lambda_\varsigma^6 \\ &= \lambda_\varsigma^6\frac{8E_2E_4(E_3+p_3)(E_1+q_1)}{[(p_4+q_1+q_2)^2-m_\varsigma^2]^2} \\ &\quad\times\left[\int_0^1 \ln\left(\frac{(q_1+q_2)^2x(x-1)+m_H^2}{m_H^2}\right)\right]^2.\end{aligned} \tag{21}$$

Note that if one lies on the $\vec{p}_4+\vec{q}_1+\vec{q}_2$ direction the obtained result is divided by two. Since the decay rate is proportional to the average spin squared amplitude integrated over the four-body phase space, the Elko particle decays in a preferred axis. Besides, the decay process in such a channel is one half lower than in any other direction.

145

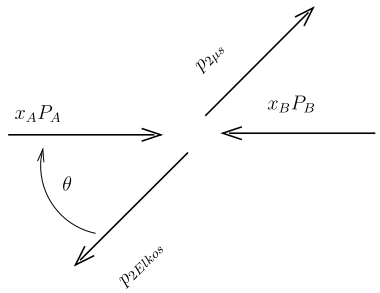

Fig. 2. Kinematics of Elko production.

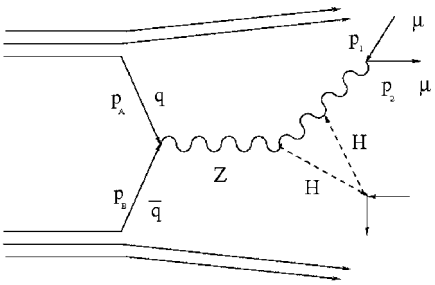

Fig. 3. $q+\bar{q}\to\mu^+ +\mu^- +2\varsigma$ scattering. The loop is composed by two Higgs and a Z boson.

The above considerations lead to an important result: if the cut applied on ϕ includes the intermediary Elko propagation axis, the measured decay is lower than any other cut in which this specific direction is not included. Therefore it breaks ϕ isotropy which is, obviously, fully observed in all Standard Model particles. Such a process makes then manifest the Elko non-locality, giving also a clue for its signature. We should also note another feature in this production, as reflect of momentum conservation, represented in Fig. 2. An increase in the Elko production, in a preferred direction, should implicate a decrease of the remain particles final momentum in the same direction (as a missing energy in the detector), reflecting in a complementary angular distribution, when compared with its possible *background*.

4. Tree level case

For tree level calculations, the non-locality effect is not manifest, and the study of possible signals of Elko decay at accelerators is addressed to the standard searching. For this purposes, we have considered the case where Elko can be produced at the LHC through the Higgs boson fusion, via quartic coupling as depicted in Fig. 3. In both cases (Higgs production or decay process), however, the production is suppressed according to the value of the coupling constant, leaving the number of events and the signature of the decay expressed as a function of two fundamental parameters of the model: the Elko mass and the Elko–Higgs boson coupling constant, which will be taken as less than or equal to one, in order to ensure renormalizability. At the LHC, signatures with leptons as a final state are preferred, specially muons, whose background can be calculated directly from the Standard Model. Besides, the identification of muons are well given as, for example, at CMS technical proposal. In this vein, we will be focused in a two muons + Elko signal, according to the process illustrated in the graph (Fig. 3). In this case the process is $q+\bar{q}\to\mu^+ +\mu^- +2\varsigma$, where 2ς stands for the two Elko particles with mass m_ς produced in the threshold were they will be on rest in the CoM frame. We do not considered here the direct production of two Higgs from Elko fusion, since the Higgs boson is, indeed, the key block to be detected

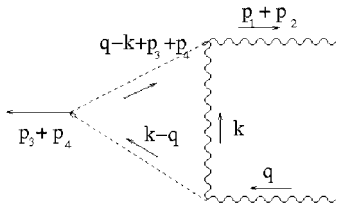

Fig. 4. Performed loop calculation.

at the LHC. We have fixed the Higgs mass boson in the experimental limit [14] and also considered jets with high energy and momentum. In such case, they will emerge almost collinear with the beam. The interaction rate is proportional to the cross section calculated as follows:

We shall label $p_A = x_A P_A$ and $p_B = x_B P_B$, respectively, as the momentum for the quark and anti-quark, related to the initial protons $P_{A,B}$ and the muons with momentum p_1 and p_2. The amplitude is given by:

$$\begin{aligned} i\mathcal{M} = {} & q^r(p_A)\left[\frac{ig_Z}{2}\gamma^\mu\left(c_V^f - c_A^f\gamma^5\right)\right] \\ & \times \bar{q}^{r'}(p_B)\left[\frac{-i}{q^2-m_Z^2}\left(g_{\mu\nu}-\frac{q_\mu q_\nu}{m_Z^2}\right)\right] \\ & \times \frac{igm_Z g^{\nu\rho}}{2\cos(\theta_w)}\left[\frac{-i}{k^2-m_Z^2}\left(g_{\rho\sigma}-\frac{k_\rho k_\sigma}{m_Z^2}\right)\frac{i}{(q-k)^2-m_H^2}\right] \\ & \times \frac{igm_Z g^{\sigma\gamma}}{2\cos(\theta_w)}\left[\frac{i}{(q-k)-m_H^2}\right]\lambda_\varsigma \bar{\lambda}^S{}_\Lambda \lambda^A_\Omega \\ & \times \left[\frac{-i}{q^2-m_Z^2}\left(g_{\gamma\delta}-\frac{q_\gamma q_\delta}{m_Z^2}\right)\right] \\ & \times \frac{-ig_Z}{2}\gamma^\delta\left(-\frac{1}{2}+2\sin^2(\theta_w)+\frac{1}{2}\gamma^5\right)\bar{u}^s(p_1)v^{s'}(p_2), \quad (22) \end{aligned}$$

following the conventions of Ref. [15], where the factors for quarks read

$$\begin{aligned} u \quad &\Rightarrow \quad c_A^f = 1/2, \qquad c_V^f = 1/2 - 4/3\sin^2(\theta_w), \\ d \quad &\Rightarrow \quad c_A^f = -1/2, \qquad c_V^f = -1/2 + 2/3\sin^2(\theta_w). \end{aligned}$$

On partonic CoM reference frame and $p_A = p_B = p_1 = p_2 \approx 0$ we can set

$$\begin{aligned} p_A &= \frac{\sqrt{\hat{s}}}{2}(1,0,0,1), \qquad p_B = \frac{\sqrt{\hat{s}}}{2}(1,0,0,-1), \\ p_1 &= \left(\frac{\sqrt{\hat{s}}}{2}-m_\varsigma\right)\big(1,\sin(\theta),0,\cos(\theta)\big), \\ p_2 &= \left(\frac{\sqrt{\hat{s}}}{2}-m_\varsigma\right)\big(1,-\sin(\theta),0,-\cos(\theta)\big), \\ p_3 &= m_\varsigma(1,0,0,0), \qquad p_4 = m_\varsigma(1,0,0,0), \end{aligned}$$

where $q = \sqrt{\hat{s}}$.

Looking at Fig. 4 we can identify

$$\begin{aligned} P_1 &= (k-q)^2 - m_H^2, \\ P_2 &= (q+2m_\varsigma - k)^2 - m_H^2, \\ P_3 &= k^2 - m_Z^2 = l_0^2 - l_\perp^2 - m_Z^2, \end{aligned} \quad (23)$$

as the denominators for the function to be integrated. In order to use the functions well established (`OneLoop2Pt`) on `xloops`

package [16] we need to reduce the number of functions on denominator (23), using Feynman trick,

$$\frac{1}{P_1P_2P_3}=\int_0^1\frac{1}{P_3}\frac{dx}{[P_1x+P_2(1-x)]^2}=\int_0^1\frac{1}{P_3}\frac{dx}{(k+q')^2-m^2},$$

$$q'=-x\sqrt{\hat{s}}+(x-1)(\sqrt{\hat{s}}+2m_\varsigma)$$

$$\Rightarrow\quad e_0^\mu=\frac{q'^\mu}{\|q'\|}=-(1,0,0,0),$$

$$m^2=\left[x\sqrt{\hat{s}}+(1-x)(\sqrt{\hat{s}}+2m_\varsigma)\right]+m_H^2-x\sqrt{\hat{s}}$$
$$-(1-x)(\sqrt{\hat{s}}+2m_\varsigma)^2, \tag{24}$$

where x integration was performed with `Maple` using of the approximation where $m_\varsigma/\sqrt{\hat{s}}\approx 0$. Obviously, such an approximation in the Elko mass is largely justified in order to guarantee Elko spinor fields as a dark matter candidate. This choice restrict the experimental analysis to events with low energy QCD jets in its final state, since almost all momentum is transferred to the initial partons, providing a signature for the Elko production. One can expect missing energy on detectors, due to the fact that Elko particles will be unobserved by detectors and the only impact in its production reduces the final $\mu^+ + \mu^-$ quadrimomentum. With this expression at hands, it is necessary to multiply by its conjugate and perform the respective polarization sums (8), taking into account, obviously, the terms $\mathcal{G}(\phi)$ responsible for the nonlocality outside $\hat{z}$ axis. Is straightforward to perform those traces for Elko polarization sums using the Elko dual definitions and the spin sums [1]

$$\sum_\kappa \lambda^S_\kappa\left(\overline{\lambda}^S_\kappa\right)^\dagger$$

$$=\sum_\kappa\left(i\epsilon^\rho_\kappa\lambda^{S\,\dagger}_\rho\gamma^0\right)\left(i\epsilon^\sigma_\kappa\lambda^{S\,\dagger}_\sigma\gamma^0\right)^\dagger=\sum_\kappa\epsilon^\rho_\kappa\epsilon^\sigma_\kappa\lambda^{S\,\dagger}_\rho\lambda^S_\sigma \tag{25}$$

$$=\lambda^{S\,\dagger}_{\{-,+\}}\lambda^S_{\{-,+\}}+\lambda^{S\,\dagger}_{\{+,-\}}\lambda^S_{\{+,-\}}=4E\mathbb{I}, \tag{26}$$

where $\epsilon^{\{-,+\}}_{\{+,-\}}=-\epsilon^{\{+,-\}}_{\{-,+\}}=-1$.

After squaring, taking traces and averaging over the spin of the initial and final particles (we approximate the masses for quarks and muons to zero), we should obtain $\sum_{r,r'}\sum_{s,s',\Omega,\Lambda}|\mathcal{M}|^2$. One could use it to calculate

$$d\hat{\sigma}=\frac{1}{2E_A2E_B}\frac{1}{2}\left(\frac{1}{64}\sum_{spin}|\mathcal{M}|^2\right)dP\,S,$$

where $dP\,S$ is the phase space for two muons with momentum p_1 and p_2 and two Elkos with mass m_ς on rest, i.e.,

$$dP\,S=(2\pi)^4\delta^4(p_A+p_B-p_1-p_2-p_3-p_4)$$
$$\times\frac{d^3p_1}{(2\pi)^3(2E_1)}\frac{d^3p_2}{(2\pi)^3(2E_2)}$$
$$=\frac{1}{4(2\pi)^2}\delta(\sqrt{\hat{s}}-E_1-E_2-2m_\varsigma)\frac{p_1^2\,dp_1\,d\Omega}{E_1E_2}$$
$$=\frac{1}{32\pi^2}\frac{\sqrt{\hat{s}}}{\sqrt{\hat{s}}-2m_\varsigma}d\Omega, \tag{27}$$

where $|p_1|dp_1=E_1\,dE_1$, being $E_1=(\sqrt{\hat{s}}/2-m_\varsigma)$. We emphasize that we are working within $m_\varsigma\approx 0$ approximation. We also stress that $d\hat{\sigma}$ has no dependence on angular coordinates, so the integration on $d\Omega$ gives a multiplicative factor 4π for the total cross section. Our final result, however, is to much huge to be presented here.

On the hadronic frame, $P_A=\frac{\sqrt{s}}{2}(1,0,0,1)$ and $P_A=\frac{\sqrt{s}}{2}(1,0,0,-1)$. Thus

$$s=(P_A+P_B)^2=\frac{\hat{s}}{x_Ax_B},$$

and we will integrate using `Cuba` routines [17]

$$\sigma_{(p+p\to\mu^++\mu^-+2\varsigma)}=\sum_q\int_0^1\int_0^1 dx_A\,dx_B\left[f_q(x_A)f_{\bar{q}}(x_B)\right.$$
$$\left.+f_{\bar{q}}(x_A)f_q(x_B)\right]\hat{\sigma}(\hat{s})\delta(\hat{s}-x_Ax_Bs).$$

With the hadronic total cross section at hands, it is straightforward to obtain the event rate R by multiplying σ by the integrated luminosity $\mathcal{L}$, estimated in 1 fb^{-1} and 10 fb^{-1}.

The results of the studied process are presented in Fig. 5. We show the total expected event rate for 2 Elkos + $\mu^+\mu-$ via the Higgs boson fusion, at the LHC, for two different values of the center-of-mass energy, as well as two different values for the total luminosity. The total number of events is presented as a function of the Elko mass. The main case we consider, with total luminosity of 10 fb^{-1}, at 7 TeV, for a coupling constant of an order of 1 shows a quite optimistic number of events, around a thousand. For a smaller coupling constant, $O(10^{-2})$, the number of events is also large. In this sense, we can consider the LHC, for instance, as a good scenario to study both, the Higgs boson and the Elko production in order to shed some light to the dark matter problem. For a 14 TeV center-of-mass energy case, in both 1 fb^{-1} and 10 fb^{-1} cases, the total number of events produced at the LHC is even bigger, for the different values of the coupling constant. By now, since the number of events is encouraging, we shall keep our attention in the exploration of a typical signature encoding the Elko nonlocality.

5. Detection possibility at LHC

Even though the decay in the preferred axis is estimated as one half lower than in any other direction, a poor detector angular resolution on this decay will smear out this effect, either due to the detector tracking, or due to the poor event reconstruction. Therefore it is mandatory to make an estimation of the minimum angular resolution requirement to detect this effect. At the LHC, the minimum angular resolution at, e.g., the CMS detector $\Delta\phi_{res}=10$ mrad [18]. The relative significance on this interval for an integrated luminosity L, taking into account our background will be given by

$$S_{rel}=\frac{S}{\sqrt{B}}, \tag{28}$$

since the background is isotropically distributed in the azimuthal angle and the efficiency on the muon measurement is about 98%. In Eq. (28), S stands for the number of events produced in the Elko decay and B denotes the number of events related to the background.

The signal is characterized by a dimuon in the final state reconstructed in a Z boson and some missing energy in the final state. Thus the irreducible SM background consists of the ZZ decaying in two muons and two neutrinos, as already studied in Ref. [19]. The background processes for the signal, considering next-to-leading order cross section are presented in Table 1 (see [18]). The irreducible SM background for the signal is the ZZ process, where one of the Z bosons decays into neutrinos. Since we

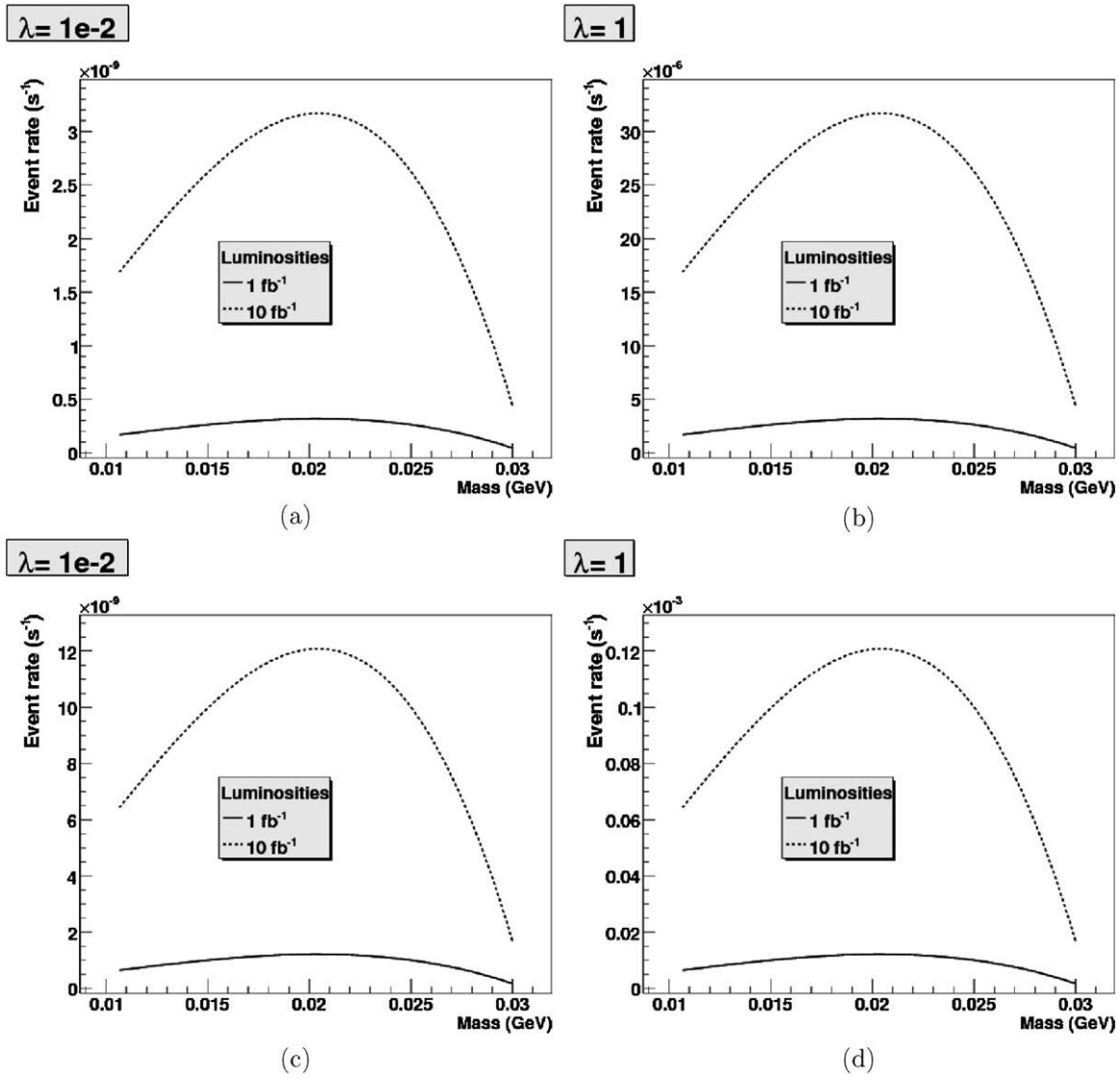

Fig. 5. Event rate $(1/s)$ versus mass (GeV) for two luminosity values and the center-of-mass energy at the LHC for 7 TeV (a)–(b) and 14 TeV (c)–(d). The range for mass was chosen to guarantee the fact that the Elko can be a possible candidate for dark matter [1]. We have considered two values for λ_ς, namely, 1 and 10^{-2}.

Table 1
Background estimative for the high-order process under study.

Channel	Cross section (pb)
$qq \to WW \to \mu^+\mu^-$	11.7
$t\bar{t}$	840
$gg \to WW \to \mu^+\mu^-$	0.54
γ^*, Z	145 000
$b\bar{b} \to \mu^+\mu^-$	710
$ZW \to \mu^+\mu^- l^\pm$	1.63
$tWb \to \mu^+\mu^-$	3.4
$ZZ \to \mu^+\mu^-$	1.52

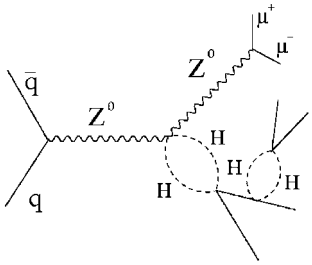

Fig. 6. Feynman diagram for the production of 4 missing Elko bosons (solid lines) and two muons, associated with some Higgs intermediary process.

are interested in making an estimate of the signal, taking into account the background without defining cuts for a detailed analysis, we only consider the ZZ process, as it is much larger than the signal. In such a case, the number of events for the background considering a luminosity of 2×10^{33} cm^{-2} s^{-1}, is around 99 000 events.

In order to explore the claimed angular dependence for the signal, we study the process $q\bar{q} \to Z^* \varsigma \varsigma^* \to 2\mu 4\varsigma$, which is shown in Fig. 6. The two final muons inherit the sensibility on azimuthal angle by momentum conservation on the final states. Actually this process is nothing but that one described in Fig. 3 followed by the decay of Fig. 1, mediated by two loops involving Higgs particles.

An analytic expression for this process can be obtained using the equation for $\frac{1}{16}\sum_{spins}|\mathcal{M}_{RG}|^2$ (see Section 3) and supposing the limit $\frac{q_1+q_2}{m_E} \approx 0, q_1 + q_2 > p_4$. One can expand the integrand, and proceed with the integration for the first term to obtain

$$\frac{1}{16}\sum_{spins}|\mathcal{M}_{RG}|^2 \approx \lambda_\varsigma^6 \frac{8E_2E_4(E_3+p_3)(E_1+q_1)}{(p_4+q_1+q_2)^4}\frac{(q_1+q_2)^4}{36m_H^4}$$
$$\approx \lambda_\varsigma^2 \frac{2E_2E_4(E_3+p_3)(E_1+q_1)}{9m_H^4}.$$

In the limit $p_3, p_4 \to 0$, and with all final state energies near to the Elko mass, we obtain a lower bound to this values given by

$$\frac{1}{16}\sum_{spins}|\mathcal{M}_{RG}|^2 \geqslant \lambda_\varsigma^6 \frac{2m_E^4}{9m_H^4}, \tag{29}$$

which shall be multiplied by the cross section obtained numerically before.

For the Elko production, on the simple decay $2\mu + 2\varsigma$ and fixing the coupling constant at its maximum value ($\lambda_\varsigma = 1$) as well as $m_\varsigma = 0.09$ GeV, we have $\sigma_{signal} = 5.06$ fb. At the LHC, for a 1 fb^{-1} integrated luminosity, one should obtain a ratio $\frac{S}{\sqrt{B}} = \frac{\sigma_{signal}\sqrt{L}}{\sqrt{\sigma_{bckg}}}$ around 5, where S stands for the number of events for the signal and B the number of events for the background (or actually one half of this value, taking account the angular asymmetry).

However as the detection of this process signature depends on the coupling constant, since under a certain value it would be required a better angular resolution in the detector to distinguish the signal from the background. For an indirect search of Elko particles via azimuthal angular asymmetry with $2\mu + 4\varsigma$ process, using the angular resolution for the CMS detector ($\Delta\phi \geqslant \Delta\phi_{res}$), $m_\varsigma = 0.09$ GeV and $\sqrt{s} = 7$ TeV, the number of events decreases substantially to $S = 4.4 \times 10^{-15}$ taking (29) into account. Hence, one can see that for these parameters Eq. (28) gives a result which is clearly insufficient to claim a discovery at the LHC. The process on study has actually a dependency on λ_ς^6, so the estimated minimum resolution for the $\lambda_\varsigma = 1 \times 10^{-2}$ case, maintaining $S_{rel} \approx 5$, is $\Delta\phi_{res} \approx 9.1 \times 10^{-11}$ rad. Lower values of λ_ς should require a better resolution on the detector. Of course, for this rough estimate, none type of cuts was performed and a detailed study using a Monte Carlo simulation for the final state Elko momenta would be in order.

The main motivation for this analysis is the possibility of Elko detection in a range of parameters making possible to address Elko as possible dark matter candidate. We now shall look at the following question: what should be the expected missing energy in the dimuon + jet system, if Elko production is occurring taking into account the Elko non-locality? Considering the proton–proton energy as $(\sqrt{s}, 0, 0, 0)$ in Fig. 2 we have the momentum configuration

$$p_{2\mu} = \frac{\sqrt{s}}{2}\left(1 + \frac{m_{2\mu}}{s} - \frac{m_{2\varsigma}}{s}, \beta\sin(\theta), 0, \beta\cos(\theta)\right),$$
$$p_{2\varsigma} = \frac{\sqrt{s}}{2}\left(1 + \frac{m_{2\varsigma}}{s} - \frac{m_{2\mu}}{s}, -\beta\sin(\theta), 0, -\beta\cos(\theta)\right),$$

where $m_{2\varsigma}(m_{2\mu})$ is the invariant mass, for instance $m_{2\varsigma}^2 = 2m_\varsigma^2 - 2\vec{p}_3\cdot\vec{p}_4 + 2E_3E_4$, as the sum of two momentum vectors, and $\beta = \sqrt{1 - 2\frac{m_{2\mu}+m_{2\varsigma}}{s} + \frac{(m_{2\mu}-m_{2\varsigma})^2}{s^2}}$. Therefore the missing energy is

$$E^{miss} = \sqrt{s}\left(1 + \frac{m_{2\mu} - m_{2\varsigma}}{s}\right) - \sqrt{s} = \frac{m_{2\mu} - m_{2\varsigma}}{\sqrt{s}}.$$

149

An important requirement is imposed by the minimum energy resolution for the search of missing energy on this channel. Considering the same parametrization as used for the CMS detector [18], we suppose that the threshold for the missing energy for the signal is given by

$$E^{miss} = \frac{m_{2\mu} - m_{2\varsigma}}{\sqrt{E}}.$$

In the limit that the two Elkos does not have a significant momenta, it is possible to approximate $m_{2\mu} \approx m_Z = 91.187$ GeV and, then, one should to select only events with $E_{miss} > 25$ GeV. This means that a detailed analysis should take into account both, angular and energy, resolutions.

6. Final remarks

By analyzing the consequences of the unusual Elko propagator behavior, it was possible to derive a typical signature to the Elko production, namely: due to the Elko non-locality, the measured decay depends on the angular cut applied, breaking therefore the angular isotropy (fully observed in all standard model processes).

We shall stress two important points: Fig. 1 may be understood as the first term of a sum involving internal Elko productions of the same type (a "cascade" of a "fork"), what means that its contribution can be improved by the sum of those graphs, faced as a finite geometric series on λ^2; second, it should be stressed for completeness, that another factor resulting as an unexpected asymmetry on ϕ (for graphs involving four Elkos coupling) arises from the inclusion of the $\overline{\eta}\overline{\eta}$ and $\eta\eta$ type propagators, which are proportional to $N(p')$ and $M(p)$ matrices, the "twisted spin sums":

$$M(p) = \begin{bmatrix} e^{-i\phi}p\cos(\theta) & p\sin(\theta) & 0 & -iE \\ p\sin(\theta) & -e^{i\phi}p\cos(\theta) & iE & 0 \\ 0 & -iE & -e^{-i\phi}p\cos(\theta) & -p\sin(\theta) \\ -iE & 0 & -p\sin(\theta) & e^{i\phi}p\cos(\theta) \end{bmatrix},$$

$$N(p') = \begin{bmatrix} \sqrt{p'^2+m_\varsigma^2} & 0 & ip'\sin(\theta') & -ie^{-i\phi'}p'\cos(\theta') \\ 0 & \sqrt{p'^2+m_\varsigma^2} & -ie^{i\phi'}p'\cos(\theta') & -ip'\sin(\theta') \\ ip'\sin(\theta') & -ie^{-i\phi'}p'\cos(\theta') & -\sqrt{p'^2+m_\varsigma^2} & 0 \\ -ie^{i\phi'}p'\cos(\theta') & -ip'\sin(\theta') & 0 & -\sqrt{p'^2+m_\varsigma^2} \end{bmatrix}. \tag{30}$$

Acknowledgements

We are grateful to Professor D.V. Ahluwalia and Professor A. Alves for valuable suggestions.

References

[1] D.V. Ahluwalia, D. Grumiller, JCAP 0507 (2005) 012, arXiv:hep-th/0412080.
[2] D.V. Ahluwalia, D. Grumiller, Phys. Rev. D 72 (2005) 067701, arXiv:hep-th/0410192.
[3] C.G. Boehmer, Ann. Phys. 16 (2007) 325, arXiv:gr-qc/0701087;
C.G. Boehmer, Ann. Phys. 16 (2007) 38, arXiv:gr-qc/0607088;
C.G. Boehmer, J. Burnett, Mod. Phys. Lett. A 25 (2010) 101, arXiv:0906.1351 [gr-qc];
S. Shankaranarayanan, Int. J. Mod. Phys. D 18 (2009) 2173, arXiv:0905.2573 [astro-ph];
C.G. Boehmer, J. Burnett, Phys. Rev. D 78 (2008) 104001, arXiv:0809.0469 [gr-qc];
D. Gredat, S. Shankaranarayanan, JCAP 1001 (2010) 008, arXiv:0807.3336 [astro-ph];
C.G. Boehmer, Phys. Rev. D 77 (2008) 123535, arXiv:0804.0616 [astro-ph];
C.G. Boehmer, D.F. Mota, Phys. Lett. B 663 (2008) 168, arXiv:0710.2003 [astro-ph];
L. Fabbri, Mod. Phys. Lett. A 25 (2010) 2483, arXiv:0911.5304 [gr-qc];
L. Fabbri, arXiv:1008.0334 [gr-qc].
[4] L. Fabbri, Mod. Phys. Lett. A 25 (2010) 151, arXiv:0911.2622 [gr-qc];
R. da Rocha, W.A. Rodrigues Jr., Mod. Phys. Lett. A 21 (2006) 65, arXiv:math-ph/0506075;

R. da Rocha, J.M. Hoff da Silva, J. Math. Phys. 48 (2007) 123517, arXiv:0711.1103 [math-ph];
R. da Rocha, J.M. Hoff da Silva, Adv. Appl. Clifford Alg. arXiv:0811.2717 [math-ph];
J.M. Hoff da Silva, R. da Rocha, Int. J. Mod. Phys. A 24 (2009) 3227, arXiv:0903.2815 [math-ph].
[5] E.P. Wigner, Ann. of Math. 40 (1939) 149.
[6] D.V. Ahluwalia, C.-Y. Lee, D. Schritt, T.F. Watson, Phys. Lett. B 687 (2010) 248, arXiv:0804.1854 [hep-th];
D.V. Ahluwalia, C.-Y. Lee, D. Schritt, arXiv:0911.2947 [hep-ph].
[7] K. Land, J. Magueijo, Mon. Not. Roy. Astron. Soc. 378 (2007) 153, arXiv:astro-ph/0611518;
P.K. Samal, R. Saha, P. Jain, J.P. Ralston, arXiv:0811.1639 [astro-ph], 2008;
M. Fommert, T.A. Ensslin, 2009; arXiv:0908.0453 [astro-ph].
[8] A.G. Cohen, S.L. Glashow, Phys. Rev. Lett. 97 (2006) 021601, hep-ph/0601236.
[9] D.V. Ahluwalia, S.P. Horvath, JHEP 1011 (2010) 078, arXiv:1008.0436 [hep-ph].
[10] P. Nath, et al., Nucl. Phys. B Proc. Suppl. 200–202 (2010) 185, arXiv:1001.2693.
[11] ATLAS inner detector: Technical design report, vol. 1, CERN-LHCC-97-16.
[12] S.P. Martin, arXiv:hep-ph/9709356.
[13] J.A. Aguilar-Saavedra, et al., Eur. Phys. J. C 46 (2006) 43, arXiv:hep-ph/0511344.
[14] The CDF Collaboration, CDF Note 10223, Preliminary results for the ICHEP 2010 Conference.
[15] M.J.G. Veltman, Cambridge Lecture Notes in Physics, vol. 4, Cambridge Univ. Press, Cambridge, UK, 1994, 284 pp.
[16] C. Bauer, H.S. Do, Comput. Phys. Comm. 144 (2002) 154, arXiv:hep-ph/0102231.
[17] T. Hahn, Comput. Phys. Comm. 168 (2005) 78, arXiv:hep-ph/0404043.
[18] CMS Physics Technical Design Report, vol. II: Physics Performance, J. Phys. G: Nucl. Part. Phys. 34 (2007) 995.
[19] K. Cheung, J. Song, Phys. Rev. D 81 (2010) 097703, arXiv:1004.2783 [hep-ph].

Capítulo 6

Considerações Finais

Apresentamos uma síntese dos mais importantes trabalhos de pesquisa que desenvolvemos nos últimos anos na área de Física de Partículas e Campos. Consideramos aqui tanto o trabalho realizado como possíveis alterações e melhorias, bem como tópicos passíveis de novos estudos e/ou análises. Salientamos que o nosso objetivo principal reside na análise crítica dos trabalhos visando uma apresentação das principais contribuições na área de pesquisa. Nesse sentido, abordamos as tres grandes linhas de pesquisa, nas quais os trabalhos foram desenvolvidos, quais sejam, Acoplamentos Anômalos, Modelos Supersimétricos em Física de Partículas Elementares e Quabra de Simetria de Lorentz. Uma observação geral a respeito dessas áreas é a de que, no tocante aos Acoplamentso Anômalos, os trabalhos publicados recentemente, refletem a atenção dedicada ao processo de revisão dos resultados à luz dos dados publicados pelos experimentos ATLAS e CMS do LHC. Do ponto de vista da Supersimetria (SUSY), a detecção do bóson de Higgs e a ausência de sinais associados à SUSY até o momento, traz à tona o questionamento da viabilidade de tal simetria. As principais críticas nesse aspecto residem

justamente na ausência de evidências diretas que corroborem a SUSY. Por outro lado, as indicações indiretas mantém nossa expectativa de que possam ser encontradas tais evidências. No que diz respeito à Quebra de simetria de Lorentz, o estudo que realizamos é uma pequena contribuição na tentativa de considerarmos todas as possibilidades de extensão do SM. Todos os trabalhos desenvolvidos sempre o foram em colaboração com grupos de pesquisa no Brasil e no exterior, acompanhados de visitas técnicas a esses grupos. Desse modo, buscamos uma integração entre diferentes instituições de ensino e pesquisa, bem como entre diferentes países, cujo intuito sempre foi o fortalecimento do trabalho de pesquisa do ponto de vista acadêmico.